# THE EVOLUTION OF RADIO GALAXIES

Simon John Lilly

Presented for the Degree of Doctor of Philosophy
at the University of Edinburgh

December 1983

This Thesis has been composed by
me and the work described in it
is my own except where specifically
acknowledged in the text.

ABSTRACT

Investigations into several aspects of the evolution of the massive elliptical galaxies associated with powerful radio sources are described. Many of the galaxies studied are amongst the most distant stellar systems presently known and observations of these allow detailed comparisons of their properties to be made over timescales that are greater than a half the present age of the Universe.

New redshifts have been measured for eight 3C radio source identifications. Several of these are very faint radio galaxies at redshifts greater than 0.5.

Infrared JHK photometry for 81 3C radio galaxies is presented. These cover the redshift range from 0.03 to at least 1.6. By analysis of the colour-redshift and magnitude-redshift diagrams it is shown that the spectral energy distributions of the radio galaxies at redshifts of order unity are different from those of nearby galaxies. Evidence is presented which argues strongly in favour of the hypothesis that these differences are caused by changes in the stellar populations of the galaxies and the observations are re-examined in the light of models for the evolution of stellar populations. It is shown that both active and passive evolution (i.e. with and without star formation activity) is occuring in these galaxies.

Infrared photometry for 39 radio sources selected to be 5-10 times fainter in the radio than the 3C sources is presented and discussed. Particular attention is paid to those radio sources whose identifications have not yet been seen in the optical waveband as these are probably very high redshift radio galaxies. Possible constraints on the epoch of galaxy formation are discussed.

Surface photometry of ten nearby 3C radio galaxies is used to compare these galaxies with other samples of giant elliptical galaxies. Some statistical differences are found and these suggest that dynamical evolution has not been as important in the radio galaxies as in the others. This is probably related to their different local environments. Some consequences of this are discussed.

CONTENTS

# Chapter 1 : INTRODUCTION TO THE THESIS

It is the aim of cosmologists to describe and understand the processes that have been important in shaping the present large scale appearance of the Universe. In this Thesis, various aspects of the evolution with cosmic time of the massive elliptical galaxies associated with the powerful radio sources are investigated.

There are two reasons why the evolution of these so-called 'radio galaxies' is particularly interesting. Firstly, the most distant stellar systems that are presently known (i.e. those at redshifts greater than 0.5) are generally members of this class of galaxy. Hence, a study of the properties of the members of the large and statistically complete samples of such galaxies that are fairly straightforward to construct using well-defined radio selection criteria, offers the possibility of observing evolutionary changes over a relatively long baseline in cosmic time. The use of radio galaxies extends the range of epochs accessible to observation to significantly earlier epochs than can be probed using the most distant 'ordinary' galaxies. Secondly, these galaxies are associated with the types of radio source that are responsible for the strong cosmological evolution of the radio source population. This evolutionary change in the radio luminosity function at different epochs was important, together with the discovery of the microwave background, in establishing the credibility of evolutionary big bang cosmologies. One of the main motivations for the work described in this Thesis is to search for possible astrophysical links between the microscopic evolution of the host galaxies and the macroscopic

evolution of the radio source population.

In this first Chapter, a brief introduction is presented of various topics to enable the reader to place the Thesis in context. Subsequently, a more detailed introduction will be given at the start of each Chapter, including a review of the relevant literature, which will relate to the particular investigation described therein.

## 1.1 : The Nature of Radio Sources

Longair (1978) has provided one of many concise introductions to the many aspects of the radio source phenomenon. In a survey to high limiting radio flux density, such as those that are used in this investigation, the majority of extragalactic sources are of an intrinsic radio luminosity that is several orders of magnitude higher than that of our own Galaxy. In the case of our Galaxy, it is possible to account for the observed emission in terms of the production of ultrarelativistic electrons from supernovae in the Galaxy. The more powerful sources, however, are not only more intense emitters, but also have a different radio structure which often bears little resemblance to the optical form of the associated object. In particular, most of the radio sources in low frequency surveys (again, such as those used in this Thesis) consist of two lobes of about the same intensity, situated approximately symetrically about the central object and forming a double source. Sometimes this central object has associated with it a compact nuclear radio source of generally somewhat lower luminosity which contributes typically less than 10% of the total flux at 5 GHz. The

two extended lobes are usually situated a few hundred kpc from the center, but the sizes range from a few kpc to a few Mpc. There is little doubt that the extended emission is produced by the synchrotron mechanism. A typical double radio source is shown in Figure 1.1 (from Jenkins et al 1977).

The 'beam' model of radio sources (e.g. Scheuer 1974) is generally accepted as being a correct basic description of the double source phenomenon. Two collimated jets, produced in the nucleus of the central object, transport energy to the distant 'working faces' where the beams interact with the ambient interstellar, or more usually intergalactic, medium. At this point the energy is converted in to that of relativistic electrons and possibly magnetic field energy. Intense synchrotron emission is produced from relatively small regions seen as 'hotspots'. However, the thermal pressure of the surrounding medium cannot contain these heads, which will expand laterally to fill a cavity of energetic electrons which will continue to radiate. If the power supply to the outer lobes is interupted, then the hotspots will diminish, and the diffuse tail regions will expand to attain pressure balance with their surroundings. This will form a 'relaxed' double source. A diagram illustrating the main features of the model, which is broadly consistent with all features seen in extended extragalactic radio sources, is shown in Figure 1.2.

The nature of the central 'optical' object located between the lobes falls in to one of two categories, with a few examples of intermediate type. The identification is either with an elliptical galaxy (where morphological classification of the galaxy can be

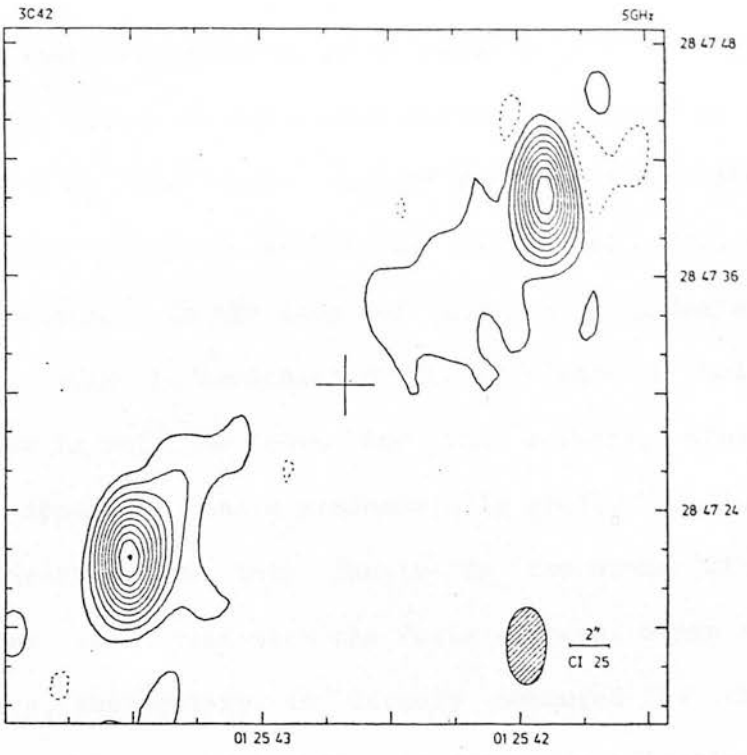


Figure 1.1: The 5 Ghz radio map of 3C 42 from Jenkins et al (1977). This is a typical Fanaroff-Riley Class II 'classical double' radio source. The cross marks the position of a 20th magnitude galaxy which is associated with 3C 42. It is a giant elliptical radio galaxy at a redshift of 0.395, and was observed with UKIRT as part of this investigation.

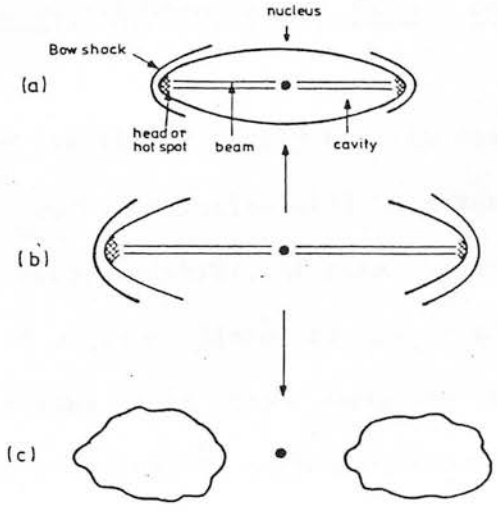


Figure 1.2: The beam model for radio sources (from Longair 1978). Two beams transport the energy from the active nucleus to the distant hotspots. The three figures show different phases in the life of such a source.

made) of above average luminosity, known as a 'radio galaxy' or with an even more luminous object of unresolved appearance, known as a 'quasar'. The properties of these latter objects are consistent with their being the highly enhanced nuclei of elliptical galaxies similar to the radio galaxies. In the case of the radio galaxies themselves the optical light is dominated by the starlight of their constituent stars. This is not the case for the quasars, whose radiation does not appear to have a predominantly stellar origin. The investigation described in this Thesis is concerned with studying the galaxies associated with the radio sources. Since in the case of the quasars, the galaxy is largely obscured by the intensity of the nucleus, the radio source identifications classified as quasars have not been included in the programme of observations described here. The few intermediate objects, known as N-galaxies, were observed, but having been recognised as such, they are not discussed in detail during the development of the interpretation of these investigations.

## 1.2 : The Evolution of Astronomical Objects with Cosmic Epoch

It is quite important to clarify precisely what is meant by the word 'evolution'. In this work, evolution will be taken to mean a change with cosmic time, or hence redshift, of some given property of an object or population of objects. Since the length of time over which astronomical observations have been made is very short compared with the timescales of interest, such evolution can only be inferred from studies of the statistical properties of well-defined samples of objects which are thought to have different ages. In the context of this investigation, this means that the objects should be

at different distances so that they are observed at different cosmological epochs. However, distinction should be made between two kinds of evolution. It is believed that the existence of some astronomical bodies, such as galaxies, is not a transitory phenomena. Although the properties of each individual galaxy may well change with time, the galaxy will nevertheless maintain its own identity, except in the unfortunate case where it undergoes a merger with another galaxy. The simple fact that some stars have lifetimes longer than the present age of the universe, for instance, indicates that this will be so. Consequently, if observations are made of say, all the galaxies in a representatively large volume of the universe (so that statistical fluctuations are small), and these are subsequently compared with observations of the occupants of a similar volume at some lower redshift (and hence later cosmic epoch), then it is reasonable to assume that the members of the first sample will, after the appropriate interval evolve in to objects with the same properties as are observed in the second sample.

On the other hand, some astronomical objects, such as radio sources (which consist only of energetic particles in a magnetic field), may not maintain their identity over cosmological timescales since their lifetimes may be very much shorter than the present age of the Universe. Consequently, one cannot assume that an individual radio source observed at a much earlier epoch will itself evolve in to a radio source similar to those observed at later epochs, but rather, only that the radio source population as a whole will evolve during this time.

Clearly, if observations are made of samples of galaxies that are selected because of their association with radio sources then any evolution that is seen must be of the second type. In other words, it is not possible to assume that the radio galaxies observed at high redshift, will themselves have, much later in their own lives, the same properties as are observed in nearby radio galaxies. This Thesis is mostly concerned with such observations of radio galaxies at different epochs, and the word evolution in the Title, and in the following pages, will be taken to include both these situations.

Too much should not be made of this distinction. In particular, it should be stressed that none of the results of this work, or of other investigations, indicate that the high redshift radio galaxies will not evolve individually in to objects looking very similar to the low redshift radio galaxies. Furthermore, since part of the motivation for this work on distant radio galaxies is to try to find astrophysical links between changes in the host galaxies and the differences that are observed in the radio source population at earlier epochs, any changes in the properties of the galaxies with redshift are of interest, regardless of whether these are purely 'evolutionary' or not. Nevertheless, it is important to stress the limitations on any cosmological investigation that are imposed by the sample selection criteria.

### 1.2.a The Evolution of Galaxies

Most galaxies, and certainly the most massive, are believed to have formed early in the history of the universe through the

dissipational collapse and subsequent virialisation of density perturbations sometime after the recombination of hydrogen, which occured at a redshift of about 1500 (see e.g. Rees 1978). However, the precise epoch at which the galaxies formed is not yet known, either theoretically or observationally. This is despite several attempts to identify primeaval galaxies (see e.g. Davis 1980). The spectrum and the nature, i.e. adiabatic or isothermal, of the initial perturbations is not known, and even the relative order in which globular clusters, galaxies, and the larger scale structure of clusters and superclusters were formed is unconstrained at present. The fact that the oldest stars that have been found have significantly non-zero abundances of metals that could not have been formed in the initial fireball suggests that there may also have been a pre-galactic population of stars (the so-called Population III).

Once the galaxy has formed, the situation becomes clearer, and a conceptual framework has been developed for investigating galactic evolution (see e.g. Gunn 1982). Most galaxies, of whatever morphological type, formed a substantial fraction of their mass in to stars at the begining of their history. These stars form the bulk of elliptical galaxies and the bulge component of spiral galaxies, and are known as Population II stars. In our own Galaxy, these are generally of relatively low metallicity, but can contain metals in above solar abundances. Unlike ellipticals which appear relatively dead at the present epoch, spirals observed today have substantial continuous star formation. This generally occurs in the spiral arms in their disks, and the rate of star formation appears to be well related to the morphological classification of the galaxy. There is

good reason to believe that the gas required for this star formation falls in to the galaxy from outside, and that this rate of infall may in fact be the prime determinant of a galaxy's morphological type. An understanding of the evolution of the star formation rate in galaxies of all morphological types is a major goal of observational cosmology.

Throughout the history of the galaxy, and indeed also in any pre-galactic phase, the stars producing metals in thermonuclear reactions will be interacting with the interstellar medium, through mass loss processes and supernovae explosions, and changing the chemical abundance of the gas and consequently of the new stars formed from that gas. This process is known as the chemical evolution of the galaxy.

These evolutionary processes are primarily concerned with the evolution of the stellar population of the galaxy. There are other forms of evolution, however, that may occur after the initial formation process, which are thought to be important in shaping the appearance of the galaxies that we see today. In particular the large size of galaxies relative to their average separations suggests that the merging of two galaxies to produce a single remnant may be important, particularly in the centres of clusters of galaxies.

One of the many motivations for trying to understand galactic evolution is, of course, the hope that some galaxies may be useful as 'standard candles' to determine the global geometry of the universe.

1.2.b The Evolution of the Radio Source Population

The observed slope (1.8) of the radio source counts at relatively high flux densities is impossible to reconcile with cosmological models, either of 'steady state' or 'Friedmannian' form, unless the radio luminosity function (RLF) changes with redshift (Ryle and Clarke 1961). The comoving space density must be higher in the past. Since this contradicts the time-invariance required by a steady state cosmology, this evolution has been taken as strong evidence in favour of evolving 'big bang' model universes. Longair (1966) showed that the form of the source counts, and in particular their rapid convergence at low flux densities, requires that the comoving space density of the more luminous radio sources must evolve much more than that of the lower luminosity sources. Longair (1966) also introduced the (P,z) plane as the basis for consideration of evolutionary models. On such a plane, the density $\rho(P,z)$ of sources at the appropriate power P and redshift z may be plotted. At any epoch, the RLF is therefore represented by a cut at constant z, while a cut at constant P shows the change in comoving space density of those sources with redshift. $\rho(P,z)$ may be conveniently decomposed in to a zero redshift RLF and an evolution function E(P,z) (Wall et al 1980).

$$\rho(P,z) = \rho_0(P) \cdot E(P,z) \qquad (1.1)$$

There have been numerous attempts to model E(P,z) as the data on the radio source population has improved. The most recent and

successful of these has been that by Peacock and Gull (1981). Whereas some earlier investigators (e.g. Wall et al 1980,1981) had assumed various analytic forms for E(P,z), Peacock and Gull (1981) modelled the function as a polynomial expansion to 6th order in log P and log (1+z). Such a model has 37 free parameters, and is effectively a free form expansion with the requirement only that E be a smooth function in these two logarithmic variables. An important consequence of adopting this approach was that it becomes clear which parts of the (P,z) plane are constrained by the available data and which are not.

Although the precise figures depend on the detailed assumptions that are made regarding the cosmological geometry, it is clear from Peacock and Gull's (1981) models that the comoving number density of sources with radio powers around $10^{28}$ $WHz^{-1}sr^{-1}$ at a redshift of unity are enhanced by a factor of about 100. This is the location on the (P,z) plane of many of the high redshift 3CR galaxies studied in this Thesis. It is not known at the present time whether this evolution is best described as either luminosity or density evolution, although the distinction is in any case blurred by the use of the combined evolution function E(P,z)

One of the most interesting aspects of recent work on the evolution of the radio source population and of the related work on the evolution of the comoving space density of optically selected quasars is the suggestion that the evolution function may decline fairly sharply at redshifts in excess of 3.5 to 4 (Peacock and Gull 1981, Osmer 1982 and Peacock 1983). Such a decline could be indicative of the epoch of galaxy formation, but since it is not

understood what causes the increase in comoving density with lookback time that is observed back to a redshift of 3, such an interpretation might be premature even if the downturn beyond that redshift is convincingly shown to be real.

## 1.3 : The Complete 3CR Sample of Bright Extragalactic Radio Sources

The radio galaxies chosen for observation in the investigations described in this Thesis were, with the exception of those in Chapter 6, selected from a complete sample of 3CR radio sources.

The Third Cambridge (3C) catalogue of 471 radio sources was constructed in the late 1950s by Edge *et al* (1959) using a four element interferometer operating at 159 MHz. The catalogue consisted of the brightest low frequency sources in the northern sky. This first catalogue was soon revised by Bennet (1962) using a better telescope with smaller side lobes. This revised catalogue (the 3CR) was based on measurements at 178 MHz, and while extending to a similar depth as the original 3C survey, it had a more uniform coverage over the sky. Subsequent careful measurements of the flux densities of these 3CR sources by Kellerman *et al* (1969) were made using the 4CT pencil beam telescope. This had a sufficiently small beam that confusion was considerably reduced, but was large enough that few sources were resolved out. These measurements enabled statistical samples that were believed to be complete with respect to fairly well defined selection criteria to be constructed (e.g. Jenkins *et al* 1977, JPR), while the development of high resolution interferometric telescopes enabled an increasing number of these sources to be identified with their associated optical objects.

The statistically complete JPR sample of 177 sources (3C 296 had been omitted from the initial sample by mistake) has formed the basis of many statistical investigations in to various aspects of the radio source phenomenon. The objects in this sample, or those in well defined subsamples, have been observed in almost all wavebands from the X-Ray to the radio in the past 6 years. Nevertheless, it was known that biases had been introduced in to the JPR sample by both confusion and partial resolution of the original 3CR sources. Laing et al (1983, LRL) therefore reexamined the original 3CR, 4C ad 4CT catalogues to reconstruct the JPR sample. Several sources were removed from the JPR sample, but 14 new sources were also introduced. The revised LRL sample contains 173 extragalactic sources which satisfy the following selection criteria: $S(178) > 10$ Jy; $\delta > 10^{o}$; and $|b| > 10^{o}$.

Although LRL had reduced the effects of the selection biases, they were unable to remove them completely, and they estimated that their new sample was 94% complete in the sense that 94% of the sources that should be in such a sample are indeed in the list in their paper. 96% of these 173 sources have been identified with optical objects, and only 7 objects do not have plausible candidate identifications in the optical waveband. For four of these, no deep optical search has yet been made in view of their late inclusion in the statistical sample and only three sources have no optical identification purely because of their extreme faintness. There is some slight doubt about the correctness of 4 more of the identifications, but of the remaining 162 sources, LRL believe that only about two could be chance associations.

## 1.4 : Cosmological Models Adopted

The interpretation of the observations presented in this Thesis will be based on the standard Hot Big Bang universe described by the Robertson-Walker metric and whose dynamics follow the Friedmannian Equations with zero cosmological constant (see e.g. Gunn 1978). Where neccessary a range of geometries will be considered. The value for the scale factor, $H_0$, will be taken to be 50 h $kms^{-1} Mpc^{-1}$. In that part of the Thesis which deals with the evolution with time of stellar populations, h will be assumed to equal unity in order to relate redshift and cosmological epoch. The principle reason for choosing this particular value is to ensure consistency of the age of the model universe with the measurements of the age of Galactic globular clusters that are based on the same models of stellar evolution that are extensively used in the Thesis to model the evolution of galaxies.

In the devolpment of the detailed interpretation of the results of this project, the redshifts of extragalactic objects will be assumed to be entirely due to the expansion of the universe, and hence they will be taken to indicate the distance and lookback time to the object. Nevertheless, it should be noted that some of the empirical 'facts' that are derived in the following chapters do not require this assumption. For instance, the validity of the change in colour with redshift that will be demonstrated in Chapter 3 does not depend on the nature of the redshift, only requiring that it is independent of wavelength.

## 1.5 : Layout of the Thesis

The following Chapters describe the results of various investigations carried out by the author in to different aspects of the evolution of the radio galaxies associated with powerful radio sources.

In Chapter 2, spectroscopic observations of nine 3CR radio sources, taken with the Mayall 4 metre telescope at Kitt Peak, are presented and analysed. These yield new redshifts for eight faint 3CR radio source identifications. Several of these new redshifts are for faint radio galaxies at redshifts greater than 0.5.

The next three Chapters contain the results of the main investigation described in the Thesis. In Chapter 3, a large programme of infrared photometry of 81 3CR radio galaxies carried out on the 3.8 metre UKIRT telescope, is described in detail. To all intents and purposes, these 81 radio galaxies form a statistically complete sample and span the redshift range from 0.03 to at least 1.62. Analysis is made of both the colours and magnitudes of these galaxies as a function of their redshift. A comparison with the data of other investigators is made. It is then shown that the colours longward of 7000 A in the rest-frame do not change with redshift over the range studied ($0<z<1.5$), but that those shortward of 4000 A are different at high redshift, indicating enhanced ultraviolet flux densities. The infrared luminosities of the radio galaxies at high redshift are also substantially enhanced if the deceleration parameter has a value less than 1.

Evidence is presented in Chapter 4 that these observed colour changes must be due to changes in the stellar populations of the radio galaxies at different redshifts.

Therefore in Chapter 5 the data on the radio galaxies presented in Chapter 3 is reexamined in the light of models for the evolution of the stellar populations of elliptical galaxies. It is shown that all the data is consistent with the idea that these radio galaxies are basically old systems that formed early in the history of the Universe, but which are undergoing small bursts of star formation as late as the epochs corresponding to a redshift of unity. The relationship of these deductions to those of other investigations is discussed.

In Chapter 6, a similar photometric investigation is described in which infrared observations were made with UKIRT of 39 radio sources selected to have a radio flux density about 5-10 times fainter than the 3CR galaxies studied in the previous Chapters. In this investigation, particular attention is paid to those radio sources which, although unidentified to a faint limiting optical r magnitude of 23.5, were nevertheless detected in the infrared waveband at 2 microns.

In Chapter 7, a different aspect of the evolution of these radio galaxies is investigated. The surface brightness profiles of ten nearby 3CR radio galaxies (at redshifts less than 0.3) are analysed using data obtained with a CCD camera on UKIRT. It is shown that dynamical evolution, in which a massive galaxy consumes its

neighbours, is unlikely to have been an important process in the evolution of these radio galaxies. Some consequences of this are explored.

Finally, in Chapter 8, the results of all these investigations are summarized. Some suggestions for future work based primarily on the imminent introduction of new technology instruments are also presented.

Note to the Reader.

Towards the end of the period during which this Thesis was being composed, two new redshifts of faint 3C galaxies were measured by Dr. Spinrad and kindly communicated by him to the author. These were for 3C 241 and for 3C 65. In some of the discussions presented in this Thesis this new information provides important confirmation of some previously more tentative ideas. In other areas little new information is gained, either because an estimated redshift was sufficient, or because some further spectroscopic information, not yet available, was required. After much thought, it was decided to incorporate the new information onto some of the Figures, and to include discussion of these galaxies into the text where appropriate, where the increase in information was significant. It was not felt that it was justified to redo every analysis that had been carried out, and so in parts of the Thesis, these two galaxies are assumed to have unknown redshifts. However, in these places the possible impact of these new redshifts are discussed in the text.

# Chapter 2 : NEW REDSHIFTS OF EIGHT 3CR RADIO SOURCES

## 2.1 : Introduction

Since the discovery of the recession of nearby galaxies and the formulation of the distance-redshift relation by Hubble, and the interpretation of this in terms of an expanding universe, the measurement of the redshifts of distant objects has been extremely important in all branches of extragalactic astronomy. Redshifts are required for all investigations that seek to relate observations of extragalactic objects to their intrinsic properties.

At low redshift, it is sensible to think of the redshift in terms of the Doppler shift. At higher redshifts however, it is more convenient to think of the redshift in terms of the scale factor of the universe, $R(z)=R(0)/(1+z)$. Knowledge of the redshift of any distant extragalactic object enables one: (a) to determine precisely the wavelengths in the rest frame of the source at which radiation observed through a given passband was emitted; (b) to fix the scale factor of the universe at the time that the radiation was emitted, under the assumption only that the distortion of the Hubble flow caused by random motions with respect to the CMB are negligible; and (c) to determine the distance to the object assuming a geometry ($q_0$) and scaling factor ($H_0$). This distance measurement may then be used to calculate the cosmological epoch at which the radiation was emitted and the intrinsic linear sizes and luminosities ( under the assumption of isotropic emission) of the objects as well as other physical parameters of interest.

In this chapter, spectroscopic observations made with the Mayall 4-metre telescope at Kitt Peak National Observatory (KPNO), are presented and analysed to yield seven secure new redshift determinations for 3CR radio source identifications. These consist of six radio galaxies and one quasar. One more galaxy redshift is more tentative, and for only one galaxy was it not possible to determine a redshift at all.

There are two main motivations for such a study. Firstly the redshifts are required for the detailed interpretation of the photometric data for these galaxies that is now available (e.g. Chapter 3 in this Thesis). Secondly, the redshifts are required to enable a quantitative description of the radio source population and its evolution with cosmic time to be made (e.g. Wall et al.1980, Peacock and Gull 1981) through the population of the (P,z) plane.

The objects associated with the 173 radio sources in the LRL 3CR sample have already been extensively studied spectroscopically for these reasons (see Laing et al.1983 and references therein). Of the 162 secure, and 4 provisional, identifications in the sample, redshifts are known for almost all of the quasars but not for all of the galaxies, and there are still several faint galaxy identifications that do not have a spectroscopically determined redshift. Nevertheless, nearly all the galaxies that are presently known to have redshifts greater than 0.5 are in fact 3CR radio galaxies. There are two reasons for this bias. Firstly the determination of a redshift is made much easier if strong narrow emission lines are present in the spectra as well as the more usual

stellar absorption lines and continuum breaks that are found in all galaxies. Emission lines are found in the majority of powerful radio galaxies (e.g. Hine and Longair 1979) and are associated with the active nucleus. In many cases, the spectra do also exhibit the absorption features expected in the integrated spectra of relatively old stellar populations, but it is unclear in the cases of the faintest radio galaxies whether these would have been sufficient to yield a reliable redshift in the absence of the emission lines. Secondly, the high mean luminosity and the small dispersion in the absolute magnitudes of these radio galaxies (Sandage 1972b and Chapter 3) mean that usually a long integration on a faint radio galaxy is rewarded by a redshift that is considerably greater than the mean redshift of the galaxy population as a whole at that apparent magnitude.

The task of obtaining redshifts for the remaining 3CR identifications for which redshifts have not been measured is challenging since most of them are fainter than 20th magnitude. The work of Spinrad and his collaborators (Smith and Spinrad 1980a, Spinrad et al 1981, Spinrad 1982, and Spinrad private communication) has contributed greatly to the number of galaxies that are known at high redshift, and has illustrated the difficulties involved in working at these faint light levels. Nevertheless, the remaining objects are likely to be some of the most distant galaxies known and their redshift determinations promise further insight in to the evolution of the radio source population and of the parent galaxies and associated galaxy clusters.

All the identified sources in the LRL sample that did not have

redshift measurements in October 1982 in the RA range from 22 hours through to 07 hours were observed, with the exception of 3C469.1. The nine objects so selected include three radio galaxies recently included (Laing et al 1983) in the complete sample (i.e. which were not in the JPR sample) which were somewhat brighter than the others. One object (3C 14) had been classified as a quasar on the basis of its optical appearance (Kristian et al 1974 and Riley et al 1980).

## 2.2 : Techniques

### 2.2.a Observations

The observations were made on the nights of the 13th to 16th October 1982 with the Mayall 4-metre telescope at Kitt Peak. The R.C. Spectrograph was used at Cassegrain focus with the cryogenic CCD camera. The dispersive element in the spectrograph was the grism numbered 770 in the KPNO system. This had 300 lines per mm, providing an undeviated central wavelength of 5970 A and a spectral coverage between 4500 A and 7900 A at a scale of 4.26 A per pixel. A long slit with an aperture of dimensions 2.5 arcsec by 4.45 arcmin was used for all the observations. This resulted in a nominal spectral resolution of 15 A FWHM, and a scale of 0.84 arcsec per pixel along the slit.

The cryogenic camera employs as detector a thinned 800 by 800 pixel Texas Instruments charge-coupled device (CCD) array. The pixel size is 15 microns square, and the readout noise is extremely low, being 8-10 electrons rms per pixel. The optical system illuminates the central 350 by 800 pixels, with the dispersion direction

parallel to the long side. The remaining area of the chip is not illuminated, and hence automatically gives a measure of the dark current signal for each exposure. In addition, a few columns in this unexposed area are read out twice to provide a direct measure of the electronic bias offset level. The CCD chip used was free from column defects over the exposed area and had only a few bad pixels.Two details of the camera affect the data reduction. Firstly, the focal plane of the camera is not absolutely flat. Consequently, the spectra were slightly defocussed at both extremities of the wavelength range. Secondly, ripples introduced onto the surface of this particular chip by the manufacturer during the thinning process resulted in further focus variations across the surface of the chip. These latter variations were not neccessarily perpendicular to the dispersion direction. The apparent width of a given night sky emission line varied across the image. One consequence of this was that it was found to be impossible to eliminate completely some night sky derivative features from the fully reduced spectra. A more complete description of the details of the instrument is given by De Veny (1982).

For the longer integrations, two or more exposures were taken. This was to enable the identification and removal of cosmic ray events and to minimize the effects of atmospheric field rotation and scale-compression between the slit and telescope guide star probe. Between each astronomical exposure, and when moving to a new object, two calibration exposures were taken. One was a flat field calibrator consisting of an exposure of a quartz continuum source viewed through a colour-balancing filter. The purpose of this was to correct for pixel to pixel variations in sensitivity at a given

wavelength across the image. The other was a wavelength calibrating exposure of a He-Ne-Ar arc. It was necessary to repeat this procedure at the start and end of each astronomical exposure in order to guard against flexure in the optical system as the telescope moved over the sky.

Periodically, exposures were taken of one of two standard stars, Hiltner 102 and Hiltner 600. This was to enable the spectra to be calibrated onto a relative energy scale. The small apertures used and the possibly imperfect centering of the very faint objects in the aperture, makes any absolute calibration rather uncertain. However this relative calibration was important in removing the large effects of the atmospheric A and B absorption bands in the far red. Finally, once a night an exposure was taken of the twilight sky. This was in order that the transmission function along the slit could be determined, since there was no guarantee that the quartz continuum source provided a uniform illumination of the slit.

The slit was positioned over the radio source identification using an offset star whose position was accurately known. The small slit width of 2.5 arcsec meant that high precision was required in the relative positions of galaxy and offset star. The COSMOS machine at Edinburgh was used in the Image Analysis Mode to measure the positions of stars within 1 degree of the radio source using the glass copy Palomar Observatory Sky Survey (POSS) plates held by the Plate Library at Edinburgh. A relatively high threshold cut (of 50% or even 125%) was used to minimize the effects of low surface brightness extensions to the stellar images. The positions of bright AGK3 stars were identified on the computer output from the COSMOS

machine, and a coordinate transformation set up using standard STARLINK software. Finally the positions of convenient offset stars were determined from this transformation. These coordinate transformations closed to the order of 0.3-0.4 arcsec on the AGK3 stars, and since the proper motions of the relatively faint stars used as offset stars are likely to be small, this probably represents the accuracy of the offset star positions. The positions of the radio source identifications were taken from Laing et al (1983). Frequently this is the position of the compact radio core of the radio source, which is accurate to 0.1 arcsec. In the other cases the position is that measured by the original identifiers, and this should be accurate to 1 arcsec. When the telescope was positioned it was possible to view the sky through the slit before the dispersive element was introduced. In many cases it was possible to see the radio galaxy on the television display even though it was below the limit of the POSS plates. This gave considerable confidence that most of the light from the galaxy was being utilised in the spectrograph.

2.2.b Data Reduction

Preliminary reductions used the standard software provided by KPNO. This initial process was undertaken by Drs Perryman and Downes in Tucson because the author was required to observe on Mauna Kea immediately after the Kitt Peak run. The reduction of CCD data is conceptually straightforward and is described in more detail in Chapter 7 in connection with another investigation. Batch programmes (Scott et al.1982) perform the bias subtraction and flat-fielding processes. The long-slit analysis package RV (Goad 1982) was then

used with the Interactive Picture Processing System to determine the curvature correction and the wavelength dispersion solution, for each image. These were applied to the data to produce two-dimensional wavelength calibrated images. The remainder of the analysis was performed by the author on the STARLINK Network using both the SPICA spectral reduction package and original software.

The identification and removal of the effects of cosmic rays on the CCD is not easy to automate on two-dimensional spectral data. The background varies greatly over the image because of structure in the night sky spectrum, and in practice even at a given wavelength it can vary a lot if that wavelength is adjacent to that of a bright sky line. Furthermore, it is difficult to construct algorithms to distinguish between narrow emission lines in faint objects and cosmic ray events. When two or more exposures are available they can be compared and a list of candidate cosmic ray events produced which may be then investigated. When only one exposure was available, it was found that the best procedure was to carefully scrutinize the images for sharp features and to remove those that were unambiguously spurious. Some features were not recognised, however, and these do appear on the final spectra.

The two-dimensional wavelength calibrated spectra were reduced to one-dimensional format as follows. The data frames were summed parallel to the dispersion direction to yield an intensity profile across the slit. The columns containing the radio source identification spectra and nearby columns containing sky spectra, uncontaminated by even fainter objects were identified. The object was always extended over several pixels. Because of the effect of

defocussing at both extremities of the wavelength range, the continuum shape of the the spectrum of the object depended on the number of columns which were coadded to produce the spectrum. In view of this, all the spectra, including those of the calibrating Hiltner stars, were extracted from two dimensional data over nine columns, corresponding to 7.5 arcsec on the sky. While this resulted in some degradation in the signal to noise ratio in the central wavelengths, it resulted in a much better relative energy calibration over the whole spectral range.

A composite sky spectrum was subtracted from the extracted object spectrum. This was produced by coadding many nearby 'sky' columns. This subtraction obviously introduces a further source of noise, which can be minimized by using a night sky spectrum produced by coadding as many 'sky' columns as possible, and in any case more than nine. If possible around 40 columns were used. It was found that it was not worth adding more because the defocussing caused by the rippled surface of the CCD resulted in progressively worse sky derivative features as the sky spectrum included columns from further away on the chip. For reference, a typical sky-spectrum is shown in Figure 2.1a. It should be noted that this spectrum has not been flux-calibrated.

The extracted one-dimensional spectra were were then calibrated on to a relative flux per unit frequency interval scale, using the spectra of the standard star Hiltner 600. The calibration for thia star of Stone (1977) was used, interpolated smoothly between his points, but avoiding the known absorption features found in the spectra of white dwarfs. The calibration curve showed both a smooth

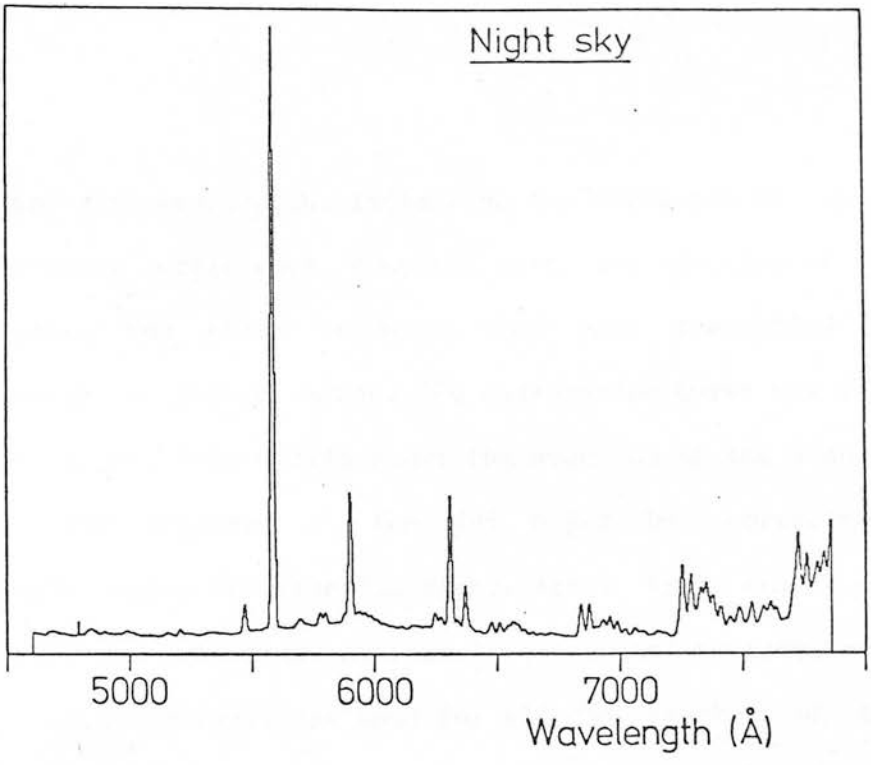


Figure 2.1a: The night sky spectrum. This has not been flux calibrated. The strong lines between 5500 A and 6500 A are O I 5577, Na I 5890-96 and O I 6300-64. Beyond 6700 A the OH bands dominate.

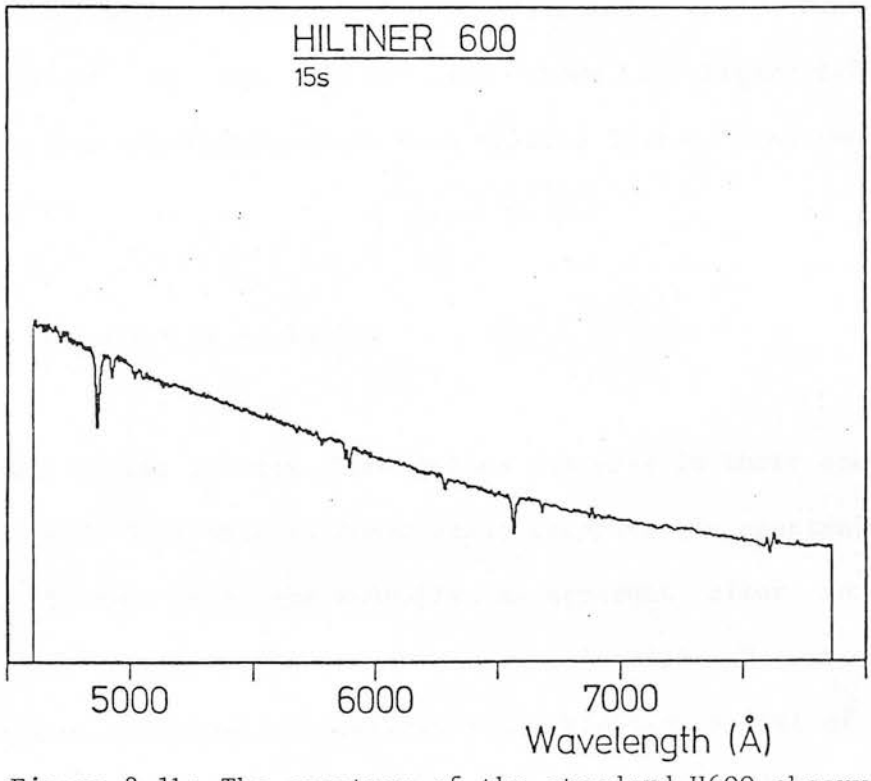


Figure 2.1b: The spectrum of the standard H600 observed on the 3rd night and calibrated using the 2nd night's calibration

variation with wavelength, reflecting the variation of spectrograph and detector efficiency coupled with the spectrum of the quartz calibrator, and sharp features that were identified with the atmospheric A and B bands. The calibration curve was stable from night to night. Figure 2.1b shows the spectrum of the standard star Hiltner 600 observed on the 3rd night but corrected with the calibration curve from the 2nd night. Apart from small derivative features, the resulting spectrum is quite satisfactory, and in fact this calibration curve was used for all the spectra of the radio sources.

Finally, the spectra were smoothed with a gaussian function of standard deviation 4.3 A to enhance the signal to noise ratio. This is of course much less than the instrumental response function. The spectra of all the objects are shown in Figure 2.2a-i. Where appropriate the spectra have been coadded if more than one exposure was taken.

2.2.c Primary Data Analysis

Most of the spectra show obvious features in their spectra. Only 3C172 and 3C65 show no immediately recognisable spectral features. Indeed in most cases the redshift was apparent after an immediate and very crude reduction at the telescope. However, two, more objective, analyses were carried out. Firstly, a list of the most common emission lines found in active galactic nucleii was compiled from the work of Yee and Oke (1978), Costero and Osterbrock (1977), Smith and Spinrad (1980b) and Spinrad (1982). Similarly, a shorter list of elliptical galaxy absorption features was taken from Corwin

Figures 2.2a-c:

The Spectra.

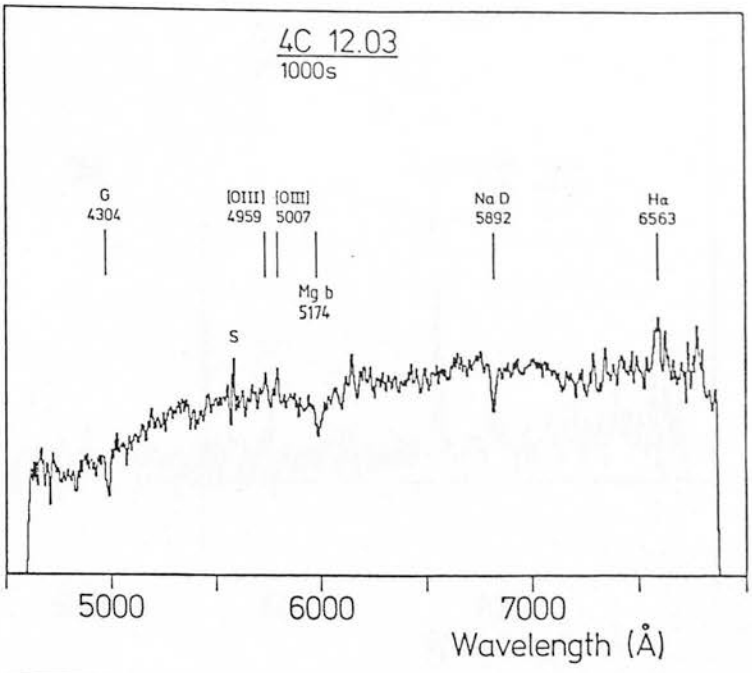


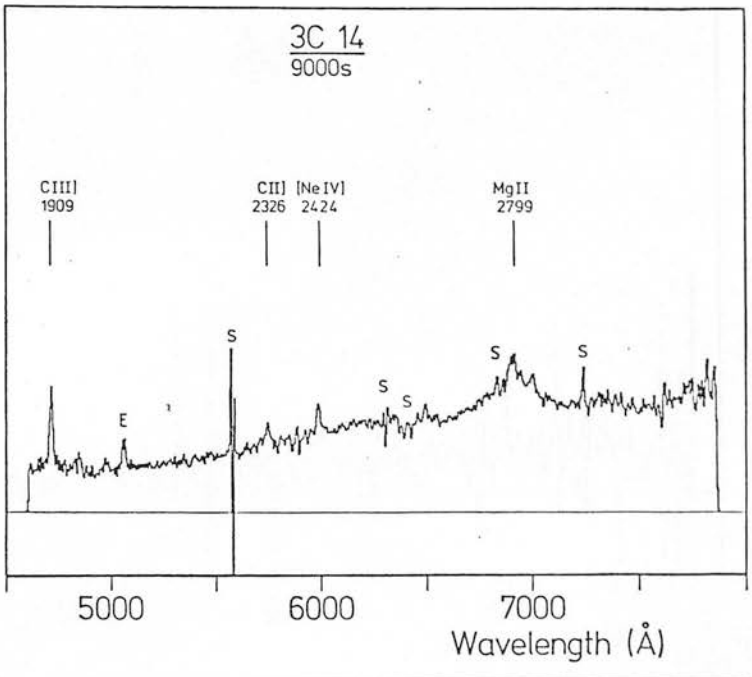


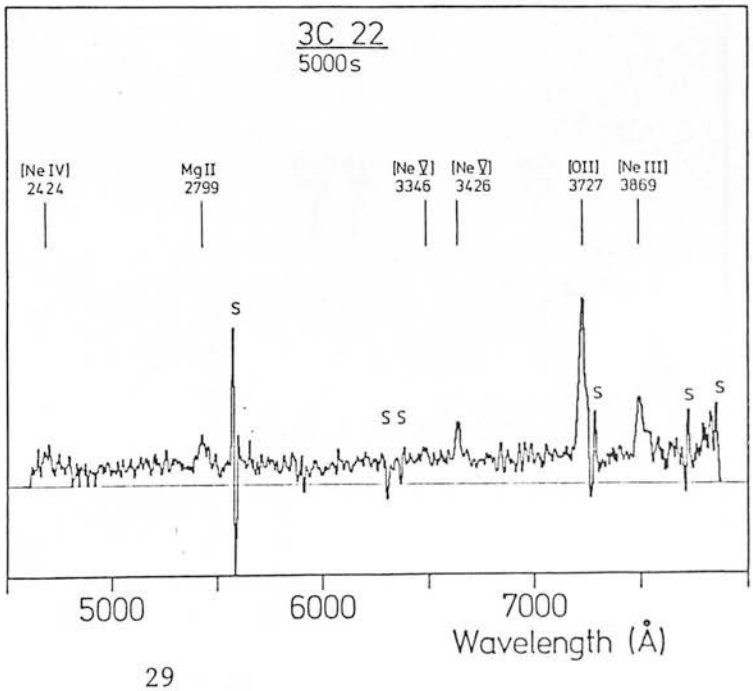

Figures 2.2d-f:

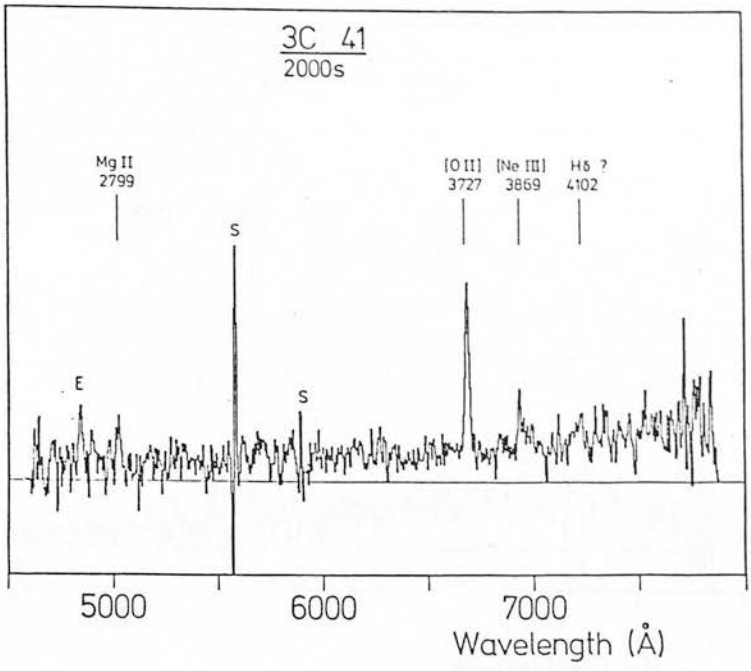


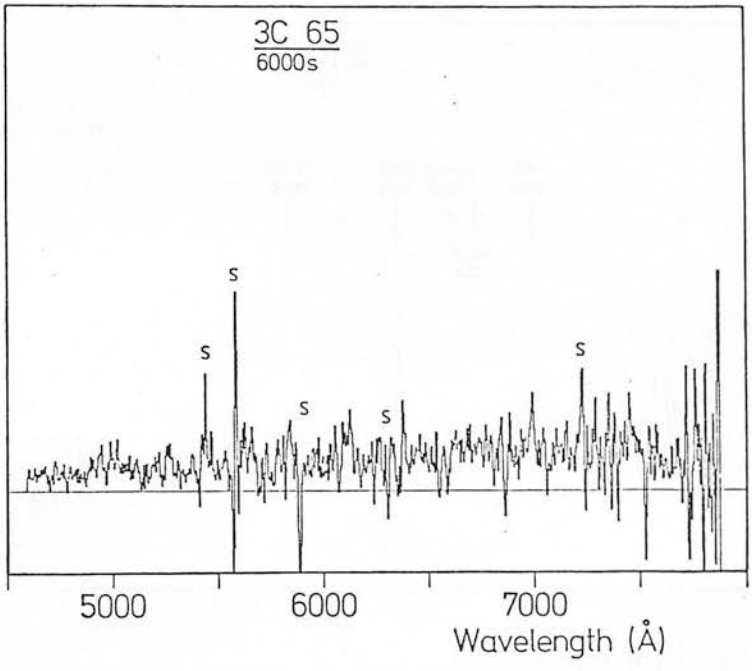


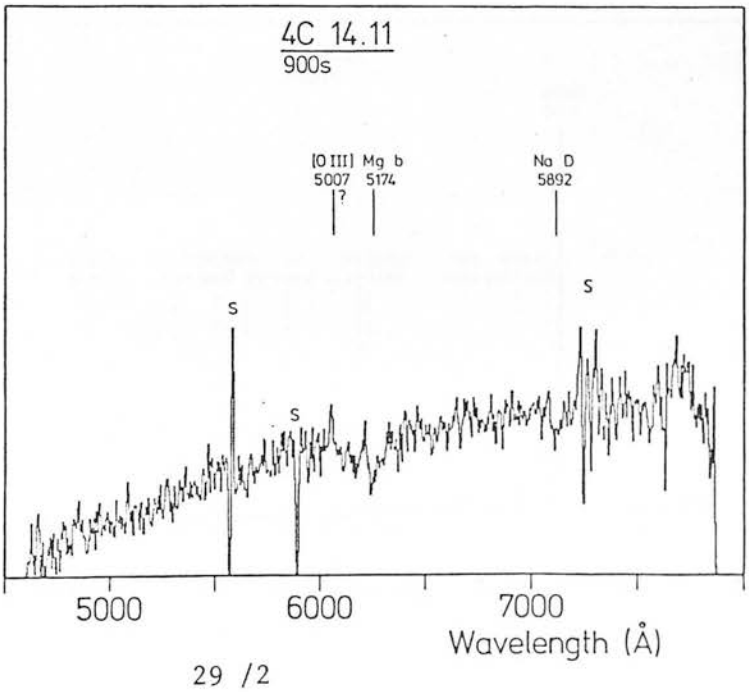

Figures 2.2g-i:

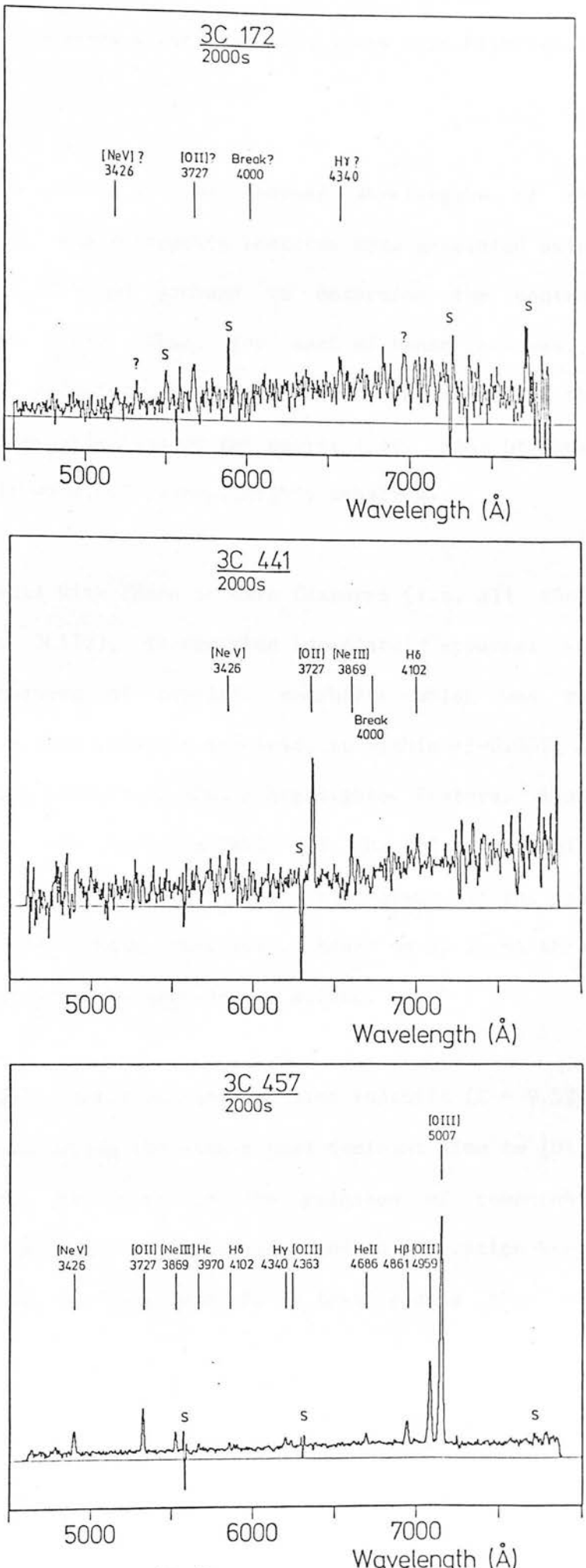

et al (1982). The most common strong emission lines were highlighted in these lists.

For each spectrum lists of the central wavelengths of the non-spurious emission and absorption features were generated using routines in the STARLINK SPICA package to determine the central wavelengths of each line. Then, for each of these features, a sequence of possible redshifts was computed by associating the feature with every possible line on the master list. Many of these 'candidate' redshifts were, of course, highly negative.

For all the objects with three or more features (i.e. all those excluding 3C65 and 3C172), it was then immediately apparent from inspecting these sequences of possible redshifts which was the correct one because this redshift appeared, to within +/-0.002, in each sequence, usually associated with a highlighted feature. These firm identifications are listed in Table 2.1, the columns of which indicate the observed wavelength, observed equivalent width, and derived redshift. All these redshifts, based on at least three clear spectral features can be regarded as secure.

For 3C172, a highly tentative emission line redshift (Z = 0.521) was derived by associating the single most dominant line to [OII] 3727. This line is the strongest in the galaxies of comparable apparent magnitude. Two other emission lines and an absorption break may then be identified, but this redshift is less secure than the remainder.

For those objects in the appropriate redshift range the

Table 2.1: Line Identifications.

| Object | Line | Rest Wavelength (A) | Observed Equivalent Width (A) | Observed Wavelength $\lambda_{obs}$ | Redshift z | |
|---|---|---|---|---|---|---|
| 4C 12.03 | G | 4304 | 6.4 | 4979.9 | 0.1570 | a |
| | [O III] | 4959 | 2.8 | 5732.2 | 0.1559 | |
| | [O III] | 5007 | 3.6 | 5786.4 | 0.1557 | |
| | Mg I b | 5174 | 7.3 | 5988.5 | 0.1574 | a |
| | Na I D | 5892 | 4.3 | 6815.5 | 0.1567 | a |
| | Hα | 6563 | 5.9 | 7583.5 | 0.1555 | |
| 3C 14 | C III] | 1909 | 39.6 | 4709.1 | 1.4668 | |
| | C II] | 2326 | 9.6 | 5740.3 | 1.4679 | |
| | [Ne IV] | 2424 | 8.4 | 5986.9 | 1.4698 | |
| | Mg II | 2799 | 74.9 | 6912.1 | 1.4694 | |
| 3C 22 | [Ne IV] | 2424 | 30.0 | 4694.0 | 0.9364 | |
| | Mg II | 2799 | 70.5 | 5424.3 | 0.9379 | |
| | [Ne V] | 3346 | 15.3 | 6475.0 | 0.9351 | |
| | [Ne V] | 3426 | 44.5 | 6636.7 | 0.9371 | |
| | [O II] | 3727 | 200-230 | 7223.3 | 0.9381 | |
| | [Ne III] | 3869 | < 87.6 | 7496.0 | 0.9375 | |
| 3C 41 | Mg II | 2799 | 67.9 | 5019.9 | 0.7935 | |
| | [O II] | 3727 | 125.9 | 6685.9 | 0.7937 | |
| | [Ne III] | 3869 | 55.5 | 6946.1 | 0.7953 | |
| | Hδ | 4102 | 30.2 | 7212.6 | 0.7600 | ? |
| 3C 65 | None | | | | | |
| 4C 14.11 | [O III] | 5007 | < 8.2 | 6046.1 | 0.2075 | ? |
| | Mg I b | 5174 | 23.6 | 6235.3 | 0.2051 | a |
| | Na I D | 5892 | 6.6 | 7110.8 | 0.2068 | a |
| 3C 172 | Hγ | 4340 | ~20.0 | 6576.7 | 0.5150 | ? |
| | [O II] | 3727 | 63.5 | 5667.3 | 0.5206 | ? |
| | [Ne V] | 3426 | ~25.0 | 5186.9 | 0.5140 | ? |
| 3C 441 | [Ne V] | 3426 | 38.3 | 5842.6 | 0.7053 | |
| | [O II] | 3727 | 95.4 | 6363.1 | 0.7073 | |
| | [Ne III] | 3869 | 31.8 | 6602.6 | 0.7065 | |
| | Hδ | 4102 | 16.0 | 7003.6 | 0.7074 | |
| 3C 457 | [Ne V] | 3426 | 63.7 | 4888.6 | 0.4269 | |
| | [O II] | 3727 | 83.9 | 5318.7 | 0.4271 | |
| | [Ne III] | 3869 | 37.1 | 5521.0 | 0.4270 | |
| | Hε | 3970 | 10.4 | 5663.0 | 0.4264 | |
| | Hδ | 4102 | 9.1 | 5852.0 | 0.4266 | |
| | Hγ | 4340 | 15.5 | 6194.5 | 0.4273 | |
| | [O III] | 4363 | 9.4 | 6229.1 | 0.4277 | |
| | He II | 4686 | 12.1 | 6688.4 | 0.4273 | |
| | Hβ | 4861 | 37.9 | 6937.2 | 0.4271 | |
| | [O III] | 4959 | 133.6 | 7076.1 | 0.4269 | |
| | [O III] | 5007 | 359.6 | 7144.4 | 0.4268 | |

ionisation parameter I (Spinrad 1982), defined as the ratio of [NeV] 3426/[OII] 3727, was calculated. This parameter is particularly useful as both the lines occur close together in the spectrum. For low redshift Narrow Line Radio Galaxies and Seyfert 2 galaxies, I is typically about 0.2 (Spinrad 1982). However, one of Spinrad's interesting results was that many of the high redshift 3CR galaxies that he observed, and particularly those with high [OII] 3727 equivalent widths, have much lower values of I, less than 0.03.

A mean redshift was calculated from the individual redshifts derived for each feature. A correction for the effects of our motion through the galaxy was applied. This was small, the velocity correction being given by $300.\cos(b).\sin(l)$ $kms^{-1}$. Table 2.2 lists these new redshifts and summarises the results of this investigation, as well as giving further observational details. The apparent magnitude in the r passband (from Laing et al 1983) and the integration times are listed, as are the derived, fully corrected redshifts, the spectral coverage in the rest frame of the galaxy and the value of the ionization parameter I.

2.2.d Cross-correlation Analysis

An analysis was also performed in which each spectrum, having had all obvious emission lines and spurious sky-derivative features removed, was cross-correlated with a standard elliptical galaxy template. There were three motivations for such an analysis. Firstly, this technique might produce a redshift for 3C 65 and confirmation of the highly tentative emission line redshift for 3C 172. Secondly, it would provide some idea of the nature of the

Table 2.2: Summary of Observations and Results.

| Object | r | Observing time (sec) | $z_e$ | $z_a$ | Rest wavelength coverage (Å) | I | $z_{pred}$ |
|---|---|---|---|---|---|---|---|
| 4C 12.03* | 17 | 1000 | 0.156 ± 0.001 | 0.157 ± 0.001 | 3900-6850 | - | 0.11 |
| 3C 14 | 20 | 3x3000 | 1.469 ± 0.001 | - | 1850-3200 | - | 1.0 |
| 3C 22 | 20.5 | 2000+3000 | 0.938 ± 0.001 | - | 2300-4100 | 0.18 | 0.60 |
| 3C 41 | 21 | 2000 | 0.795 ± 0.001 | - | 2500-4400 | < 0.08 | 0.78 |
| 3C 65 | 23 | 2x3000 | - | - | - | - | 2.0 |
| 4C 14.11* | 19 | 900 | - | 0.206 ± 0.001 | 3750-6550 | - | 0.38 |
| 3C 172 | 20 | 2000 | 0.520 ** | - | 2950-5200 | ~ 0.3 | 0.52 |
| 3C 441 | 21 | 2000 | 0.708 ± 0.001 | - | 2650-4600 | 0.32 | 0.78 |
| 3C 457* | 19.5 | 2x2000 | 0.428 ± 0.001 | - | 3150-5550 | 0.75 | 0.31 |

* additions to the original 10 Jy sample proposed by Laing et al (1982)
** redshift requiring confirmation

underlying spectral continuum, and indicate whether it was dominated by old stars or by some other component. Finally, it would indicate whether this technique could have been used to determine redshifts of normal galaxies of this apparent magnitude in the absence of emission lines.

The spectra of the radio galaxies were correlated with a template constructed from the optical to red spectrum of a standard elliptical galaxy taken from Pence (1976), extended shortwards of 3400A using the ultraviolet spectra of the bulge of M31 given by Bruzual (1981). Figure 2.3 shows the template spectrum on a flux per unit wavelength interval scale. This template, and each radio galaxy spectrum, was rebinned in intervals of $\delta(\log\lambda)=0.001$. The wavelength range of the template is such that a potential redshift range of -0.2 to +2.7 can be investigated. All obvious emission lines and incompletely subtracted night sky features in the radio galaxy spectra were removed by linear interpolation with the addition of a gaussion noise component of appropriate amplitude.

To avoid the appearance of spurious trends with redshift in the correlation function these binned spectra were further processed in the following way. Firstly, a highly smoothed version of itself was subtracted from each galaxy and template spectrum. This produced a 'features' spectrum, which was then multiplied by a normalising function so that the root mean square (rms) deviation of the features was unity when averaged over a large enough range. This produced two 'normalised features' spectra, one for the radio galaxy and one for the template, $S_i$ and $M_i$. Figure 2.4 shows these two normalised feature spectra for the template and for 4C 12.03, the

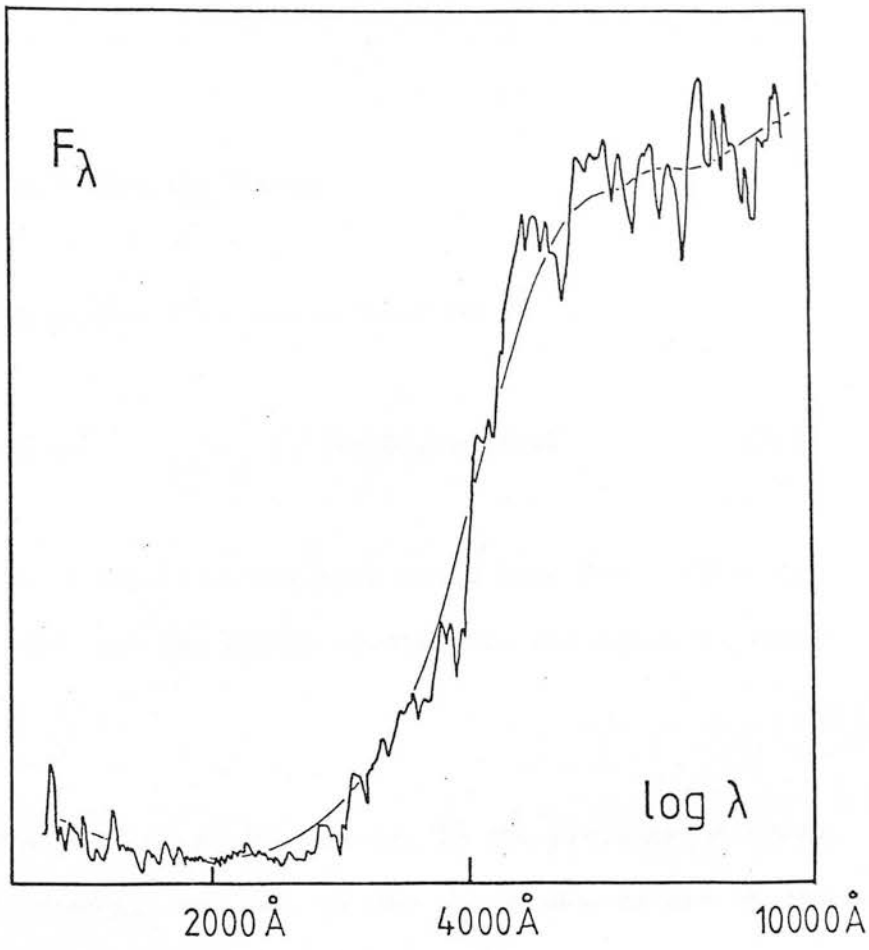


Figure 2.3: The elliptical galaxy template spectrum, used in the correlation analysis, and the smoothed version

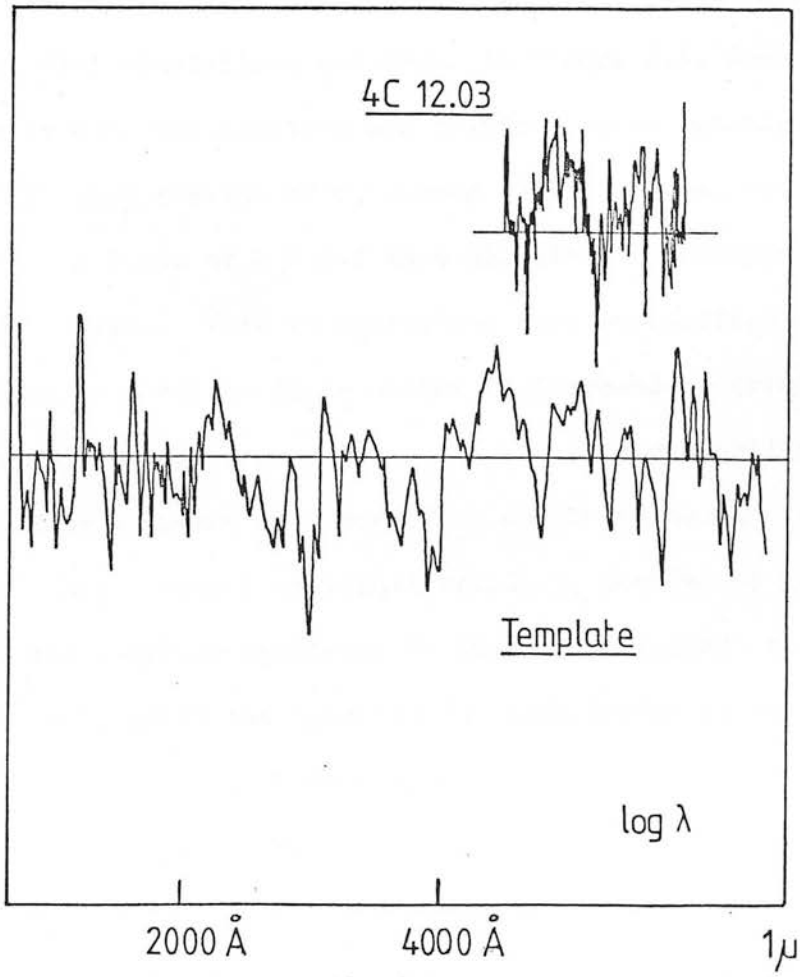


Figure 2.4: The normalised features spectra of the template galaxy and (displaced) of 4C 12.03.

latter being displaced from the former.

A correlation statistic C(z) was defined thus:

$$C(z)=\sum_i M_{i-j}.S_i \quad ; \quad j=1000.\log(1+z) \qquad (2.1)$$

A spectrum that was identical to the mask would have C = 1 since the rms of both the mask and the galaxy spectra are set equal to unity in the mean.

The precise significance of any feature in the presence of noise is difficult to assess, because of the non-random nature of the mask. A series of five simulations correlating a random noise spectrum with the standard galaxy template indicated that no feature arising by chance has $|C| > 0.20$. The C(z) functions that were obtained in these five simulations are shown in Figure 2.5. Such a limit makes sense; if both the spectrum and template were gaussian noise with rms = 1, then the rms of C, summed over 190 bins, would be $(190)^{-\frac{1}{2}}$, or 0.07. A limit of C = 0.2 thus plausibly corresponds to roughly a '3$\sigma$' limit. This is equivalent to a probability of 0.1%. However, there is a fairly large number of independent trials in the whole redshift range from -0.2 to 2.7, so this probability should be multiplied by a number of order 50 or so. This number is smaller than the total number of actual trials j, because of the smoothed nature of the template spectrum. It should be noted that the existence of a 'significant' peak in the correlation function with $|C| > 0.2$ indicates only that there are significant features in the spectrum, i.e. that the spectrum is not a featureless continuum with only noise added. Hence, given one significant feature with

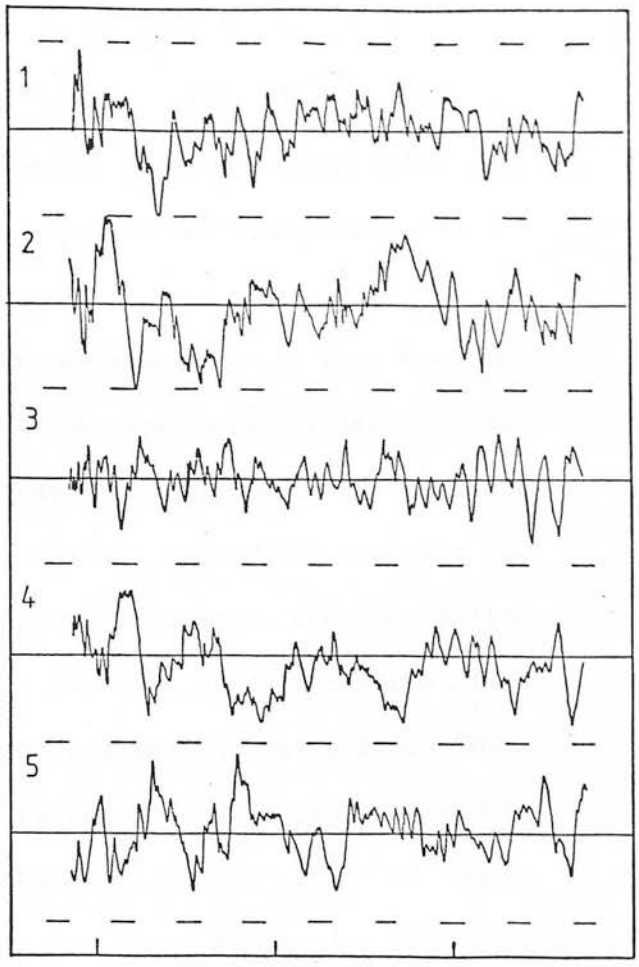


Figure 2.5: The correlation functions that were found during five Monte carlo simulations in which the standard galaxy was cross correlated with a spectrum containing only noise. The dashed lines indicate an amplitude of ± 0.2.

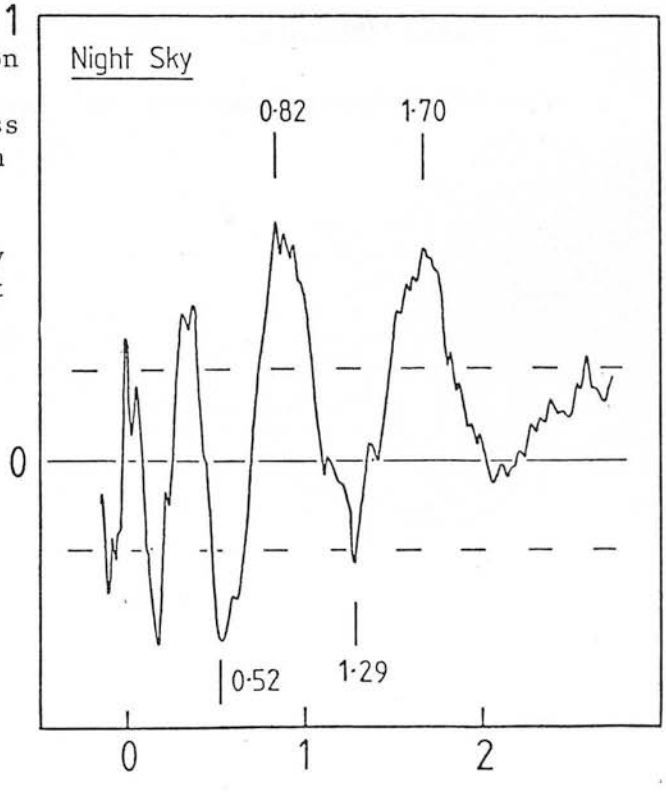


Figure 2.6: The correlation function that is obtained when the template is cross correlated with a spectrum derived from that of the night sky. The strength of the strongest night sky lines were reduced so that they did not completely dominate the normalised features spectrum. The dashed lines again mark an amplitude of ± 0.2.

$C(z) > 0.2$, there will frequently be others with $|C| > 0.2$, at different redshifts with both positive and negative values of C. The most likely redshift is that at which C(z) is maximally positive.

As a final check on possibly spurious results, a sky spectrum was correlated with the mask. This sky spectrum was derived from that in Figure 2.2. The most prominent emission lines were reduced in amplitude, however, so that they did not completely dominate the 'features' spectrum. Significant peaks were found in the correlation function, at redshifts of 0.52, 0.82, 1.29 and 1.70. The correlation function of the sky with the template is shown in Figure 2.6. These 'significant' peaks are entirely expected since the sky spectrum is clearly not featureless. The implication of this is that if peaks are found in the faint galaxy spectra at these particular redshifts then they may conceivably be due to spurious features in the galaxy spectra caused by inadequate subtraction of the night sky.

Figure 2.7a-g shows C(z) for all the radio galaxies except 3C 65. These diagrams are discussed in the next section for each individual object.

Figures 2.7a-c:

The correlation function C(z) for the radio galaxy spectra. In most cases, the emission line redshift is marked.

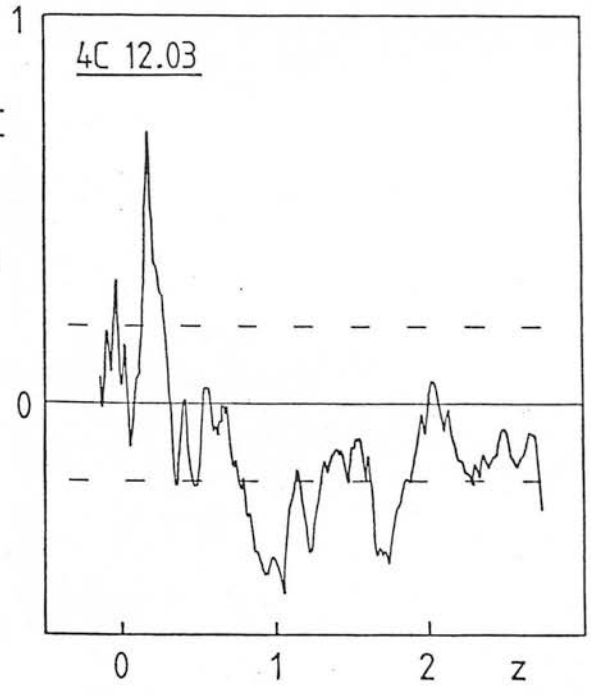


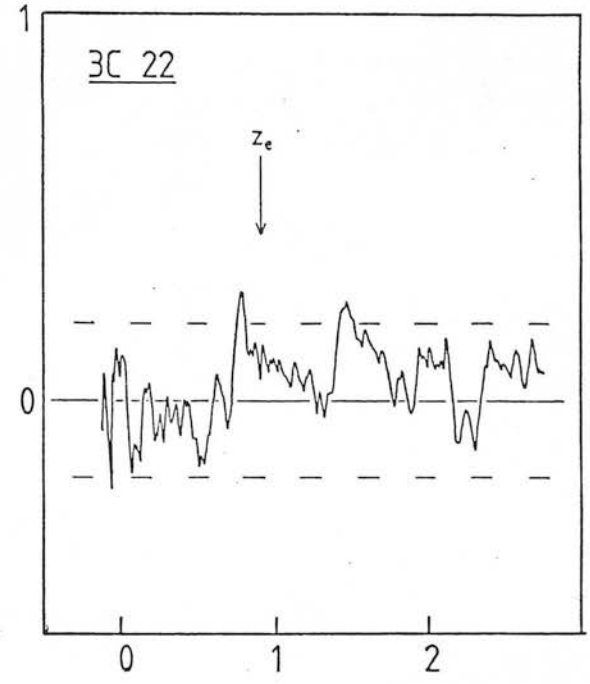


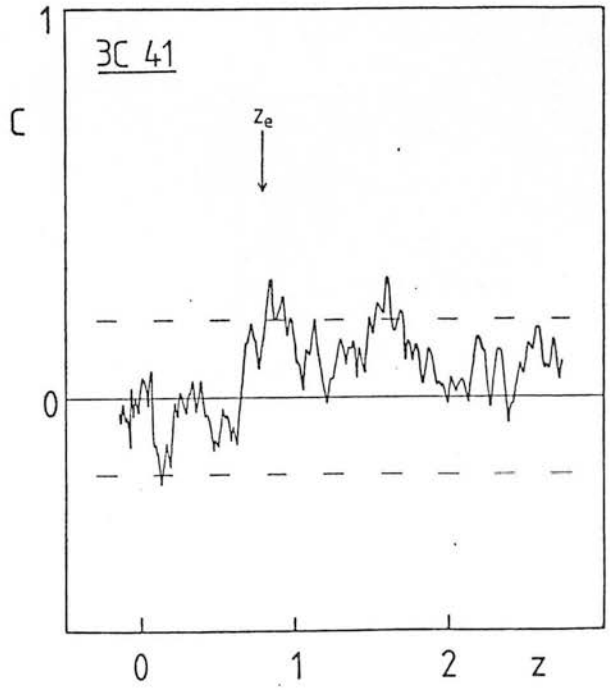

Figures 2.7d-f:

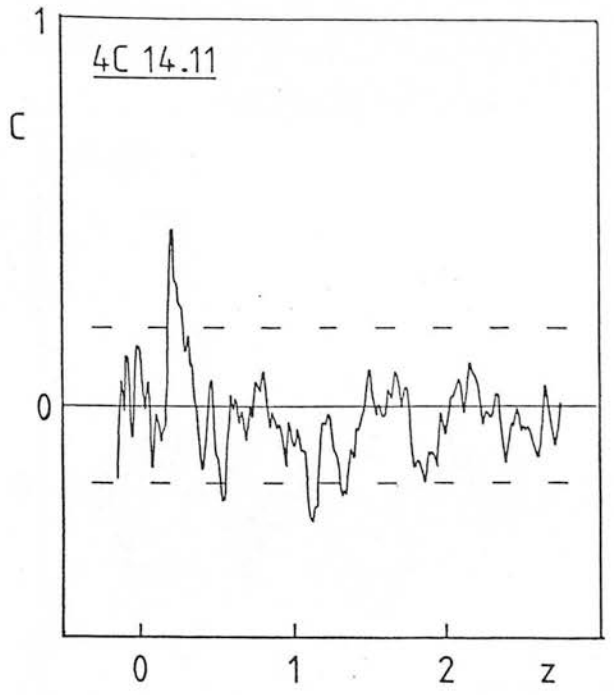


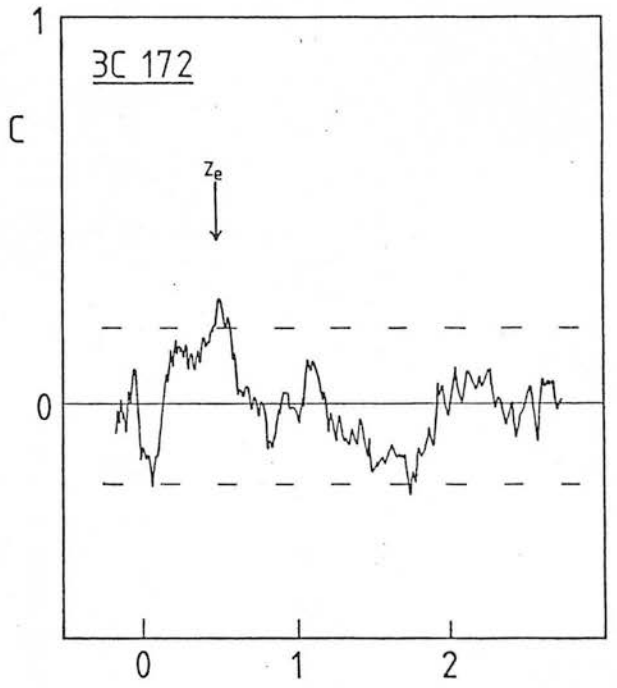


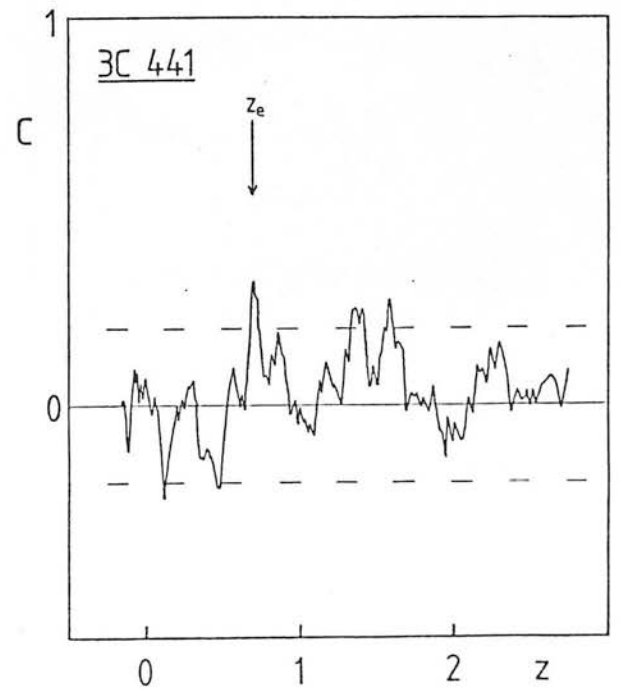

Figure 2.7g:

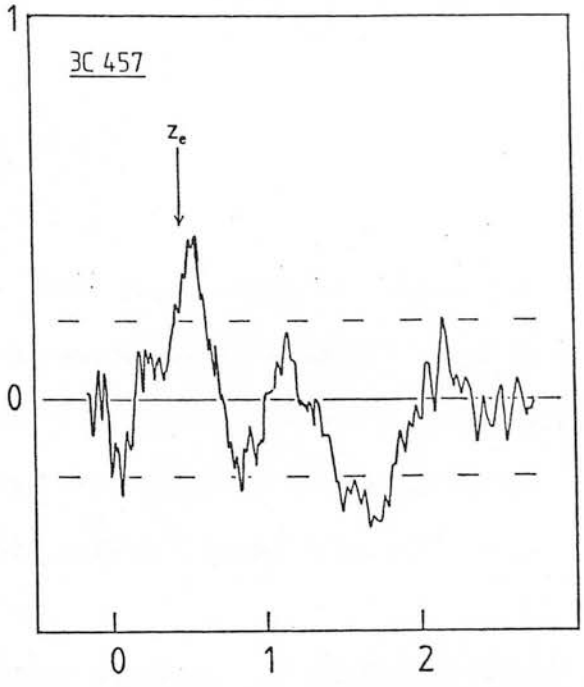


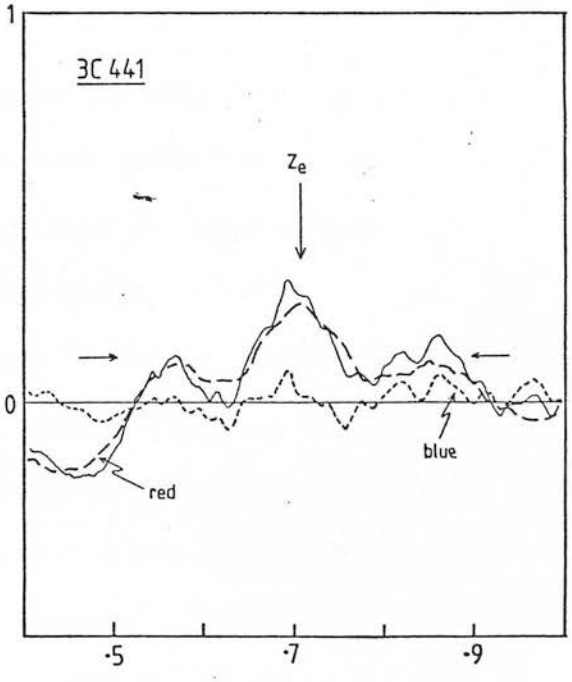


Figure 2.8: C(z) is decomposed into that fro the red and blue halves of the spectrogramme. The peak at the emission line redshift clearly comes only from the long wavelength region. The two small arrows mark the amplitude that corresponds to the 0.2 limit of the other plots.

2.3 : The Spectra

4C 12.03: This bright object has weak emission lines. but the absorption features give an unambiguous redshift of 0.157. The correlation function also gives a highly significant peak at this redshift. It is interesting that this is indeed by far the most significant peak over the whole redshift range from -0.2 to 2.7.

3C 14: Both Kristian et al (1974) and Riley et al (1980) noted the quasi-stellar nature of this identification. The spectrum confirms that this object is a quasar. Its steep continuum (with frequency spectral index 2.4) and the equivalent widths of the emission lines make 3C 14 a typical example of the faint red QSOs studied by Smith and Spinrad (1980b).

3C 22: The redshift of this galaxy is clear from the prominent lines of [NeV] 3426, [OII] 3727, and [NeIII] 3869. The latter two are unfortunately both affected by night sky edges. MgII 2799 is also certainly present on the spectrogram, and from a comparison of the two individual spectra, both [NeIV] 2424 and [NeV] 3346 are likely to be present too. There is clearly a strong ultraviolet continuum in this galaxy. No correlation peak is found at the redshift of the emission lines, although the 4000 A feature has been redshifted out of the spectral range and the reddest third of the spectrum is seriously affected by the emission lines which, although removed, will to a certain degree destroy any features in the underlying continuum. This ultraviolet continuum could be due to either a young stellar population or to a non-thermal component.

3C 41: The emission line redshift, based principally on the strong lines of of [OII] 3727 and [NeIII] 3869, appears to coincide with a peak in the correlation function. The two are displaced by 0.03 however, and the correlation peak could concievably be caused by a sky feature. The high excitation line [NeV] 3426 is weak if present at all, and the ionization parameter I must be correspondingly small.

3C 65: This is the faintest object observed in this programme, with an r magnitude of about 23. Although the continuum is clearly detected, there are no recognisable emission or absorption features. No peak in C(z) was found with an amplitude greater than 0.2, and the least insignificant peaks occured at redshifts that could correspond to sky features. No redshift determination has been possible for this galaxy.

4C 14.11: Although based on only two absorption features and a weak [OIII] 5007 line, this redshift is clearly correct from the correlation analysis.

3C 172: A tentative redshift measurement of 0.52 may be made by identifying the most prominent emission feature with [O II] 3727 (c.f. the other spectra). Other possible weak emission lines at this redshift are [Ne V] 3426 and $H_\gamma$ 4340. The stellar correlation function shows a peak at this redshift, and the 4000 A continuum break feature may be present in the spectrum. However, the correlation peak could concievably be due to inadequately subtracted sky features. This redshift is rather less certain than the others

that have been measured, and needs confirmation.

3C 441: The redshift is based on four emission lines, especially the strong [OII] 3727. A strong peak is found at precisely this redshift in the correlation function. The correlation function can be decomposed to show the contributions of the red and blue halves of the spectrum. Figure 2.8 shows that the positive signal in C(z) at a redshift of 0.70 comes almost entirely from the red end of the spectrum, and indeed the 4000 A feature can be identified in that part of the spectrogram. The small arrows on Figure 2.8 represet the confidence limits in each half of C(z) that correspond to the dashed lines in the other diagrams.

3C 457: This spectrum shows a large number of emission lines on a featureless continuum. The spectrum exhibits lines with a wide range of ionization potentials, and I is very high (0.75). No correlation is found with the template, although the spectrum has been badly cut up in removing the numerous emission lines. The very high ionization ratio suggests that this is probably an ionizing non-thermal continuum.

## 2.4 : Discussion

The success rate in obtaining redshifts for these galaxies was high. Indeed, if 3C 172 is included, the redshift content of the LRL sample in the RA range from 00 hours to 08 hours is now 95% complete. Only two sources (3C 65 and the 'empty field' source 3C 68.2) out of the 53 in this part of the sky do not now have redshift determinations. With this completeness, it is tempting to reanalyse the sample in terms of the classical tests such as the V/Vmax analysis. However, one feature of the new redshifts is the generally rather good agreement that is found with the LRL predicted redshifts. These were based on the apparent optical magnitudes and the optical Hubble diagram for radio galaxies, and are listed in the final column of Table 2.2. This agreement is not very surprising since the new redshifts are in the range where many 3CR galaxies define the Hubble relation well and where, to a large degree, random evolutionary effects on the r magnitude are not very large (Chapter 3). The V/Vmax analysis carried out for the entire 173 source sample by LRL is therefore unlikely to be in error, and is likely to be more useful than a repeat analysis using the much smaller sample of 53 sources that has almost complete redshift information which is available as a consequence of this observing programme.

The high success rate amongst the faint 3CR radio galaxies is almost entirely due to the strong narrow emission lines in the spectra. For the objects at high redshift the correlation analysis proved relatively dissapointing, and it is unlikely that much credence would have been put on the results if the emission lines

were not present. One problem is that the best features, and those that are least sensitive to changes in the stellar population, are found at wavelengths of around 4000 A and longer. Even in 3C 441, in which a correlation peak is clearly seen, the signal for this peak comes from the red half of the spectrum. The ultraviolet spectrum of M31 used at wavelengths shortward of 3400 A may not be appropriate for elliptical galaxies with redshifts greater than 0.5. Whatever the reason, an implication of this fact is that there will be considerable demand for optimum far-red performance in future faint object spectrographs so that features such as the 4000 A break can be seen to as high redshifts as possible.

The origin of the blue continuum in the radio galaxies at high redshift is of considerable interest, and this topic will be discussed throughout this Thesis. It might have a non-thermal origin, but it could also be produced by a young population of massive stars produced by continuing star formation in these presumably elliptical galaxies. Unfortunately, the continua of both of these possible components are expected to be relatively featureless, and over the short wavelength interval covered by the spectrograms both can have essentially power-law form. A test between these two hypotheses is provided however by observations of the location in the galaxy of the source of the excess ultraviolet radiation. A non-thermal component would be concentrated at the nucleus, whereas a young stellar component could be either nuclear or extended throughout the galaxy, depending on the location of the star-forming regions. This test will be examined in greater detail later in the Thesis (see Chapter 4). For the moment, however, one interesting aspect of the results in this chapter and of previous

spectroscopic investigations merits attention in this context. This is the remarkable success of the original identifiers of the radio sources in distinguishing between the spectroscopic classifications of broad line quasar (BLQ) and narrow line radio galaxies (NLRG) on the basis of the optical morphology of the objects on the deep identification plate material. This alone indicates that the rest-frame near uv light of the NLRG is not dominated by a component produced at the nucleus.

## Chapter 3 : INFRARED PHOTOMETRY OF EIGHTY ONE 3C RADIO GALAXIES

### 3.1 : Introduction to Extragalactic Infrared Astronomy

There have been two comprehensive reviews of the state of extragalactic infrared astronomy published in the last five years. These are by Riecke and Lebofsky (1979) and Smith (1983). The first covered the whole period up to 1978, while the second covers the four years up to 1983. It is an indication of the rapid growth of the field that Smith's review contains as much new material as the earlier one by Riecke and Lebofsky. In this introductory section, a brief review of previous research in to related topics is presented in order to set the research described in this Chapter, and in Chapters 5 and 6, in to their historical context.

Both of these two published reviews used a classification scheme for extragalactic objects that places them in to one of three categories: (a) Those whose near-infrared output is dominated by the direct radiation of late-type stars. These include ordinary elliptical galaxies and many spirals too. (b) Those which are dominated by thermal reradiation by dust of energy produced by massive stars associated with obscured star forming regions. In many cases, the luminosity of the infrared continuum radiation is considerably greater than the entire optical luminosity output. These are truly 'infrared galaxies', and this class includes many spirals and irregular galaxies. (c) Those whose ultimate energy source is believed to be non-stellar (i.e. non-thermonuclear) in origin, i.e. the active galactic nuclei (AGN). There are many

manifestations of the AGN phenomenon throughout the electromagnetic spectrum. In the infrared, it is by no means clear generally what the precise radiation mechanisms are, or of their relative importance in the different classes of AGN activity observed. In some cases, there is evidence of direct emmision (e.g. synchrotron radiation) while in others it is more likely that the infrared emission comes from thermally reradiating dust.

The objects studied in this Thesis are the elliptical galaxies associated with powerful radio sources. A priori, it would be expected that they would fall in to either category (a) or (c), depending on the degree of optical or infrared activity in the nucleus, and the following brief review will concentrate on these two categories.

3.1.a Infrared properties of Active Galactic Nuclei.

There has been a huge observational effort directed at the near-infrared properties of active galactic nuclei aimed at understanding the emission processes concerned. The general shapes of the observed continuum infrared energy distributions of each class of AGN (e.g. BL Lac, Quasar, Seyfert 1 and Seyfert 2) have been well established, although there appears to be considerable variation within, and overlapping between, the various classes. Soifer and Neugebauer (1981) have recently reviewed the main results of these programmes, which are outlined in the next few paragraphs.

AGN are generally characterized by an increasing flux density in to the infrared. This 'infrared excess' is certainly not starlight,

whatever the ultimate energy source. At 2 microns, however, there is a wide variation in the relative strengths of the non-stellar component and of the starlight associated with the underlying galaxy. In ascending order of importance of the non-stellar component, the classes of AGN may be ranked as follows; Seyfert 2, Seyfert 1, Quasar, BL Lac. The principal question is the nature of the mechanisms that are responsible for the non-thermal continuum component in the different types of AGN.

In the case of NGC 1068, the archetype Seyfert 2 galaxy, there is considerable evidence that the infrared radiation is produced by thermally reradiating dust. The continuum slope from 1 to 20 microns is steeper than in any source thought to be dominated by non-thermal emission, with a spectral index of 3, and is similar to that found in definitely thermal systems such as galactic HII regions. Crucially the 10 and 20 micron images are significantly resolved (Becklin et al. 1973, Telesco et al. 1980), to a degree expected of a thermal source. There is also no convincing evidence of variability in this source, which is consistent with a dust model.

At the other extreme of activity, the observational evidence on BL Lac objects suggests strongly that they are dominated by non-thermal emission, probably incoherent synchrotron radiation. The high degrees of polarization, and the rapid variability of luminosity, polarised intensity and polarisation position angle that have been observed all argue strongly in favour of a non-thermal origin. The continuum is smooth and continuous from the radio, through the millimetre and submillimetre wavebands, to the infrared and optical, suggesting that a single emission mechanism may be

responsible for the dominant emission over many decades of frequency. There is also some evidence that this emission must be anisotropically emitted.

However, the situation in Seyfert 1 galaxies and quasars is considerably less conclusive, although the optically violently variable (OVV) quasars do share many properties with the 'nonthermal' BL Lacs. Searches for the spectral signatures of dust in the optical and infrared spectra of quasars and Seyfert 1's have generally proved negative when carried out sufficiently carefully (Lee et al 1982). On the other hand, the continuum shapes are generally slightly more complex than are found in OVV quasars and BL Lacs, but certainly do not resemble thermal sources such as the HII regions or NGC 1068.

3.1.b Infrared emission of nearby normal stellar systems

Johnson (1966a) was the first to determine the J, K and L colours of external galaxies. In a small sample, he showed that the nuclei of galaxies exhibited only a small variation of colour with Hubble type, and that a few very late stars (e.g. M10) were required to match the broad band colours. More recent work has consisted of a number of quite large surveys of photometric observations of early-type systems (i.e. globular clusters, elliptical galaxies and the bulges of spirals). This has been both broad and narrow band work, and has confirmed Johnson's early results and greatly extended them. Particularly important has been the work of the group consisting of Aaronson, Cohen, Frogel, Persson and Matthews, who have produced a long series of papers (e.g. Frogel et al 1978,

Persson et al 1979, Frogel et al 1980, Persson et al 1983). Other studies on smaller samples that have been undertaken include those by Strom et al.(1976, 1978), Glass (1976), and Penston (1973).

Although the composite nature of the integrated spectra of elliptical galaxies has been known for many years (e.g. Whitford 1975 and references therein), only fairly recently has it been possible to determine the relative proportions of high and low luminosity stars in the red and infrared wavebands. Johnson (1966) had shown that the near infrared is dominated by stars that are cooler than those which are apparent at optical wavelengths, but was unable to distinguish between giants and dwarfs. The ratio of giants to dwarfs in the infrared is important because it leads to: (a) constraints on the slope of the Initial Mass Function, x , (b) the stellar M/L ratio, and (c) constraints on the luminosity evolution of the elliptical galaxies that are sometimes used as cosmological standard candles.

Frogel et al (1978) presented J, H, and K photometry and measurements of the luminosity sensitive infrared CO index at 2.3 microns (Baldwin et al 1973) in 51 early-type galaxies, and showed that the infrared light from these galaxies was dominated by giants. The inferred M/L ratios are less than about 10, and x is less than or equal to 1. However the form of the giant branch was relatively unconstrained. Aaronson et al (1978a) presented measurements of the $H_2O$ index which is sensitive to the effective temperature of the stars, and showed that the $H_2O$ indices of the galaxies were the same as that of an M5III star, indicating that stars of this type and later must make a significant contribution to the integrated

spectrum. Whitford (1977) had also showed that the giants must dominate at a wavelength of 1 micron by analysing the strength of the Wing-Ford molecular band at 9910 A.

By analysing the positions of M31 globular clusters and elliptical galaxies on the (U-V)/(V-K) plane, and comparing the CO and $H_2O$ indices of the two types of object, Frogel et al.(1980) showed that elliptical galaxies must contain a population of cool luminous stars not present in globular clusters. These stars are something of a mystery. They may be identified with stars on the upper assymptotic giant branch (AGB) that have bolometric luminosities greater than -5.5. The need to include these stars had also been shown by Tinsley and Gunn (1976) and Tinsley (1978) who had used in their models of the giant population of elliptical galaxies a Galactic old disk giant population (ODG). This ODG population contains the upper AGB stars anyway, since they are found in both the disk and bulge of the Galaxy, while the theoretical models of Aaronson et al (1978b) used by Frogel et al (1980), do not. These models do give a good fit to the globular cluster data, however. The evolutionary status of these upper AGB stars is unclear at present. They could either represent a population of stars significantly less old than the remainder, or alternatively they could represent the tail of a very metal rich old population. Recently Frogel (private communication and preprint) has shown that the metal rich globular clusters of the nearby giant elliptical NGC 5128 (Cen A) also appear to contain these upper AGB stars, despite their inferred old age. This tends to support the second hypothesis. Why metal-rich stars should be able to ascend the AGB to a higher level than more metal-poor stars is not yet known, although it is

presumably related to the mass-loss process.

However, the outcome of this large observational effort by Frogel and his collaborators, has been that there is general agreement on the basic constituents of the stellar populations that contribute mostly to the infrared light of globular clusters and elliptical galaxies.

3.1.c Infrared observations of galaxies at higher redshift

The studies described above were all based on observations of galaxies at very low redshift. In the years immediately preceding 1980, when the investigation described in this Chapter was begun, the first infrared observations were being made of more distant galaxies at cosmologically interesting redshifts. Lebofsky (1980) and Grasdalen (1980) both reported preliminary results from programmes to obtain infrared photometry for distant elliptical galaxies.

Lebofsky (1980) had data on six non-radio giant ellipticals, although the most distant ($z=0.95$) was only just detected at a two sigma level. The remainder had redshifts between 0.1 and 0.55. Grasdalen (1980) had data on many galaxies at redshifts smaller than 0.2, on two at redshifts around 0.5 (including the radio galaxy 3C 295) and on two radio galaxies with redshifts around unity. His results were already suggestive of two important effects. Firstly, the two galaxies with redshifts close to 0.5, had (V-K) colours that were between 0.2 and 0.5 magnitudes bluer than was predicted from unevolving K-corrections. Secondly, the galaxies at redshifts

greater than 0.3 appeared to be somewhat brighter than expected in the absence of luminosity evolution, assuming that the deceleration parameter $q_0$ was less than unity.

Both of these investigations were hampered by the very small number of objects that had been observed at that time. The present investigation was therefore undertaken with the principal motivation of extending this kind of study to much larger samples of objects at generally higher redshift and selected in a systematic way from statistically complete samples. To work at the highest redshifts known requires the use of radio galaxies. However, there had been no systematic investigation of the near-infrared properties of this kind of galaxy at low redshift. This neglect of the radio galaxies by observers of other classes of active galactic nuclei is probably due to their relative faintness (due to their rarity) compared with their more common counterparts, the Seyfert 1 and 2 type galaxies. In view of the wide diversity in the infrared properties of other classes of active galactic nuclei described above, it was clearly neccessary also to observe a complete sample of the radio galaxies at low redshifts, if the observations of the most distant galaxies were to be correctly interpreted.

Since then, the preliminary results of this project have been published (Lilly and Longair 1982a,b,c and Lilly 1983). In addition, three other groups have also published accounts and results from similar research. Lebofsky (1981) observed a sample of 34 galaxies, seven of which are at redshift greater than 0.5. Four of the latter, and a few of those at lower redshift are 3C radio galaxies. Puschell et al.(1982) published photometry of 22 3C radio galaxies, most of

which had z>0.5, and 10 other objects. Finally, in a rather different approach, Ellis and Allen (1983) have studied a number of radio-quiet giant elliptical galaxies with redshifts less than 0.5. A detailed comparison of the data, results and interpretations of these other investigations will be made at appropriate points in this Chapter.

3.1.d A complete sample of 90 3CR radio galaxies

The sample of extragalactic 3CR radio sources constructed by Laing et al.(1983, LRL), on the basis of earlier work by Jenkins et al.(1977, JPR) is the basis for the sample used in this investigation. It has been briefly described in Chapter 1 of the Thesis. For the present investigation, the major attractions of this sample are the virtually complete identifications of the optical objects that are associated with the radio sources, and the relatively high percentage of these identifications for which accurate redshifts are available (see Chapter 2). These redshifts allow precise descriptions of the intrinsic properties of the radio galaxies to be made. Even if there is room for discussion as to the correct astrophysical interpretation of the data, the observed behaviour is at least unambiguous. Furthermore, given the limitations imposed by the finite number of galaxies available for observation, the completeness offers, in principle, the ability to delineate precisely the range of behaviour seen at a given redshift with no limitation imposed by additional selection criteria in, for example, apparent magnitude or colour. The whole LRL sample contains a total of 173 radio sources. The sample investigated here is a subsample of this produced by the imposition of three further

selection criteria.

Firstly, all sources with declinations than $+55.0^{\circ}$ are excluded. This is because UKIRT has an absolute declination limit of $+59^{\circ}$ (see Section 3.2.a), and in the region below this limit the telescope enters the 'extended operating region' (EOR) in which there are a few constraints on telescope operation. The principal effect of the declination limit is to reduce the number of sources in the sample to a level which can be observed in a reasonable amount of observing time. Hence, the declination limit is not a serious problem at all, although one or two 'interesting' objects are excluded from the sample in this way. The limit of $55^{\circ}$ is selected to avoid the EOR in addition to the absolute limit.

Secondly, a lower redshift limit of 0.03 is imposed. The principal reason for applying this selection criterion is that the large apparent angular size of the galaxies below this limit has the following two consequences: (a) it is more difficult to determine the sky background level, and (b) The aperture correction neccessary to relate measurements of objects at different redshifts observed through a constant observing aperture is approximately proportional to the logarithm of the redshift. This of course varies rapidly at very low redshift, and the redshift limit therefore limits the total range in log z covered by the sample, and hence reduces the reliance on an accurately known growth curve. The deletion of the sources at very low redshift is also not serious scientifically. In a flux density limited sample such as the 3CR, the limiting logarithmic intrinsic luminosity is also proportional to log z. Hence the very low redshift sources in the 3CR have a much lower radio luminosity

than the bulk of the sample, and there is some evidence (e.g. Chapter 7) that several of their properties are different.

Finally, all sources that are classified as quasars are exluded (i.e. those that are Q or Q* in the notation of LRL). Nearly all of these are now spectroscopically confirmed quasars. Their colours are clearly dominated by the non-stellar radiation associated with their powerful nuclei. About 25% of the LRL sample is excluded by this criterion. This is the least objective of the selection criterion, and in particular is conceivably dependent on the redshift of the object. In fact, it will be found later in this Chapter that it is necessary to exclude from most of the discussion the Broad Line Radio Galaxies, which have broad quasar-like emission lines at generally low redshift, and this in practice then allows for any change in the quasar criterion with redshift.

The selection criteria may be summarized as follows:

1. $S_{178} \geq 10$ Jy
2. $|b| > 10^{\circ}$
3. $+10^{\circ} < \delta < +55^{\circ}$
4. $z > 0.030$
5. Identification not classifed as a quasar.

90 radio galaxies satisfy these criteria. Their apparent V magnitudes range from 14 to at least 24, while the redshifts extend to at least 1.62, and probably beyond. The sample includes three 'empty field' sources which have not been optically identified on even very deep plate material (3Cs 68.2, 437, and 470), and three other sources that have not been identified only to a brighter

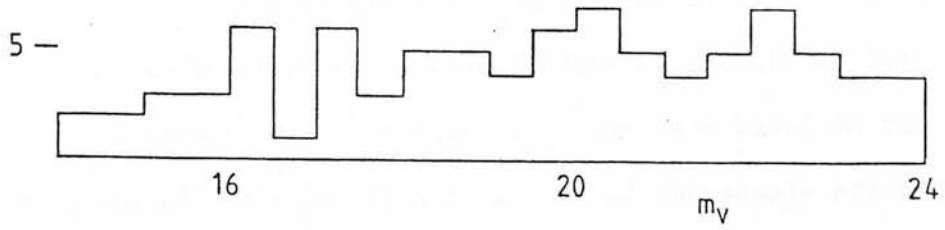


Figure 3.1a: The distribution of apparent optical magnitude of the 90 sources in the statistically complete sub-sample of the 3CR. The three empty field sources have been assigned an apparent magnitude of 23.8.

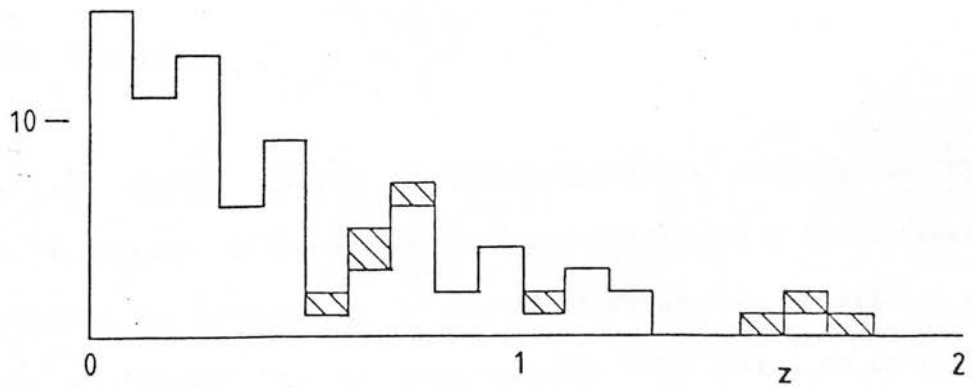


Figure 3.1b: The distribution of redshifts of the 3C radio galaxies that have been identified. Galaxies for which only an estimate of the redshift is available are represented by hatched boxes. About one half of the sample have redshifts greater than 0.4.

limiting magnitude. The field of 3C 294 is obscured by a nearby bright star, while it is only known that 3C 292 and 4C 13.66 are below the limit of the POSS survey plates. They were included in the LRL 'complete' sample only after the deep identification programme had been completed.

The distributions of the redshifts and the approximate apparent V magnitudes of the galaxies in the sample are shown in Figures 3.1a and 3.1b. The hatched boxes in the former indicate redshifts that have not been obtained spectroscopically, but are based on the apparent magnitudes of the identifications. 40% of the sample are at redshifts greater than 0.5 and, to a large degree, these represent the most distant stellar systems presently known.

The members of the sample are listed in Table 3.2 later in the chapter (p. 76).

## 3.2 : UKIRT and observational techniques

### 3.2.a The Telescope

The 3.8m United Kingdom Infrared Telescope (UKIRT) is the largest telescope in the world designed specifically for infrared observations. Its location on the summit of Mauna Kea, Hawaii, at an altitude of 13,800 ft, is particularly well suited to infrared observations because of its low water vapour pressure and general aridity. The telescope is unique amongst large telescopes in the lightweight nature of the design, made possible by the use of an unusually thin primary mirror with a novel support arrangement. A

number of additional features were incorporated in to the design of the telescope to enhance its infrared performance. These include less baffling and a smaller secondary mirror than would be found on conventional optical telescopes. This small secondary acts as an aperture stop to reduce thermal effects. The effective aperture of the telescope is in fact 3.75m.

The telescope is a Serrurier Truss mounted in an English Yoke Equatorial mount. This limits the range of accessible declinations to between $-46^{\circ}$ and $+59^{\circ}$. The small dome size restricts the permissable elevations to greater than 23 degrees above the horizon. A more serious limitation is that the small dome and lightweight structure make the telescope more sensitive to vibration by the wind than most others, although the effects of this can normally be minimized by flexibility in the observing programme. The telescope is completely computer controlled. A DEC PDP11/40 computer is used for this. The telescope can at present be operated in two modes. These are f/9 and f/35 Cassegrain focus. The change requires a complete change of the top end of the telescope.

The basic configuration of the telescope and instrumentation is shown in Figure 3.2 (which is not to scale). Below the primary mirror (B) is the instrument rotator flange (C). All common user instrumentation is mounted on the 'gold dustbin' (D) that can be attached to the instrument rotator. A dichroic mirror (E) reflects the infrared radiation through $90^{\circ}$ in to the sideways looking cryostats (F). Optical light passes through the dichroic, and a TV camera (H) is mounted on an X-Y crosshead (G) that is attached to the base of the gold dustbin. This TV is normally used to guide the

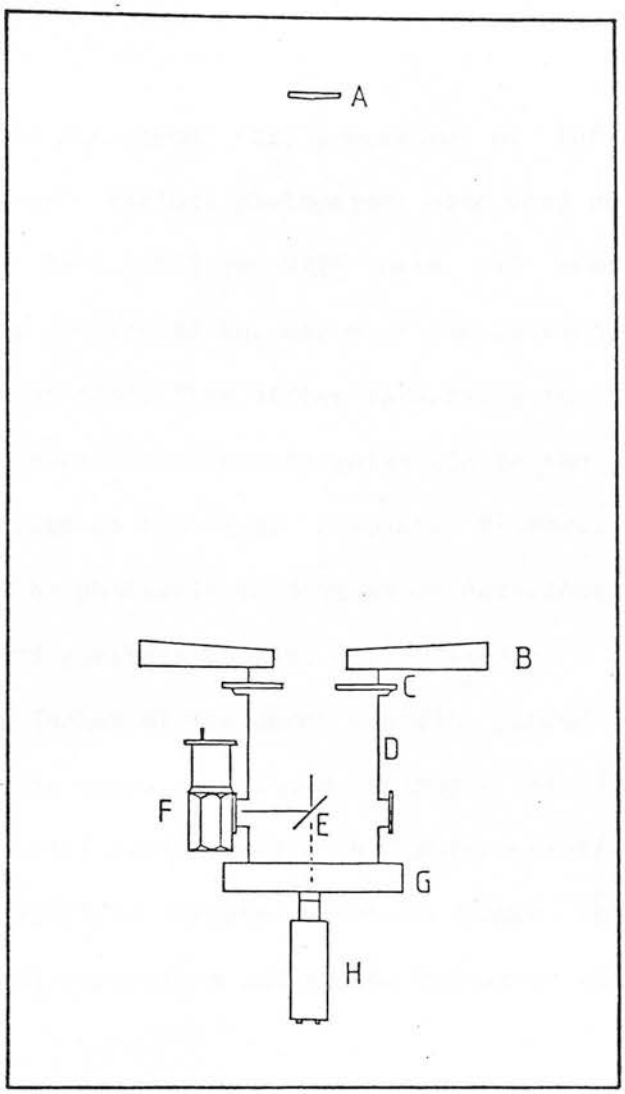


Figure 3.2: A schematic representation of the observing system used on UKIRT. The important components of the telescope are as follows:

A: Secondary mirror which may be used to chop.

B: Lightweight primary mirror.

C: Instrument rotator flange.

D: Instrument support unit (gold dustbin).

E: Dichroic mirror which may be used to chop.

F: Sideways looking cryostat in dewar.

G: Precision x-y crosshead.

H: Acquisition and guiding TV camera on the x-y crosshead.

telescope.

The instrumentation used throughout this programme of infrared observations was 'common user'. Various photometers were used during the project. Those known as UKT1, UKT5 and UKT6 were all used at least once. The first was configured for use with the telescope at f/9, the other two for use at f/35. They differ internally in their Fabry optics, but were essentially indistinguishable to the user, except for the details of some of the less standard filters. All used Indium Antimonide (InSb) photovoltaic devices as detectors. The detector, and the filter and aperture wheels, are located in a dewar cooled to 55 K. The inner jacket of the dewar contains pumped solid Nitrogen, while the outer one contains liquid Nitrogen at 77 K, which it is neccesary to refill periodically. The instrumentation is controlled by another DEC PDP11/40 computer which is linked through CAMAC links both to the instrumentation and to the telescope control computer.

3.2.b Chopping and Nodding

The level of the infrared background is very high. Particularly at wavelengths longer than 3 microns, the background is completely dominated by thermal emission from the atmosphere and from the telescope itself, which are both radiating at 250-300 K. Even at 2.2 microns, the background signal through a 12 arcsec aperture is the same as a 12th magnitude star (whereas a giant elliptical galaxy at a redshift of unity has a magnitude of around 17 at K). In addition, this background can exhibit quite large fluctuations over a short

time interval. These problems have been overcome by the use of techniques known as 'chopping' and 'nodding'. Although these problems are in fact not nearly as severe at wavelengths as short as 2 microns, these techniques are still used for photometry at J, H and K.

Chopping consists of oscillating the focal plane image of the sky over the aperture of the photometer, at a frequency of 5-10 Hz. Ideally the oscillations would have a square wave form; in practice there is a short rise time of between 5 and 10 milliseconds. The signal from the detector is first amplified by a preamplifier at the cryostat, before being sent to the control-room. Here the signal is modulated by a square-wave that is phase locked to a signal from the chopping device. The preamplifier has two different feed-back resistors for use with high and low signals, and the differing impedances mean that the phase of the lock-on amplifier must be adjusted whenever the feed-back resistor is changed. The square-wave modulation has the effect of subtracting the flux from the reference area from that recieved from the object area. The modulated signal, measuring the emission from the source only is displayed on a strip chart pen recorder and sent to the instrument computer via the CAMAC link.

The oscillation of the focal plane image was performed during this programme in one of two ways. In the f/9 configuration, a 'focal-plane' chopper was used, whereas at f/35, the chopping secondary mirror was employed.

The focal-plane chopper was very simple. The dichroic mirror (E

in Figure 3.2) is translated horizontally towards and away from the cryostat. This does not change the location of the optical image viewed by the TV through the dichroic, but the infrared image reflected by the dichroic is moved vertically over the cryostat aperture. One feature of this arrangement is that the infrared radiation received by the detector has always been reflected off the same part of the dichroic mirror throughout the chop cycle. However, although there is some flexibility in the chop size, up to a rather small maximum of 22 arcsec, the direction of the chop can only be changed by rotation of the whole gold dustbin (D) on the instrument rotator (C). Apart from the slight inconvenience of this the main problem is that this also rotates the X-Y crosshead on which the guider TV is mounted. This means that the offsets must be recalculated, which is a hazardous procedure at 14000 ft for a general rotation angle, and this effectively limits the chopping direction to either exactly North-South or East-West.

The chopping system used at f/35 is much more flexible. The secondary mirror is oscillated to move both the optical and the infrared images in the focal plane. The dichroic mirror is fixed and the TV camera sees two oscillating, but effectively superimposed, images of the sky displaced from each other by the chop. The secondary mirror is hydraulically moved, and the direction can be varied at will to any position angle and the chop size has an ample maximum for this work, of about 100 arcsec.

The effect of the chop may be thought of as projecting two circular infrared beams onto the sky. Ideally these would be of uniform illumination, i.e. of constant cross-section, but the

effects of astronomical seeing and of the imperfect optics causes a small rounding of the edges of the beam, and the finite rise time of the chopper mechanisms also degrades the beam particularly in a direction parallel to that of the chopping motion. These two beams will have slightly different ray-paths through the telescope, and will 'see' different areas of the primary mirror. To allow for this and to allow for any other systematic drifts in the system, the technique of nodding is used. This technique also removes the effects of a uniform gradient in the background.

At the end of a period of integration of the modulated signal, a period that may last up to 20 seconds, the whole telescope is moved, either manually or automatically, to place the object in the other beam. The new reference beam is then located on a piece of sky diametrically opposite the previous reference beam position. A new integration is started and run for the same length of time to produce a single 'pair'of integrations. The modulated signal is now of course of opposite sign, and for an object brighter than a K magnitude of about 16, this change will be apparent on the strip chart above the random noise. The difference in the two integrations is equal to the flux recieved from the object, and this number is printed out by the instrument control computer at the end of each pair. Apart from the analogue strip chart recording, this is the smallest bit of data recieved by the astronomer. A new integration is then started, before the telescope is nodded back to the original position for the second integration to complete the next pair.

At the end of each pair, the instrument computer calculates and outputs the running mean, associated instrumental magnitude, and the

standard deviations of the integrated signals derived from all the previous pairs. Provided that there are several pairs, this uncertainty estimate is therefore the minimum statistical uncertainty in the data. The total number of pairs taken in a given observation varied, depending on the brightness of the object. For some of the faintest sources 128 pairs of two integrations of 15 seconds each were taken. A conscious effort was made to stop the observation after a predetermined number of pairs in order not to be influenced by the fluctuations in the computed uncertainty. The decision as to how long to integrate for was made as soon as it became clear approximately how bright the object was. These fluctuations in the computed signal to noise ratio are to a large degree caused by fluctuations in the mean integrated signal rather than in the standard deviation, and hence stopping the integration when a certain formal uncertainty in the measurement has been attained not only leads to a spuriously low estimate of the true uncertainty, but will also systematically bias the measurement to higher flux densities.

### 3.2.c Telescope Guidance

Most of the galaxies observed in this programme are too faint to be seen on the TV even when using the maximum available memory integration. Precise offset guiding was therefore used. The X-Y crosshead, to which the TV guider is attached, has a range of travel that corresponds to +/- 13 arcmin at f/9 and +/- 4 arcmin at f/35. The TV itself has a field of view of about 1 arcmin in both configurations. Unfortunately the area of sky available for guide stars is too small to include, in more than a few cases, AGK3 stars

and for nearly all the fields it was neccessary to measure accurate positions for the guide stars.

Except for those fields that were prepared for spectroscopic investigation (see Chapter 2), and for which the COSMOS machine was used, these positions were measured manually using the Packman x-y measuring table at Edinburgh. This machine digitizes to 10 microns, which corresponds to 0.7 arcseconds on POSS scale plates. Glass copy POSS plates were used for this work, and the positions on these of the dozen or so AGK3 stars that were nearest to the position of the radio source were measured. Standard STARLINK software was used to set up a six parameter coordinate transformation. Under this transformation, the AGK3 stars closed to about 0.7 arcseconds. Proper motions of the generally faint offset stars should be small over the thirty years that have elapsed since the POSS plates were taken, and the accuracy of their positions should also be slightly better than 1 arcsec. If the radio galaxy was bright enough to be seen on the POSS plates, then its position too was measured. For the remainder, it was often possible to use the accurate (0.1) arcsec position of the radio central core if that had been detected. Otherwise it was neccessary to rely on the positions given by the original identifiers of the radio galaxies. The uncertainties in these latter positions may conceivably be as high as 1-2 arcsec in some cases.

The procedure for setting up the telescope on a faint galaxy was as follows: The telescope was first slewed to the position of a bright star near to the radio galaxy position. This was sometimes the guide star itself and sometimes the nearest AGK3 star. It had to

be bright enough to have a strong signal on the strip chart. The optical datum point (zero offset) was then aligned with the centre of the infrared beam by locating the half-power points of the beam. The telescope was then driven to the position of the radio galaxy and simultaneously, the X-Y crosshead was motored to the appropriate position. A small correction must be applied to the offset if the telescope moves out from under the dichroic mirror to compensate for the refraction in the optical beam introduced by the dichroic mirror. The telescope was then guided, either manually or later automatically, on the image of the offset star on the TV. This is a rather more direct way of offset guiding than normally practised on other telescopes that have a better absolute pointing and tracking performance. It should be very accurate. The only concern is possible flexure in either the TV mounting or in the cryostat as the telescope moves over the sky, particularly if the meridian is transitted during an observation. Where possible, long integrations through the zenith were avoided. When they were undertaken, a careful check of the alignment was made at the end of the integration, but no observations needed to be rejected for this reason.

### 3.2.d The choice of aperture size

There are as yet no sensitive array detectors available for use in the infrared, although these should become available on UKIRT in 1984. The photometry described here had to be single-element aperture photometry, and the choice of the size of aperture required some consideration.

Smaller apertures are generally more sensitive. Particularly at K, the dominant source of noise in the photometric measurements of faint objects is the photon statistics of the background produced by the sky and by telescope itself. The noise from the background scales as the diameter of the aperture, and for an unresolved faint object, the sensitivity of the system will vary accordingly. The limiting magnitude at K is indeed about 0.3 magnitudes fainter through an 8 arcsec aperture than through a 12 arcsec aperture. The savings in observing time to reach a given signal to noise ratio on a faint object are therefore quite substantial. At J, and to a lesser extent H, the noise from the instrument itself is more important. This is not a function of aperture, and hence the sensitivity gains are somewhat smaller in these passbands. For extended sources such as nearby galaxies, the apparent decrease in sensitivity with the larger apertures is to a certain degree reduced by the inclusion of more light from the galaxy.

The other major advantage of the smaller aperture is that both the 'object' aperture and the two reference 'sky' apertures are less likely to contain other sources. As will be discussed further in Chapter 6 (Section 6.1.c(i)), almost all objects that will contaminate the infrared measurements will be visible on the deep plate material that is available for all of these radio galaxy fields (since elliptical galaxies at high redshift are amongst the reddest objects in the sky). Particularly with the flexibility of the f/35 chopping system, it is nearly always possible to locate the reference beams on 'empty' sky. The possible contamination of the measuring beam itself is potentially more serious, however, since that cannot be moved, for obvious reasons.

The principal advantage of the larger aperture (12 arcsec) is the increased tolerance that it provides to positional errors. Because almost all the radio galaxies are too faint to be seen on the TV system, the offsetting was completely blind. Possible sources of positional error in the centering of the measuring aperture over the galaxy are as follows: (a) The offsets calculated from the relative positions of object and guide star. Although these were normally accurate to 1 arcsec, the worst cases could conceivably be up to 2 arcsec in error, and (b) flexure in the offset system itself. Although usually negligible, it is known that this was occasionally as large as 1 arcsec. Since the beam was always slightly rounded, and since windshake could in addition sometimes oscillate the telescope with an amplitude of about 1 arcsec, it is clear that the most reliable (i.e. repeatable) measurements would be made through the large (6 arcsec radius) aperture rather than the smaller one (4 arcsec radius), especially as even the most distant galaxies are extended over 2 or 3 arcsec.

Therefore, the philosophy adopted was to use, wherever possible, the larger beam, except in those cases where this would have led to the inclusion of contaminating objects in the primary 'object' beam. Great care was taken to ensure that no stars were included. Very faint galaxies (i.e. those significantly fainter than the radio galaxy) were not so serious, as these are almost certainly cluster galaxies at the same redshift as the radio galaxy and in most cases these will be intimately associated with the radio galaxy.

3.2.e Calibration and infrared photometric systems

Unfortunately the photometric system in use at UKIRT does not at present have a set of well defined standard stars for calibration, although this is presently being remedied. The largest list of faint infrared standards is that from Caltech (e.g. Elias et al 1982) which defines the 'CTIO' system. This is a different system from that used at UKIRT, and colour equations exist between the two systems. The colour equation is important because elliptical galaxies at moderate to high redshift have infrared colours that are much redder than those of the standard stars that are available, having both (J-H) and (H-K) around unity. In view of the large amount of work on extragalactic stellar populations carried out on the Caltech system, all of the photometry of the radio galaxies taken on UKIRT have been transformed onto this system.

From careful work in ideal observing conditions, the following colour equations have been found by Dr. Williams at UKIRT, and have been kindly communicated to the author by him.

$$(H-K)_U = (H-K)_{CTIO} \qquad (3.1)$$

$$(J-K)_U = 1.09\,(J-K)_{CTIO} \qquad (3.2)$$

During the observing sessions for the current investigation, observations were regularly made of standard stars selected from the

list of Caltech standards (Elias et al 1982) throughout the periods when data was being taken. The instrumental calibration derived from these observations was extremely stable, and the small drifts that were present on the records of some nights' observations could usually be attributed to small changes in the atmospheric conditions. On the few occasions when observations of the standards indicated that the conditions were not photometric to the 3% level, no long integrations were taken, and the brighter galaxies were observed in a cyclical fashion K-J-H-K. The whole cycle was rejected if the two K measurements differed by more than the statistical uncertainties of each measurement.

All the data taken on each run were reduced onto the UKIRT system referenced to a single primary standard that was observed many times on each night of the run. The other standards observed were basically used to monitor the conditions. The data was then transformed onto the CTIO system using the colour equations, and the colours of the primary standard.

However, because the corrections applied to the photometry are based upon extrapolations of the colour equations well beyond the colour range covered by the standards, since the high redshift galaxies are redder by virtue of the redshift than almost any star, systematic errors may be introduced in to the colours of the reddest galaxies in the sample. These should be at the 2% level at most, and this in practice is not a serious problem, not least because the high redshift colours are principally compared to synthetic colours computed from the assumed Spectral Energy Distribution which are also uncertain at this level.

3.2.f Further corrections to the photometry

Up to four corrections were applied to the photometry of each radio galaxy. These were all fairly small, however, being on the level of a few percent in each case.

The first was to eliminate the effects of atmospheric extinction. This is low in the infrared on a good site such as Mauna Kea, and the effects were minimized by observing objects only when they were relatively close to the zenith. This was facilitated by the 'survey' nature of the project, and only towards the end of the sequence of observing sessions did it become neccessary to work at airmasses greater than 1.25, i.e. at more than 35° from the zenith. The normal extinction corrections at Mauna Kea are 0.05 per airmass for H and K, and 0.08 per airmass for J. The corrections to the photometry should be very small therefore, and rather than derive possibly uncertain corrections from the observations of the standard stars, the radio galaxy photometry was corrected using the nominal figures given above, while the general atmospheric conditions were monitored by frequent observations of standard stars located fairly close to the programme objects. The airmass correction was rarely greater than 0.02 magnitudes.

The second correction that was applied was to correct for the galactic extinction produced by dust near to the plane of the Galaxy. The worst effects of this were avoided since the sample of radio galaxies is selected to have $|b|$ greater than $10^{\circ}$, and the corrections in the infrared were typically a few percent or less.

Corrections were applied to all the photometry on the basis of the E(B-V) maps given by Burstein and Heiles (1982). These are based upon column density measurements of HI. The accuracy of the method is believed (Burstein and Heiles 1982) to be 0.01 magnitudes in E(B-V) or 10% of the reddening, whichever is greater. The positions of all 3CR galaxies were computed in galactic coordinates, and the reddening in each direction read from the maps. The absorption in B, V, R, J, H, and K was assumed to be 4.0, 3.0, 2.15, 0.78, 0.48, and 0.3 times E(B-V) respectively. The corrections in the infrared are generally small, but galactic extinction can have a large effect on the optical-infrared colours such as (V-K), since E(V-K) is 2.7 times E(B-V). The reddenings derived from the HI maps are generally similar to the well-known polar-cap model of Sandage (1973), except for the region around $l=180^{\circ}$, $b=-10^{\circ}$, where the extinction is considerably higher than produced by the Sandage formulation. 3C 123 is in this area, and the correction for this galaxy ($A_V=1.5$) is rather uncertain because of the high reddening gradients in this area.

The other two corrections applied to some of the data were required by instrumental effects. They were applied only to the data obtained at f/9. The beam profiles were significantly poorer in this configuration than at f/35, and this required a correction to be applied so that the flux densities referred to those which would be measured through an aperture of the quoted size with a uniform illumination. Furthermore the small chop displacement used resulted in some contamination of the reference beam from the outer regions of the galaxies with largest apparent size on the sky. Both these corrections are functions of redshift. Their size was computed from

the growth curve for giant elliptical galaxies given by Sandage (1972a). It will be shown in Chapter 7 that this is a good representation also of radio galaxies. These two corrections were both less than 0.04 magnitudes for even the worst affected galaxies.

## 3.3 : Data

### 3.3.a Observations

Infrared photometry of these radio galaxies was taken during 6 observing runs on UKIRT between September 1980 and November 1983. The dates of these are listed in Table 3.1, with the telescope configuration. The author was present for all the observing runs except the first which was exploratory in nature. Subsequently, all but one of the ten observations made at this time were repeated on later runs.

During these observing sessions, 81 of the 90 galaxies in the complete sample were observed. The other 9 were omitted for one of three reasons. Firstly, a number of the galaxies were so close to stars that it would not have been possible to obtain a meaningful magnitude for the galaxy alone with the size of apertures used. The sources so affected were 3Cs 132, 153 and 247. Secondly, observations were not made of the unidentified sources that did not have deep optical plate material available. This lack made it impossible to have confidence that the observations would not be contaminated by other objects. These sources are 3Cs 292 and 294, and 4C 13.66. Finally, three galaxies (3Cs 263.1, 266 and 340) were not observed because, unfortunately, the guide star data taken to

Table 3.1: Observing runs on UKIRT.

| | | |
|---|---|---|
| 1. | 12th - 15th September 1980 * | f/9 |
| 2. | 6th - 11th March 1981 | f/9 |
| 3. | 19th - 24th November 1981 | f/35 |
| 4. | 18th - 22nd October 1982 | f/35 |
| 5. | 11th - 18th March 1983 † | f/35 |
| 6. | 3rd - 6th November 1983 † | f/35 |

Notes: * The author was not present.

† The run was not wholly dedicated to the programme described in this Chapter.

the telescope was inadequate. The problem was that the dichroic mirror is supported by four relatively thick supports which obscure the view of the TV below for certain offsets of the X-Y cross-head. For these three sources, all the measured offset stars (two or three in each case) were so obscured.

The first reason will discriminate against fainter galaxies, because the stellar surface density increases fairly rapidly with increasing depth. The second will also bias against faint sources below the POSS. The final effect however is completely random. However, none of the exclusions should be related to either the colours or the absolute magnitudes of the galaxies, and especially since almost 90% of the sample has been observed, the impact of these omissions on the results and conclusions of this work should be negligible.

The fully corrected data for the 3CR galaxies is listed in Table 3.2.

In addition to the 81 3CR radio galaxies, four nearby NGC giant elliptical galaxies were also observed during November 1981. The purpose of this was to ensure consistency between the measurements of the radio galaxies and the large amount of data on bright elliptical galaxies presented by Frogel et al (1978, FPAM). These four ellipticals were selected from those observed by FPAM and were NGCs 1600, 1700, 2672 and 3158. Data for these galaxies are listed in Table 3.3.

Finally, during the last observing period, in March 1983, a

Table 3.2: Infrared Photometry of 3C Radio Galaxies.

| 3C | z | d | K | | H | | J | | |
|---|---|---|---|---|---|---|---|---|---|
| 4C12.03 | 0.157 | 12 | 13.41 | 0.03 | 13.92 | 0.02 | 14.54 | 0.03 | Oct 82 |
| 13 | 0.477 | 12.3 | 16.36 | 0.10 | 17.00 | 0.12 | 17.83 | 0.17 | Nov 81 |
| 16 | 0.405 | 12.3 | 15.91 | 0.07 | 16.86 | 0.12 | - | - | Nov 81 |
| 19 | 0.482 | 12.3 | 15.55 | 0.05 | 16.50 | 0.09 | 17.08 | 0.09 | Nov 81 |
| 20 | 0.350 | 12 | 14.30 | 0.04 | 14.93 | 0.06 | - | - | Oct 82 |
| 22 | 0.936 | 7.8 | 15.67 | 0.10 | 16.88 | 0.14 | 17.30 | 0.14 | Oct 82 |
| 28 | 0.195 | 12 | 13.77 | 0.02 | 14.39 | 0.02 | 14.91 | 0.04 | Oct 82 |
| 33 | 0.060 | 12.3 | 12.35 | 0.01 | 12.85 | 0.01 | 13.48 | 0.02 | Nov 81 |
| 34 | 0.690 | 10.8 | 16.02 | 0.07 | 16.80 | 0.09 | 17.53 | 0.20 | Sep 80 |
| 35 | 0.067 | 12.3 | 12.45 | 0.03 | 12.85 | 0.03 | 13.51 | 0.02 | Nov 81 |
| 41 | 0.793 | 7.8 | 15.95 | 0.10 | 16.87 | 0.10 | 18.02 | 0.24 | Oct 82 |
| 42 | 0.395 | 12 | 15.12 | 0.06 | 15.85 | 0.06 | - | - | Oct 82 |
| 46 | 0.437 | 12 | 15.05 | 0.06 | 15.60 | 0.06 | - | - | Oct 82 |
| 49 | 0.621 | 7.8 | 16.68 | 0.06 | 17.65 | 0.20 | - | - | Oct 82 |
| 55 | 0.240 | 12 | 16.42 | 0.05 | 17.57 | 0.26 | - | - | Nov 83 |
| 65 | - | 7.8 | 16.78 | 0.20 | 18.03 | 0.32 | - | - | Oct 82 |
| 67 | 0.310 | 7.8 | 15.25 | 0.07 | 16.06 | 0.08 | 16.92 | 0.12 | Oct 82 |
| 68.2 | - | 7.4 | 17.73 | 0.20 | - | - | - | - | Nov 83 |
| 76.1 | 0.032 | 12 | 12.07 | 0.02 | 12.25 | 0.01 | 13.00 | 0.01 | Oct 82 |
| 79 | 0.256 | 7.8 | 14.43 | 0.04 | 15.28 | 0.07 | 15.88 | 0.08 | Oct 82 |
| 98 | 0.031 | 12.3 | 11.90 | 0.02 | 12.01 | 0.02 | 12.74 | 0.01 | Nov 81 |
| 109 | 0.306 | 12.3 | 12.46 | 0.01 | 13.40 | 0.01 | 14.36 | 0.03 | Nov 81 |
| 4C14.11 | 0.206 | 12 | 14.49 | 0.04 | 15.23 | 0.05 | 15.92 | 0.07 | Oct 82 |
| 123 | 0.218 | 10.8 | 14.15 | 0.03 | 14.76 | 0.03 | 15.79 | 0.04 | Mar 81 |
| 132 | 0.214 | - | - | - | - | - | - | - | - |
| 153 | 0.276 | - | - | - | - | - | - | - | - |
| 171 | 0.238 | 10.8 | 14.69 | 0.11 | - | - | - | - | Mar 81 |
| 172 | 0.520 | 12 | 15.62 | 0.06 | 16.24 | 0.10 | 17.02 | 0.20 | Oct 82 |
| 175.1 | 0.920 | 5 | 17.58 | 0.20 | - | - | - | - | Oct 82 |
| 192 | 0.060 | 12.3 | 12.47 | 0.01 | 12.86 | 0.01 | 13.56 | 0.01 | Nov 81 |
| 200 | 0.458 | 12.3 | 15.16 | 0.04 | 16.02 | 0.05 | 16.95 | 0.07 | Nov 81 |
| 4C14.27 | - | 12 | 15.66 | 0.10 | 16.41 | 0.11 | - | - | Mar 83 |
| 217 | - | 10.8 | 17.76 | 0.24 | - | - | - | - | Mar 81 |
| 219 | 0.174 | 10.8 | 13.55 | 0.01 | 14.16 | 0.01 | 14.93 | 0.02 | Mar 81 |
| 223 | 0.137 | 10.8 | 13.82 | 0.02 | 14.36 | 0.02 | 15.10 | 0.02 | Mar 81 |
| 225B | - | 7.4 | 15.9 | 0.10 | - | - | - | - | Nov 83 |
| 226 | - | 12 | 16.14 | 0.10 | 17.18 | 0.13 | - | - | Mar 83 |
| 228 | - | 12 | 16.19 | 0.10 | | | - | - | Mar 83 |
| 234 | 0.185 | 10.8 | 12.65 | 0.01 | 13.99 | 0.01 | 15.04 | 0.02 | Mar 81 |
| 236 | 0.099 | 12.3 | 12.69 | 0.01 | 13.24 | 0.02 | 13.88 | 0.02 | Mar 81 |
| 239 | - | 10.8 | 17.67 | - | - | - | - | - | Mar 81 |
| 241 | 1.62 | 10.8 | 17.29 | 0.15 | 10.16 | 0.34 | - | - | Mar 83 |
| 247 | 0.75 | - | - | - | - | - | - | - | - |
| 252 | 1.105 | 12.3 | 17.32 | - | - | - | - | - | Mar 81 |
| 263.1 | 0.36 | - | - | - | - | - | - | - | - |
| 265 | 0.811 | 10.8 | 16.01 | 0.09 | 16.65 | 0.10 | 17.39 | 0.10 | Mar 81 |
| 266 | 1.275 | - | - | - | - | - | - | - | - |
| 267 | 1.14 | 12 | 17.28 | 0.17 | 18.17 | 0.23 | - | - | Mar 83 |
| 1227+119 | 0.084 | 12 | 12.04 | 0.01 | - | - | - | - | Mar 83 |
| 274.1 | 0.422 | 10.8 | 15.39 | 0.09 | 16.09 | 0.06 | 17.00 | 0.04 | Mar 81 |

.....(cont)

Table 3.2 (continued)

| | | | | | | | | | |
|---|---|---|---|---|---|---|---|---|---|
| 277.2 | 0.766 | 7.4 | 17.66 | 0.22 | 17.84 | - | - | - | Mar 83 |
| 280 | 0.994 | 7.2 | 16.87 | 0.14 | 17.84 | 0.20 | - | - | Mar 81 |
| 284 | 0.239 | 10.8 | 14.17 | 0.02 | 14.75 | 0.03 | 15.51 | 0.04 | Mar 81 |
| 285 | 0.079 | 10.8 | 13.11 | 0.01 | 13.49 | 0.01 | 14.26 | 0.02 | Mar 81 |
| 288 | 0.246 | 10.8 | 13.59 | 0.02 | 14.20 | 0.02 | 15.08 | 0.02 | Mar 81 |
| 289 | 0.970 | 11 | 16.54 | 0.08 | 17.25 | 0.33 | - | - | Mar 83 |
| 293 | 0.045 | 12 | 11.68 | 0.01 | 12.08 | 0.01 | 12.76 | 0.01 | Mar 83 |
| 292 | - | - | - | - | - | - | - | - | - |
| 294 | - | - | - | - | - | - | - | - | - |
| 295 | 0.459 | 7.4 | 14.49 | 0.03 | 15.33 | 0.07 | 16.08 | 0.06 | Mar 83 |
| 299 | 0.367 | 10.8 | 15.91 | 0.06 | 16.61 | 0.08 | 17.35 | 0.08 | Mar 81 |
| 300 | 0.270 | 12 | 15.20 | 0.05 | 15.95 | 0.07 | 16.57 | 0.11 | Mar 83 |
| 303 | 0.141 | 12 | 13.27 | 0.01 | 13.86 | 0.01 | 14.67 | 0.02 | Mar 83 |
| 310 | 0.054 | 12 | 12.49 | 0.01 | 12.86 | 0.02 | 13.50 | 0.05 | Mar 83 |
| 315 | 0.109 | 12 | 13.36 | 0.03 | 13.82 | 0.03 | 14.42 | 0.08 | Mar 83 |
| 318 | 0.752 | 7.2 | 16.96 | 0.15 | - | - | - | - | Mar 81 |
| 319 | 0.192 | 12 | 15.11 | 0.06 | 15.41 | 0.06 | 16.21 | 0.08 | Mar 83 |
| 321 | 0.096 | 12 | 12.72 | 0.01 | 13.26 | 0.02 | 13.73 | 0.02 | Mar 83 |
| 324 | 1.21 | 12 | 16.84 | 0.17 | 18.07 | 0.17 | 0.20 | | Mar 83 |
| 326 | 0.089 | 12 | 13.60 | 0.02 | 13.96 | 0.02 | 14.58 | 0.02 | Mar 83 |
| 337 | 0.63 | 12 | 16.34 | 0.11 | 17.34 | 0.14 | - | - | Mar 83 |
| 340 | 0.76 | - | - | - | - | - | - | - | - |
| 341 | 0.448 | 12 | 15.31 | 0.03 | 15.99 | 0.06 | 16.88 | 0.12 | Mar 83 |
| 346 | 0.161 | 12 | 13.37 | 0.02 | 13.96 | 0.02 | 14.73 | 0.05 | Mar 83 |
| 349 | 0.205 | 10.8 | 14.70 | 0.03 | 15.32 | 0.03 | 16.13 | 0.06 | Mar 81 |
| 352 | 0.806 | 7.2 | 17.24 | 0.12 | - | - | - | - | Mar 81 |
| 356 | 1.079 | 12 | 16.75 | 0.13 | 17.35 | 0.13 | - | - | Mar 83 |
| 4C13.66 | - | - | - | - | - | - | - | - | - |
| 368 | 1.132 | 7.4 | 16.68 | 0.16 | 17.68 | 0.16 | 18.06 | 0.16 | Mar 83 |
| 381 | 0.161 | 10.8 | 13.89 | 0.01 | 14.64 | 0.02 | 15.41 | 0.03 | Mar 81 |
| 382 | 0.059 | 10.8 | 10.87 | 0.01 | 11.74 | 0.02 | 12.59 | 0.01 | Mar 81 |
| 388 | 0.091 | 10.8 | 12.55 | 0.02 | 13.09 | 0.01 | 13.69 | 0.02 | Sep 80 |
| 433 | 0.102 | 12 | 12.37 | 0.01 | 13.26 | 0.01 | 14.21 | 0.06 | Oct 82 |
| 436 | 0.215 | 12.3 | 14.00 | 0.02 | 14.65 | 0.02 | 15.43 | 0.04 | Nov 81 |
| 437 | - | 7.4 | 18.02 | 0.19 | - | - | - | - | Nov 83 |
| 438 | 0.290 | 12 | 13.98 | 0.03 | 14.65 | 0.05 | - | - | Oct 82 |
| 441 | 0.70 | 10.8 | 16.5 | 0.10 | 17.22 | 0.15 | - | - | Oct 82 |
| 452 | 0.081 | 7.8 | 12.91 | 0.02 | 13.34 | 0.02 | 14.03 | 0.02 | Oct 82 |
| 457 | 0.427 | 12 | 15.71 | 0.14 | 16.80 | 0.15 | - | - | Oct 82 |
| 470 | - | 7.4 | 18.49 | 0.26 | - | - | - | - | Nov 83 |

Table 3.3: Photometry of FPAM Elliptical Galaxies.

| NGC | 1600 | 1700 | 2672 | 3158 |
|---|---|---|---|---|
| UKIRT Data: | | | | |
| d | 12" | 12" | 12" | 12" |
| J | 10.99 | 10.46 | 11.05 | 11.28 |
| H | 10.26 | 9.73 | 10.33 | 10.54 |
| K | 9.96 | 9.46 | 10.03 | 10.24 |
| (H-K) | 0.30 | 0.27 | 0.30 | 0.30 |
| (J-K) | 1.03 | 1.00 | 1.02 | 1.04 |
| FPAM Data: | | | | |
| d | 15" | 15" | 15" | 15" |
| J | 10.87 | 10.29 | 10.86 | 11.05 |
| H | 10.07 | 9.55 | 10.10 | 10.29 |
| K | 9.76 | 9.27 | 9.82 | 9.99 |
| (H-K) | 0.31 | 0.28 | 0.28 | 0.30 |
| (J-K) | 1.11 | 1.02 | 1.04 | 1.06 |

large number of radio sources selected from a different radio catalogue were observed. That data, which was reduced in an identical fashion to that of the 3CR sources will however be presented and discussed in Chapter 6 of this Thesis.

3.3.b Internal consistency of the data

During most of the observing runs, a small number (between one and three) of radio galaxies were observed on more than one night, with an identical instrumental set-up. These measurements were always found to be repeatable to within the statistical uncertainties associated with each observation, and these measurements were therefore averaged. In addition to this, 18 of the galaxies were also reobserved on subsequent runs. It is however important to note that of these, six were reobserved because there was some reason to doubt the initial measurement, either because there was some specific evidence of a discrepancy (e.g. by comparison with published data) or because the observation did not follow trends established by the bulk of the data, and hence merited confirmation. The remaining 12 repeat observations represent a more random check on the repeatability of the data. In general it will be found that, while the 12 latter checks agreed well, the six galaxies for which there was some initial doubt did on reobservation have different magnitudes.

Four of the six repeats of 'suspect' observations concerned data taken in the first, exploratory run in September 1980, at which the author was not present. The two lowest redshift galaxies were suspect because, as noted in Lilly and Longair (1982a, Paper 1), the

derived (V-K) colours of these galaxies appeared anomalously blue, compared with the nearby ellipticals of Frogel et al.(1978,FPAM). On reobservation in November 1981, both these galaxies appeared to be substantially brighter in the infrared, by 0.15 magnitudes in the case of 3C 33 (z=0.06) and by as much as 0.5 magnitudes in the case of 3C 98 (z=0.03). At higher redshifts, 3C 46 (z=0.48) was reobserved because it had a very red colour for its redshift (Paper 1), while the original measurement of 3C 65 was substantially fainter than reported by both Grasdalen (1980) and Puschell et al.(1982,POL). Both of these galaxies were also substantially brighter when reobserved. There are a number of possible explanations for these discrepancies: the beam profiles could have been much poorer than thought, the calculated offsets could have been less precise, or the reference beams could have been contaminated. Five other galaxies from this first run were however reobserved 'randomly'. Although 3C 382 was affected by these problems the variation in the measurement was erroneously attributed (Paper 1) to the variability in this source reported by O'dell et al.(1978). 3C 381 did not appear to be affected (Paper 1), while 3Cs 388 and 441 were both unchanged on reobservation. The 'empty field' source 3C 68.2 was slightly, but not significantly, fainter when it was reobserved through a smaller aperture over three years after the initial measurement.

In summary of the above, several of the ten observations made in September 1980, and reported in Paper 1, are underestimates of the true flux density. However, all these galaxies have either been subsequently reobserved on UKIRT during later runs, or, in the case of 3C 34, have been independently checked by other investigators.

There is no reason to doubt further the data on these ten galaxies presented in Table 3.2, and analysed in the remainder of this Chapter.

The data from the second, and subsequent, runs is believed to be more reliable. This corresponds to over 75% of the data in Paper 1, and 97% of the data in table 3.2. The problems that affected the earliest observations had been mastered.

Of the 27 galaxies observed in March 1981, only 3C 295, which is in a difficult crowded field, was suspect, although 3C 200 had a slightly blue (H-K) colour (c.f. Lebofsky 1981). Three other relatively bright radio galaxies, 3Cs 109,192, and 236, were all found to be the same to within the statistical uncertainties of the observatios, once allowance had been made for the slightly different sized apertures used. The very faint galaxy 3C 241 was also measured to have almost exactly the same flux density when reobserved in November 1983. 3C 200 also agreed well at J and K, but H decreased by 0.3 magnitudes, to produce a more consistent colour. The original measurement was only two sigma from the new one, and this may represent simply a statistical variation. 3C 295 was found to be substantially brighter in all wavebands. It is thought that the lack of flexibility in the chop size and direction with the f/9 configuration in March 1981 led to contamination of the reference beam that was avoided on subsequent reobservation at f/35 with the chopping secondary.

3C 228 was observed in both March and November 1983, and a very satisfactory agreement was found between these two measurements.

In summary, a small fraction of the data published in Paper 1 has been found to be in error. These occassionally poor observations were made mainly during the first observing run of this programme, and improved measurements of these galaxies have been included in Table 3.2.

The data in Table 3.2 represents the final data set which will be subject of analysis in the remainder of this Chapter.

3.3.c Consistency with the data for low redshift galaxies of FPAM

The infrared photometry obtained with UKIRT of the four NGC giant elliptical galaxies that have also been observed by Frogel et al (1978,FPAM) are presented in Table 3.3 with FPAM's original data. The UKIRT data were reduced in an identical fashion to the radio galaxy data, although the correction for galactic extinction has not been applied. The colour equation has been used, of course, to place the UKIRT data on nominally the same photometric system as the FPAM data. The UKIRT data was taken through a 12 arcsec aperture, whereas the smallest aperture employed by FPAM was 15 arcsec. The uncertainties in each measurement are formally very small (0.01 magnitudes).

The agreement in (H-K) colour is very satisfactory. The mean difference between the two measurements for each galaxy is zero, and for only one galaxy is the difference larger than 0.01 magnitudes.

In (J-K), the agreement is slightly less good. All the UKIRT

measurements are too blue, i.e. (J-H) is too small. The mean difference is slightly over 0.03 magnitudes. There are two possibilities: Either the colour equation has a smaller coefficient than is believed (i.e. the passbands are more similar) or some other systematic effect is present. For instance, because the nearby galaxies will have a relatively flatter profile across the aperture, the measurements of these will be more sensitive to small variations in the outer regions of the beam profiles.

Finally in K, although the magnitudes are discrepant by 0.20, 0.21, 0.19, and 0.25 magnitudes respectively, this size of effect is entirely consistent with the different apertures used and the growth curve given by FPAM. There is no evidence that there is any significant systematic effect.

In summary, it appears that some systematic effects could be present in the radio galaxy data, particularly in the J passband, at the level of around 3%. This however is thought to be acceptable. In most cases the random errors are much bigger than this, and most of the observations will be compared with modelled predictions of behaviour which are unlikely to be more precise than this in any case.

3.3.d Consistency with other observers

Excluding 3C 68.2, for which Grasdalen (1980) obtained an upper limit only, 20 of the 81 galaxies for which data is listed in Table 3.2 have been observed by either Lebofsky (1981) or Puschell *et al.*(1981, POL). The overlap is most complete at K. This is generally

the most sensitive waveband for objects that are as red as these galaxies. Lebofsky (1981) measured H and K magnitudes, while POL concentrated on J and K, although many galaxies were in fact also observed in H also.

A comparison of the K magnitudes is shown diagramatically in Figure 3.3a. Both Lebofsky (1981) and POL used apertures which were generally smaller than those used in this investigation on UKIRT, and so a small aperture correction must be applied to their data. This has been done; it was usually around 0.1 magnitudes in most cases. In all cases, the error bars shown in Figure 3.2a are those derived from the statistics of the observations, and hence are the minimum statistical uncertainties in the magnitudes.

For objects brighter than about 16.5 in K, the agreement is satisfactory, with two curious exceptions. It is not at all clear what has happened to 3C 265 and 3C 318, both observed by POL. They are both at approximately the same redshift (0.8). Peculiar is the fact that both these galaxies have anomalous colours (see Section 3.4.d(i)), and that this is largely true whichever of the K magnitudes (either from UKIRT or POL) is used. The measurements of the galaxies are almost as if transposed (indicated by their symmetrical location on Figure 3.3a) and one may speculate that at some stage in the reduction procedure these two objects were confused. However, from a thorough examination of the observing records (extending to the computer records of the actual position of the telescope) there is no doubt that this has not occured in the reduction of the UKIRT data.

Figures 3.3a-c:
Comparison of UKIRT photometry taken in the current investigation with measurements made on other telescopes (e.g. Lebofsky 1981 and Puschell et al 1982).

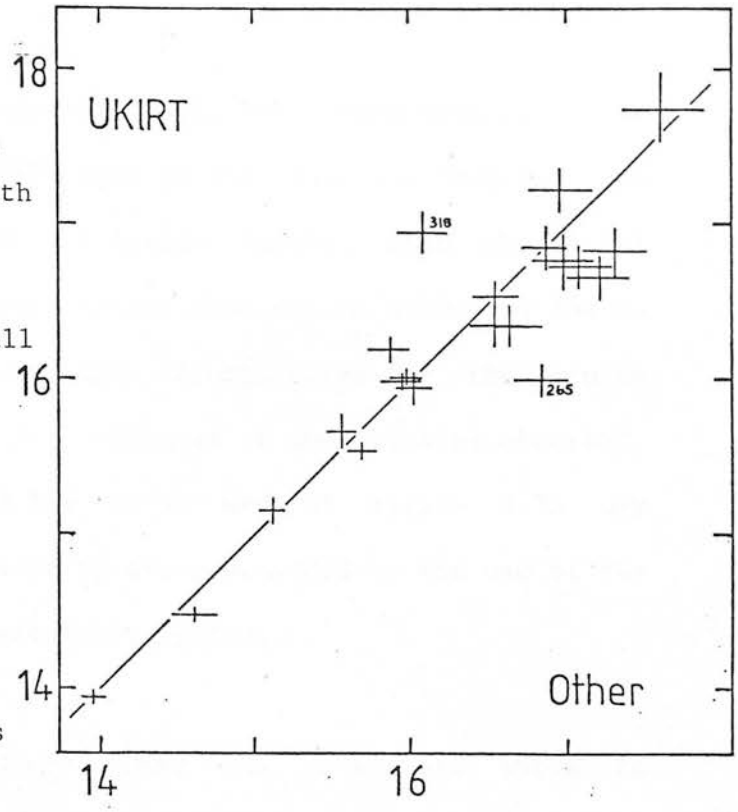


(a) K magnitudes

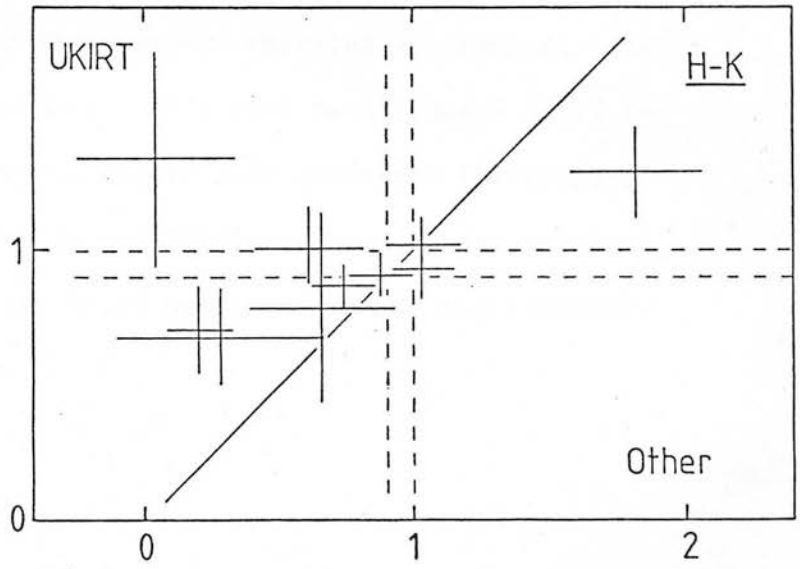


(b) (H-K) colours

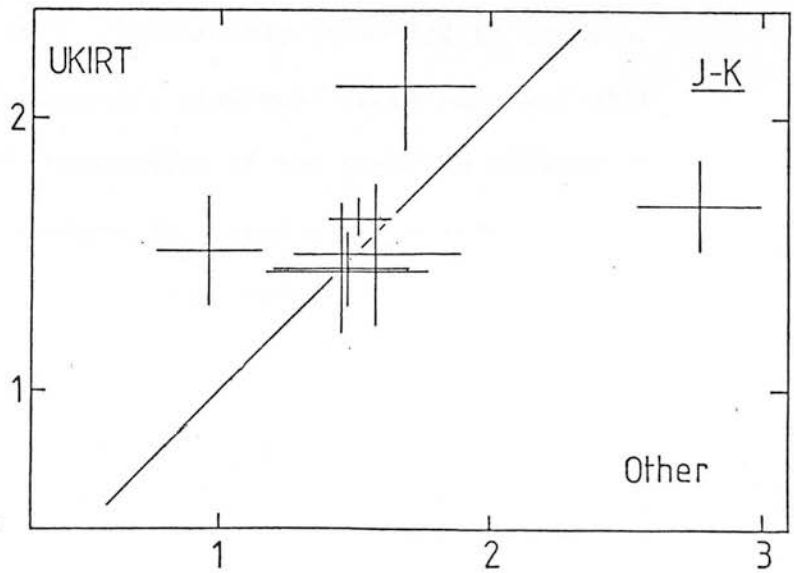


(c) (J-K) colours.

Fainter than a K magnitude of 16.5, the agreement is less satisfactory. All the non-UKIRT data in this case are from POL, and some of these appear to be systematically fainter than the UKIRT measurements. This is a larger affect than can be accounted for in terms of the different apertures and uncertainties in the growth curve. These are amongst the faintest of the galaxies observed, requiring long exposures, and the faint end of Figure 3.3a may reflect the increased tolerance to error provided by the use of the larger apertures in the present investigation.

The comparison of the colours (H-K) and (J-K) are shown in Figures 3.3b and 3.3c. The agreement is not very good. Unfortunately, resolving this discrepancy inevitably involves the interpretation of these colours. This will be discussed later in this Chapter. The dashed lines in Figure 3.3b represent the range of colours that are expected by redshifting an unchanging spectral energy distribution. Few of the UKIRT measurements are significantly displaced from these colours.

## 3.4 : Presentation of Results

Because of the high redshift information content of the sample, the photometric data is most conveniently presented in terms of colour-redshift and magnitude-redshift diagrams. These diagrams will be shown after an initial discussion of the possible effects of strong emission lines on the colours and after a description of a classification scheme for three classes of radio galaxy that will be required in the discussion.

In the remainder of this chapter, the emphasis will be on the experimental results. Empirical 'facts' will be derived that are associated with the minimum of assumption or interpretation. Even the cosmological nature of the redshift does not have to be assumed for much of the remainder of this chapter. Then, at the end of the chapter, various possible interpretations for these 'facts' will be outlined. These interpretations will then be explored more fully, both in the next chapter, and particularly in Chapter 5.

### 3.4.a The Effect of Strong Emission Lines

The majority of 3CR radio galaxies have emission lines in their spectra (Hine and Longair 1979 and references therein, and also Chapter 2), and it is important to assess the effect that these could have on the magnitudes measured through various passbands. In particular, Spinrad (1982 and private communications) has measured some very large equivalent widths in the [OII] 3727 line in some of the radio galaxies that have redshifts close to unity. The change in magnitude observed through a passband of width D produced by a line of observed equivalent width W is :

$$\delta M = -2.5 \log (1 + W/D) \qquad (3.3)$$

The observed equivalent width of a line of given fixed strength increases as (1+z) because the line does not suffer the K-term wavelength stretching that the continuum does. This alone increases the effect of the emission lines at high redshift, although there also appears to be an underlying trend for the more distant galaxies to have intrinsically stronger lines.

An examination of the spectrophotometric line ratios given by Costero and Osterbrock (1977) and by Yee and Oke (1978) for radio galaxies shows that the strongest lines in the optical spectrum of Narrow Line Radio Galaxies (NLRG) are [OII] 3727, [OIII] 5007 and Hα. When account is taken of the relative strengths of the continuum at the appropriate wavelengths, it is found that the equivalent widths of these lines are typically in the approximate ratio 1:3:1. At high redshift (and hence shorter wavelengths) Mg 2799 is also often evident (Spinrad 1982, Chapter 2), but this line is generally not very strong. Spinrad (1982) has shown that the observed equivalent widths of [OII] 3727 in high redshift radio galaxies are typically in the range of a few hundred A (c.f. similar values found in Chapter 2) but that in a few cases (e.g. 3C 324 and 3C 368) they can be as high as 1000 to 2000 A.

Fortunately, the infrared passbands J, H and K are very broad in wavelength, and are hence less sensitive to emission lines than the narrower optical V and r (Thuan and Gunn 1976) passbands. Figure 3.4 shows diagramatically the redshifts at which these four most important emission lines are in the five passbands that are most of interest for this investigation, namely V, r, J, H, and K.

The following general statements may be made concerning the likely effects of this contamination on the colours at high redshift. Firstly, in the optical, where in any case the spectra are normally available for direct inspection and the equivalent widths of the most prominent lines often measured, the r magnitude is unlikely to be seriously affected at redshifts greater than 0.85,

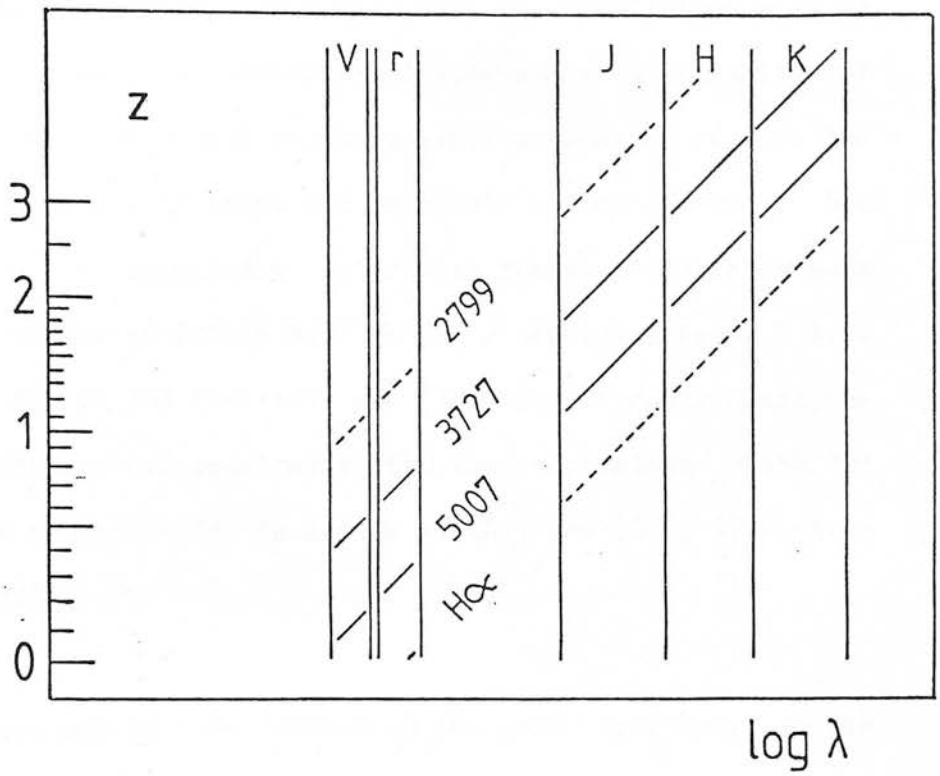


Figure 3.4: Diagram showing the redshifts at which the four strongest emission lines found in the spectra of 3C radio galaxies are within the 5 passbands that are most of interest in the current investigation.

when [OII] 3727 moves out of the passband. Secondly, in the infrared, where no spectra are available, both J and H may be affected by both $H\alpha$ and [OIII] 5007. If the line ratios are similar to those found at lower redshifts then the [OIII] line will be particularly important. $H\alpha$ enters the J passband at a redshift of 0.6, but does not reach the H passband until a redshift of 1.2. The effect of this line should be at the level of a few percent, but could rise to 0.2 magnitudes in extreme cases. Potentially more serious is the effect of [OIII] 5007 on the J magnitude for $z > 1.1$. In particular, for 3C 368 ($z=1.13$), the (J-K) colour could easily be reduced by as much as 0.5 magnitudes if the equivalent width of [OIII] 5007 is substantially in excess of that for [OII] 3727 given by Spinrad (1982).

To summarize, and to look forward to the next sections, it is unlikely that either the (r-K) or the (H-K) colours are affected for any of the objects of interest. However, the (J-K) colour may be slightly affected for redshifts greater than 0.6, and may be severely contaminated for redshifts greater than 1.1.

### 3.4.b Differentiation between various classes of Radio Galaxies

It will be found neccessary to differentiate, in the discussions to follow, between three types of radio galaxy identification.

The first distinction will be between those radio galaxies that are associated with extended radio sources, and those which are associated with compact sources (CRS). In fact there are only two radio galaxies in the latter category, 3C 299 and 3C 318. They have

a radio brightness distribution that for frequencies above 1 GHz is dominated by an unresolved nuclear component that is smaller than 1 arcsec in size (Laing et al 1983). It is worth noting at this stage that the vast majority of 3C radio sources which have CRS structure are associated with quasars. The second, and more important, distinction will be between the narrow line radio galaxies (NLRG) and the broad line radio galaxies (BLRG). Grandi and Osterbrock (1978) have shown that the spectra of those radio galaxies that have emission lines in their spectra can be divided in to these two distinct classes. The NLRG have forbidden and recombination lines that have full widths at half maximum (FWHM) of the order of 500 $kms^{-1}$, while the BLRG have FWHM in excess of 2000 $kms^{-1}$. Grandi and Osterbrock (1978) also showed that this difference was even more striking when the full width at zero intensity (FWOI) was considered. Whereas the FWOI of NLRG are about 1000 $kms^{-1}$, those of the BLRG are larger than 14 times this figure. They also showed that there was a good correlation between the spectral classification (NLRG or BLRG) and the optical morphological classification of the radio galaxies. The BLRGs are associated predominantly with N-galaxy morphology, whereas the NLRG are associated with more normal giant elliptical types such as E, D, and cD. In the discussion to follow, the classifications of Grandi and Osterbrock (1978), Yee and Oke (1978) and Yee (1980) will be followed. It is natural to view the N-galaxy BLRGs as low luminosity quasars.

### 3.4.c The Infrared Colours (H-K) and (J-K)

The observed infrared colours (H-K) and (J-K) for all the 3C radio galaxies for which such colours were measured are shown in

Figures 3.5 and 3.6. Because the three infrared magnitudes were measured through the same aperture the derivation of the colours from the data tabulated in Table 3.2 is straightforward. The error bars plotted on these colour-redshift diagrams are derived from the statistical uncertainties listed in Table 3.2, and therefore represent the minimum possible uncertainty in the colours. The galaxies for which a redshift has not yet been determined are plotted in the diagrams as short horizontal bars, of arbitary length, centred on the redshift that they are most likely to have. These redshift estimates are based on their infrared K magnitudes and the infrared (K,z) Hubble diagram (Section 3.4.e, Table 3.8). In practice, all the galaxies are likely to be at high redshift where the (H-K) and (J-K) colours are very weak functions of redshift. Hence the precise positions of these galaxies on the diagrams are not very important.

The small histograms on the vertical axes of the two diagrams represent the data on very low redshift ellipticals of Frogel et al (1978, FPAM). The short arrows extending from these histograms indicate the low redshift K-corrections derived by them. The FPAM data is on the same photometric system as the data for the radio galaxies. The solid lines in the diagrams represent the predicted colour-redshift relations in the two colours for an unchanging giant elliptical galaxy spectral energy distribution. Its construction will be detailed later in this section.

The uncertainties in the colours of these galaxies without known redshifts have been omitted from Figures 3.5 and 3.6 for reasons of clarity. They are easily derivable from the figures given in Table

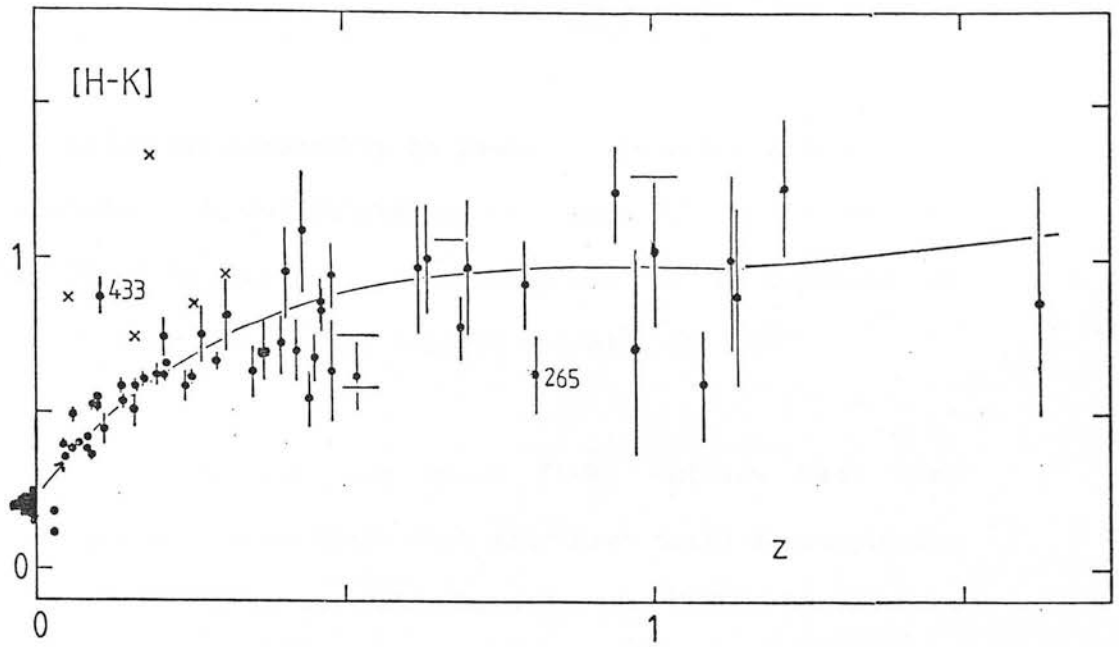


Figure 3.5: The infared colour (H-K) as a function of redshift for NLRG (circles), BLRG (crosses), CRS (square). Galaxies with unknown redshift are represented by short horizontal bars of arbitary length at the most likely redshift that they are at (Table 3.8). 3C 433 is an anomalous NLRG while 3C 265 has unusually blue optical colours. The solid curve shows the colour-redshift relation that is predicted for an unchanging SED appropriate to an elliptical galaxy.

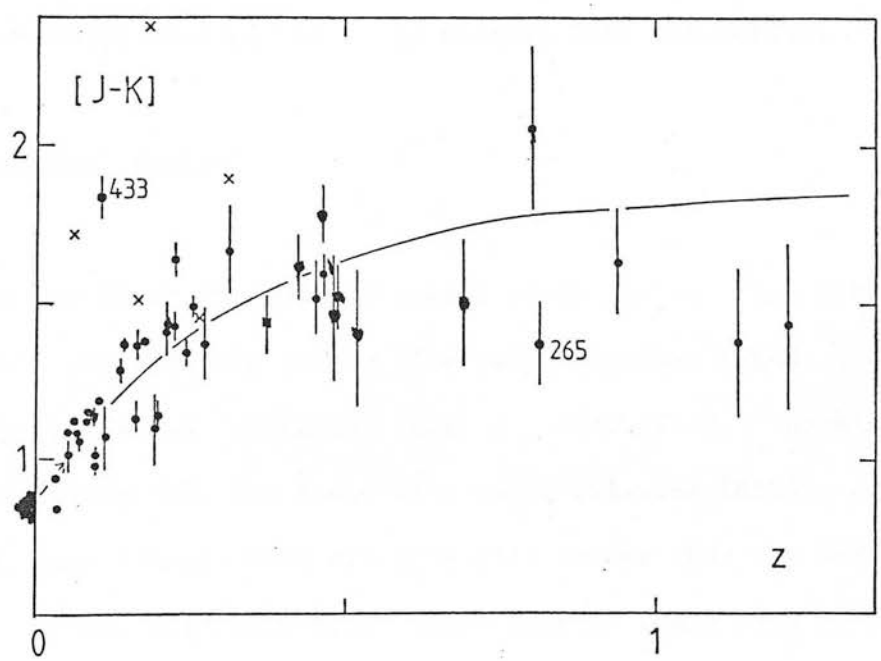


Figure 3.6: The infrared (J-K) colour as a function of redshift. The symbols are as in Figure 3.5.

3.2, and are generally comparable to those of the other galaxies at similar redshifts. 3C 241 is plotted on Figure 3.5 at its redshift of 1.62, but 3C 65 is shown as a horizontal bar at a redshift of unity. This is very close to its correct redshift of 1.17

The number of galaxies for which (H-K) colours have been measured is greater than those that also have (J-K) measurements. There are two main reasons for this. Firstly, the UKIRT photometers are optimised for longer wavelength observations. This, combined with the intrinsic redness of the high redshift galaxies, makes measurements much easier at H and K than at J. This is illustrated by the uncertainties in Table 3.2, which are nearly always largest for the J measurement, even though the integration times were normally longer in this wavelength. Secondly, the fact that at high redshift the (J-K) colours may be contaminated by emission lines makes the detailed analysis of (J-K) colours less attractive.

3.4.c.(i) General Results

Considering first the overall trends exhibited by the data in Figures 3.5 and 3.6: The narrow line radio galaxies (NLRG) broadly follow the predicted relations for a redshifted, unchanging elliptical galaxy SED. The broad line radio galaxies (BLRG), on the other hand, have colours that are generally redder than the NLRG at the same redshift. The two Compact Radio Sources (CRS) have infrared colours that are not significantly different from those of the NLRG. This difference between the 1-2 micron continua of NLRG and BLRG is similar to that found between Seyfert 1 (broad line) and Seyfert 2 (narrow line) galaxies shown by McAlary et al (1979).

The red colours of the BLRG are almost certainly due to the presence in the SED of a non-stellar component that is redder than the underlying stellar continuum, which is presumably the same as dominates the NLRG continuum. This interpretation is also suggested by the infrared absolute magnitudes that are generally found to be brighter than the NLRG on the (K,z) diagram (Section 3.4.e). Such a non-stellar component would be associated with the optical component that is responsible for the bright star-like nucleus that is present and which leads to the classification of these BLRGs as N-galaxies. The red infrared colours of the BLRGs do not have a stellar origin, and these objects which are of intermediate type between the NLRGs and the quasars, will not be discussed in more detail here, since a proper treatment requires, preferably simultaneous, photometry over a much wider baseline in wavelength than is available in this study. The remainder of this discussion, and indeed of the Thesis, will focus on the NLRGs. Mention should be made of 3C 433. This galaxy has very red colours in both (J-K) and (H-K), and is clearly separate from the rest of the NLRG on Figures 3.5 and 3.6. Spectroscopically it is a typical NLRG with rather weak emission lines (Schmidt 1965), and in the radio it does not have the 'classical double' structure that is normally assocaiated with powerful sources. This galaxy was reobserved in November 1983 as part of another investigation, and there is no doubt that the photometry given in Table 3.2 is correct. The nature of this galaxy is a mystery. It is one of only a few dumb-bell systems in the sample, and the interaction with the other galaxy may provide a clue to the unusual colours. It is clearly different from the other NLRGs, and will be omitted from the sample that is investigated

further in the remainder of the this section. One other NLRG is also omitted. This is 3C 265. This galaxy is excluded because, as will be shown in Section 3.4.d, it has peculiar optical and optical-infrared colours. These two omissions from the sample to be analysed further are regrettable. Nevertheless it is felt that they are justified in view of the large difference which exists between their properties and those of the great majority of the NLRGs.

Figures 3.5(i) and 3.6(i) are the same as Figures 3.5 and 3.6 but have the BLRG, CRS and the two peculiar NLRG removed, the better to illustrate the NLRG data.

One of the advantages of using infrared passbands to study the colours of galaxies at moderate to high redshift is that the K-corrections for the infrared passbands should be known more accurately at high redshift than is possible for optical passbands. This is because at high redshift the optical passbands are redshifted in to the rest-frame ultraviolet whereas the infrared passbands are shifted in to the well studied optical region of the spectrum. However the actual detailed prediction of the colour-redshift relations is not trivial. The principal reason for this is that there is no spectrophotometry of galaxies available that covers the continuous wavelength range from 1 to 3 microns. The available data consists of broad band colours and measurements of a few narrow band indices. A further uncertainty is that the absolute calibration is based on theoretical models of the stellar atmosphere of an A0V star (e.g. Kurucz (1979)). This calibration must be accurate over a wide range of wavelengths if the predicted colours are to be correct over the corresponding range of redshift. At a

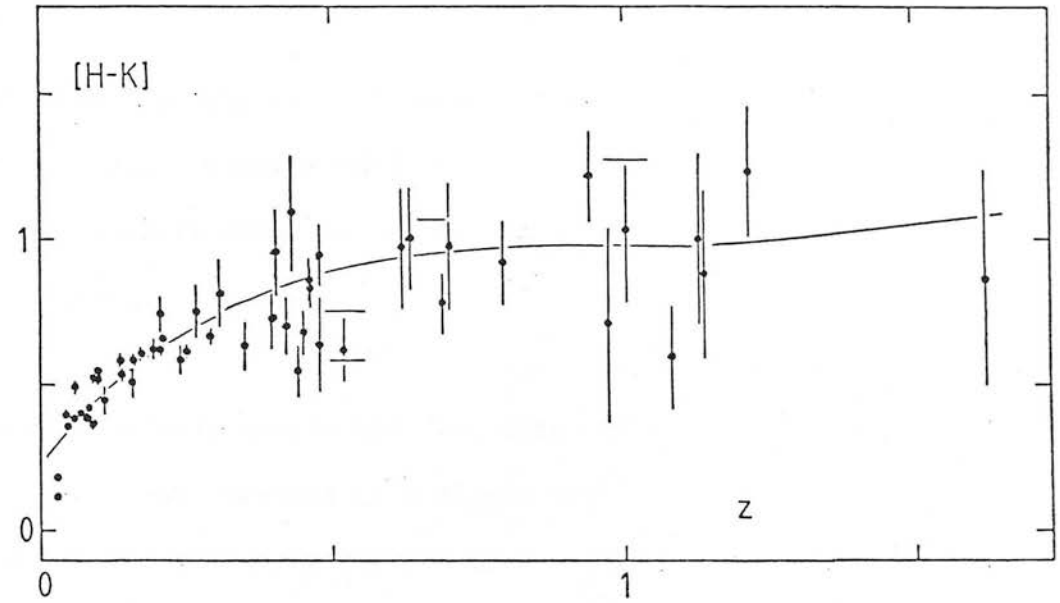


Figure 3.5(i): The (H-K) colours for the NLRG only and excluding 3Cs 433 and 265. The symbols are as in Figure 3.5. The mean displacement of the colours from the predicted relation and the intrinsic scatter in the colours are analysed in Table 3.4. 3C 241 (z=1.62) is excluded from that analysis because of its high redshift.

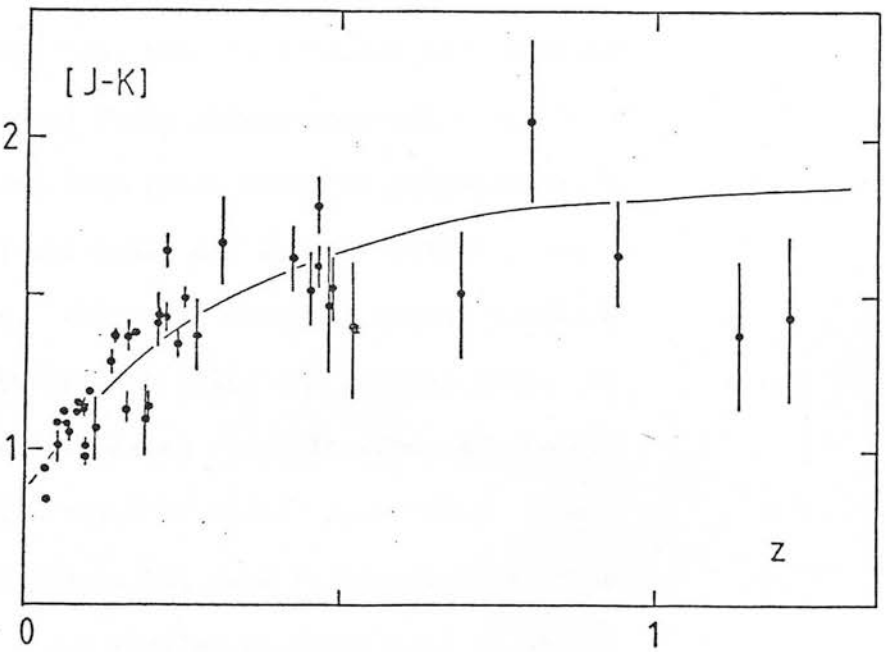


Figure 3.6(i): The (J-K) colours of the NLRG only and excluding 3Cs 433 and 265. The symbols are as in Figure 3.6.

redshift of 1.5, the J passband is at about 5000 A in the rest frame, and so if high redshift (J-K) colours are to be accurately compared with low redshift data the calibration of Vega must be accurate from 0.5 to 2.5 microns.

There have been several approaches to this problem. Lebofsky (1981) used an infrared spectrum of a single star ($\alpha$ Tau) that had been normalised to give the correct broad band colours and narrow band indices for an elliptical galaxy. In an earlier report on the current investigation, Lilly and Longair (1982a) used a free-form construction that was constrained to fit the data at redshifts less than 0.4. Bruzual (1981) used an infrared SED based upon the broad band colours of the stars present in his evolving stellar populations. For the population that dominates in the infrared, the Giant Branch stars, he used the R2 population of Tinsley (1978). Finally, Puschell et al. (1982, POL) used a similar synthetic spectrum, based on the Giant Branch of O'Connell (1976), in their analysis, although their colour-redshift relations were not actually published. Apart from small detailed differences, the predictions of Bruzual (1981) and Lilly and Longair (1982) agree fairly well, and in particular, the high redshift colour predictions for redshifts around unity (where the Lilly and Longair curve is constrained by the low redshift data) are in close agreement. As far as can be judged, the high redshift (J-K) prediction from POL is also in agreement with these. POL used filter profiles from the NASA 3m IRTF telescope which are similar to those used on UKIRT. These agreements are reassuring, but not very surprising since the giant populations of the synthetic models were to a large degree constructed to be consistent with the broad band galaxy data on which Lilly and

Longair's predictions were largely based.

A serious discrepancy exists, however, with the (H-K) prediction of Lebofsky (1981). Whereas the colour-redshift relation in Figure 3.5 flattens at redshifts greater than about 0.5, Lebofsky's curve continues to rise. By redshifts of around unity, this discrepancy amounts to slightly over 0.3 magnitudes, in the sense that her relation is too red. The most puzzling feature is that this discrepancy extends to sufficiently high redshifts that both the H and K passbands are in to the optical wavebands at a micron and shorter, where spectrophotometry is available, so it is not clear exactly why this discrepancy exists.

In the current analysis the Bruzual (1981) relations have been used, but have been modified in two respects. The original method of a free-form continuum was abandoned because it assumed that the continua were unchanging out to a redshift of 0.4. The two modifications that were applied to Bruzual's curves are as follows. Firstly the good agreement in high redshift colours between the Bruzual relations and the predictions of Lilly and Longair (1982a) and POL (which were based on UKIRT filters) suggest that, as the UKIRT data have had a colour equation (3.2) correction applied, then so should Bruzual's curves. Accordingly, since (J-H) is close to 0.7 over the whole redshift range of interest, a value of 0.07 has been subtracted from his J predictions at all redshifts. Secondly, it is apparent that the zero-redshift colours of the Bruzual predictions do not match those of the elliptical galaxies of FPAM, although this discrepancy has been removed by a redshift of 0.05 because of the differing zero-redshift slopes of the colour K-corrections from FPAM

and Bruzual. Such a steepening in the colour-redshift relation at redshifts less than 0.05 is seen in Lebofsky's curve (which explicitly incorporates the narrow band index measurements) but not in Bruzual's curve, and this effect probably represents the progressive removal of the 2.3 micron CO absorption feature (Baldwin et al 1973) from the K passband. Therefore, below redshifts of 0.05, the FPAM colour K-corrections have been used. These link up at that redshift with the Bruzual relations that are used for all higher redshifts.

In summary, the colour-redshift relations plotted on Figures 3.5 and 3.6 represent what is believed to be the best estimate of the effect of the redshift on the observed (H-K) and (J-K) colours. However, it should be borne in mind that, particularly at high redshifts, these must be regarded as uncertain to the level of about 5%.

The NLRG data follow these relations well. Particularly in (H-K), for which the number of high redshift galaxies is greater, it is immediately apparent that there are no large systematic deviations from these relations, implying the the broad shapes of the red and near-infrared continua of the high redshift galaxies are basically unchanged from those at low redshift.

3.4.c.(ii) A More Quantitative Analysis

In order to investigate the agreement between the data and the modelled prediction in more detail, the following analysis was performed. For the N objects in a given interval of redshift, it is

possible both to measure the weighted mean deviation of the observations from the prediction, $\delta c$ , and to estimate the underlying scatter in the data once allowance has been made for the formal uncertainties in the observations, $\sigma_c$ . This underlying scatter may be composed of both genuine 'cosmic' scatter (i.e. a range in the intrinsic properties of the population) and any scatter introduced in to the colours by observational errors that might affect the colour measurement but not be present in the statistics of the individual integration pairs in each passband. Both $\delta c$ and $\sigma_c$ are assumed to be independent of redshift within the redshift interval considered. A $\chi^2$ statistic is defined in terms of the observed colours of the galaxies, $c_i$, the formal uncertainties in those colours, $\sigma_i$, and the predicted colour of an elliptical galaxy at the same redshift, $c_z$ :

$$\chi^2 = \sum_i \frac{(c_i - c_z - \delta c)^2}{\sigma_c^2 + \sigma_i^2} \qquad (3.4)$$

With $\delta c$ a completely free parameter, $\sigma_c$ is slowly increased from zero until the minimum value of $\chi^2(\delta c)$ is such that $\chi^2_{min} = N-1$. This indicates the minimum value to the underlying scatter such that a single colour-redshift relation, of the same slope, but not neccessarily the same normalisation, as the modified Bruzual relation, is a satisfactory fit to the data. The value of $\delta c$ associated with this minimum in $\chi^2$ is therefore the weighted mean deviation from the relation. It is in fact insensitive to $\delta c$, because varying the latter changes only the relative weighting of the different galaxies, and since at a given redshift most of the galaxies have similar statistical errors oi the change in weighting is very small. The uncertainty in $\delta c$ may be found by finding the

values of $\delta c$ such that, with $\sigma_c$ set to the minimum value found above, $\chi^2 = \chi^2_{min}+1$.

Particularly at high redshift, where the analysis is of particular interest in placing upper limits to the change in the intrinsic SED of the galaxies, the number of galaxies in most of the useful groups is small. This not only increases the uncertainty in $\delta c$, but also makes the estimate of $\sigma_c$ less certain, particularly as the statistical uncertainties, $\sigma_i$, may be quite large. In particular for some groups, an imaginary value for $\sigma_c$ may be required to find $\chi^2_{min}=N-1$. This means, of course, that the data show less scatter about the mean relation than would be expected from the formal observational uncertainties alone. Consequently, the values of $\sigma_c$ should be treated with some caution. Nevertheless, this analysis does give a useful indication of the amount of scatter in the data underneath quite large error bars. In particular, it is interesting to assess whether the apparently rather dramatic onset of scatter in the colours in the diagrams at redshifts around 0.4 is accountable for by the increased formal uncertainties in the measurements alone.

This analysis has been carried out for a number of groups of galaxies for both (H-K) and(J-K). The results of the analysis are presented in Table 3.4, and illustrate several interesting features of the data. 3C 241 is excluded because of its very high redshift, and 3C 65 is analysed only in those groups containing the galaxies with unknown redshift.

In (H-K), $\sigma_c$ and $\delta c$ are both generally rather small, in all the groups considered. At low redshift (Groups A, F and G) the mean

Table 3.4: The Statistical Analysis of the Infrared Colours of High Redshift Galaxies.

| | | (H-K) | | | | | (J-K) | | | | |
|---|---|---|---|---|---|---|---|---|---|---|---|
| | z | N | $\sigma_c$ | < | $\delta_c$ | > | N | $\sigma_c$ | < | $\delta_c$ | > |
| A: | 0.00 - 0.30 | 29 | 0.078 | 0.000 | -0.015 | -0.035 | 28 | 0.100 | -0.010 | -0.035 | -0.055 |
| B: | 0.30 - 0.60 | 13 | 0.103 | -0.040 | -0.080 | -0.120 | 8 | 0.070 | 0.045 | -0.005 | -0.055 |
| C: | 0.60 - 1.50 | 12 | imag | 0.035 | -0.015 | -0.070 | 5 | 0.170 | -0.080 | -0.210 | -0.340 |
| D: | > 0.50 * | 17 | 0.082 | -0.015 | -0.065 | -0.115 | 7 | 0.300 | -0.145 | -0.250 | -0.450 |
| E: | 0.00 - 0.50 | 41 | 0.084 | -0.010 | -0.025 | -0.045 | 35 | 0.095 | -0.010 | -0.030 | -0.050 |
| F: | 0.05 - 0.20 | 18 | 0.073 | 0.020 | 0.000 | -0.020 | 18 | 0.094 | -0.025 | -0.050 | -0.075 |
| G: | 0.00 - 0.20 | 21 | 0.089 | 0.005 | -0.015 | -0.040 | 15 | 0.093 | -0.030 | -0.055 | -0.080 |
| H: | All | 58 | 0.068 | -0.020 | -0.040 | -0.055 | 42 | 0.116 | -0.015 | -0.040 | -0.065 |
| I: | 0.40 - 0.55 | 10 | 0.120 | -0.030 | -0.085 | -0.140 | 7 | 0.063 | 0.030 | -0.020 | -0.070 |

* This group included all those galaxies with unknown redshift. A redshift was assumed for each one on the basis of it's K magnitude and the infrared (K,z) Hubble relation. These galaxies were excluded from the other groups.

deviations from the stellar continuum prediction are insignificantly different from zero, while the underlying scatter is around 0.07 to 0.09 magnitudes, depending in particular on the inclusion or otherwise of the two lowest redshift galaxies. This dispersion is both larger than found by FPAM in their very low redshift elliptical galaxies (0.02) and than the dispersion in the colours of the four FPAM galaxies observed on UKIRT (0.015). This latter fact might suggest that the cause of the scatter in the colours of the radio galaxies may be intrinsic to them, rather than an observational effect. At some level, there are almost certain to be some non-stellar radiation components in the continuum due to the presence of the active nucleus in the galaxies. This would generally be expected to be somewhat redder than the stellar component, and the low redshift (H-K) colour should be fairly sensitive to the addition of such a component due to the different effective spectral indices of the two components. In addition, since the metric size on the galaxy of the constant observing aperture (around 10 arcsec) is smallest at low redshift, the effect of any given additional component will also be greatest at lower redshifts. On the other hand it should be noted that the mean colour is not displaced at all from the stellar relation. If the scatter was caused by the varying strengths of a red non-stellar addition to the continuum, then the mean colour would be expected to be displaced to the red also.

In the two intermediate redshift groups considered (B and I), $\sigma_c$ is slightly larger than found at low redshift, being between 0.1 and 0.12. In addition, the mean colour is displaced to the blue, although in both cases the upper limit to the mean colour is within 0.05 magnitudes of the predicted line. The important point is that

the rather dramatic apparent increase in scatter in the data at redshifts around and greater than 0.4 is to a large degree accounted for by the, largely unavoidable, increase in the formal statistical uncertainties of the observations as the galaxies get progressively fainter.

At high redshift (C and D) both $\sigma_c$ and $\delta c$ are still quite small. The predicted relation is still a relatively good fit to the observations. The results are slightly different depending on the inclusion or otherwise of the galaxies without known redshift, but neither of the $\delta_c$ values are significantly displaced from zero. One interesting feature is the approximately constant value of $\sigma_c$ in the (H-K) part of Table 3.4 over the entire redshift range from zero to unity. This is despite the fact that at low redshift $\sigma_c$ is usually greater than the formal observational uncertainties, whereas at high redshift the converse is true.

For the (J-K) colour the results are much the same as for the analysis of the (H-K) colour except at high redshift. The scatter is slightly larger at low redshift, but there is no increase in this out to redshifts of 0.6. It may be recalled that the scatter in the observed (J-K) colours of the four FPAM ellipticals observed on UKIRT was also higher than in (H-K). The mean colours are consistently bluer than the prediction, but the effect is not large, and it should be recalled that the mean (J-K) colour of the four FPAM ellipticals was also displaced from the values given by them. At high redshifts however (i.e. greater than 0.5) the mean colour of the rather few radio galaxies that have been observed in this colour is over 0.20 magnitudes too blue, and the underlying scatter also

shows a large increase. However, inspection of Figure 3.6 makes it clear that the effect is caused by the three galaxies with redshifts greater than unity. In the case of at least two of these, those with spectroscopically determined redshifts, it has been argued in Section 3.4.a that the (J-K) colour can be seriously affected by the [OIII] 5007 emission line. The strengths of this line in these galaxies can only be estimated from the known strengths of [OII] 3727 at present, but if it is responsible for causing the deviations in the colours, then the equivalent width should be sufficiently high and the line sufficiently narrow that it will be detectable with infrared array spectrographs in the near future. On the other hand, J has been redshifted to sufficiently short wavelengths, near to the rest-frame V passband, that modest changes in the continuum can be accommodated in reasonable models for the evolution of the stellar population of these galaxies (Bruzual 1981). However, the uncertainty introduced by the emission lines means that at present, little can be said about the (J-K) colours of the galactic continua at the highesr redshifts studied.

In summary, the infrared colours of the NLRGs show no evidence for systematic change with redshift once the K-correction is accounted for. In particular, the (H-K) colour, which corresponds approximately to the rest-frame (R-J) colour at redshifts close to unity, is unchanged. This statement may be made from the data with a statistical accuracy of about 0.05 magnitudes, which is in any case also approximately the uncertainty in the model predictions.

3.4.c.(iii) Comparison of these results with those of other workers

Lebofsky (1981) presented a colour-redshift diagram in (H-K) that is fairly well populated with non-radio galaxies for redshifts less than 0.5, and which has five galaxies with redshifts around unity, although one of these (3C 13) now has a revised redshift of 0.477 (Spinrad, private communication), and is in any case probably not the correct identification (Spinrad, another private communication). Despite her use of an erroneous colour-redshift prediction, Lebofsky's general conclusion that there is little intrinsic change in the infrared colours of elliptical galaxies is correct. The large scatter in colour seen in her data, and discussed by her, in the redshift interval between 0.1 and 0.2, and which extends down to (H-K) colours as small as 0.1, is not seen in the radio galaxy data. Ellis (1983) has suggested that this scatter could be caused by the passage of steam bands through the filter passbands, although the effect does seem rather large to be accounted for by this. Although there are unfortunately no galaxies in common in the two samples in this redshift range, the lack of this effect in the radio galaxies suggests that, whatever the reason, it is likely to be an 'observational' effect of some kind rather than a property of the galaxies that requires further explanation.

Lebofsky (1981) also noted that two of her high redshift radio galaxies had, in her view, 'anomalously' blue colours, and these were subsequntly excluded from her analysis of the (K,z) Hubble diagram. One of these was in fact 3C 13, although Lebofsky's (H-K)

colour of 0.22 is still very blue even at the revised redshift. This galaxy has also been observed on UKIRT, and was measured then to be considerably redder, with a colour of 0.65. The other high redshift 'blue' galaxy was 3C 427.1. This galaxy would not be at all anomalous on Figure 3.5, however, and the classification of this galaxy as 'blue' is a consequence of Lebofsky's much redder colour prediction at high redshift. Although the underlying scatter of these four high redshift galaxies is much higher than seen in the UKIRT data, being about 0.25 when the purely observational uncertainties are accounted for, the mean colour displacement from the modified Bruzual relation is not significant, being only 0.19 magnitudes with an uncertainty in this number of 0.17. This is in the sense of the galaxies being generally redder than the prediction.

In contrast, Puschell et al (1982, POL) have published photometry on 22 3CR radio galaxies, most of which were at high redshift. Their analysis was primarily aimed at obtaining improved estimates of the redshifts of those galaxies that had not had spectroscopically determined redshifts by using their photometric broad-band colours. In this analysis they were only partially successful. Only about a half of the galaxies that did have spectroscopic redshifts had 'photometric' redshifts based on the simplest model that were consistent with the known redshifts even at the $2\sigma$ level. This fraction did increase, though, if evolutionary models were used. They did note that "for galaxies whose colours were not consistent with these models, deviations occur not only in the optical bands but also in the infrared". This is illustrated in Figures 3.7 and 3.8, in which (H-K) and (J-K) colours, constructed

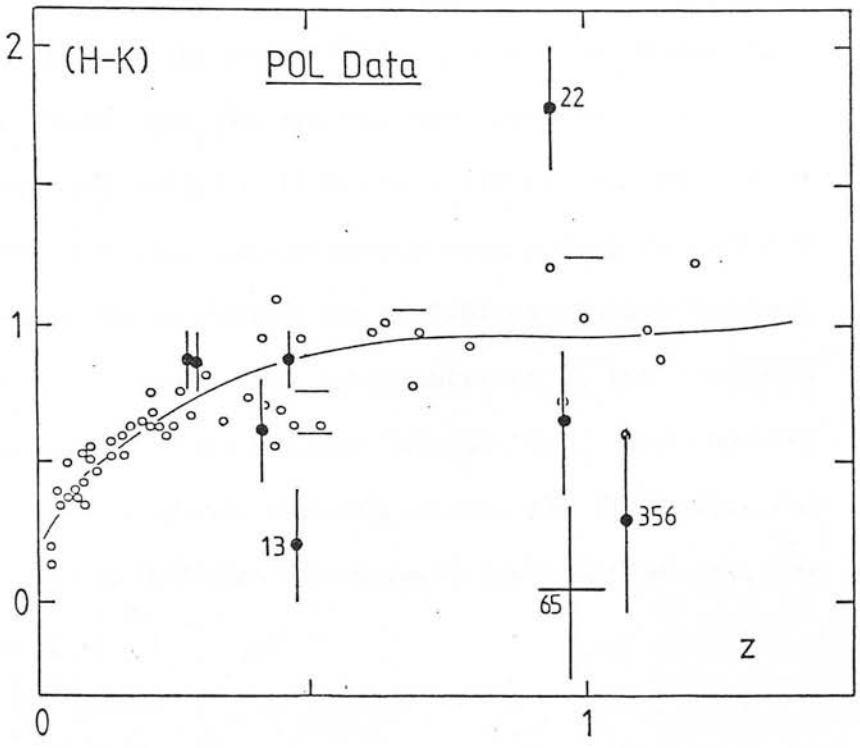


Figure 3.7: The (H-K) colours measured for NLRGs by Puschell et al (1982) (solid circles) compared with the results of the current investigation (open circles). The UKIRT data do not exhibit the scatter seen in the other work.

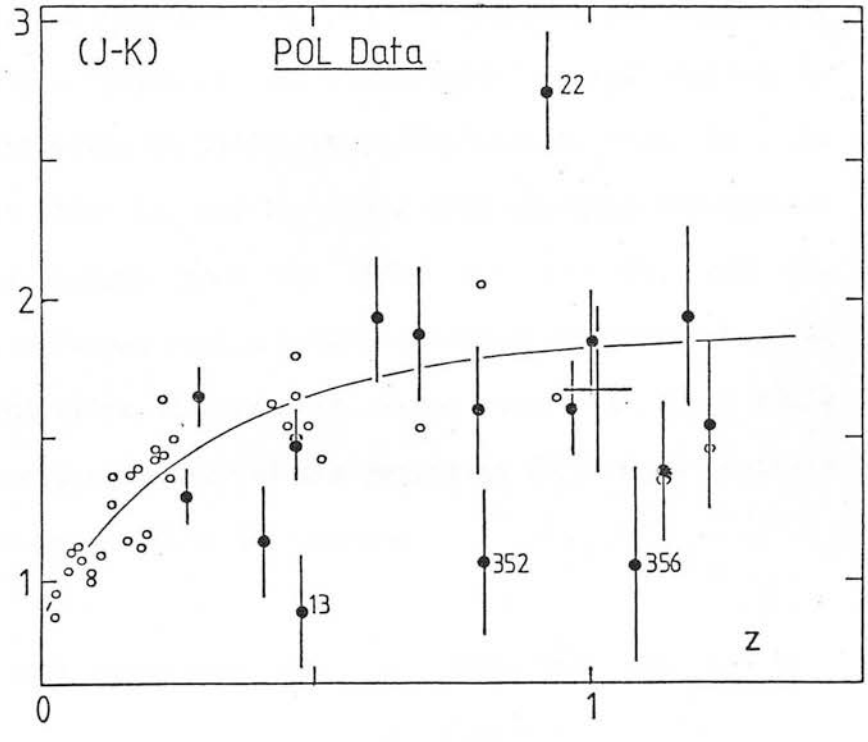


Figure 3.8: As for Figure 3.7 but for (J-K). The large scatter in colours is again not seen in the UKIRT data.

from the flux densities and the calibration listed by them, have been plotted. One BLRG and the two CRS have been omitted for the same reason that they are excluded from the analysis of the UKIRT data, namely their possible contamination from strong non-stellar components. A colour equation correction of 0.07 magnitudes has been applied to the J data, though this is unimportant in the following discussion. The contrast between Figures 3.5 and 3.7, and between Figures 3.6 and 3.8 is clear. For comparison, the UKIRT data has been replotted on Figures 3.7 and 3.8 as small open circles without error bars.

The large and general scatter in the POL data is not seen in the UKIRT sample. The explanations (POL) for this scatter in terms of the addition of non-stellar quasar-like components is unconvincing. There is a significant fraction of sources in common between the two samples. In (H-K), the four most extreme POL objects, 3Cs 13,22,65, and 356 have all been found to have essentially 'normal' colours in the present investigation on UKIRT, while the same is true for the (J-K) colours of 3Cs 13 and 22. Given this apparent discrepancy between the observations made on UKIRT and by POL, and the consistency of the former with a single infrared continuum shape at essentially all redshifts studied, it seems unlikely that POL's suggestion of the possibility of the necessity of a major revision of current evolutionary models is correct.

Over the redshift range over which a comparison may be made (i.e. out to a redshift of 0.5), the colours of the radio-quiet elliptical galaxies studied by Ellis and Allen (1983) follow the same colour-redshift relation in (J-K) as the radio galaxies

observed in the current investigation.

3.4.d The Optical to Infrared Colours (V-K) and (r-K)

Whereas the data presented in this chapter has created a large and homogeneous data set of infrared photometry for 3CR galaxies, the optical photometry that has been published on these objects is much less uniform in coverage. Indeed, for almost half of the galaxies that were observed in the infrared, the best available optical measurement is an eye-estimate from the photographic plate material on which the galaxy was first identified. These estimated magnitudes are believed to be accurate to only about 1 magnitude, and have in any case been made in a variety of ill-defined passbands. Hence they are virtually useless for constructing the optical to infrared colours.

Sandage (1972b) published much data on most of the 3CR galaxies that had been identified at that time. With the odd exception, however, these are at redshifts less than 0.30. Kristian et al. (1978) published some photometry on a limited number of more distant radio galaxies in connection with their optical Hubble diagram programme, but the greatest contribution came with the introduction of the PFUEI CCD system on the Palomar 5m telescope. This readily provided fairly accurate magnitudes for the faintest identifications that had not been previously identified on photographic plates. The consequence of this is that optical photometry is therefore available for many of the brightest sources, at redshifts less than 0.25, and for many of the faintest, at redshifts close to unity or even greater, but is much sparser for galaxies at intermediate

redshifts.

At the faint end of the sample, where the galaxies for which (r-K) colours are derivable are found, there is therefore a crude selection in apparent magnitude since in order to have a CCD magnitude the identification would have to be sufficiently faint that non-photographic identification or confirmation of a doubtful identification had been required. This selection is not directly related to either the redshift, absolute magnitude or colour, but a bias in the colour distribution at a given redshift may still conceivably be introduced. At any given redshift the preferential inclusion of the optically faintest galaxies will, all other things being equal, bias the colour distribution against the bluer galaxies in any population that exhibits a spread in colour. The effect of this is very difficult to estimate because it will depend on the relative importance of the scatter in both colour and absolute magnitude, and on the possible interelation of the two. Furthermore, the initial selection by apparent magnitude is in any case difficult to quantify. It is not thought that this bias will be serious, at least in a sample as small as is available here, but its possible presence should, however, be noted.

Optical to infrared colours (V-K) and (r-K) have been derived for all those galaxies that have been observed in the infrared on UKIRT, and which have either published photoelectric V, or r CCD, photometry. The derivation of these colours is slightly less straight forward than that of the infrared colours, since in some cases both aperture corrections and sometimes quite sizeable corrections for the effects of galactic extinction in the optical

Table 3.5: The Derivation of the (V-K) colours.

| | z | $V_{pub}$ | Ref | $\Delta m_{ap}$ | $A_v$ | $V_{corr}$ | K | (V-K) |
|---|---|---|---|---|---|---|---|---|
| 13 | 0.477 | 22.10 ± 0.30 | SSB | +0.40 | 0.18 | 21.52 | 16.36 ± 0.10 | 5.16 ± 0.32 |
| 19 | 0.482 | 20.47 ± 0.10 | KSW | - | 0.18 | 20.29 | 15.55 ± 0.05 | 4.74 ± 0.11 |
| 28 | 0.195 | 17.84 ± 0.05 | S5 | - | 0.12 | 17.72 | 13.77 ± 0.05 | 3.95 ± 0.07 |
| 33 | 0.060 | 15.82 ± 0.05 | S5 | - | 0.03 | 15.79 | 12.32 ± 0.01 | 3.47 ± 0.05 |
| 76.1 | 0.032 | 15.88 ± 0.05 | S5 | - | 0.30 | 15.58 | 12.07 ± 0.02 | 3.51 ± 0.05 |
| 79 | 0.256 | 18.75 ± 0.05 | S3 | - | 0.27 | 18.48 | 14.43 ± 0.04 | 4.05 ± 0.06 |
| 98 | 0.031 | 15.42 ± 0.05 | S5 | - | 0.36 | 15.06 | 11.90 ± 0.02 | 3.16 ± 0.05 |
| 109 | 0.306 | 18.01 ± 0.05 | S3 | - | 0.75 | 17.26 | 12.52 ± 0.02 | 4.74 ± 0.05 |
| 123 | 0.218 | 20.37 ± 0.20 | KSW | -0.04 | 1.17 | 19.24 | 14.23 ± 0.03 | 5.01 ± 0.21 |
| 171 | 0.238 | 18.90 ± 0.05 | S3 | -0.04 | 0.18 | 18.76 | 14.69 ± 0.11 | 4.07 ± 0.12 |
| 192 | 0.060 | 16.10 ± 0.05 | S5 | - | 0.12 | 15.98 | 12.47 ± 0.01 | 3.51 ± 0.05 |
| 219 | 0.174 | 17.44 ± 0.05 | S5 | -0.05 | - | 17.49 | 13.55 ± 0.01 | 3.94 ± 0.05 |
| 223 | 0.137 | 17.41 ± 0.05 | S3 | -0.05 | - | 17.46 | 13.82 ± 0.02 | 3.64 ± 0.06 |
| 234 | 0.185 | 17.27 ± 0.05 | S3 | -0.04 | 0.03 | 17.28 | 12.65 ± 0.01 | 4.63 ± 0.05 |
| 236 | 0.099 | 16.23 ± 0.05 | S3 | -0.20 | 0.03 | 16.40 | 12.69 ± 0.01 | 3.71 ± 0.06 |
| 265 | 0.811 | 20.04 ± 0.10 | KSK | - | - | 20.04 | 16.01 ± 0.09 | 4.03 ± 0.14 |
| 285 | 0.079 | 16.59 ± 0.05 | S3 | -0.06 | - | 16.63 | 13.11 ± 0.01 | 3.52 ± 0.05 |
| 295 | 0.459 | 19.76 ± 0.10 | S5 | - | - | 19.76 | 14.49 ± 0.05 | 5.27 ± 0.12 |
| 299 | 0.367 | 19.43 ± 0.05 | KSW | -0.10 | - | 19.53 | 15.91 ± 0.06 | 3.62 ± 0.08 |
| 310 | 0.054 | 16.33 ± 0.05 | S3 | - | - | 16.33 | 12.49 ± 0.01 | 3.84 ± 0.05 |
| 315 | 0.109 | 16.49 ± 0.05 | S3 | -0.20 | 0.09 | 16.60 | 13.36 ± 0.03 | 3.24 ± 0.07 |
| 318 | 0.752 | 20.90 ± 0.10 | SS | +0.15 | 0.09 | 20.66 | 16.96 ± 0.15 | 3.70 ± 0.18 |
| 381 | 0.161 | 17.66 ± 0.05 | S5 | -0.05 | 0.12 | 17.59 | 13.90 ± 0.02 | 3.69 ± 0.06 |
| 382 | 0.059 | 15.39 ± 0.05 | S5 | -0.04 | 0.27 | 15.16 | 11.00 ± 0.02 | 4.16 ± 0.06 |
| 388 | 0.091 | 16.04 ± 0.05 | S5 | -0.06 | 0.18 | 15.92 | 12.60 ± 0.02 | 3.32 ± 0.06 |
| 433 | 0.102 | 15.74 ± 0.05 | S3 | -0.20 | 0.30 | 15.64 | 12.37 ± 0.01 | 3.27 ± 0.06 |
| 438 | 0.290 | 19.18 ± 0.05 | KSW | -0.05 | 0.78 | 18.45 | 14.01 ± 0.03 | 4.44 ± 0.07 |
| 452 | 0.081 | 16.99 ± 0.05 | S5 | - | 0.51 | 16.48 | 12.91 ± 0.02 | 3.57 ± 0.06 |

References:


S3 Sandage (1972b)
S5 Sandage (1973)
SS Spinrad and Smith (1976)
SSB Spinrad et al (1981)
KSW Kristian et al (1978b)
KSK Kristian et al (1978a)

wavebands are required. The aperture correction was based on the optical growth curve for 1st ranked cluster galaxies given by Sandage (1972a). It will be shown in Chapter 7 that this is a reasonable representation of the growth curve of 3CR radio galaxies. The correction for galactic extinction was derived from the reddening maps of Burstein and Heiles (1982, see Appendix 1). Table 3.5 lists the galaxies for which (V-K) colours have been derived and details the optical photometry, its source, and the corrections applied to it in deriving the colour, since these can be quite large.

In the case of the r CCD photometry, the published photometry of Gunn et al (1981, GHWPL) was not used. In order to obtain a more precise value for the uncertainty in each measurement that is given by GHWPL, rather than the cautious 0.5 magnitudes uncertainty which they took for all their measurements regardless of the brightness of the galaxy, the original CCD exposures and a few others not previously published, were re-reduced and re-analysed. The principal motivation for this was that, with errors on the colours of over 0.5 magnitudes, it was difficult to determine from the distribution of the colours whether they showed an underlying scatter. The re-reduction of this data followed exactly the standard procedure described by GHWPL and in Chapter 7 of this Thesis. New magnitudes were measured, using the interactive E2D software package on STARLINK, by placing a circular aperture of known size over the galaxy image. The size of this aperture was chosen to be similar to that used for the infrared measurements. The uncertainty in this measurement was found by repeatedly measuring the standard deviation of the sky flux measured through the same aperture when it was moved

over 'empty' areas of sky. During this analysis, it was noticed that the magnitudes of some of the faintest galaxies had been measured to be significantly brighter than the values given by GHWPL, despite the use of exactly the same basic data. Discussions with Dr. Perryman (who originally analysed this data and who produced the GHWPL magnitudes) have suggested that this discrepancy may be attributable to the very inferior image display devices available to him, compared with the extremely flexible ARGS television monitors that can be used today. For instance, GHWPL were unable to see the image of 3C 65 in r in 1980, although this galaxy is clearly seen on an ARGS display, and a magnitude can be easily measured. Similarly, it is likely that an identification for the GHWPL 'empty field' source 3C 68.2 is in fact visible on the exposures of that field. An r magnitude of 23.6 has been measured for this object. The revised r (and i) magnitudes, corrected for galactic exrinction, for these galaxies are listed in Table 3.6 together with the extinction correction. Those data not previously published in any form (i.e. that do not appear in GHWPL) are indicated by an asterisk. The apertures used for the optical measurements are sufficiently similar to the infrared apertures used and the galaxies are sufficiently distant that no aperture corrections are neccessary, and the (r-K) colour may be constructed from the magnitudes given in Tables 3.2 and 3.6.

Because all but two of the galaxies with (V-K) colours have redshifts less than 0.5, while all those with (r-K) colours have redshifts larger than this, a composite optical-infrared colour-redshift diagram has been constructed in Figure 3.9. The data have been represented on Figure 3.9 using the same conventions that

Table 3.6: CCD r Photometry for Faint 3C Radio Galaxies.

| 3C | d(") | $A_r$ | $A_i$ | r | i | Comments. |
|---|---|---|---|---|---|---|
| 34 | 6.0 | 0.08 | 0.06 | 20.93 ± 0.05 | - | |
| | 8.6 | " | " | 20.60 ± 0.07 | - | |
| | 12.9 | " | " | 20.13 ± 0.10 | - | |
| 61.1 | 8.6 | 0.21 | 0.16 | 19.55 ± 0.06 | - | GHWPL 'a' |
| | 8.6 | " | " | 18.61 ± 0.06 | - | GHWPL 'b' |
| 65 | 5.2 | 0.11 | 0.08 | 23.00 ± 0.25 | 21.51 ± 0.10 | |
| | 8.6 | " | " | 22.65 ± 0.30 | 21.22 ± 0.30 | |
| 68.2 | 4 | 0.19 | 0.14 | 23.61 ± 0.35 | - | New cand. ? |
| 175.1 | 5.2 | 0.26 | 0.20 | 21.59 ± 0.15 | - | |
| 184 | 8.6 | 0.04 | 0.03 | 21.94 ± 0.14 | 21.14 ± 0.30 | |
| 220.3 | 8.6 | 0.06 | 0.04 | 20.14 ± 0.15 | - | |
| 239 | 8.6 | 0 | 0 | 21.96 ± 0.30 | 21.25 ± 0.30 | |
| 241 | 6.0 | 0.02 | 0.01 | 22.90 ± 0.21 | 22.33 ± 0.25 | |
| 250 | 8.6 | 0 | 0 | 22.04 ± 0.16 | - | |
| 267 | 8.6 | 0 | 0 | 22.06 ± 0.12 | - | |
| 268.3* | 8.6 | 0 | 0 | 19.94 ± 0.05 | - | |
| 272 | 6.0 | 0 | 0 | 23 ± 1 | - | |
| 280 | 6.0 | 0 | 0 | 21.57 ± 0.07 | - | |
| 289 | 8.6 | 0 | 0 | 21.93 ± 0.15 | - | |
| 305.1* | 8.6 | 0.04 | 0.03 | 21.10 ± 0.06 | - | |
| 322* | 8.6 | 0.02 | 0.01 | 23.03 ± 0.50 | - | 3 galaxies. |
| 324 | 8.6 | 0.06 | 0.04 | 21.34 ± 0.16 | - | Cent. on No 1. |
| 356* | 4.3 | 0.04 | 0.03 | 21.84 ± 0.22 | - | |
| 368 | 8.6 | 0.39 | 0.30 | 21.00 ± 0.20 | - | |
| 469.1 | 4.3 | 0.47 | 0.36 | 22.00 ± 0.16 | - | |

Note: The magnitudes for the galaxies indicated by an asterisk have not been published in any form. The remaining magnitudes are from a reanalysis of the CCD frames that originally appeared in Gunn et al (1981). Some of the fainter ones are significantly revised.

were used in Figures 3.5 and 3.6. Three lines have been drawn on the diagram to aid discussion. The first, labelled NE, is the equivalent of the line drawn on the infrared colour diagrams, and represents the colour that is predicted as a function of redshift for an elliptical galaxy spectrum that does not change with redshift. This has been constructed using the K-corrections given for the V band by Whitford (1975) for redshifts less than 0.5, those for the r band given by Schneider et al.(1983a) at higher redshift, and those given by Bruzual (1981) for the infrared K passband over the entire redshift range.

Some consideration should be given to the possible effects of colour gradiants in these galaxies since the change in redshift corresponds to a change in the metric size of the aperture on the galaxies. In fact the change in size betwen redshifts of 0.1 and 1 is not very large, being at most a factor of 4. There would have to be a very large colour gradient to produce a significant change to the integrated colour over such a range.

Although it is the intention to avoid the introduction of interpretation in to this presentation of data and basic results, the fit to the data at high redshift of this prediction is so poor (c.f. Figure 3.5) that another line has also been plotted. This second curve (C) is based upon the colours predicted for an elliptical galaxy whose spectrum does change with redshift in the way expected due to the evolution with cosmic time of the integrated spectrum of a coevally formed population of stars. This has been derived from the models of Bruzual (1981), and will be discussed much further in Chapter 5. For the present, the curve represents an

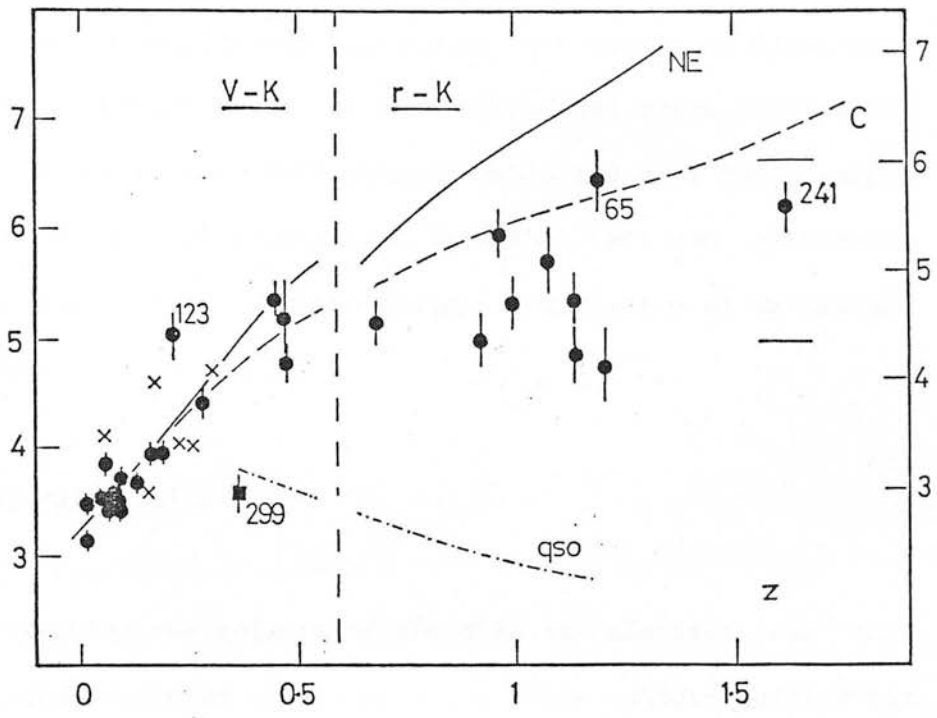


Figure 3.9: The optical-infrared colours (V-K) and (r-K) for 3C radio galaxies. The data have been plotted with the same conventions as Figures 3.5 and 3.6. The solid line represents the expected colour-redshift relation for an elliptical galaxy spectrum that does not change with redshift. The line labelled C is the relation predicted by a model for the stellar population that incorporates the ageing of the main sequence turnoff (Bruzual 1981). The dot-dash line marks the approximate upper envelope of typical quasar colours.

alternative 'null hypothesis' by which the the observed colours may be compared at different redshifts. The vertical normalisation of the two halves of Figure 3.9 has been adjusted so that these two predictions are approximately continuous, the better to illustrate the trend that is exhibited by the data. The final curve (QSO) marks the upper envelope of the (V-K) colours exhibited by a large sample of quasars. This has been constructed from the infrared photometry of Hyland and Allen (1982) and the optical compilation of Hewitt and Burbidge (1980).

3.4.d.(i) General Results

Broadly speaking the colours of the NLRG at redshifts less than 0.5 follow the predicted relations well. Their colours quickly get redder with increasing redshift as the K passband moves up to the maximum in the galaxy spectral energy distribution, while the V band moves down in to the restframe ultraviolet below 4000 A. A few anomalies are however apparent: 3C 123 has a rather redder colour than expected. Although a galactic extinction correction of 1.25 magnitudes has been applied to the colour, the residual redness probably indicates that this is not sufficient. The two other galaxies that show most deviation from the relation at low redshift (3C 310, which is blue and 3C 315, which is red) are both dumbell systems. Although very similar apertures were used for both optical (Sandage 1972b) and infrared measurements, the derived colours will be very sensitive to the relative positioning of the optical and infrared apertures. The infrared aperture was always centred on the position of the nucleus of the radio source.

The colours of the BLRG, however, show considerable scatter about the 'stellar' relation, and are found to be both bluer and redder. The interval of 10 years between optical and infrared measurement of these possibly variable objects makes detailed interpretation uncertain. Nevertheless, the BLRG with infrared colours that differ most from starlight (Figures 3.5 and 3.6) are all redder than starlight in (V-K) while those that have less discrepant colours in the infrared are bluer than the standard elliptical galaxy in (V-K). A power-law component of spectral index of 1.5 has a (V-K) colour of about 4.3, and hence quite large non-stellar components of this form may be added to otherwise normal galaxies at redshifts around 0.2 without producing large colour changes in the integrated (V-K) colour.

The two compact radio sources (CRS), 3C 299 and 3C 318, have (V-K) colours, 3.6 and 3.7 respectively, that are very different from those of the NLRG at the same redshifts. The two CRS have similar colours even though they are at different redshifts, a behaviour which is also shown by a power-law SED. Both the CRS have colours that are close to the upper envelope of quasar colours. These two galaxies have unusually blue optical colours too (Kristian et al 1978and Spinrad and Smith 1976). A deep CCD image of 3C 318 obtained on UKIRT by the author is clearly dominated by an unresolved nuclear component, while the plate of 3C 299 given by Spinrad and Smith (1976) also appears to show some central condensation of the image. It should be recalled that the majority of 3CR sources with compact radio structure are identified with quasars, and there is little doubt that the colours of these two remaining objects are dominated by non-stellar radiation components.

The (r-K) colours of the 12 radio galaxies at high redshifts are clearly substantially and systematically bluer than the (NE) prediction, a trend that is becoming apparent in the (V-K) colours of the three galaxies with redshifts around 0.5. The size of this gross deviation is about 1.5 magnitudes at a redshift of one. The effect is reduced somewhat if the 'passively evolving' spectral energy distribution (C) is used, but is nevertheless still significant. However, the r passband is shifted in to the near ultraviolet (3200 A) at a redshift of unity, and hence it is neccessary to first check that, at low redshift, the ultraviolet colours of the radio galaxies match the ultraviolet spectral energy distribution of normal non-radio elliptical galaxies, on which, of course, the two curves in Figure 3.9 are based.

3.4.d.(ii) The near-ultraviolet continua of low redshift radio galaxies

The data on the near-ultraviolet continua of radio galaxies comes from two sources. These are the UBV photometry of Sandage (1972b) and the spectrophotometry of Yee and Oke (1978).

Figure 3.10 shows the (U-B) colours of all the radio galaxies observed by Sandage (1972b). These colours have been corrected for galactic extinction. BLRGs (crosses) and NLRGs (circles) have been distinguished on Figure 3.10 using exactly the same criteria as used in the rest of this investigation (i.e. principally the classification of Grandi and Osterbrock 1978). Those NLRG that are in the 90 source sub-sample and that have been observed in the

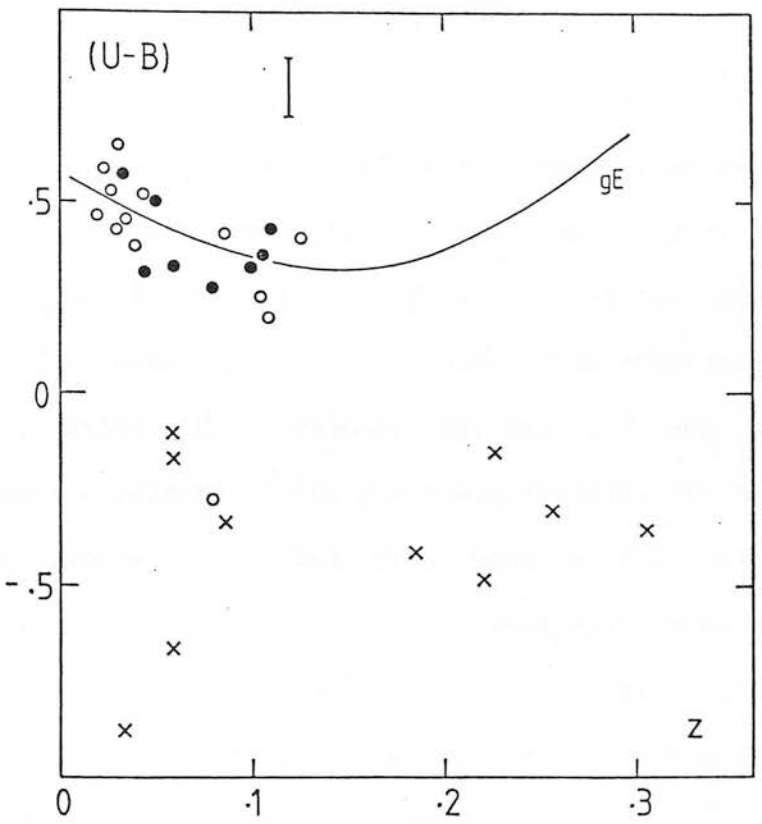


Figure 3.10: The (U-B) colours of a sample of 3C radio galaxies observed by Sandage (1972b). Distinction between NLRG (circles) and BLRG (crosses) has been made on exactly the same criteria as in the previous diagrams. The solid circles represent 3C galaxies that were observed on UKIRT in this programme. All but one of the NLRG are very close to the colour of a normal giant elliptical at that redshift which is shown as the solid line. The small bar represents typical observational error.

infrared as part of this investigation are indicated by filled circles on Figure 3.10. The solid line represents the K-corrected colour prediction of Coleman et al (1980), and the typical observational uncertainty in the data is indicated by the short error bar.

With the clear exception of 3C 198, all of the radio galaxies in Sandage's sample that are classified as NLRG have colours that are essentially indistinguishable from those of a radio-quiet giant elliptical galaxy. The BLRG, on the other hand, show substantial ultraviolet excesses, having (U-B) colours between 0.5 and 1.0 magnitudes bluer than the colours of the giant ellipticals. One NLRG in the 20 in the sample (i.e. 5%) does have a substantial ultraviolet excess. It is difficult to assess whether any biases are present in this data set. Sandage analysed his data primarily in terms of the optical morphology of the galaxy, and distinguished between N-systems and other more normal elliptical types (e.g. E, D, cD etc)

Yee and Oke (1978) obtained spectrophotometry for 17 NLRG and 9 BLRG (assuming that 3C 17 and 3C 456 are BLRG: see their discussion). Their data cover the spectral range from about 3000 A in the rest frame to around 1 micron. In their discussion of the ultraviolet continua of these galaxies, Yee and Oke divided the objects in to 4 groups depending to a large degree on the relative strengths of the galaxy and non-stellar components. Those in the first group, which contained over half the NLRGs in the sample, have energy distributions that were the same as the standard elliptical galaxy. The second group contained a further five NLRG and contained

objects that had 'small ultraviolet excesses'. However the (U-B) colours of those two in this group which were observed by Sandage (e.g. Sandage 1972a) are not abnormal on Figure 3.10 and the small excesses in these galaxies probably do not have a large effect on the colours. The two remaining NLRGs were in Yee and Oke's third group, which also contains most of the BLRGs in their sample. One of these two is 3C 198, which it was noted above had a (U-B) colour similar to the BLRGs and it is likely that the other NLRG in this group (Cygnus A, 3C 405) also has similar colours. Yee (1980) claims that these radio galaxies form a representative sample of 3CR galaxies at redshifts less than 0.09. Thus two out of 17 NLRGs in the sample (i.e. 12%) probably have ultraviolet excesses of the order of 0.5 magnitudes.

In summary, the evidence from low redshift 3C NLRG is that most have continua from 3000 A to 2 microns that are indistinguishable from those of radio-quiet giant elliptical galaxies. However, a small fraction of radio galaxies at low redshift (probably around 15% or less) do show quite significant enhancements of their near ultraviolet flux densities that can amount to 0.5 magnitudes. These are believed to be caused by non-stellar radiation components of approximately power-law form (Yee and Oke 1978).

3.4.d.(iii) The (r-K) colours of radio galaxies at redshifts of unity

The twelve galaxies for which (r-K) colours are available form a small homogeneous sample. As discussed above the only possible selection effect that could make this sample unrepresentative of the

larger sample, for which optical data is not available, is that the sub-sample may conceivably be biased against the inclusion of the bluest galaxies at a given redshift. Nine of these galaxies have a spectroscopically determined redshift, including 3C 241 at a redshift of 1.62 (Spinrad private communication).

The colours of these nine radio galaxies that can be precisely placed on the colour-redshift diagram are all substantially bluer than the 'NE' colour-redshift relation and many are significantly bluer than the passively evolving 'C' model prediction. Indeed, no galaxy with measured redshift in this sample has a colour that is redder than this 'C' model prediction, and there is a considerable range in colour, of about 1 magnitude, that extends bluewards of this line. This may be contrasted with the much smaller scatter shown in both Figures 3.5 and 3.10. From the very poor fit of the NE line to the data, there is clearly a difference in the continuum spectral energy distributions (SED) between the 3C radio galaxies at high and low redshift. An additional component that enhances the ultraviolet flux density must be present in many if not all of the high redshift radio galaxies. The data rather suggests that in fact two processes may be occuring, the first in all galaxies and the second in about two thirds of the sample.

One important clue as to the identification of this component is the scatter in colours that is observed. This implies that the strength of the new component must vary from galaxy to galaxy. This strongly suggests that it is caused by a process that can occur independently in each galaxy. For instance, it is unlikely to be caused by the appearance in a coeval stellar population of a

hitherto unsuspected (or unmodelled) population of stars, because that would, assuming all the galaxies were formed at a similar time, lead to a similar strength component in all the galaxies at a given redshift. In other words, the data do not simply suggest that the 'C' model has been incorrectly constructed or that colour gradients are more important than thought. On the contrary, the fact that the 'C' model colour-redshift prediction follows the red limits of the colour distribution rather supports its correctness. This point will be explored much further in Chapter 5.

In order to investigate the additional component that causes the change in colour it is convenient to quantify the colour excess in the galaxies. A blueness parameter, $\Delta$(r-K), was defined to be the difference between the predicted 'C' model colour and the observed colour for each galaxy. Most of the galaxies with measured redshift are at redshifts between 0.9 and 1.2, and this a sufficiently small range that the $\Delta$(r-K) values may be directly compared. 3C 34 is at a lower redshift of 0.69. It would be expected that the effect of any given addition would be greater as the r passband is redshifted further in to the ultraviolet. To compensate for this effect, the value of $\Delta$(r-K) has been increased by 25% from 0.4 to 0.5, although this does not in fact change the ranking of the galaxy colours. Because of the very small aperture used for the infrared measurement of 3C 175.1, and the subsequent possibility that the infrared flux density may have been underestimated, the value for $\Delta$(r-K) given for 3C 175.1 should be regarded as an upper limit. Finally the three galaxies with unknown redshift (including 3C 65), and 3C 241 (at a redshift of 1.62), have been assigned a qualitative value of the (r-K) parameter, since a precise estimate is impossible due to the

Table 3.7: The Blueness Parameter Δ(r-K).

| | z | Δ(r-K) | $W_{\lambda 0}$ A | I | $S_{c5}$ mJy | log $P_{c5}$ $WHz^{-1}sr^{-1}$ | Θ " | d kpc |
|---|---|---|---|---|---|---|---|---|
| 34 | 0.69 | 0.5a ± 0.20 | 91 | <0.1 | 0.6 | 24.60 | 48 | 380 |
| 175.1 | 0.92 | <1 ± 0.25 | 52 | <0.1 | 1.8 | 25.22 | 7 | 59 |
| 267 | 1.14 | 1.0 ± 0.20 | 360 | - | 3.2 | 25.57 | 38 | 326 |
| 280 | 0.99 | 0.9 ± 0.15 | 235 | 0.18 | 1.2 | 25.08 | 13 | 110 |
| 289 | 0.97 | 0.2 ± 0.15 | 104 | - | 1.2 | 25.07 | 10 | 85 |
| 324 | 1.21 | 1.7 ± 0.30 | 340 | - | <0.6 | <24.87 | 10 | 86 |
| 356 | 1.08 | 0.6 ± 0.25 | 165 | 0.32 | 0.9 | 24.99 | 75 | 643 |
| 368 | 1.13 | 1.4 ± 0.25 | 700 | 0.03 | <0.6 | <24.83 | 9 | 78 |

Galaxies with Qualitative Δ(r-K):

| | |
|---|---|
| 65 | small |
| 68.2 | small |
| 239 | large |
| 241 | small |

Table 3.8: Estimated Redshifts.

| 3C | K | z* |
|---|---|---|
| 68.2 | 17.73 | 1.64 |
| 4C14.27 | 15.66 | 0.51 |
| 217 | 17.76 | 1.67 |
| 225B | 15.79 | 0.55 |
| 226 | 16.14 | 0.68 |
| 228 | 16.19 | 0.70 |
| 239 | 17.67 | 1.59 |
| 437 | 18.02 | 1.91 |
| 470 | 18.49 | 2.34 |

quite large variation in the predicted colour of over the redshift range in which these sources are most likely to lie. Provided, however, that they are between redshifts of 1 and 2 (which is likely on the basis of their K magnitudes and the infrared Hubble diagram presented in the next section) then it is clear from Figure 3.9 that 3C 239 has a relatively 'large' colour excess, while 3C 65, 3C 68.2 have 'small', or even negative values of $\Delta(r-K)$. Given the higher redshift of 3C 241, it is also clear that the colour excess of this galaxy is towards the lower end of the range exhibited by the others at redshifts near to unity. The adopted values of $\Delta(r-K)$ are listed in Table 3.7 for all twelve galaxies.

In spite of the small numbers of galaxies available for analysis, possible relations between $\Delta(r-K)$ and other properties of the radio galaxies have been examined. In particular, the values of one spectroscopic parameter, the equivalent width of the [OII] 3727 line, and one radio parameter, the nuclear core luminosity, have been found for as many of the galaxies as possible. The equivalent width of [OII] 3727 is available (Spinrad 1982 and private communication) for all those galaxies with measured redshift except 3C 241, which is at sufficiently high redshift that the line has been redshifted out of the optical waveband. Equivalent widths in the rest-frame of the galaxy are tabulated in Table 3.7 for the eight other galaxies. The nuclear core radio luminosities have been derived from the flux densities at 6 cm (5 GHz) kindly supplied by Dr. Laing (Private communication) from data obtained with the VLA radio telescope. Measurements or upper limits are available for all the galaxies in this reduced sample except 3C 241, which is insufficiently resolved. The nuclear core luminosity is more useful

than the total radio luminosity because the latter, in a flux density limited sample such as the 3CR, is inevitably strongly correlated with the redshift because most of the sources will be close to the flux density limit. In any case, the nuclear luminosity is probably a better indicator than the total radio luminosity of the current level of activity in the nucleus, since the latter is dominated by the two radio lobes situated several hundred kiloparsecs from the nucleus and which therefore must reflect the activity of at least $10^5$ years ago. The core luminosity was derived assuming $H_0 = 50$ kms$^{-1}$Mpc$^{-1}$, $q_0 = 0.5$ and a spectral index for the radio cores of 0.0. Since the sources are all at approximately the same redshift these assumptions have only a weak effect on the relative luminosities.

$$P(\mathrm{WHz^{-1}sr^{-1}}) = 1.73\ 10^{28}.\ (1-(1+z)^{-\frac{1}{2}}))\ .\ (1+z)^{-1}\ .\ S(\mathrm{Jy}) \qquad (3.5)$$

The equivalent widths of [OII] 3727, radio core luminosities and radio source size are plotted against the blueness parameter $\Delta(r-K)$ in Figures 3.11a-c.

While there is clearly no trend of colour with nuclear luminosity or source size, there is a fairly clear relation between colour and oxygen equivalent width. The significance of this has been examined using the Spearman Rank Test. Even if 3C 175.1 has a colour excess of 1 (i.e. the worst case) the correlation is still significant at the 95% level. In other words, this diagram has only a 5% chance of representing an underlying population in which colour and line equivalent width are unrelated. If 3C 175.1 is completely excluded from the analysis then the significance increases to 99%.

Figure 3.11a-c:
The blueness parameter $\Delta(r-K)$ for 8 3C radio galaxies at high z is plotted against:

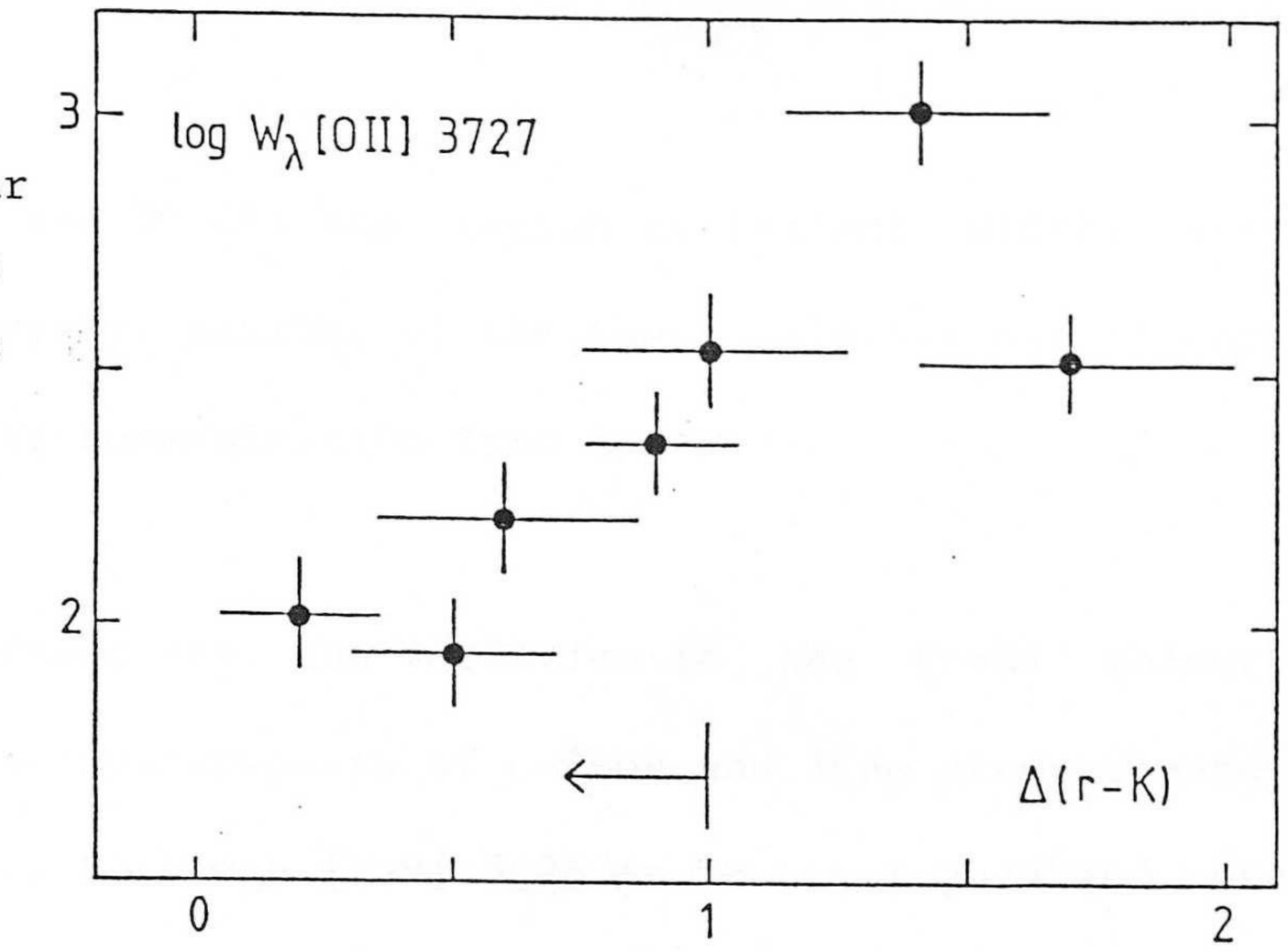


(a) The log of the Equivalent Width in A of |O II| 3727.

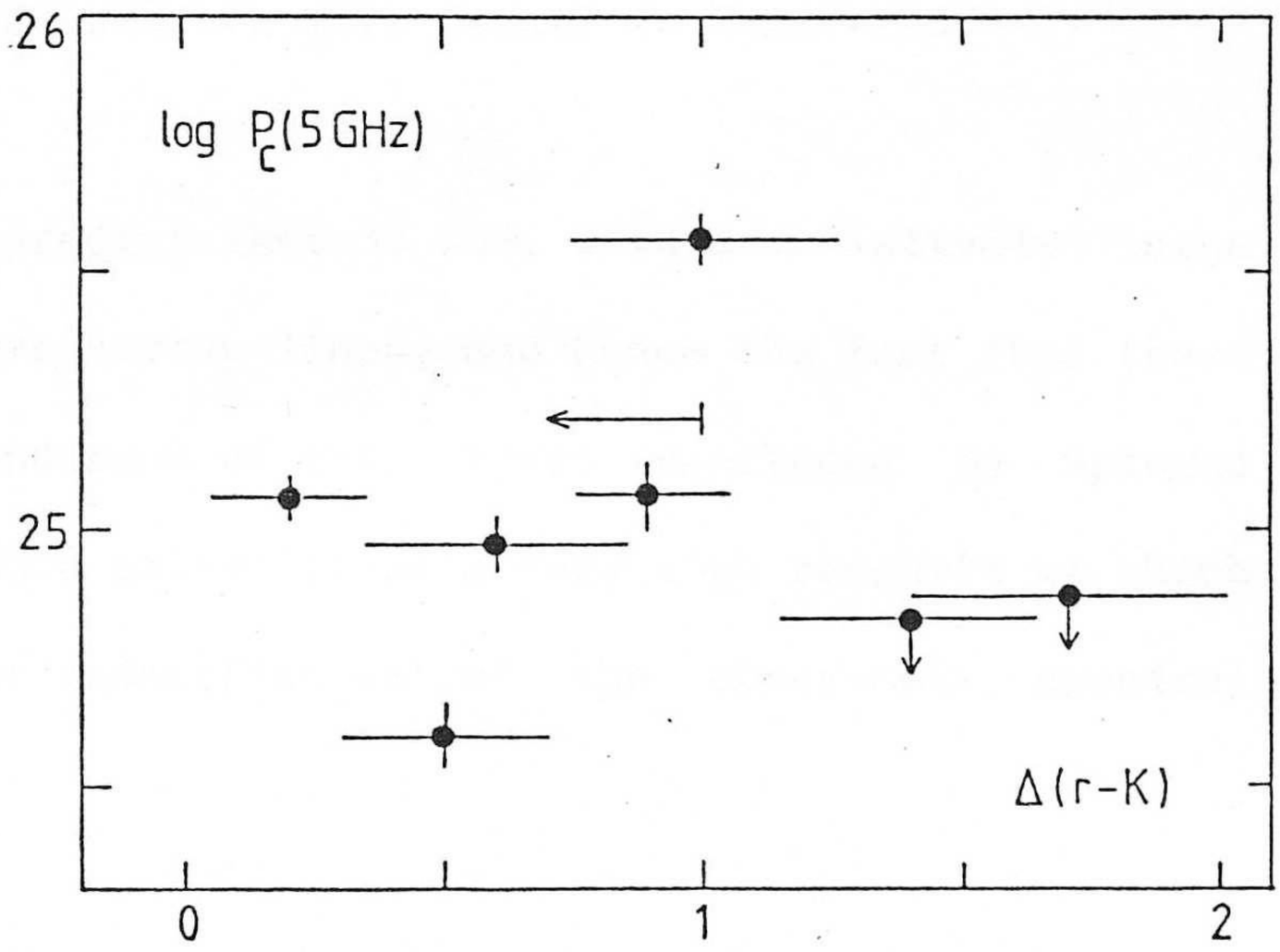


(b) The log of the nuclear core radio luminosity in $WHz^{1}sr^{1}$.

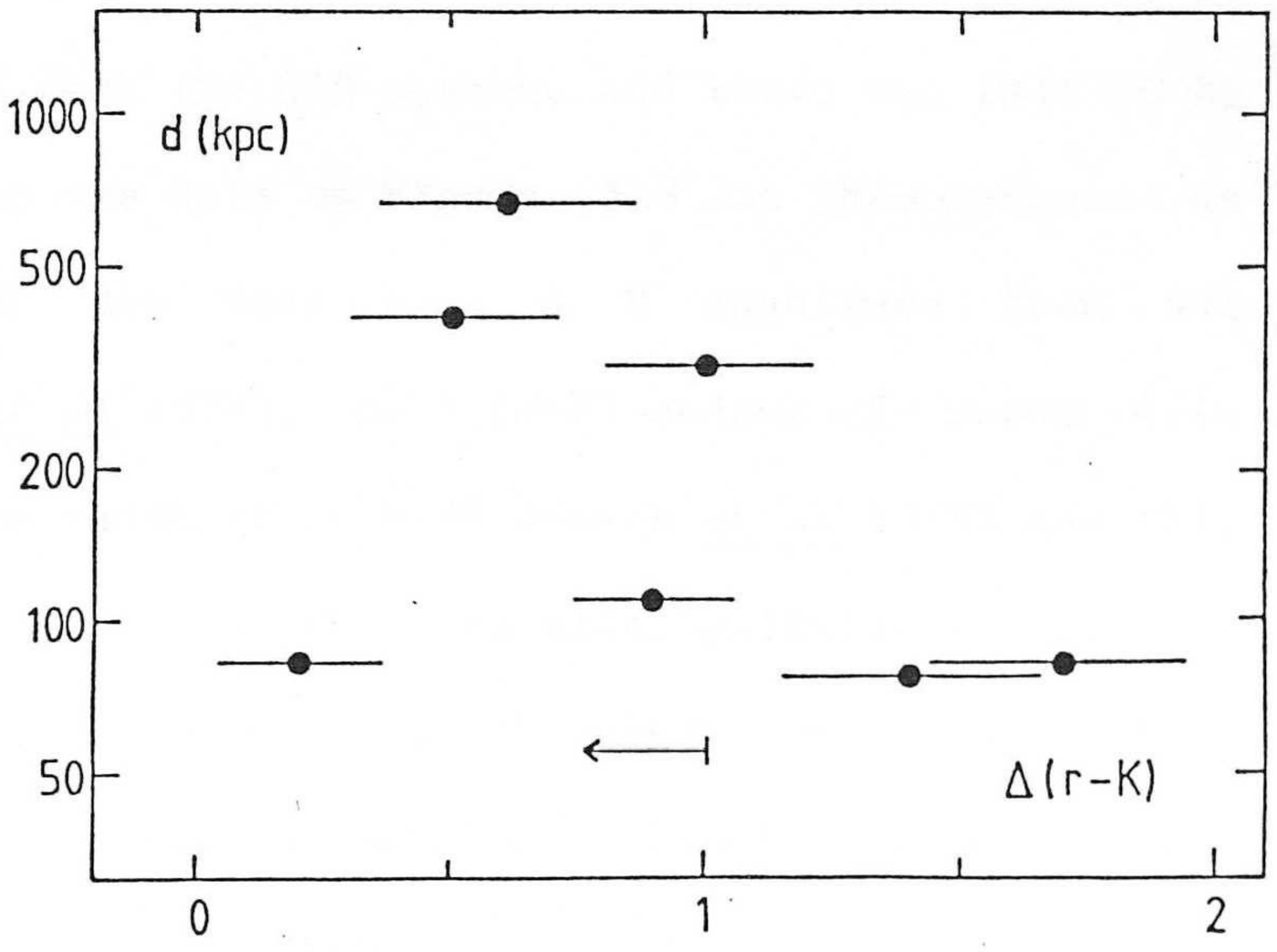


(c) The log of the projected linear size in kpc. of the double radio structure.

In the cases of 3C 65 and 3C 241 the precise equivalent widths are not yet availabe. However, neither of the these galaxies has strong emission lines (private communication from Spinrad)

This correlation shows that the variation in the (r-K) colour must be real, since the measurements of colour and line strength are completely independent. Although [NeV] 3426 is in the r passband for most of these galaxies, the strength of this line is not sufficient to account for even a small part of the observed correlation. This correlation will be discussed in more detail in Chapter 5.

The correlation would predict that 3C 239, with a relatively large colour excess would have strong lines, and hence the fact that these were not seen on the spectrum of this object mentioned by Spinrad (1982) suggests that this galaxy is at a very high redshift at which the prominent lines are redshifted out of the observable spectral range.

Before leaving this discussion of the optical-infrared colours of the radio galaxies at high redshift, brief mention should be made of 3C 265. This galaxy has not been plotted on Figure 3.9 because it had not been observed with the CCD system, and there was felt to be an advantage in keeping the data on Figure 3.9 as homogeneous as possible. However, 3C 265 does have a V magnitude from SIT photometry (Kristian et al 1978), and a (V-K) colour of about 4.1. 3C 265 has a secure redshift of 0.81 (Smith et al 1979) and this galaxy is clearly somewhat bluer than the other galaxies at similar redshifts (Figure 3.9). If the infrared photometry of Puschell et al (1982) is used the colour is a magnitude bluer, or even more

extreme. Several authors have noted the blue optical colours and generally rather peculiar nature of this identification (e.g. Kristian et al 1978, Saslaw et al 1978 and Smith et al 1979). The deep red photograph of 3C 265 presented by Smith et al (1979) shows a chaotic morphology, and there are almost certainly cluster galaxies interacting with this radio galaxy. Smith et al were unable to detect any sign of a stellar continuum in their spectrum, and remarked that the continuum appeared to be non-thermal in nature with a spectral index of about 1.1. Their deep direct photograph appears to show a strong unresolved nucleus (c.f. their image of 3C 352 in the same paper, see also Figure 4.2). It is thought that 3C 265 represents one of the 5% or so of the NLRG that do have a strong blue non-stellar continuum.

### 3.4.e The Infrared (K,z) Hubble Relation for Radio Galaxies

#### 3.4.e.(i) Introduction

For many years it was thought that the curvature of the Hubble diagram constructed from photometry of massive elliptical galaxies could produce a believable value for the cosmological deceleration parameter, $q_0$ , and a large observational effort was expended on obtaining large data sets to examine the magnitude-redshift relation for these objects. It is now generally realised, however, that this will not be possible at the present level of understanding. The principal difficulties arise not in the difficult observations, but in the methods of selection of a uniform sample over a wide redshift range, and in the quantitative evaluation of the effects of various possible evolutionary processes that may be occuring to alter the

luminosities of the 'standard candles' as a function of cosmic epoch.

Although the use of radio galaxies allows the use of well-defined 'complete' samples of objects, the connection of the selection criteria with astrophysical processes that are as yet poorly understood (i.e. the active galactic nucleus phenomenon) makes the use of radio galaxies no less hazardous.

Nevertheless, the Hubble diagram is the only way of studying and comparing the luminosities of these objects at different redshifts, and effects may possibly be so gross as to make the uncertainty in the correct cosmology relatively unimportant when interpreting the Hubble diagram.

Figure 3.12a shows the observed (K,z) Hubble relation for all the NLRGs with measured redshift, the 2 CRS and 6 BLRGs. The form of this diagram is slightly unconventional in that the observations are plotted on the diagram with the minimum of correction or adjustment. The corrections for aperture effects and the K-correction (which may contain an evolutionary term) can then be incorporated in to the predicted (K,z) relations, since they may both be functions of the assumed geometry. The data on Figure 3.12a have however been corrected to a single standard observing aperture of 10 arcsec. Since virtually all the data were taken through apertures that were between 7 and 12 arcsec, this correction is small, and to first order it is independent of the chosen geometry since the correction is between two observed apertures. In the construction of Figure 3.12, as opposed to the actual numerical analysis when all possible

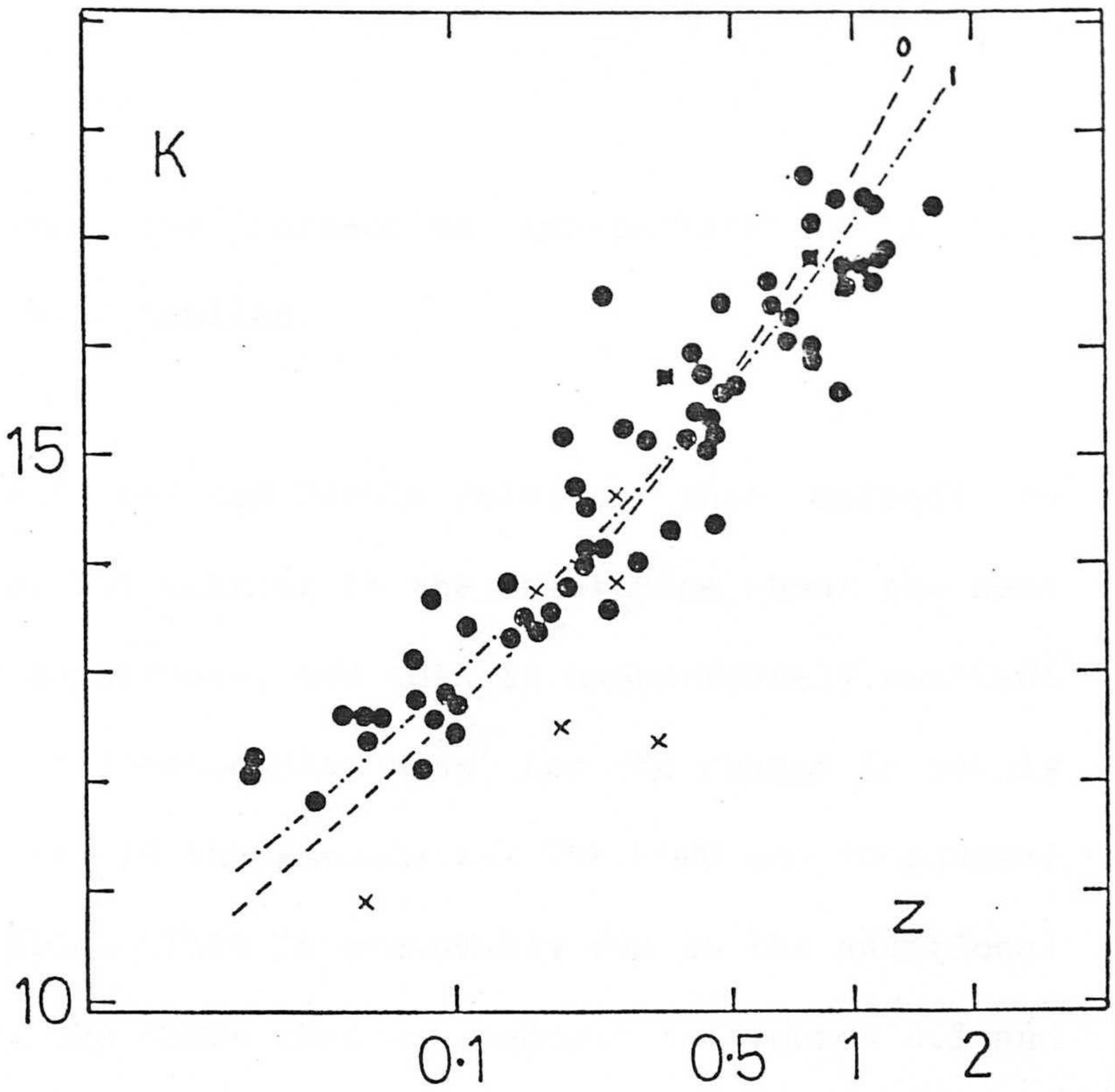


Figure 3.12a: The K,z diagram for all 3C radio galaxies with measured redshifts, NLRG (solid circles), BLRG (crosses) and CRS (squares). The two dashed lines show the predicted K(z) relations for $q_0$ = 0 and 1 with optimum vertical normalisation. They are nevertheless poor fits to the data.

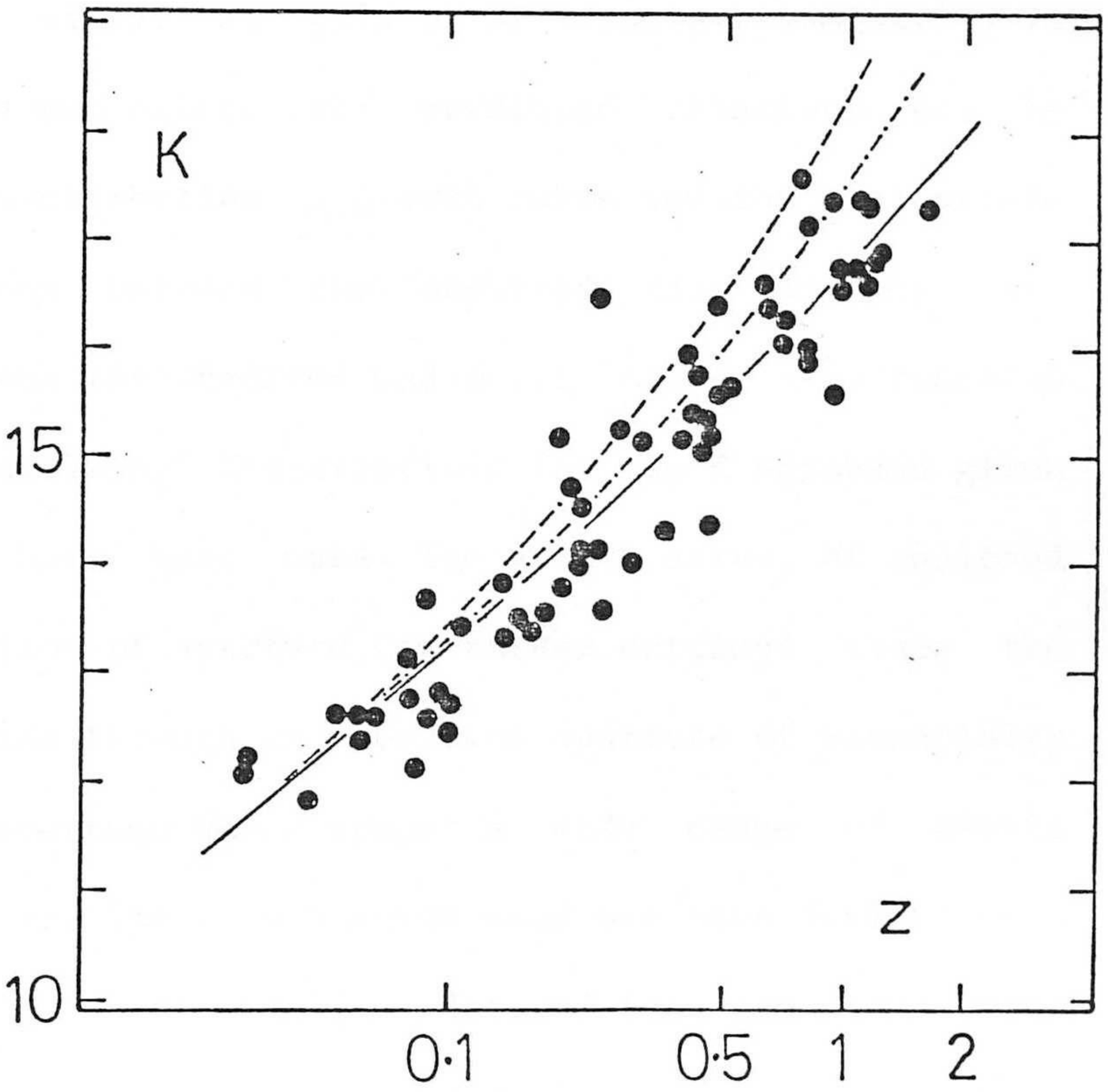


Figure 3.12b: To show the change in absolute magnitude better, the NLRG data have been replotted and the two dashed lines renormalised to fit the modelled best fit to the data (solid curve) at low z.

geometries are considered, the correction appropriate to a flat geometry ($q_0$=0.5) has been applied.

The NLRGs form a well-defined Hubble relation that extends to the highest redshifts. The scatter in the magnitudes about the mean relation is about 0.5 magnitudes, and this is approximately constant with redshift, once allowance is made for the change in purely observational uncertainty in the photometry. The BLRG are in general brighter than the NLRG. This is presumably due to the additional non-stellar component. The BLRGs that are reddest in Figures 3.5 and 3.6 are the most luminous in Figure 3.12.

At this stage of the analysis, it is interesting to compare the observed (K,z) relation for the NLRG with the relations predicted for various simple models, and in particular those that are appropriate for an elliptical galaxy of constant luminosity in simple Friedmannian cosmologies. The predicted relations may be constructed using a K-correction, a growth curve and the appropriate cosmological relations between the observed flux density and luminosity, and between the observed and metric sizes, as a function of redshift. The 'unevolving' K-corrections for the K passband given by Bruzual (1981) have been used. The growth curve, of enclosed luminosity as a function of aperture, is rather critical since the observations were made through an observing aperture of essentially constant size. This aperture hence spans a wide range of metric sizes on the galaxies. The growth curve used has been derived from the mean value of $\alpha$ (Gunn and Oke 1975) derived for ten 3CR radio galaxies in Chapter 7. This is in fact very similar to that given by Sandage (1972). However, both these growth curves have been derived

from optical data, and the existence of a colour gradient in (V-K) across the galaxy will introduce a systematic error with redshift. The data of Frogel et al. (1978) indicates that there may be a radial colour gradient in elliptical galaxies that would produce a difference of 0.1 magnitudes between the infrared and optical growth curves over a a range of metric aperture of a factor of 10, which is about the range over which the growth curve is used. This will in fact be in the sense of overestimating the predicted infrared luminosity at high redshift.

The two dashed lines on Figure 3.12a indicate the predicted (K,z) relations for standard candle elliptical galaxies in Friedmannian cosmologies with values of the deceleration parameter, $q_0$ , of 0 and 1 respectively. The vertical normalisation of the two curves (which is arbitary since it represents the combination of $H_0$ and the absolute magnitude of the galaxies) has been adjusted to give the best fit to the data. Nevertheless, it is clear that the data do not follow either of the two predicted relations for low values of $q_0$ in the absence of evolution.

3.4.e.(ii) A quantitative analysis

In order to quantify this effect, an analysis has been made of the goodness of fit of the various modelled predictions. This has been done with a $\chi^2$ statistic. Because there is both a cosmic dispersion (of in principle unknown size) in the absolute magnitudes of the radio galaxies at any given redshift, and also observational errors in each measurement (which should at least be known), the choice of the variance in the statistic is non-trivial. However,

because it was possible to produce a model that was clearly an acceptable fit to the data, it was decided to fix the cosmic dispersion so that, when it was taken in quadrature with the observational uncertainties for each object, $\sigma_i$ of the best fitting model was such that this model was a 'good' fit to the data, and was equal to the number of degrees of freedom.

$$\chi^2 = \sum_i \frac{(K_i - K_z(z_i) - K_0)^2}{\sigma_c^2 + \sigma_i^2} \qquad (3.6)$$

K is a free parameter that contains the absolute magnitude and H. combination, while $\sigma_c$ is the cosmic dispersion found iteratively using the criteria described above.

The results of this analysis are shown in Figure 3.13, for two samples. The first contained all the 64 radio galaxies with measured redshifts (including both 3C 65 and 3C 241) while the second included all the galaxies that had a measured redshift between 0.05 and 0.3. The complete data set is best modelled by an apparent value of q in excess of three, and values smaller than unity may be excluded with a high degree of confidence. The $1\sigma$ confidence limits to the apparent value of $q_0$ are 2.8 and 5.1. The low redshift sample has so few galaxies (29) that any $q_0$ less than 4 is an acceptable fit to the data. Nevertheless it is noticeable that the best-fitting value (1.0) is much closer to zero or unity than that which is found in the sample that includes the high redshift data.

There are many reasons to believe that the correct value of $q_0$ is smaller than this apparent value of 3.5. The principal arguments are based on the observed abundance of deuterium produced in the initial

Figure 3.13:
Values of $\chi^2$ for different values of the apparent deceleration parameter.

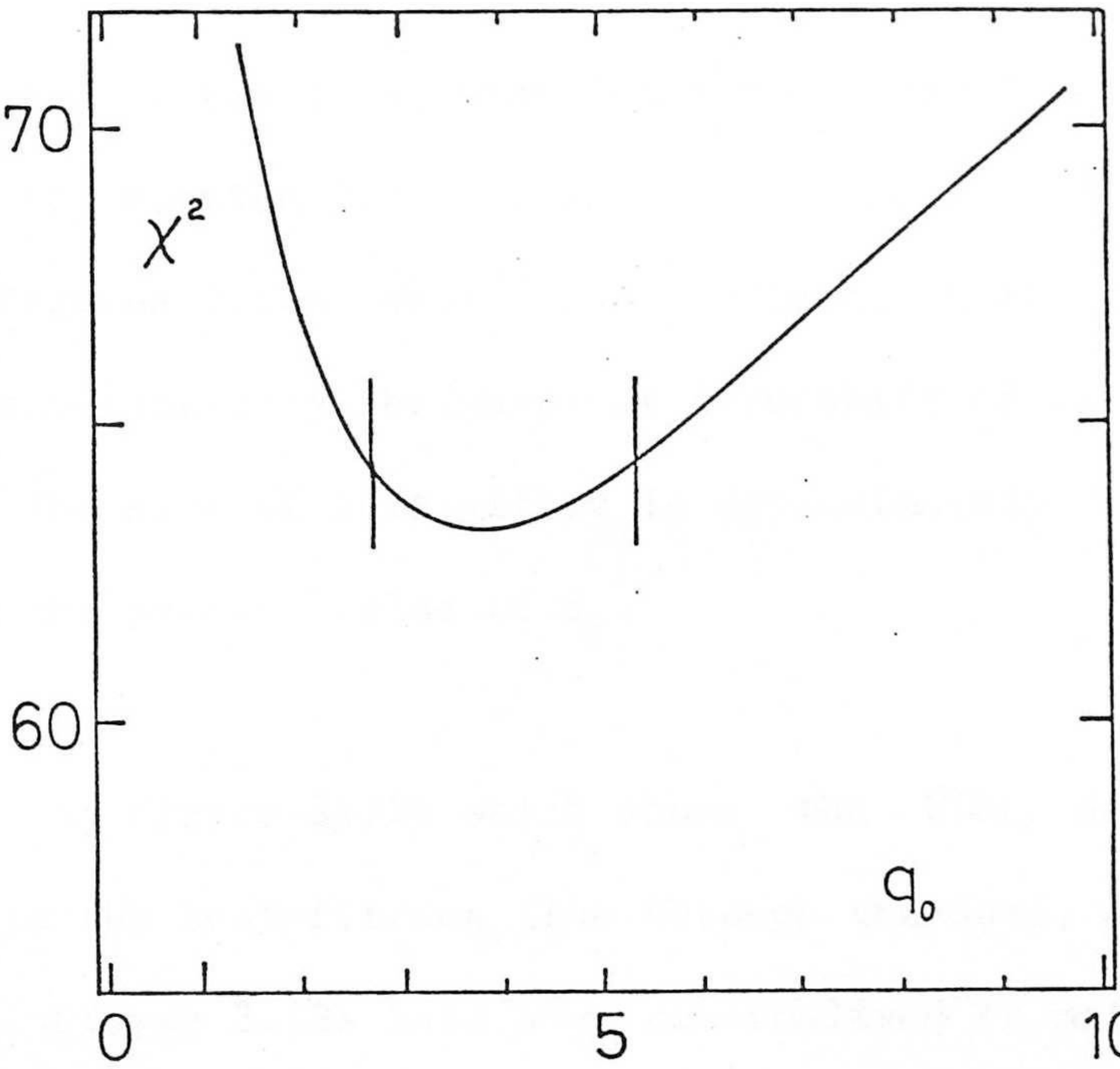


(a) The complete data set of all 64 NLRGs that have measured redshifts. The two vertical lines mark where $\chi^2 = \chi^2_{min} + 1$. The best fitting model has $q_0 = 3.8$.

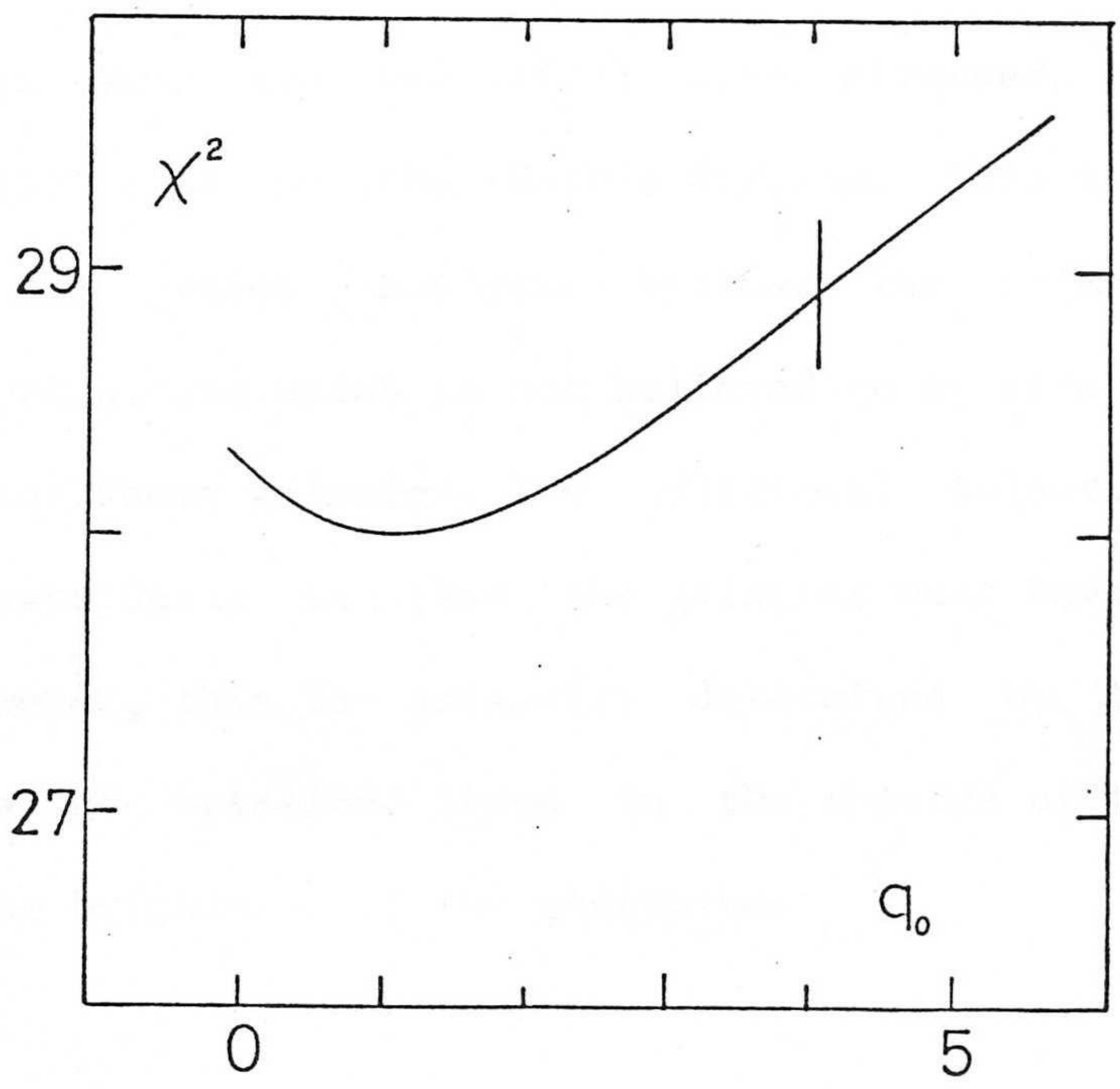


(b) The set of 29 NLRGs in the redshift range from 0.05 to 0.3. The best-fit model has $q_0 = 1.0$, but all values less than 4 are acceptable.

fireball, and on estimates of the local mean density of the universe (see the discussion in section 5.3). If the true value is indeed between 0 and 1, then Figures 3.12a and 3.13a indicate that the radio galaxies are substantially brighter at a redshift of unity than they are locally. The size of this effect is approximately one magnitude depending on the precise value of $q_0$.

This is illustrated by Figure 3.12b which shows the NLRG data only. The solid line is the best-fitting line through the data, and the two dashed lines of Figure 3.12a have been renormalised to match the solid line at very low redshift. The difference between the solid line and the two dashed lines is approximately 1 magnitude at a redshift of unity, and this indicates the most likely evolutionary change.

Many authors (e.g. Gunn and Oke 1975) have stressed the importance of Malmquist bias on the Hubble diagram. This bias should be avoided in the present analysis because the primary selection is in radio brightness which is not believed to be related to optical luminosity for these galaxies. The additional selection criterion that is unavoidable is that the galaxies must have a measured redshift. However, this is primarily determined by the presence or otherwise of emission lines in the spectra of the galaxies rather than the brightness of the continuum.

3.4.e.(iii) Comparisons with other Hubble diagrams

Despite the problems of interpretation, it is interesting to compare the values of the apparent value of $q_0$, in the absence of

any evolutionary corrections, derived from different investigations. Detailed comparisons are difficult because of the variety of observational and analytical methods used. Nevertheless, gross effects of the kind shown in Figure 3.12b should be evident. Four previous Hubble diagrams for massive elliptical galaxies that have been published merit particular attention. These are the two optical Hubble diagrams for 1st ranked cluster galaxies (but including a few radio galaxies) of Gunn and Oke (1975, GO) and Kristian et al.(1978, KSW), the second of which was itself a continuation of earlier work by Sandage (e.g. 1972a, 1973). Of more direct relevance are the optical Hubble diagram for 3CR radio galaxies of Smith (1977) and the infrared diagram for 1st ranked elliptical galaxies, again including a few radio galaxies, of Lebofsky (1981).

The first two of these investigations produced two apparently rather discrepant 'uncorrected' values of $q_0$. GO found low values of $q_0$, $0.31\pm0.68$ or $-0.15\pm0.57$, depending on the inclusion or otherwise of 3C 295 ($z=0.46$), while KSW found values considerably in excess of unity, again depending on the detailed composition of the samples used. Typically the values found ranged between 1.5 and 2.2, with a formal uncertainty of around 0.5. The observations, reductions, and analyses all have significant differences in the two investigations, and hence it is very difficult to identify the cause of this discrepancy. One problem with particularly the GO study was that the 'high redshift' galaxies were at relatively low redshifts around 0.3. Cosmological effects are small at these redshifts, and the low redshift end of the Hubble diagram must be anchored using large samples of galaxies. In the GO study, these very low redshift galaxies had been observed by other investigators, and it is

possible that systematic error was introduced at this stage. The higher values found by KSW are certainly more in accord with the present investigation (Figures 3.13a and b), but it should be remembered that the evolution of first ranked cluster ellipticals may be different from radio galaxies (see in particular Chapter 7).

Smith (1977) constructed an optical Hubble diagram for 3CR radio galaxies, and his sample included 4 at redshifts greater than 0.5. Although no formal solution was made for $q_0$, it is very clear from his Figure 4 that these four high redshift galaxies lie substantially above (i.e. are brighter than) the $q_0$ =1 curve. This effect is as large as 1 magnitude even at a redshift of 0.6, and this is clearly the same effect as seen on Figure 3.12 with the additional effect of the evolution in the (V-K) colour that begins to occur at redshifts greater than 0.4 in Figure 3.9.

The most direct comparison with the current investigation may be made with the infrared Hubble diagram of Lebofsky (1981), for which the observational techniques and reduction procedures are almost identical. The only significant difference is that most of her data is for 1st ranked cluster galaxies, and the number of galaxies at the highest redshifts is smaller. However, her results are not in good agreement with those deduced from Figure 3.12. Analyzing the data for those galaxies with redshifts smaller than 0.5, Lebofsky found an apparent value of $q_0$ of -0.15 with an uncertainty of 0.3, while the inclusion of the five galaxies at higher redshift increased $q_0$ to 0.7. However, three criticisms may be made of this analysis which reduce its usefulness. Firstly her Figure 2 contains 17 galaxies at redshifts less than 0.05, that are not in her Table

1, and are probably the low redshift ellipticals from Frogel et al (1978) and Persson et al (1979) that were plotted on her Figure 1, and described in the text at that point. Although it is not stated in the text, it is fairly clear from her Figure 2 that these galaxies must have been used in the quantitative analysis of the Hubble diagram. Unfortunately, Frogel et al (1978) and Persson et al (1980) observed ellipticals covering a wide range of absolute magnitudes brighter than about $M_V$=-19. Lebofsky therefore imposed an absolute magnitude selection criteria in K of brighter than -25.5. This appears to be rather arbitrary in view of the fact that "most [of these low redshift ellipticals] are not in clusters" (Lebofsky 1981). Indeed, inspection of her Figure 2 makes it fairly clear that her apparent value of q is determined principally by the slope of the (K,z) relation between the low redshift sample with redshifts less than 0.05 and the mean magnitude of her own data, rather than the slope of the relation in her own data, which is clearly steeper (and hence indicates a larger $q_0$) than the 'best fitting' curves that have $q_0$ close to zero. In other words, it would seem that the value of $q_0$ derived in her analysis depends largely on the cut-off in absolute magnitude used to construct the low redshift sample. Secondly, the method of the estimation of the errors is less conventional than that used here. The hypothesis to be tested should be as follows: For each of a range of all possible values of $q_0$, what is the chance that a universe with this particular value could produce the observed data. This is distinct from that tested by Lebofsky's Monte Carlo statistical analysis which determines, if the universe really had her best fit value as the true value, the probability that she could have measured another value. Finally, there is some evidence (Chapter 7) that investigations such as

Lebofsky's that mix 1st ranked cluster galaxies and radio galaxies may be difficult to interpret as they may have different absolute magnitudes and evolutionary histories. In view of these problems, and particularly the first, the apparent discrepancy with the present results is not considered serious.

3.4.e.(iv) Estimated redshifts for 9 Faint Galaxies

Nine galaxies that do not have measured redshifts have been observed in the infrared, including some sources that have not been seen in the optical (see Section 3.4.f). If it is assumed that these are all radio galaxies with absolute magnitudes that are comparable to those of the other 3C radio galaxies that do have spectroscopically determined redshifts, then an estimate of the likely redshifts of these nine remaining galaxies can be obtained. This has been done for many years using optical photometry (e.g. Laing et al 1983). Particularly at high redshift, the infrared magnitudes have the advantage that they should be less sensitive to evolutionary effects. The most likely redshift, $z^*$, is found by finding the redshift at which the mean 3C relation has that infrared magnitude. These estimated redshifts were used on the colour-redshift diagrams discussed in the previous sections, and are listed in Table 3.8 (page 125). The cosmic scatter of 0.5 magnitudes means that these estimated redshifts will generally be in error by as much as 30%, and there is really no substitute for a spectroscopically determined redshift.

3.4.e.(v) Summary

The apparent value of $q_0$ indicated by an infrared Hubble diagram for 63 3CR radio galaxies is in excess of 3. However, there would be every expectation that either substantial evolution in the luminosites with epoch, or selection biases introduced by the radio selection criteria, could be present in the radio galaxy data set to make this apparent value of $q_0$ very different from the true value of this parameter. If $q_0$ is indeed smaller than unity, then these effects must combine to produce a change in the mean absolute magnitude of these galaxies of about one magnitude between redshifts of zero and unity. The Hubble diagram will be reexamined in more detail in Chapter 5 in terms of some possible evolutionary effects.

3.4.f The Observations of the Empty Field Sources

In addition to 3C 68.2, which it was suggested in Section 3.4.d may actually now have been seen at the limits of a very deep red CCD exposure, two other 'optically unidentified' sources were included in the statistical sample of 90 sources and were observed in the infrared. These were 3Cs 437 and 470.

Much of the discussion that is presented in Chapter 6 of this Thesis concerns various aspects of the detection in the infrared of radio sources that are too faint to be seen, at present, in the optical wavebands. In that Chapter, observations of 12 such sources selected from a new radio sample are described and analysed. The observations of these three 3C empty fields followed exactly the

same procedures as are described in Section 6.2.b, and the reader is refered forward to Chapter 6, in which many aspects of the detection of 'empty field' radio sources are discussed. All three 3C sources were observed in November 1983, with a 7.4 arcsec aperture. This was chosen to avoid nearby contaminating objects. The radio sources are all extended doubles, but an aperture of this size should cover the most likely positions of the associated objects. 3C 68.2 was also observed, with a 10.8 arcsec aperture, in September 1980.

For each of the three sources, a significant detection at a high level of significance (i.e. greater than 4 sigma above the background) was obtained after an integration of 64 minutes. The K magnitudes ranged from about 17.7 for 3C 68.2, through 18.0 for 3C 437, to 18.5 for 3C 470. The two measurements of the K flux density of 3C 68.2 agreed to within 0.18 magnitudes, which is well within the combined statistical uncertainties. If these are radio galaxies of comparable absolute magnitudes to the other 3C radio galaxies, then they must lie at high redshifts (Table 3.8).

If these infrared detections are taken to represent identifications of the objects (i.e. radio galaxies or, less likely, quasars) that are associated with these radio sources, (see e.g. Section 6.1.c.(ii)), then at last no 3C radio source remains unidentified because of its proven faintness. The four remaining sources that have not been identified have not yet been thoroughly examined in the optical.

## 3.5 : Summary

Infrared J, H and K photometric data on 81 3CR radio galaxies in the redshift range from 0.03 to at least 1.62 have enabled many empirical conclusions to be drawn. The most interesting are summarized thus.

1. The near infrared continua of NLRG at low redshift are dominated by the giant stars in their stellar populations. In contrast, the BLRG have redder colours and show varying degrees of excess at K. The additional component probably has a power-law form over the short wavelength range covered.

2. At high redshift, the mean observed (H-K) colour is within 5% of the prediction based on the zero-redshift spectral energy distribution. No significant evolution at all is seen in this colour.

3. In contrast, the optical-infrared colours (r-K) of radio galaxies at high redshift are substantially different than would be predicted from the continuum energy distributions of nearby radio galaxies. The colours show a real scatter, and the enhancements in the rest-frame ultraviolet flux densities relative to those in the infrared are between 1 and 2 magnitudes.

4. There is a relation between the size of this enhancement and the strength of [O II] 3727 emission, but not between it and two

radio properties of the sources.

5. The infrared K(z) relation for the NLRG is well defined. If $q_0$ is less than 1, then the data indicate that the galaxies at a redshift of unity are significantly brighter than those nearby. The size of this effect is probably about one magnitude.

6. Three 'empty fields' for which no optical identification had been found despite intensive efforts were detected at 2.2 microns. This means that no 3C radio source remains unidentified by virtue of its proven faintness.

It should be remembered though that a few exceptions to these general statements do exist (e.g. 3Cs 265 and 433),

There are two main candidates for producing these changes that are observed in the radio galaxies. These are (a) an evolution or change of the stellar populations of the galaxies, and (b) the addition of non-stellar radiation components associated with the active nucleus. The latter might plausibly be produced by the increase in the radio luminosity that is associated with the high redshift radio galaxies. The former could be either an evolutionary effect, related to the earlier cosmological epochs involved, or could also be related to the increase in luminosity. This is because some of the population changes can have effects which last a time that is very much shorter than the cosmological timescales of interest

In the next Chapter, evidence is presented that distinguishes

between the 'stellar' and 'non-stellar' hypotheses (in favour of the former), and in Chapter 5 these empirical facts on the NLRG summarized above are reexamined in the light of different models of the stellar populations of these galaxies.

# Chapter 4 : EVIDENCE FOR STELLAR EVOLUTION IN 3C 352 AND OTHER GALAXIES

## 4.1 : Introduction

It was shown in the preceding Chapter that 3CR radio galaxies at high redshift have bluer optical-infrared colours than expected on the basis of the colours of nearby galaxies with generally similar radio properties, albeit with lower radio luminosities. This ultraviolet excess could have either a stellar origin (i.e. be caused by a population of hot blue stars), or it could be non-stellar emission associated with the active nucleus that powers the radio source. This latter radiation could be either non-thermal in nature (e.g. synchrotron radiation) or thermal (e.g. emission from a hot accretion disc). However, a study of the surface brightness distribution of the galactic image, in a range of passbands offers the possibility of distinguishing between the 'stellar' and 'non-stellar' hypotheses. An image containing a component that is emitted from the nucleus should appear increasingly unresolved as the nuclear flux becomes more dominant, until eventually the object will appear quasi-stellar. If however blue stars are responsible for the ultraviolet excess, then the distribution of excess light in the image will follow their distribution. In particular, if the colour change is produced by a very young population of stars, then these stars will still be close to where they were formed. It is, of course, possible that the star forming regions could be close to the nucleus, in which case the light will be again unresolved (and hence indistinguishable from nuclear emission), at high redshift. On the other hand, if the

ultraviolet light that causes the colour change is distributed throughout the galaxy, then a strong argument can be made for a stellar origin.

An investigation of this kind has been undertaken on 3C 352. This is a typical high redshift member of the 3CR galaxy sample studied in the previous Chapter. It is a faint galaxy (23rd magnitude in V) and was identified by Kristian et al (1974). 3C 352 has a secure redshift of 0.806 based on five narrow emission lines. (Smith et al.1979). In addition the 4000 A stellar absorption feature is "probably present in the spectrum". The identification is symmetrically located between the two lobes of the 10 arcsec double radio source, but no central radio component has been detected (Laing et al 1983).

In addition, an analysis of the surface brightness profiles of most of the CCD images used in the previous chapter has been carried out. This is a very direct test, since it was these images that produced the r magnitudes that revealed the changes in the (r-K) colours.

## 4.2 : Multicolour Observations of 3C 352

Four photometric exposures of 3C 352 were taken using the Royal Observatory Edinburgh Imaging Spectropolarimeter (ISP) during an observing run on UKIRT during April 1982. Four similar exposures were also taken of 3C 284, a radio galaxy at rather lower redshift (0.239). The instrument was mounted at f/9 cassegrain focus, and telescope guidance was performed using the instrument's own TV guidance system.

The ISP (McLean et al. 1981) consists of a versatile photometer with a CCD detector that can be operated in a number of modes, including that of photometric direct imaging. This was the mode used for this experiment. Four photometric passbands defined by interference filters were used. These are similar to those that define the standard BVRI system, but they are not identical, however, and will be refered to as B′V′R′ and I′. Details of these passbands are given in Table 4.1. Each exposure was 15 minutes in duration. The astronomical seeing was about 1.5 arcsec for all the images.

During this observing run with the CCD camera on UKIRT, several other, unfortunately unphotometric, exposures were taken for another investigation (see Chapter 7). The preliminary reduction of the raw CCD data for 3C 352 and 3C 284 was undertaken by the batch programmes that were developed for this other programme. A description of the basic reduction procedure is given in Chapter 7, and so will be omitted here.

4.2.a Photometric calibration

Because of the non-standard nature of the filters used in this investigation, the photometric calibration of the data is not trivial. It was carried out as follows. The few hours of photometric conditions that were available during the run meant that only five standard stars were observed. These are listed in Table 4.2. Although not ideal, these are nevertheless sufficient to set up a system that should be accurate to within a few percent.

Because there was no particular requirement for the CCD data to be placed onto the standard BVRI magnitude system, since the observations would be compared principally with a continuous zero redshift spectral energy distribution, the analysis set up first a 'natural' instrumental magnitude system, $M_{ccd}$, then converted this to a proper B'V'R'I' system in which the A0V star $\alpha$ Lyrae is defined to have zero colours and magnitudes in all passbands. The calibration of this system in terms of flux density (i.e. $Wm^{-2}Hz^{-1}$) can then be found from the known flux densities of $\alpha$ Lyrae. One advantage in staying in the non-standard passbands all through the analysis is that it avoids the neccessity of using colour equation transformations outside the range of colours in which it is empirically defined by the standard stars. This is otherwise normally neccessary because of the very red colours of the galaxies at high redshift. A colour equation is of course still used, to transform $\alpha$ Lyrae onto the non-standard system, but this is done in the part of the curve that is well defined by the standards.

Table 4.1: Details of the Filters.

| | $\lambda_c$† | FWHM† | $S_\nu(0)$¶ |
|---|---|---|---|
| B' | 4647 | 730 | -22.36 |
| V' | 5266 | 937 | -22.40 |
| R' | 7591 | 772 | -22.58 |
| I' | 8488 | 950 | -22.63 |

Notes: † Angstroms.

¶ log ($Wm^{-2}Hz^{-1}$).

Table 4.2: Standard Stars Observed with the CCD.

| Star | (B-V) | (V-R) | (R-I) | V |
|---|---|---|---|---|
| HD 122693 | 0.55 | 0.19 | 0.30 | 8.0 |
| HD 128428 | 0.77 | 0.26 | 0.37 | 7.7 |
| HD 132683 | 1.41 | 0.81 | 0.83 | 9.4 |
| HD 165475 | 0.29 | 0.00 | 0.23 | 7.1 |
| HD 165475B | 0.28 | -0.08 | 0.12 | 7.5 |

Four-colour exposures were taken of each of the five standard stars. A natural magnitude system was set up in each of the passbands, M, in terms of the integrated number of data-numbers, which should be directly proportional to the number of photo-excited electrons:

$$M_{ccd} = -2.5 \log dn \qquad (4.1)$$

For each standard star, the three instrumental colours in this natural system, $(B-V)_{ccd}$, $(V-R)_{ccd}$, and $(R-I)_{ccd}$ were constructed. In addition dV, defined as the difference between the natural $V_{ccd}$ magnitude and the true Vo magnitude was also found:

$$dV = V_{ccd} - Vo \qquad (4.2)$$

Graphs of these three colours and dV plotted against the appropriate Johnson colours and against (B-V) in the case of dV, enable one to find the colours and magnitudes that $\alpha$ Lyrae would have in the natural CCD system, since this star will have all Johnson magnitudes, and hence all colours, equal to zero. Inspection of Figures 4.1a-d indicates that, for $\alpha$ Lyrae:

$$V_{ccd} = -11.20$$
$$(B-V)_{ccd} = 0.25$$
$$(V-R)_{ccd} = -1.75$$
$$(R-I)_{ccd} = -1.55$$

Figure 4.1a-d: The Photometric Calibration of the CCD. Johnson magnitudes are plotted against those measured in the 'natural' CCD system.

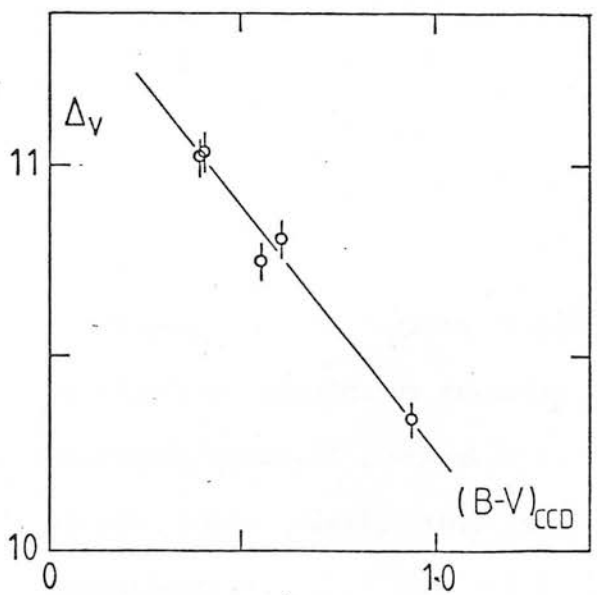


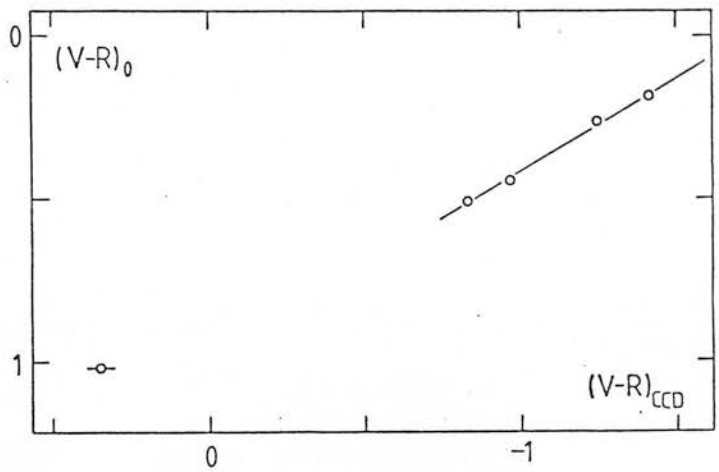


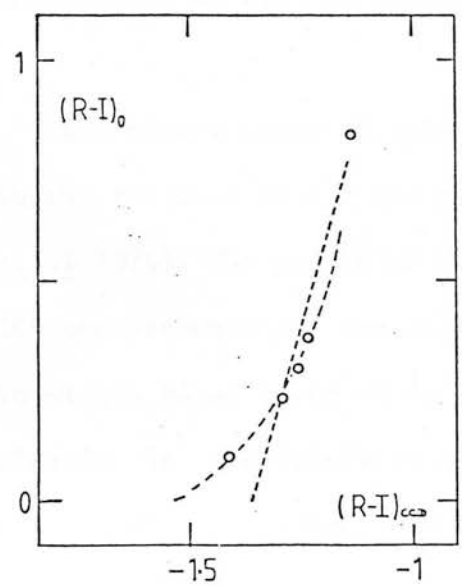


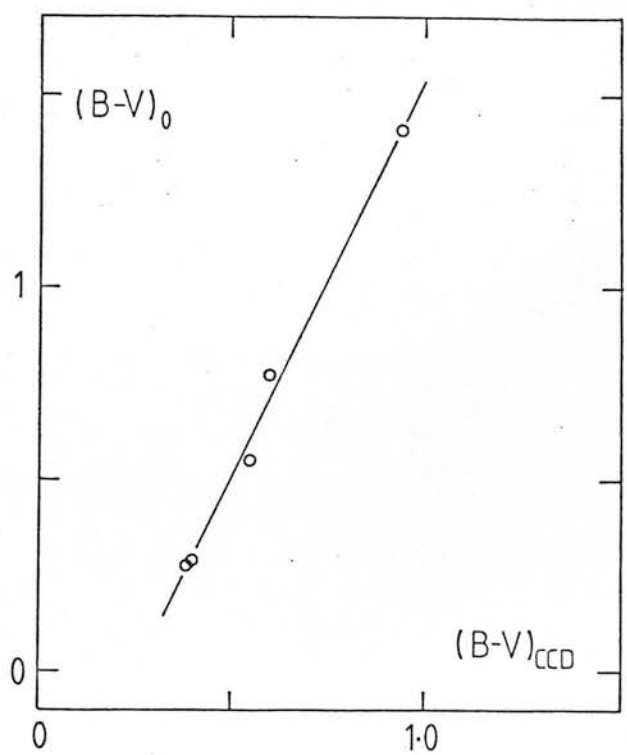

And hence, since $\alpha$ Lyrae also must have $B'=V'=R'=I'=0.00$ , it follows that:

$$B' = B_{ccd} + 10.95$$
$$V' = V_{ccd} + 11.20$$
$$R' = R_{ccd} + 9.45$$
$$I' = I_{ccd} + 7.90$$

Inspection of Figures 4.1a-d suggests that internally this calibration should be accurate to about 0.05 magnitudes in all the passbands except I', where it is likely to be around 0.10. Although by no means ideal, this will be sufficient for the present investigation.

The final flux density calibration of the B'V'R'I' magnitude system is based on the flux densities of $\alpha$ Lyrae at the central wavelengths of the filters. The logarithm of the adopted flux density (in $Wm^{-2}Hz^{-1}$) for zero-magnitude is listed in Table 4.1.

One direct check of this analysis is possible. The bright star in the field of 3C 352 has published photometry in B and V (Kristian et al 1974). The values of B and V for this star derived from the CCD measurements and the relations shown in Figures 4.1a and d agree to within 5% at V and 6% in (B-V). One additional check that this affords is the linearity of the exposure times, since the standard star exposures were very short compared with those for the astronomical images of the radio galaxies.

4.2.b Data for 3C 352 and 3C 284

The fully reduced image of 3C 352 is shown in Figure 4.2. The radio galaxy is the faint object that lies between the two white crosses which mark the positions of the radio lobes. The grey scale in picture has been set proportional to the noise in the sky background, so that signals of equal significance above the noise appear with equal intensity in Figure 4.2.

Magnitudes on the B'V'R'I' system were found for the two radio galaxies, by summing the pixel values on the CCD. For 3C 284 a circular aperture of exactly the same radius as that used for the infrared measurements (10.8 arcsec, Chapter 3) was used for this summation, while for 3C 352, a rectangular aperture that was 5 by 7 arcsec was used, aligned with the major axis of the galaxy. This is sufficiently close to the infrared aperture (7.2 arcsec) that no aperture correction is necessary. The uncertainties in the measurements for 3C 352 are quite large. They arise from the photon statistics of the sky and other difficulties in fixing the value of the flat sky background. The size of the uncertainty in each measurement was estimated by repeatedly summing over areas of 'empty' sky with the same sized aperture, and then calculating the standard deviation of these measurements. Table 4.3 lists the observed magnitudes and flux densities of the two radio galaxies, with the total uncertainties derived for 3C 352. The uncertainties in the actual measurements for 3C 284 are smaller than the uncertainties in the calibration discussed above.

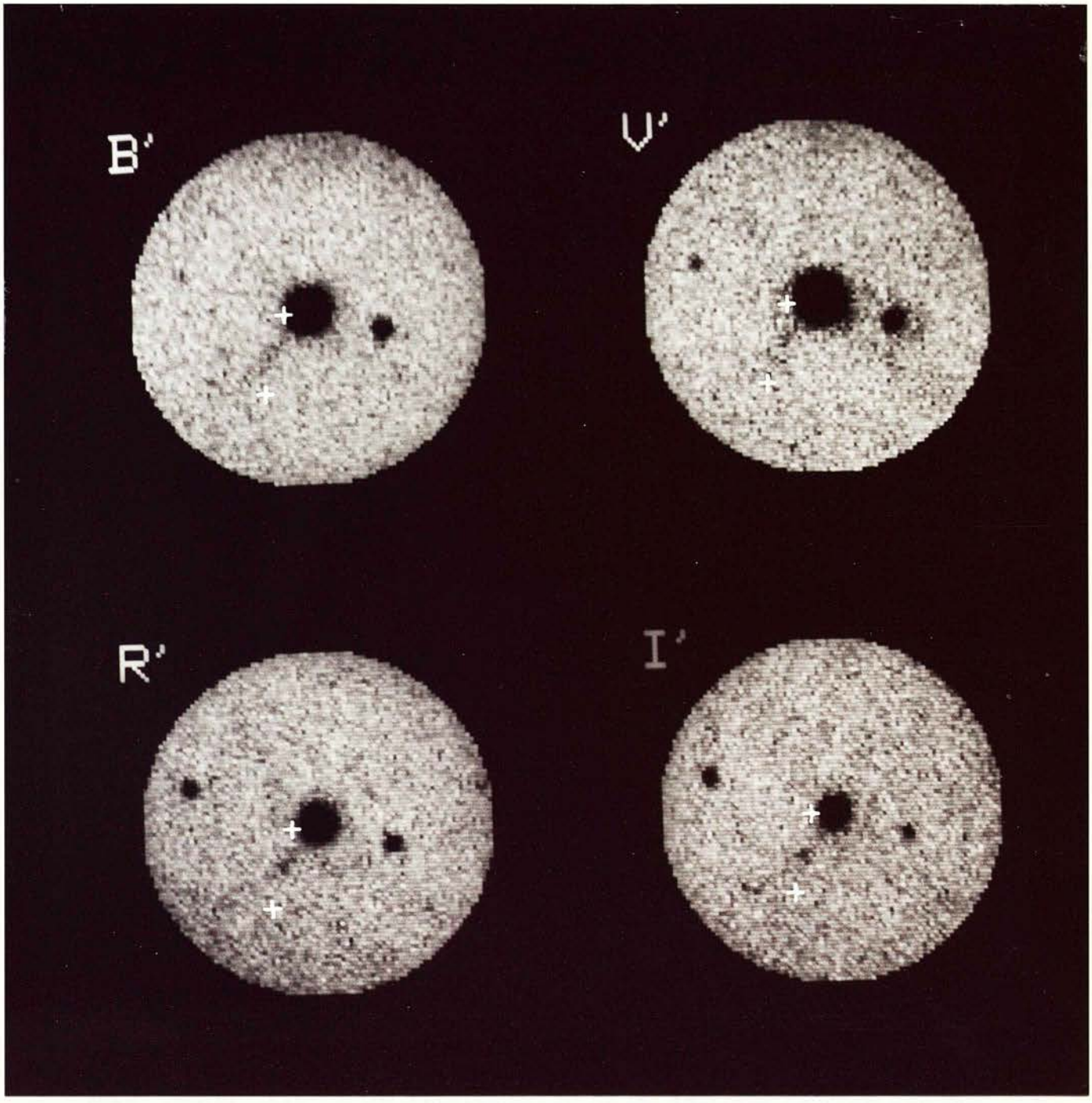


Figure 4.2: CCD images in four colours of 3C 352. The radio galaxy is the faint object situated between the two white crosses which represent the positions of the two radio lobes. These are separated by 10 arsec.

## 4.3 : Discussion of the Results

These flux-density measurements are compared graphically in Figure 4.3a,b with the spectrophotometry of 3C 192 published by Yee and Oke (1978). This low redshift 3C radio galaxy (z=0.060) has been chosen from their sample to be a reasonably typical Narrow Line Radio Galaxy with similar radio properties to 3C 284 and 3C 352. The optical spectrophotometry has been extended in to the infrared using the infrared data on this galaxy presented in Chapter 3, plus a single L (3.5 micron) magnitude that had been obtained at the same time. The vertical scale of Figure 4.3 is in units of $2.5.\log(\nu f_{\nu})$, and the measurements of 3C 284 and 3C 352 have been shifted arbitarily in the vertical direction for comparison with the continuous Spectral Energy Distribution (SED) of 3C 192.

The lower diagram (b) shows that the Broad Band SED of 3C 284 at moderate redshift is the same as that of 3C 192. However, 3C 284 is at sufficiently low redshift (z=0.239) that no strong evolutionary effects would be expected, and the data on this galaxy provide a further check on the calibration of the B′V′R′I′ passbands.

The Broad Band SED of 3C 352 in the upper diagram, (a), is a much poorer fit to the continuum SED of 3C 192. The spectra may be adjusted vertically but not horizontally since the redshifts of both galaxies are accurately known. Several things are clear from Figure 4.3.a. Firstly, the flux density is considerably enhanced at around 3000 A compared with 3C 192. The apparent upturn between V′ and B′ is not significant and the two measurements should be regarded as

Table 4.3: Photometry for 3C 352 and 3C 284.

| | 3C 352 | | 3C 284 | |
|---|---|---|---|---|
| | Mag | μJy | Mag | μJy |
| B' | 22.56±0.2 | 4.12±0.9 | 19.54 | 66.6 |
| V' | 22.59±0.2 | 3.66±0.8 | 18.68 | 134 |
| R' | 20.69±0.15 | 13.9±2.5 | 17.06 | 394 |
| I' | 19.63±0.2 | 33 ± 10 | 16.39 | 650 |
| J | - - | - - | 15.55 | 928 |
| H | - - | - - | 14.76 | 1284 |
| K | 17.24±0.12 | 82 ± 10 | 14.17 | 1396 |

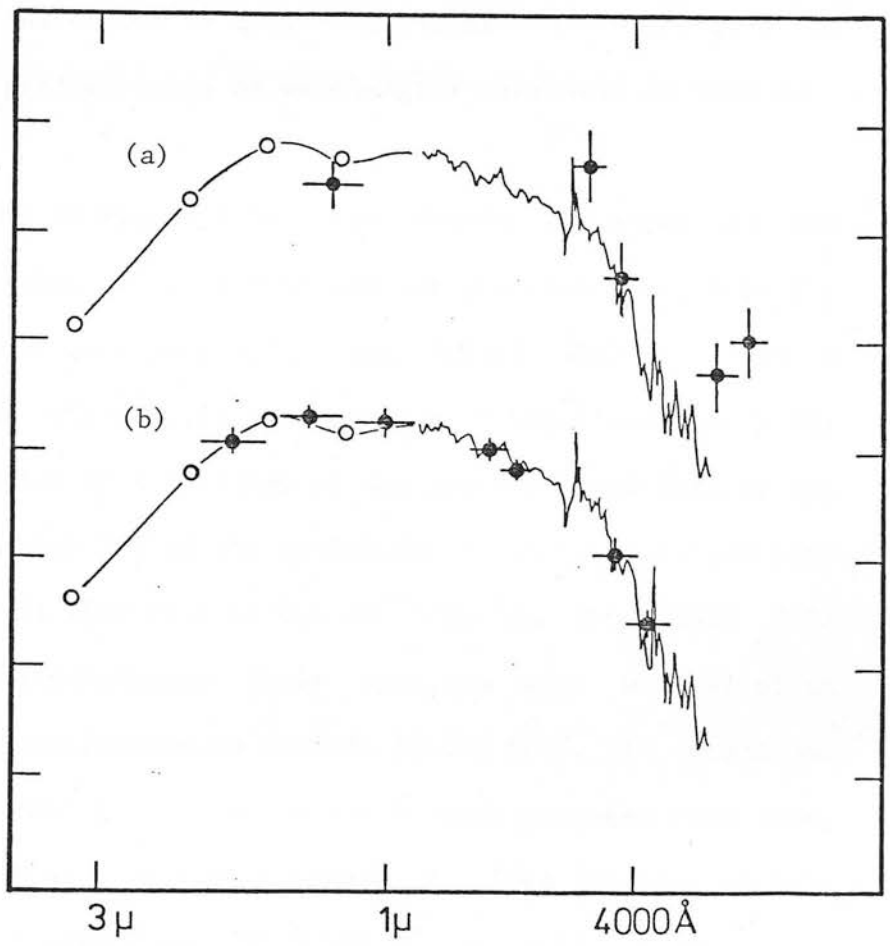


Figure 4.3: Comparison of the broad band SEDs of (a) 3C 352 and (b) 3C 284 with the continuous SED of 3C 192. The redshifts of these radio galaxies are 0.81, 0.24 and 0.06 respectively.

effectively independent measurements of the continuum level near to 3000 A. This enhancement in the ultraviolet flux density over that in 3C 192 is about one magnitude, and this is clearly the same effect that produces the change in (r-K) colours that was demonstrated in the previous Chapter (Section 3.4.d(iii)). Note that the continuum longward of 4000 A is relatively unchanged, and that in fact the (R′-K) colour for 3C 352 would not show a substantial change. However the R′ passband has a considerably longer effective wavelength than the r passand (7600 A compared with 6500 A), and 3C 352 is also at a slightly lower redshift than most of the radio galaxies whose (r-K) colours were discussed in Chapter 3. The lack of change in (R′-K) colour is quite consistent with Figure 3.9. The evolution occurs predominantly at wavelengths shortward of 4000 A.

Another feature of Figure 4.3a that should be noted is the enhancement, by about 0.5 magnitudes of the flux density in I′. However, as is clear in Figure 4.3a, the [OIII] 5007 line at a redshift of 0.81 will lie in the red wing of the I′ passband. The relative transmission of the filter at the precise wavelength of the line is actually about 35% of the maximimum. Smith et al.(1979) have measured an observed line flux of $0.6\ 10^{-17}$ $Wm^{-2}$ in the [OII] 3727 emission line. Unfortunately their spectrum does not extend to sufficiently long wavelengths to include [OIII] 5007. It would be expected, though, that [OIII] 5007 would be much stronger than this, possibly by as much as a factor of around 3, (see Section 3.4a). Thus the line emission from [OIII] 5007 could easily account for a substantial fraction of the observed flux of about $1.3\ 10^{-17}$ $Wm^{-2}$ observed in the I′passband, since the increase in the I′ flux density requires that the total line flux in [OIII] 5007 be

approximately $1.5\ 10^{-17}\ Wm^{-2}$. A study of the other line strengths (Smith et al. 1979) indicates that it is unlikely that any of the other passbands are seriously affected; both the strong [NeIII] 3869 and [OII] 3727 are outside the B′, V′ and R′ passbands.

The crucial result from these observations of 3C 352, however, is apparent on the CCD image shown in Figure 4.2. The short wavelength B′ image, which is clearly (from Figure 4.3a) substantially brighter than would would have been found if there had been no change to the SED, is distinctly non-stellar in appearance. In particular, there is a clear difference in structure between the B′ image and the I′ image, in which it has been argued there is a substantial contribution from the nucleus associated with a powerful emission line. The I′ image looks much more centrally concentrated than the others, and this is especially true for those shortward of rest-frame 4000 A.

One may therefore conclude that the ultraviolet excess that causes the change in optical-infrared colours observed in the previous chapter has, in at least one high redshift galaxy, a stellar origin.

## 4.4 : Further Empirical Evidence Concerning Image Structure

In an effort to investigate further the question of the origin of the emission responsible for producing the blue (r-K) colours, the images of the radio galaxies on the CCD exposures, from which were derived the r magnitudes used in the previous Chapter, were analysed to produce quantitative estimates of their structure. It is important to stress the direct nature of this investigation; the images examined structurally are precisely those that produced the r magnitude used to construct the (r-K) colours. On the other hand, the information on the change in structure as a function of wavelength, that was available in the case of 3C 352, is of course absent for these galaxies.

Eight of the twelve galaxies for which (r-K) colours are available were analysed. No analysis was attempted on the remaining four. These were either too faint (3C 68.2 and 3C 239) or were located so close to either defects (3C 356) or to so many other nearby objects in the image (3C 175.1) that analysis of the surface brightness profiles of the images would have been unjustified.

In each of the remaining fields, the profiles of many images of stellar appearance were fitted by a gaussian function using interactive STARLINK software. These measurements provided an estimate of the seeing $\sigma$ in each exposure, and also allowed the selection of a star of approximately the same brightness as the radio galaxy for detailed comparison during the analysis. This comparison star was required only to have a value of $\sigma$ close to the

minimum seen in the measurements of the objects in that exposure.

For each of the radio galaxies and the eight comparison stars the structure parameter alpha, defined by Gunn and Oke (1975), was determined. This parameter will be the subject of a more extended discussion in Chapter 7 (Section 7.1a). For the present, $\alpha$ may be defined as being equal to twice the ratio of the mean surface brightness at a sampling radius of 19.2 $\bar{h}^{-1}$kpc to the mean surface brightness interior to that radius.

$$\alpha_{\gamma} = 2 \frac{\text{Surface Brightness at } \gamma}{\text{Surface Brightness within } \gamma} \qquad (4.5)$$

Alpha is related to the de Vaucouleurs characteristic radius (Figure 7.1). The apparent size of the sampling radius will be a function of both redshift and the assumed cosmological geometry. The dependence on the former is fairly weak at high redshift, but the apparent size on the sky of this standard radius will change by 50% between cosmological models with $q_0 = 0$ and 1. In this analysis a flat geometry with $q_0 = 0.5$ is assumed. Since this is probably greater, if anything, than the real value, the most likely effect of this assumption, if there is one at all, will be to overestimate the sampling radius on the sky, and hence underestimate $\alpha$ since the galaxy will be sampled further from the nucleus than it should have been. However the weak dependence of the sampling radius on redshift means that the uncertainty in $q_0$ should not effect the relative measurements of the radio galaxies. It is however one reason why direct comparison of these measurements with those for the low redshift galaxies presented in Chapter 7 should be treated with caution.

The procedure for measuring $\alpha$ is identical to that described in Chapter 7 (see Section 7.2c). Redshifts of unity were assumed for 3C 65 and 3C 241. Although the measured redshift of 3C 241 (1.62) is considerably larger than the assumed value, the effect on the sampling radius will not be large, and in fact may be of either sign (depending on the cosmological geometry), and it was felt that this new redshift determination did not warrant a reanalysis of the image of this galaxy. The redshift of 3C 65 (1.17) is very close to the assumed value. The images of the comparison stars were analysed exactly as if they had been the radio source identification.

A correction to account for the effects of atmospheric seeing was applied. In principle a different correction should be applied to the galaxies and stars, since they will probably have different underlying surface brightness profiles. However, since the main aim of the investigation is to determine whether the images of the radio galaxies and the stars are different, the same correction was applied to both. This correction was derived from the corrections for a galactic profile computed in Chapter 7 and shown in Figure 7.4. In Table 4.4, the uncorrected values of $\alpha$, given by upper and lower bounds, the ratio $\sigma/\gamma$ and resulting correction to $\alpha$, $\delta\alpha$, and the corrected values of $\alpha_c$ are listed for the eight radio galaxies. In some cases, the correction was quite large, particularly for those with $\sigma/\gamma$ greater than 0.3 and the resulting values of $\alpha_c$ should be treated with considerable caution. In particular, it would be again unwise to compare directly these results with those of the investigation carried out in Chapter 7 on much brighter, lower redshift galaxies. Nevertheless, the alpha parameters for these

galaxies should measure, at least crudely, the deviation from a stellar profile.

Figure 4.4a shows the corrected measurement of $\alpha$ for the eight radio galaxies and eight reference stars as a function of their apparent r magnitude. The stars, plotted as open symbols have values of $\alpha$ that are close to zero, the value expected for unresolved objects. It is worth noting parenthetically that this is only after the seeing correction based on a galactic profile has been applied. The seeing correction that is actually derived for an unresolved star and a gaussian seeing disk is much smaller than this. The fact that a larger correction is actually required to bring the measured values of $\alpha$ for the stars to close to zero probably illustrates that the seeing point spread function is not purely gaussian in form, but has more power at large radii. This will obviously have some effect on the galaxies too, but the importance of this analysis is in the relative measurements of the radio galaxies and comparison stars.

At least four of the radio galaxies are clearly resolved in Figure 4.4a, by virtue of their non-zero alpha measurement. Interestingly, 3Cs 267, 280 and 324 are amongst the bluest galaxies on the (r-K) diagram. The remaining four galaxies are unresolved by the seeing disk. Although this may indicate that they are dominated by a nuclear source, this is not required by their location on Figure 4.4a. Their unresolved appearance can be caused by either compact size or poor resolution. In order to investigate this further, the corrected values of $\alpha$ are plotted in Figure 4.4b against the ratio of the seeing to the apparent size of the sampling radius, $\sigma/\gamma$. For $\sigma/\gamma$ less than 0.35, the corrected value of $\alpha$ for

Table 4.4: The α-parametre for faint 3C galaxies.

| 3CR | α | σ/γ | δα | $\alpha_c$ | Δ(r-K) |
|---|---|---|---|---|---|
| 34 | 1.01-1.04 | 0.21 | 0.05 | 0.96-0.99 | 0.6 |
| 65 | 0.10-0.47 | 0.23 | 0.07 | 0.03-0.40 | ≃ 0 |
| 241 | 0.13-0.45 | 0.35 | 0.24 | -0.11-0.21 | ≃ 0 |
| 267 | 0.94-1.08 | 0.31 | 0.18 | 0.76-0.90 | 1.0 |
| 280 | 0.71-0.79 | 0.35 | 0.24 | 0.47-0.55 | 0.9 |
| 289 | 0.30-0.49 | 0.42 | 0.40 | -0.10-0.09 | 0.2 |
| 368 | 0.27-0.47 | 0.40 | 0.35 | -0.08-0.12 | 1.4 |
| 324 | 0.47-0.65 | 0.30 | 0.16 | 0.31-0.49 | 1.7 |

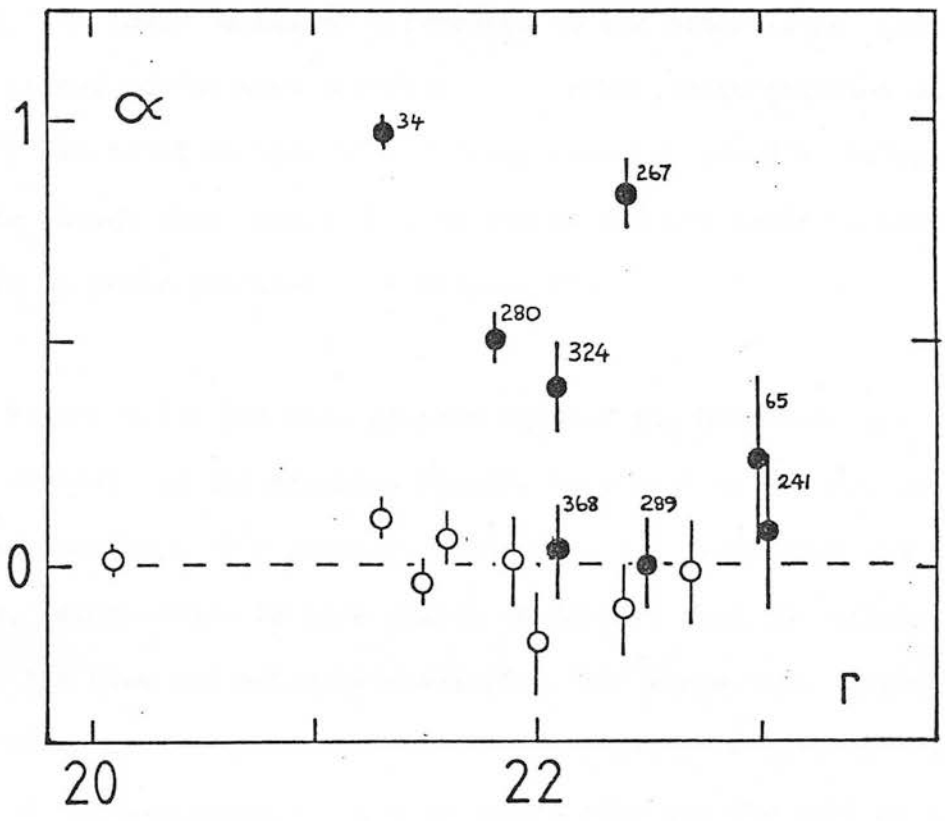


Figure 4.4a: The values of the α parameter found for 8 faint 3C radio galaxies (solid circles) and 8 comparison stars (open circles) as a function of their r magnitudes.

the different radio galaxies does not appear to depend on the ratio. At a given $\sigma/\gamma$ there is a spread in the values of $\alpha$ measured. This is reassuring since the seeing correction is intended to remove the effects of having different $\sigma/\gamma$ ratios for different galaxies. It is noticeable in Fig. 4.4b, however, that both the radio galaxy images that have $\sigma/\gamma$ greater than 0.4 have 'unresolved' profiles indicated by values of $\alpha$ close to zero, and this may indicate the point at which the analysis breaks down in the presence of increasingly poor seeing. Reference to Figure 7.4 and Table 4.4 certainly indicate that it is around this point that the computed seeing corrections to $\alpha$ begin to increase dramatically with further deteriorations in $\sigma/\gamma$. In the two cases of 3C 65 and 3C 241, however, the lower values of $\alpha$ compared to the other radio galaxies would appear to be more reliable since other radio galaxies at the same $\sigma/\gamma$ are found to have higher (i.e. more 'resolved') values of $\alpha$. Note though that values of $\alpha$ of around 0.2 are found in some low redshift 3C radio galaxies (see Chapter 7).

In Figure 4.5 $\alpha$ has been plotted against the blueness parameter $\Delta(r-K)$ defined in the previous Chapter (see Section 3.4.d). The two galaxies that have $\sigma/\gamma$ greater than 0.4 are indicated by open circles, since there is some reason to believe that the values of $\alpha$ derived for them are not very meaningful. If these are neglected, then there is a trend for the bluer galaxies to have the higher values of the $\alpha$ parameter. In other words they are the most extended and the two galaxies that remain in the sample with $\Delta(r-K)$ close to zero, are the least resolved. Of course, this trend is in exactly the opposite sense to that expected if the colour change in (r-K) is due to the addition of a nuclear ultraviolet component. It is

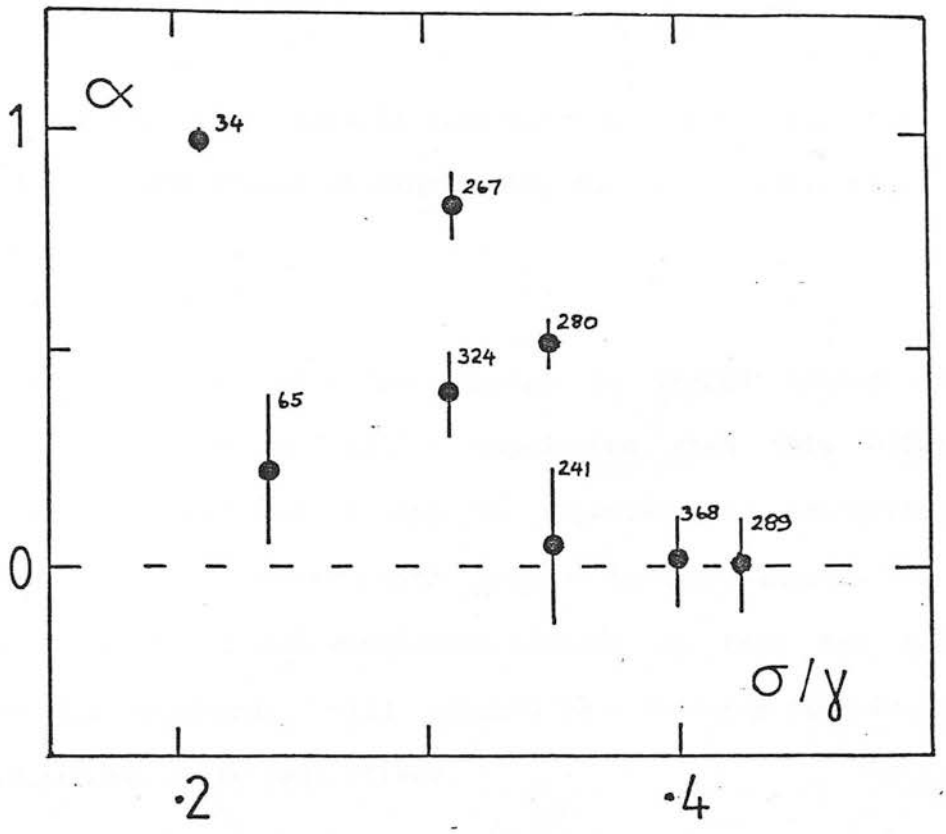


Figure 4.4b: The corrected measurement of α plotted against the seeing of each exposure expressed as the ratio σ/γ.

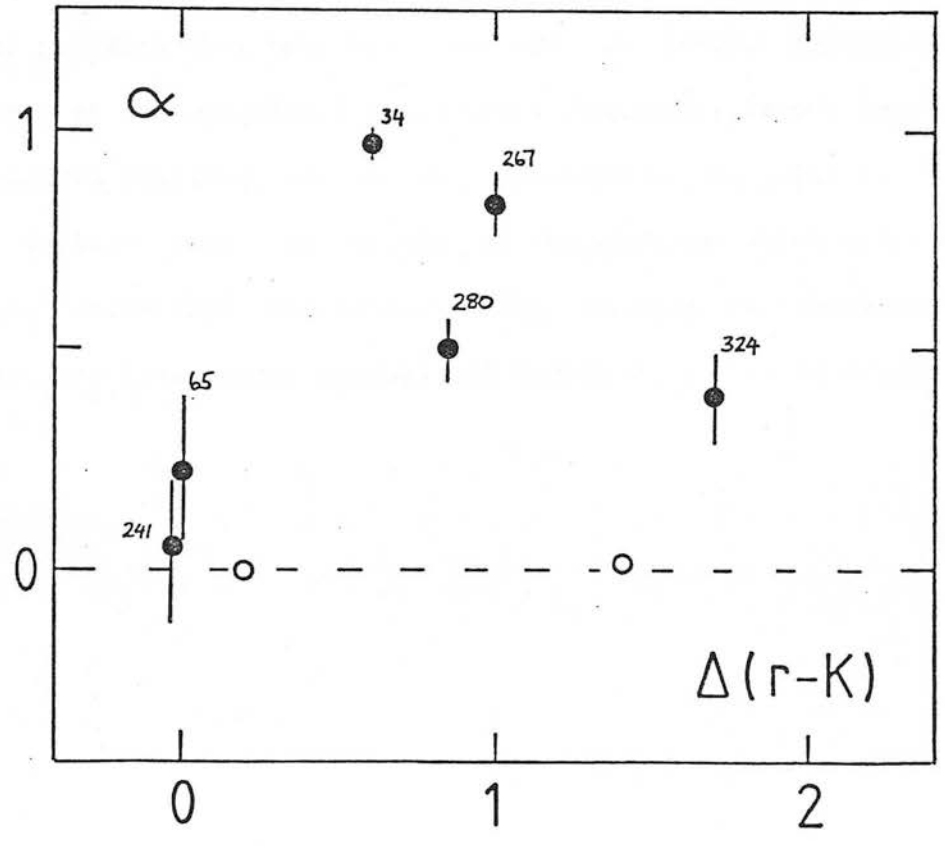


Figure 4.5: The variation of α with the blueness parameter Δ(r-K). The two open circles represent the two galaxies with σ/γ greater than 0.37 in Figure 4.4b.

unfortunate that this possible link between $\Delta(r-K)$ and the image size is at the limits of credibility due to the small size of the sample.

Nevertheless, if the colour change is indeed caused by the existence of a young stellar population then this effect, if confirmed in larger samples, may be important in indicating the locations of the star-forming regions in the galaxies. The Space Telescope, with its high resolution imaging in both the red and ultraviolet wavebands, will clearly be a valuable tool in further investigations in to this effect.

In the meantime, the most important result from this analysis is the demonstration from Figures 4.4a, and particularly 4.5, that most of the galaxies that have blue colours in (r-K), indicating the presence of the additional ultraviolet component, have r images that are clearly resolved, and are not dominated by the galactic nuclei. This implies that the origin of the emission which produces the 'excess' rest-frame ultraviolet flux density is throughout the galaxy, and this argues strongly in favour of a stellar origin.

## Chapter 5 : THE STELLAR POPULATIONS OF RADIO GALAXIES AT HIGH Z

In the preceding two chapters, evidence has been presented to the effect that the broad-band continua of radio galaxies change, in some wavebands, with redshift. There is furthermore evidence that these changes are caused by a change in the stellar populations of these galaxies and it is the intention, in this Chapter, to explore in more detail the information on the stellar populations of these high redshift radio galaxies, that can be gained from the data presented in the previous two chapters.

### 5.1 : Models of the Stellar Populations of Elliptical Galaxies

Because elliptical galaxies appear on first sight to be rather simple stellar systems, and because of the historical importance of 1st ranked cluster ellipticals in cosmological investigations, there has been considerable work on understanding their stellar populations, and on modelling the evolution of these populations over cosmological timescales. Two approaches have been taken, which particularly when considered as complementary to each other, have yielded important results. These are conveniently referred to as 'population synthesis' and 'evolutionary synthesis' modelling.

In the former, the spectral energy distribution (SED) of the model galaxy is represented as the linear combination of the SEDs of as many different stellar types as possible. The optimum mix of these different stellar types is then found by comparison with available data on nearby galaxies. Various obvious astrophysical

constraints may be applied to exclude some 'impossible' combinations. The usefulness of this technique, which has been used by, amongst others, Faber (1972) and O'Connell (1976,1980), is that the population is sufficiently unconstrained that the presence of small minority populations can be detected. On the other hand, the models give no information on how these populations might have arisen and hence on the change in these populations with cosmic time that one might expect to observe. The most recent application of this approach has been the paper by Gunn et al (1981).

In the 'evolutionary synthesis' technique, simple analytic forms are assumed for the logarithmic slope of the stellar Initial Mass Function (IMF), x, and the Star Formation Rate (SFR) history. Using theoretical or 'semi-theoretical' evolutionary tracks for stars of different masses, the density of stars at all points on the HR diagram are computed as a function of time for a coevally produced population of single stars (a simple stellar population SSP). Hence, using a library of stellar SEDs, the integrated spectrum of the SSP as a function of time after the stars were formed, is constructed. These spectra may then be convolved with the desired SFR history to produce the spectrum of the model galaxy at all epochs. These 'predictions' may be compared with observations of galaxies at any epoch. Since the early work of Tinsley (1972), these models have been progressively refined, particularly as a result of the outcome of the 'population synthesis' models described above. Although some detailed aspects of the work were subsequently found to require modification (e.g. the Giant Branch) the paper by Tinsley and Gunn (1976) established many of the basic features of the evolution of a simple stellar population.

The models of Bruzual (1981) (see also Bruzual 1983) incorporated several new features. In particular Bruzual made extensive use of satellite data on the ultraviolet continua of stars, especially new data on the cooler stars, to extend the wavelength coverage of the model SEDs to include the range from 300 A to 3 microns. This was important since the evolutionary changes are generally larger in the ultraviolet than in the region longwards of 4000 A where the continuum is increasingly dominated by Giant Branch stars, and because the ultraviolet waveband is observed through optical passbands for objects at high redshift. This work will be refered to several times in the discussion of this Chapter, and will be discussed in some more detail later.

An important contribution to the evolutionary synthesis literature has also been made by Renzini (1981). Although his use of only bolometric luminosities (and effective temperatures) makes comparison with observation difficult, his analysis of the relative contributions to the total luminosity of an SSP, from stars in the various evolutionary phases on the HR diagram, derived from considering the mass of fuel burnt, is particularly clear. His argument that the changes in the later evolutionary stages (i.e. those associated with the Giant Branch) should be most important in evolutionary synthesis models, because of the high fraction of the total bolometric luminosity that is produced by these stars, is particularly true when considering infrared data, which is virtually unaffected by the evolution of the main sequence turn-off colour. Many modellers have concentrated on the main sequence turnoff point, which contributes only a small fraction of the bolometric

luminosity.

### 5.1.a General Results and a Simple Analytic Evolutionary Model

It is worthwhile to describe briefly the evolution of stars of low and intermediate masses. Figure 5.1 shows an idealized HR diagram (after Renzini 1981) showing the various phases of stellar evolution for such stars. Apart from a short 'pre-main-sequence' phase, the stars appear initially on the zero age main sequence (MS). The star spends a relatively long period burning core hydrogen on the main sequence, a time which is a strong function of the stellar mass and which probably exceeds the present age of the universe for masses less than 0.8 solar masses. After this, the star moves rapidly across (as a sub giant) to the base of the giant branch with the onset of hydrogen-shell burning. The star then proceeds to ascend the red giant branch (RGB), until at the tip of the 1st ascent, core-helium ignition takes place. Subsequently, the star moves very quickly down to the horizontal branch (HB), which is in fact often merged with part of the RGB to form a so-called 'clump'. After a period on the HB, the star, which by this stage may have lost a significant fraction of its original mass in the form of a stellar wind, moves up the assymptotic giant branch (AGB), before a rapid post-AGB evolution takes the star to the white dwarf state, or other appropriate remnant, via a hot post-AGB phase (such as the nucleus of a planetary nebula). The location of the HB can be a very strong function of the metallicity of the star, and stars of low metallicity can be very hot.

As far as evolutionary changes between ages of 1 and 20 Gyrs are

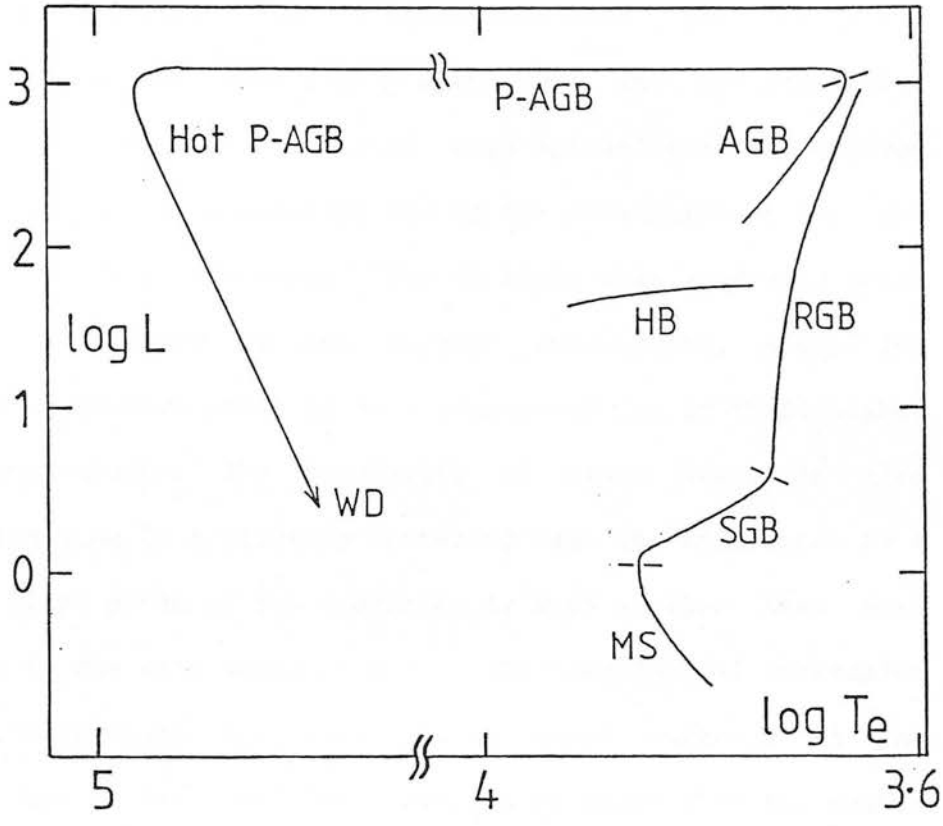


Figure 5.1: The evolution of stars of low to moderate mass on the Hertzsprung-Russell diagram (after Renzini 1981). The phases of the evolution are progressively the main sequence (MS), sub-giant branch (SGB), red giant branch (RGB), horizontal branch (HB), assymptotic giant branch (AGB), post-AGB and hot post-AGB, and finally the white dwarf (WD) or other remnant. The RGB, HB and AGB are collectively referred to as the giant branch. The main sequence phase is by far the longest in duration.

concerned, the populations that are most important are (a) the main sequence stars (MS) and (b) the giant branch stas, including both the 1st ascent red giant branch (RGB) and the assymptotic branch (AGB). In a coeval, simple stellar population (SSP), both the MS and giant branch populations will change with time. The MS population will become progressively depleted with age as stars are removed from the upper (i.e. more massive) end of the population at the end of their individual lifetimes. The MS light will gradually decay with time, particularly at the shorter wavelengths, where the contribution of massive stars is most pronounced due to their higher effective temperatures. The population of giant stars is also changing with time in a slightly different way. The time spent by a star in the giant phase of its evolution is much smaller than both its lifetime on the main sequence and of the cosmological timescales of interest. This means that there is a rapid turnover in the population, and in fact the giant phase is so short that the number of giants at any epoch can safely be assumed to be proportional to the rate at which stars are leaving the main sequence at that time. In practice, since the colours of a giant star do not appear to be a strong function of the mass of its progenitor, the colours of the giant population will not change much, although the luminosity can change markedly due to the changing number of stars at different times.

Broadly speaking, the effect of these changes on the integrated colours of the stellar population is basically to make the galaxy redder with age as the MS light decays. A very simple analytic scheme representing these effects is useful to illustrate some interesting features of this evolution that are found in more

complex models.

In any passband i, the total flux density may be assumed to be made up of the sum of the contributions of the MS and giant branch stars. The giant branch contribution is assumed to be given by the number of red giants multiplied by the mean luminosity in that waveband, $\bar{f}_{iRG}$. This is assumed to be independent of the mass of the progenitor star.

$$f_i = \int dm.\Psi(m).f_{iMS}^{(m)} + N_{RG}.\bar{f}_{iRG} \qquad (5.1)$$

$\Psi(m)$ is the Mass Function. In a SSP this will be represented by the IMF, which is usually parameterized as a powerlaw in mass, truncated at the turnoff mass.

$$\Psi(m) = \bar{m}^{(1+x)} \quad ; m < m_{TO} \qquad (5.2)$$
$$\Psi(m) = 0 \quad ; m > m_{TO}$$

The number of red giants at any epoch for a SSP will be given by:

$$N_{RG} = \Psi(m).\frac{\delta m_{TO}}{\delta t}.\bar{\tau}_{RG} \qquad (5.3)$$

So the total flux density for a SSP as a function of time may be written as:

$$f_i = \int_0^{m_{TO}} dm.\, m^{-(1+x)}.f_{iMS}^{(m)} + m_{TO}^{-(1+x)}.\frac{\delta m_{TO}}{\delta t}.\bar{\tau}_{RG}.\bar{f}_{iRG} \qquad (5.4)$$

One important thing is already apparent. The initial mass function enters in to both the MS and red giant contributions. Furthermore, if all the functions of mass in the above equations could be represented as simple power-laws of the mass, then the dependence of both the MS and red giant components on the

logarithmic slope of the IMF, x, will be the same. If this was the case, then when considering the change with time of a colour (i.e. the ratio of the flux densities through two passbands in which the two components will generally be of differing relative importance), the slope of the IMF would not therefore, on this simple model, be important, since the dependence on x would not be changed by the integral. On the other hand, the flux density change in a single passband will depend strongly on the form of the IMF. The important consequence of this 'decoupling' of the colour and luminosity evolution is that it would be impossible to determine the predicted luminosity change from measurements of the (relatively easily observed) colour change, even in a simple coeval population. In fact, the various functions of mass in equation 5.4 are not all best represented by such simple power-laws (see e.g. Table 5.1), and so there is some dependence on x in the predicted colour evolution.

To make further progress it is neccessary to assume analytic forms for $f_{iMS}(m)$, $\bar{f}_{iRG}$, $\bar{\tau}_{RG}$ amd $m_{TO}(t)$. These were derived for the U, R and K passbands using the data tabulated by Bruzual (1981) and the colours of stars with various spectral types given by Johnson (1966b). These analytic forms are tabulated in Table 5.1. Using these, it is possible to compute the colours and magnitudes of the SSP as a function of its age. The results of this are shown in Figure 5.2 for the U and K passbands only, since the R curve is very similar to that for K.

The important feature of this diagram is that the evolution is more marked in the ultraviolet than in the infrared (the curves have been normalised at an age of 16 Gyrs). This of course leads to the

Table 5.1: Polynomial Expressions for U, R, K and $\tau$.

$y = a_0 + a_1x^1 + a_2x^2 + a_3x^3 + a_4x^4$

$x = \log (M/M_0)$; $\tau =$ log (MS lifetime in years)

| y | $a_0$ | $a_1$ | $a_2$ | $a_3$ | $a_4$ |
|---|---|---|---|---|---|
| U | 5.298 | -15.643 | 13.632 | -8.427 | 0.198 |
| R | 4.006 | -9.277 | 6.693 | -4.319 | 1.016 |
| K | 3.141 | -5.826 | 4.422 | -3.984 | 1.101 |
| $\tau$ | 9.922 | -3.873 | 1.485 | -0.210 | 0.000 |

$\tau_{RG}$= 0.86 $10^9$yr. $\bar{K}_{RG}$=-1.86 $\bar{R}_{RG}$=0.86 $\bar{U}_{RG}$=3.80

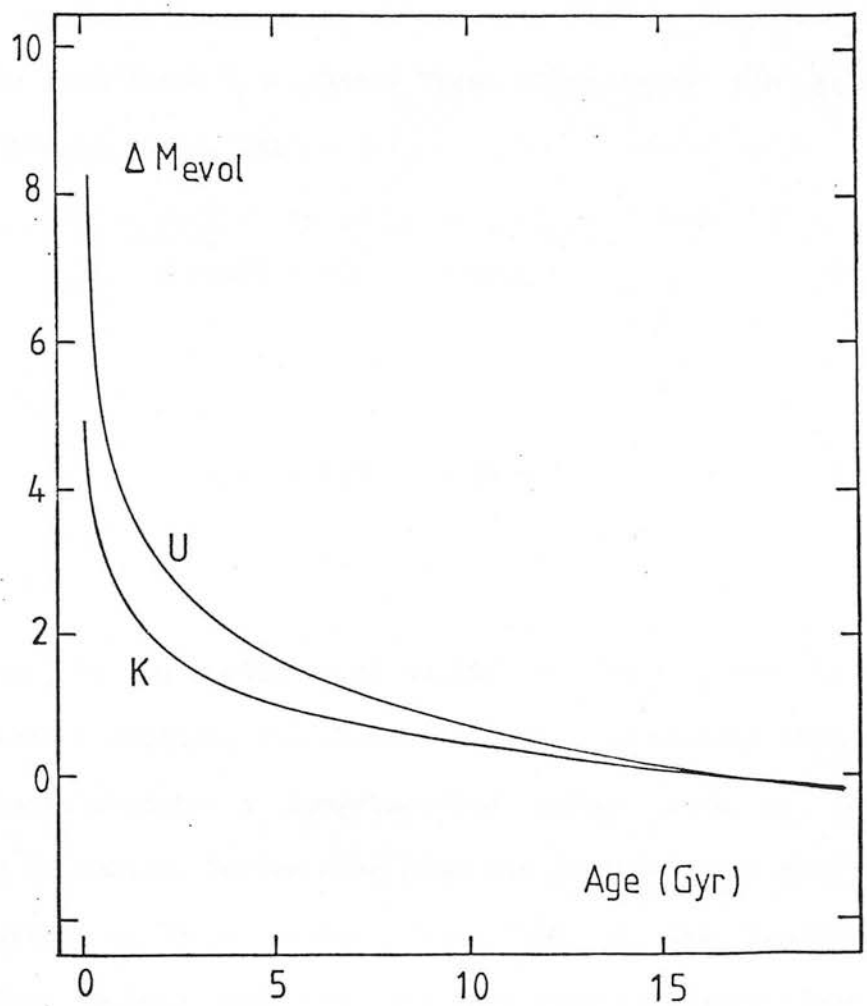


Figure 5.2: The change in the rest-frame U and K absolute magnitudes as a function of time after formation that is predicted for an SSP using the simple analytic model described in the text with a value for x of unity. The curves have been normalised at an age of 16 Gyr.

reddening of the population with age. It is straightforward to examine the dependence of both the luminosity and (U-K) colour evolution on x, the slope of the IMF. Of particular interest, is the change that may be predicted in the infrared absolute magnitude and in the (U-K) colour, between ages of 6 and 16 Gyrs, because this is probably the change in epoch that corresponds, at least roughly, to a change in redshift from unity to zero. A change in the rest-frame (U-K) colour at a redshift of unity will, of course, be observed to a large degree as a change in the (r-K) colour. In fact, the r passband at a redshift of unity is at about 3250 A, compared with 3600 A for the rest-frame U passband. These differences are given, in this very simple model, by:

$$\Delta\,(U-K) = 0.46 - 0.06.x \qquad (5.5)$$

$$\Delta\,K = 1.12 - 0.26.x \qquad (5.6)$$

Notice that, in the evolution of an SSP in which there is no continuing star formation, the change in colour is smaller than the luminosity change even for a long-baseline colour such as (U-K) (given that x is small). Notice also that the dependence on x of the colour evolution is much weaker than that of the luminosity evolution. This merely reflects the fact that the expressions in Equation 5.4 are almost power-laws in the mass, but does suggest that an empirical determination of the size of the luminosity evolution from observations of the colour evolution is not possible, given all the additional uncertainties that will affect the precise

values of the coefficients in Equation 5.5 that are produced by a more sophisticated model.

In passing, it is reassuring to note that Equation 5.5 reproduces exactly the evolutionary effects found in apparently more complex models (e.g. Bruzual 1981). Of course, the polynomial expressions in Table 5.1 were derived using the data that Bruzual used in his models, so the agreement is not very surprising. Nevertheless, it does show that nothing is lost by making the very simple assumptions about the causes of the evolution. The more detailed models are still very useful for studies of precise effects, such as the evolution of absorption line strengths, but the simple analytic form is sufficient to at least make clear the cause and size of the broad-band colour changes, which, at present, are in any case the only data that are available on very high redshift galaxies.

When the curves in Figure 5.2 are multiplied by a function representing the age distribution of the stellar population in a model galaxy, which will be the reverse of the SFR history, then it is clear that the ultraviolet luminosity will be very sensitive to the presence of any minority population of extremely young stars that have virtually zero age. Furthermore, because the evolution is much smaller in the infrared than in the ultraviolet, it is possible to have large changes (of order at least 1 magnitude) in the ultraviolet flux density of the galaxy accompanied by much smaller (0.1 magnitudes) increases in the infrared flux density. Hence large colour changes can occur without large infrared luminosity changes in a system that has some continuing star formation activity. This

is in contrast to the system that has no such activity, in which the colour change will generally be rather smaller than the luminosity change, over the time intervals of interest.

Brief mention should be made about the effects of chemical evolution. If there is star formation in a galaxy at more than one epoch then, because some of the metals produced in stars are returned to the interstellar medium during the later phases of stellar evolution, the stars produced at later epochs may have different metallicities than those formed earlier in the life of the galaxy. Infall of 'primordial' material from outside the galaxy may also modify the chemical composition of the interstellar medium. If the mean metallicity of the stellar population does change with epoch, then the colours will evolve also, regardless of any other effects. This is because the ultraviolet flux densities of stars are sensitive to the blanketing effects of metal absorption lines. However, in a pure SSP in which all the stars are formed at a single time, the mean metallicity will not change with time, provided that the IMF is not a function of metallicity. In a more realistic model galaxy, some very rapid chemical evolution of the interstellar medium must occur at the beginning of the history of the galaxy in order to allow the formation of the old stars of solar metallicity or greater that are presently seen in elliptical galaxies. However, the epoch at which this rapid chemical evolution must have occurred is well before those that are relevant to the current investigation. In a model galaxy that contains a spread of stellar ages, for example one in which a burst of star formation occurs after the bulk of the population formed, the mean chemical composition of the stars may well change. However, there are so many other uncertainties such

as the slope and cut-off mass of the IMF of the young population, and the precise SFR history of the burst, that it is sufficient with the present data to assume that the mean metallicity stays constant at all epochs.

5.1.b The models of Bruzual (1981)

The models of Bruzual (1981) have become widely used in the past two years to interpret and discuss observational data on distant galaxies. The models are easy to use in this manner since they are tabulated in terms of observed colours as a function of redshift. The loss of generality that this entails, because of the need to specify a cosmological model, is not a problem given the rather crude state of the observational material with which the models can at present be compared. Bruzual's (1981) models also include a wide range of SFR histories. The models inevitably have their limitations, and a slavish use of them would be unwise. Nevertheless, they are a useful tool in discussing observational results and intercomparing the results obtained by different observational methods.

Mention should first be made of the terminology that is used to describe the different models. The basic model is the passively evolving 'C' model. This has a burst of star formation lasting 1 Gyr, during which the star formation rate is constant. After this period, however, the SFR is zero. The models that are most of interest have this burst occuring 16 Gyr before the present time, and assume values of $H_0 = 50$ kms$^{-1}$ Mpc$^{-1}$ and $q_0 = 0$ to relate cosmic time and redshift. The Nonevolving 'NE' model is in fact based on the

present spectrum of the 'C' model rather than on observations of galaxies at zero redshift. Actively evolving galaxies are represented by a series of models (the '$\mu$' models) in which the star formation is an exponentially decaying function of time. The parameter $\mu$ is used to describe the SFR and, taking values in the range $0<\mu<1$, this parameter represents the mass fraction of the galaxy that is in the form of stars at the end of the first Gyr. A model with $\mu$ close to unity thus looks very like a 'C' model, while those with $\mu > 0.5$ are very similar to the passively evolving models for ages greater than 10 Gyr. These models that have little, if any, star formation at the present epoch are probably relevant at some level to elliptical galaxies. A model with $\mu < 0.1$ however, has an SFR that decays only slightly with epoch. It is probably more appropriate for late spiral type galaxies.

A single IMF is assumed for the star formation at all epochs. This is taken to have a logarithmic slope of 1.35 which is the Salpeter (1955) value. Such a slope is probably slightly steeper than the actual slope, but it has been shown above that x has only a weak effect on the colour evolution. Solar metallicity is assumed for all the stars in the model galaxies.

There are two particular limitations to the models that will affect the discussion in this Chapter. The first concerns the treatment of the giant branch. Unfortunately, the evolution of stars in these later phases of their lives is still rather uncertain, principally on account of the uncertainty that surrounds the mass-loss process. Bruzual employs an empirical Giant Branch Luminosity function that is assumed to be independent of the mass of

the progenitor star for masses which are less than about twice solar; in fact the R2 population of Tinsley (1978) is used. Examination of the models for Giant evolution (e.g. Sweigart and Gross 1978) indicates that this assumption, while justified to a certain degree, is unlikely to be completely correct. The complete lack of evolution exhibited by the models in those colours such as (H-K) that are dominated by the giant branch stars, is a consequence of this assumption. This will be discussed further in Section 5.2. For stellar masses above two solar masses, evolutionary tracks are used but these do not extend beyond the point of Helium ignition. In practice, this is actually less of a problem in the current investigation, because the observations do not extend to galaxies at sufficiently high redshift that the effects of these massive stars is likely to be important.

The second problem concerns the ultraviolet flux densities of the models between 2000 and 4000 A. Models of old stellar populations of an age greater than 10 Gyr, which are required by the observed red visual colours such as (B-V), have an ultraviolet flux density that is too small when compared with nearby elliptical galaxies. This deficiency has been noted by many authors (e.g. Faber 1977 and references therein). It has the immediate practical effect that the colour-redshift predictions of the non-evolving 'NE' model do not match, at all redshifts, those that would be predicted on the basis of redshifting the spectral energy distribution of a low redshift elliptical galaxy. The 'NE' model prediction is redder than that based on 'real' elliptical galaxies. Fortunately, the empirical unevolving K-corrections based on observations of nearby galaxies are quite well known, and have been published for almost all

passbands. However, although it is possible to adjust the models to be consistent with the zero-redshift data, this discrepancy does indicate the presence of a population of hot stars, which are not present in the models, and whose evolutionary properties are not known.

The nature of these hot stars has recently been reviewed and investigated by Gunn et al (1981,GST). The possibilities include the following: (a) Blue horizontal branch stars. These can be produced in an elliptical galaxy from stars at the turnoff mass (about 0.8 $M_\odot$) either by having a minority population of much lower metallicity than the average, or, if the stars are metal rich, by having unusually severe mass loss, so that they are effectively of lower mass. (b) Young stars. These stars would be produced by continuing star formation. GST considered two possible populations. One was based on the empirically determined population of young stars in the solar neighbourhood, while the other, reflecting the uncertainty of the IMF in elliptical galaxies, was based on the same population but omitted the O and early B stars. (c) Blue stragglers. These are stars located on the main sequence above the turnoff point but within a factor of two in apparent mass of that point. Their nature and evolution is controversial. Possible mechanisms involved in producing these stars include anomalous mixing in single stars and mass transfer in binaries. (d) O stars. These can arise either in a young population with an IMF that is rich in massive stars, or they may represent pre-white dwarf or even subdwarf stars. The status of stars in the last category is not at all clear.

GST found that either of the first three groups matched well the

observed spectra of nearby ellipticals when they were combined with the basic old population. The HB stars could be ruled out, however, because a substantial metal poor population would be seen elsewhere on the HR diagram (e.g. on the red giant branch) while the effect was too large to be explained by the fraction of anomalous mass loss metal rich stars that could be plausibly produced. GST were, however, unable to differentiate between the other two possibilities.

## 5.2 : Infrared Colours and the Evolution of the Giant Branch

At a redshift of unity, the observed infrared colour (H-K) is roughly equivalent (apart from an additive term) to an (R-J) colour in the source rest frame. The lack of deviation in the mean observed (H-K) colour at redshifts close to unity shown by Figure 3.5(i) (see also Table 3.4) means that the rest frame (R-J) colour is the same at a redshift of unity as at zero redshift.

(R-J) is at sufficiently long wavelengths that the light from all but the very youngest SSPs is dominated by the contribution from the post main sequence (PMS) giant branch stars. In terms of bolometric luminosity, about 80% of the total SSP luminosity is produced by PMS stars if turn-off mass is below 3 $M_{\odot}$, while even at 7 $M_{\odot}$ the fraction is still around 70% (Renzini 1981). The corresponding fractions for discrete passbands at wavelengths greater than 6000 A will be even larger because the PMS stars are redder than all the other stellar types (see Figure 5.1). The galaxies may well not be single aged SSPs, of course. Nevertheless, provided that the SFR at the epoch of observation is not very high,

the giant dominance will still hold. This is illustrated by the lack of a significant difference in the observed (H-K) colour of Bruzual's (1981) actively and passively evolving models. Furthermore, if as seems most plausible, the SFR in elliptical galaxies was so much higher at the start of the galaxies' lives that most (e.g. more than 90%) of the stars were formed at that time, with only a small dribble, or perhaps intermittent bursts, of Star Formation after that period, then the population of giants will be dominated by the oldest stars in the population. Again, this may be illustrated by reference to the small difference between the predicted infrared luminosity evolution of Bruzual's (1981) actively and passively evolving models. It is therefore reasonable to make the simplifying assumption that the observed (H-K) colour is sampling exclusively the population of giant stars that were formed from stars that were created during the period of maximum SFR, which was probably at the beginning of the life of the galaxy. With this assumption, the observed lack of a change in (R-J) may be used to try to place some constraints on the evolution of the giant branches in these galaxies.

Figure 5.3 shows an empirical HR diagram in (R-J),J. The location of the main sequence is shown, with two turnoff points marked. For reference, the mean present day colour of giant elliptical galaxies is also indicated. The giant branch is shown in more detail. The sizes of the circles represent the logarithm of the number of stars in a population at each point on the diagram, which is proportional to the inverse of the time spent by a single star at that point as it traverses the evolutionary track. Tinsley's (1978) 'R2' giant branch, based on the population of old disk giants

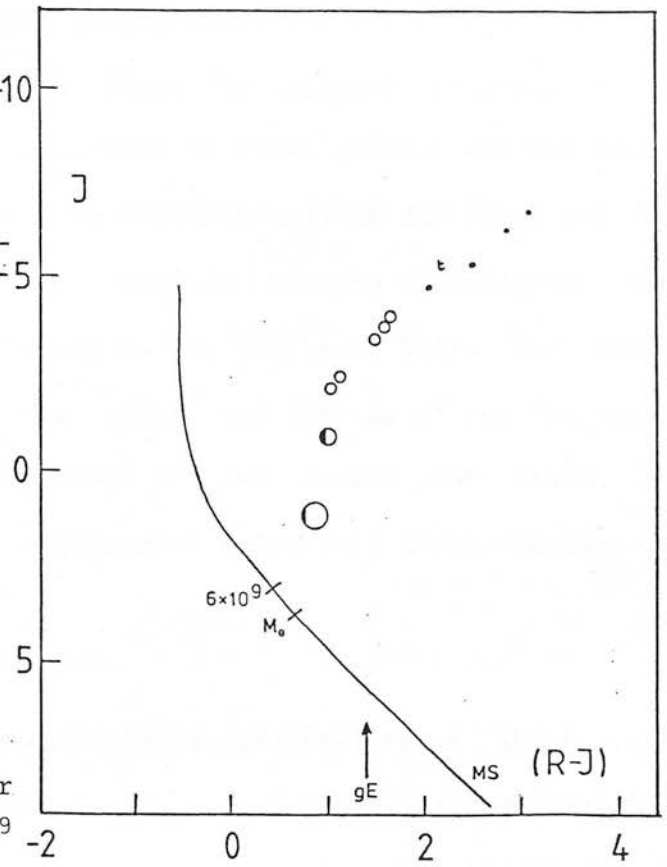


Figure 5.3: The H-R diagram in (R-J),J. The number of stars along the giant branch is represented logaritmically by the size of each circle. The clump stars are shown as the shaded portions of the two lowest circles. The tip of the 1st ascent of the RGB is shown as a small 't'. Two turn-off points are shown on the MS, corresponding to a solar mass and an age of $6.10^9$ years respectively. The integrated colour of a nearby giant elliptical galaxy is shown.

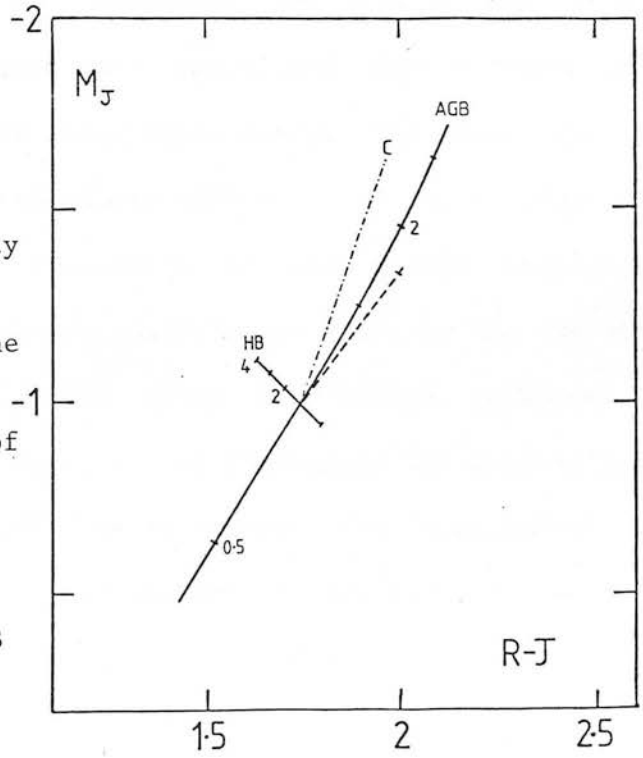


Figure 5.4: The change in colour and magnitude that is associated with changing the numbers of stars in the two minority populations (HB and AGB) by various factors f. The dash-dot line shows the effect of the addition of carbon stars, while the dashed line represents the change if only the reddest stars on the AGB are changed.

(ODG) in our own Galaxy, has been used, while the colours were taken from Johnson (1966b) using the spectral types for Tinsley's Giant Branch given by Bruzual (1981). Since the primary interest is in differential effects, the precision of these colours and the efects on them of assumptions about the metallicities of the stars are not critical. The HB clump stars occupy two bins on the diagram. They are represented by solid shading in the two lower bins. The giants that are found between the clump and the tip of the 1st ascent (indicated by a 't') are a mixture of 1st ascent RGB stars, and post-HB AGB stars, in the approximate ratio 4:1. Above the tip, all stars are AGB stars.

The effect of altering the relative proportions of these stars on the integrated colour and luminosity of the giant Population was investigated. For each of the 'minority' populations, the HB and AGB in turn, the number of constituent stars in each bin was multiplied by a single factor, f. The new integrated (R-J) colour and mean J absolute magnitude per star was calculated for a range of f, including values greater and less than unity. The mean absolute magnitude change that is associated with a given colour change will be of some interest in the discussion of the Hubble diagram to follow. The results of this analysis are shown as the two solid lines in Figure 5.4. The labels along the curves indicate the appropriate values of f. The effect of increasing the proportion of stars on the different branches is to increase the luminosity, and to change the colour either redwards or bluewards depending on whether the mean colour of the minority population is higher or lower than that of the integrated population. Two other changes were also investigated. These were to increase just those AGB stars in

the last two bins at the top of the AGB, and to include a number of Carbon stars. The effect of adding only the latest AGB stars is obviously to produce a given colour change for a smaller increase in luminosity, since no stars with colours close to that of the original population are added. In the case of the carbon stars, the (R-J) colours were derived from the data of Cohen et al (1981) and Blanco et al (1980). Although they are generally very red stars, C stars are not in fact as red in (R-J) as late M giants, and have a correspondingly smaller effect on the colours.

It can be seen from Figure 5.4 that changes in the HB contribution are relatively unimportant to either the colour or the luminosity. The influence of the AGB stars is clearly much greater, and the observed lack of change in the mean (H-K) colour at high redshift can be used to set constraints on the change in the relative contributions of RGB and AGB stars. Although a 'conspiracy' between changes occuring in both the HB and AGB populations could conceivably produce no net colour change, this is not very likely since theoretically (Renzini 1981) changes in the AGB are expected to be very much larger than those in the HB.

The intrinsic (R-J) colour of the radio galaxies at a redshift of unity is at most 0.04 magnitudes redder than at low redshift (Table 3.4). In fact it will be recalled that the mean colour was 0.02 magnitudes bluer. Taken literally, this upper limit of 0.04 magnitudes suggests from Figure 5.4 that the number of AGB stars, relative to the RGB stars, has not increased by more than 15%. This assumes that this is the dominant change that can occur.

However, one factor that should be considered is the probability that the mean colours of the RGB itself will depend on the mass of the progenitor star for masses smaller than 2 $M_{\odot}$ (i.e. contrary to the assumption made by Bruzual 1981 and others). The models of Sweigart and Gross (1978) show that the mean effective temperature of the 1st ascent giant branch may change by about 0.03 in the log between progenitor masses of 1.8 and 0.9 $M_{\odot}$. This could produce a change in (R-J) colour of up to 0.20 magnitudes, in the sense that the higher mass stars will have a bluer giant branch.

Even if the whole giant branch is shifted by 0.2 magnitudes to the blue at a redshift of unity, the new upper limit to the colour change of 0.24 magnitudes would still indicate that the relative numbers of AGB and RGB stars had not more than doubled. Parenthetically, the high turn-off mass that is required to produce such a big colour change in the giant branch is very unlikely to be found at a redshift of one, since it corresponds to an age of only 1 Gyr.

Renzini (1981) has emphasised the importance of the changing relative contributions of the AGB and RGB stars to the integrated luminosities of SSPs and, in principle, the rather small change that is observed could be used to place constraints on the relative ages of the SSPs that are observed at redshifts of order unity and those that are nearby. However, the details of Renzini's calculations are very susceptible to the current uncertainties regarding the amount of mass loss that occurs from the giant stars during the later phases of their evolution, i.e. when on the HB and AGB. In addition, there is one particularly good reason why the results of these

calculations may not be applicable to the present investigation. Renzini's SSP at the present age of the universe has 5 times more bolometric luminosity emitted by the RGB than by the AGB. While this is a good representation of the case in metal-poor old globular clusters, it is not correct in the case of present day elliptical galaxies, in which the bolometric luminosities of the two populations are comparable. The additional AGB light in the ellipticals is believed to come from an old metal-rich population in the galaxies (communication from Dr. Frogel). This is based on observations of the globular cluster system of Cen A. Such old stars can form an upper AGB if the mass loss during the later stages of evolution is small enough, and the fact that they do not appear in the SSP models is simply an indicator of our general lack of understanding of the mass loss phenomenon and its dependence on the metallicity of the star. The evolution of this population, which obviously contributes greatly to the infrared luminosity of metal rich systems is not obvious. A large effort is required, theoretically and observationally, to understand the PMS evolution of stars of high metallicity and moderate mass (i.e. less than 2.0 $M_{\odot}$).

Although they are unfortunately of low metallicity, the globular cluster systems in the Magellanic Clouds offer the possibility of a purely empirical comparison with the high redshift data. These appear to span a very wide range in age from some with virtually zero age to some with ages that are comparable wih those of the Galactic globular clusters. Ideally, observations of these clusters could be used to map out quite empirically the changes in the colours of an SSP with age. In the context of the current

investigation, the work of Persson et al (1983) is particularly interesting. They measured a number of infrared photometric parameters for a large sample of Globulars from both Magellanic Clouds. These were plotted against the 't' parameter of Searle et al (1980, SWB). There are reasons to believe, not least from the well ordered appearance of the diagrams presented by Persson et al, that the t parameter is a single valued monotonic function of the age. Persson et al showed that a number of clusters with $160<t<260$ had very red colours. They deduced from narrow band infrared measurements that these were caused by the presence in these clusters of a very small number of carbon stars.

Figure 5.5 shows a plot of a quantity, that is roughly equivalent to an (R-J) colour, against t. The colour is in fact (V-J)-(g-r), and was constructed by combining the data of Persson et al and the optical photometry of SWB. The approximate colours of the old Galactic globular clusters and those of M31 are also shown. Those clusters with the luminous infrared C stars are clear on the diagram as having red '(R-J)' colours. The scatter in colours at a given t value is caused by the very small numbers (of order one) of luminous C stars that are present in the relatively small stellar populations of the globular cluster. An SSP representing a galaxy would not suffer from this, and would have a colour represented by the mean of the Globulars at a given t. With decreasing age the colour reddens by 0.3 magnitudes when the C stars appear. Although in a system with higher metallicity than these Magellanic globular clusters C stars would not be expected, the corresponding late M giants would in fact have just as large an effect on the (R-J) colour (see Figure 5.4).

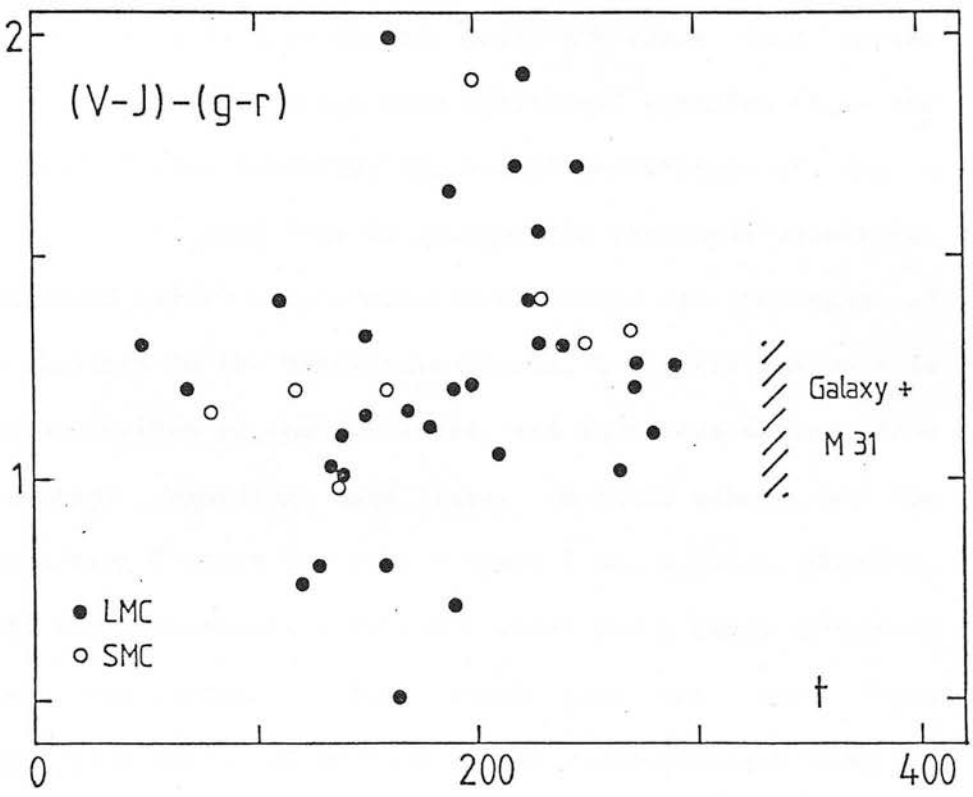


Figure 5.5: The variation of (V-J)-(g-r), which approximates to (R-J), with the SWB t parameter for globular clusters in the two Magellanic Clouds. The range of colours of the old globular clusters found in our Galaxy and in M31 is also shown.

This colour change of about 0.3 magnitudes is larger than is observed in the radio galaxy colours at a redshift of unity. However, there are two problems with using this empirical comparison. Firstly, the lower metallicity of the Magellanic globulars means that they lack the old upper AGB stars that appear to be present in the more metal rich elliptical galaxies (i.e. the same problem as before). Secondly, the actual calibration of the t scale in terms of elapsed time is in any case extremely uncertain. Aaronson and Mould (1982) have presented estimates of the ages of many of the clusters in the Magellanic Clouds, but their analysis is based on the properties of the AGB stars, and therefore suffers from the uncertainties regarding mass loss. On their scheme, all the clusters containing C stars had ages between 1 and 4 Gyrs. However, a study of the Main Sequence Turn-Off point for a small number of such clusters has indicated that these ages may have been overestimated by a factor of as much as ten (communication from Dr. Hodge).

In view of these problems, which are traceable to our lack of understanding of the rate of mass-loss during late giant evolutionary phases, no quantitative statement on the age of the radio galaxies at high redshift can be made at the present time. Nevertheless, the lack of any change in the integrated (R-J) colour larger than 0.1 magnitudes does suggest that these systems were not very young when observed, i.e. when the Universe was somewhat less than a half of its present age.

Having abandoned the attempt to use the lack of colour change to

constrain the age of these galaxies, it is worth making the most reasonable assumptions about the age, and then stating the consequences of this assumption on the composition of the giant branch. Let it be assumed that the ages of these galaxies at redshifts of unity are about 6 Gyrs. This corresponds to a turnoff mass of only 1.1 solar masses. Consequently, the giant branch colour should have evolved by only about one third of the change derived above, or 0.07 magnitudes. The most likely observed colour change (Table 3.4) is -0.02 magnitudes, so the most likely colour change due to any changes in the relative numbers of AGB and RGB stars is about 0.05 magnitudes. It is therefore unlikely that the relative contributions of RGB and AGB have changed by more than the order of 10-20%.

## 5.3 : The Infrared Hubble Diagram Revisited

The analysis of the (K,z) Hubble relation for NLRG showed that the apparent value of the deceleration parameter $q_0$, was considerably in excess of unity. Indeed values larger than 3 were indicated. However, it has long been realised (e.g. Gunn and Oke 1975) that, as shown in Figure 5.2, the luminosity of a coeval population dominated by giant stars will be higher in the past. This is due to the changing number of such stars in the population, and there will be more stars in the past if the slope of the IMF is flatter than 4 . If this is so, the much more rapid evolution of the main sequence turnoff at high masses is able to overcome the countering effect of the IMF, which has more stars at lower masses. It is therefore of interest to repeat the analysis of Section 3.4.e removing as carefully as possible the effects of this evolution. It

is worth stressing at this stage that this evolution should not in any direct way be associated with the radio source activity since one would expect that it will occur in every stellar population.

The two most important parameters in modelling this evolution are the slope of the IMF, x, and the epoch, $T_f$, or equivalently the redshift, $z_f$, at which the SSP was formed. The former obviously determines the relative numbers of stars at different turnoff masses, while the latter determines both the turnoff mass and also the rate at which the main sequence mass function is traversed. Given values for these two parameters, neither of which are presently known reliably, and assuming that $H_0 = 50$ kms$^{-1}$Mpc$^{-1}$ so that the stellar ages are consistent with cosmological ages, the evolution function $E(z,q,x,z_f)$ can be calculated using equation 5.4 and the appropriate relations between epoch and redshift.

$\bar{f}_{KRG}$ has been assumed to be constant for masses below twice solar. This assumption, made by many workers (e.g. Tinsley 1972), can be justified as follows. The 1st ascent of the Giant Branch can be represented by stellar evolution models more successfully than later stages, in which our lack of understanding of the mass loss process is more critical. The bolometric luminosities of the model stars of different initial masses computed by Sweigart and Gross (1978) have been integrated over the time spent between leaving the main sequence and the point of core helium ignition at the top of the 1st ascent of the giant branch. The bolometric magnitude as a function of age is shown in Figure 5.6. The large increase in luminosity for RGB stars which are older than $5\ 10^8$ years is due to the formation of a degenerate helium core in these stars. In the

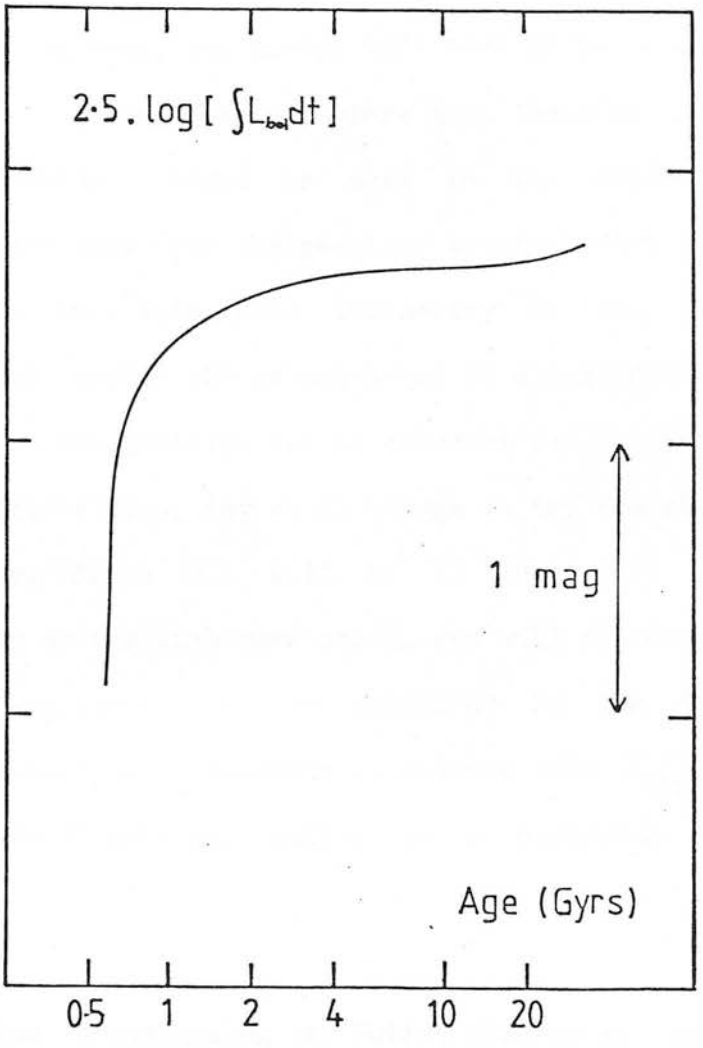


Figure 5.6: The variation of bolometric luminosity output on the first ascent of the RGB with turnoff point age, found by integrating the luminosities of the stellar models of Sweigart and Gross (1978) from the point of leaving the main sequence to the onset of core helium burning.

lifetime interval of interest however, i.e. between 2-3 and 20 Gyrs, the integrated luminosity per star is remarkably constant to within about 0.1 magnitudes. Furthermore, any change will tend to be in the sense of making the younger, more massive, stars less luminous. The empirical fact that no colour change is seen in the observed infrared (H-K) colour indicates (see the previous section) that the relative contributions to the integrated luminosity of the 1st ascent RGB and the 2nd ascent AGB is unchanged at a redshift of unity, and hence since the RGB contribution is constant per star, so should the total be constant also. Any small change in the relative contributions permitted by Figure 5.4 will be in the sense of increasing the luminosity of the high mass stars, and will therefore be acting in the opposite sense to the trend exhibited by the RGB star models. It is therefore reasonable to believe that $\bar{f}_{KRG}$ is constant between redshifts of zero and unity, to a precision of around 10 or 15%.

The formalism used for investigating the Hubble diagram in this analysis is the same as that used in Chapter 3. The modelled K(z,q) relation is modified by the addition of the evolution function $E(z,q,x,z_f)$. The resultant relation $K(z,q,x,z_f)$ is compared with the data using a $\chi^2$ statistic. Two values of $z_f$ were chosen as representative. These were formation redshifts of 4 and 25. The former was taken to represent scenarios with a relatively late epoch of galaxy formation, and coincides with the location of a possible turndown in the quasar evolution function (Osmer 1982, Peacock 1983). It is however a sufficiently high formation redshift that the assumptions regarding the simple form of the evolution are still valid at the redshifts of interest. A $z_f$ of 25 is representative of

galaxy formation scenarios with early collapse of galaxies, and for these purposes, is indistinguishable from all models with $z_f$ greater 25. There is no reason to prefer either of these formation redshifts. Similarly, the only constraint on x is that it is likely to be less than one (e.g. Frogel et al 1978).

A single sample of radio galaxies was used. This comprised all the NLRG with z>0.05, and excluded the two CRS (see Section 3.4.b). The results of this analysis are illustrated graphically in Figure 5.7. For each of the two $z_f$, two curves have been plotted which represent the 30% rejection contours of the models on the (x,q) plane. The quality of the 'best fit' is essentially constant down each set of curves, and is to all intents and purposes the same for both values of $z_f$. This illustrates the well-known fact that the effects of evolution are practically indestinguishable from those of cosmological geometry. Excluding 3C 241 from the sample has the effect of shifting the curves to the left on Figure 5.7, to lower apparent $q_0$. For a $z_f$ of 4, the change is 0.02, while for a $z_f$ of 25, it is 0.04.

Figure 5.7 does not bring the determination of $q_0$ any closer. This is because of not only the uncertainty in the value of x (and $z_f$), but also because of the possible occurence of other systematic changes in the mean absolute magnitude with redshift. These might be caused by another evolutionary effect, candidates for this being the merging of cluster galaxies or the accretion of substantial amounts of hot cluster gas over cosmological timescales. In addition, the sample selection criteria may introduce biases. For instance it should be remembered that the 3CR galaxies at high redshift are much

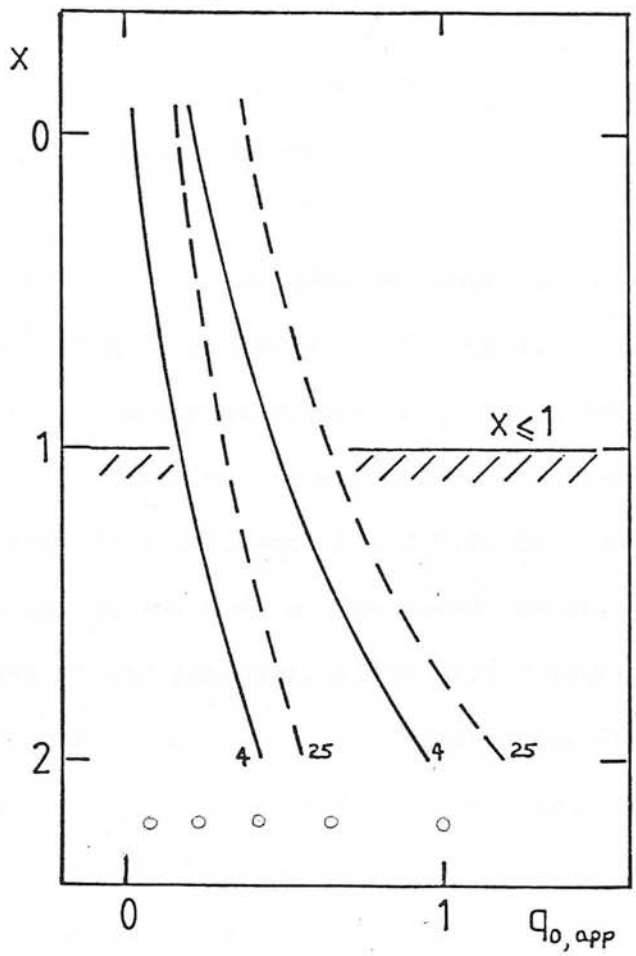


Figure 5.7: The range of $q_{0_{app}}$ that is found from the 3C K(z) Hubble diagram after a correction has been applied for the effects of stellar evolution on the population. This evolutionary correction is defined by the slope of the IMF, x, and the formation redshift of the population, $z_F$. All x were examined for two values of $z_F$. The shading represents the constraint on x found from studies of nearby galaxies.

more powerful radio sources than those nearby. Furthermore, although the sample of galaxies that was observed in the infrared is reasonably complete, the sample that can be used on the Hubble diagram is regrettably not as complete, since the redshifts have not yet been measured for all of the galaxies.

Nevertheless, this analysis does produce one interesting result. Assuming that x is less than 1, as seems to be indicated in nearby elliptical galaxies, then the apparent values of $q_0$ found on Figure 5.7 after the effects of stellar evolution have been removed as carefully as possible, are clearly between 0 and 0.7. This range is precisely that in which conventional wisdom would currently place the true value. Estimates of the cosmological density parameter, $\Omega_0$, ( $\Omega_0 = 2\, q_0$ in Friedmannian cosmologies) from 'local' studies range from 0 to 1. For example, the present abundance of deuterium in the Universe produced by primordial nucleosynthesis suggests that the baryonic contribution to $\Omega_0$ is less than about 0.15 (see e.g. Audouze 1982). Dynamical arguments based on the Virgocentric infall of the Local Group and other galaxies give $\Omega_0 < 0.6$ (see e.g. Davis 1982). On the other hand, the application of GUT theories developed for high energy particle physics to the conditions in the early universe produces a post inflation prediction of $\Omega_0 = 1$. There are certainly loopholes in the interpretation of the observational data which make it quite possible that either $\Omega_{0_{bar}}$ or $\Omega_0$ could be larger than the upper limits given above. These arguments are dependent on the precise way in which the mass is distributed in the universe. Nevertheless, the strong expectation is that $q_0$ will lie between 0.1 and 0.5.

The fact that the apparent value of $q_0$ shown by the data, after the removal of the effects produced by the evolution of the stellar population, spans those expected of the true value implies that the net effect of all the other evolutionary and sample selection effects that may be operating, must be much smaller than the effect of the stellar evolution. The line of circles along the bottom of Figure 5.7 shows the change in $q_0$ that would be produced by any smooth drift in the mean absolute magnitude that resulted in a total change at a redshift of unity of 0.2 magnitudes. 0.2 magnitudes is also probably approximately the precision of the stellar population models used to calculate the luminosity evolution even once the two parameters were specified.

If $0 < q_0 < 0.5$, then clearly the mean absolute magnitude of the radio galaxies at a redshift of unity must be within 0.3 magnitudes of that at low redshift, once the effects of an evolutionary process that would be expected to occur in all galaxies have been accounted for. In other words, underneath the change in the number of red giants in the galaxy, these 3C radio galaxies must be surprisingly good standard candles over long cosmological timescales.

There are a number of reasons why the two other evolutionary effects mentioned above are not expected to be important on the K,z relation for radio galaxies. An investigation is presented in Chapter 7 that strongly suggests that the merging of cluster galaxies is not as important in these particular giant ellipticals as in others, such as the cDs in the centers of Abell clusters. Any intergalactic gas surrounding the radio galaxies has also been shown (Fabbiano et al 1983) not to be radiating strongly in the X-Ray

wavebands, and substantial cooling flows of the type seen in some clusters (see e.g. Fabian et al 1981 and references therein) are not therefore likely to occur in the vicinity of the radio galaxies.

## 5.4 : Evolution in (r-K) and Star Formation

Unlike the infrared colours, the optical-infrared (r-K) colours of the radio galaxies at redshifts around unity are substantially different than those expected from radio galaxies nearby. Furthermore, evidence was presented in the last chapter to the effect that these changes were caused by changes in the stellar populations of these galaxies rather than an increase in the strength of a non-stellar component. It will be recalled that there are two possible causes for an increase in the ultraviolet flux density with lookback time. Firstly, the main sequence turnoff point will evolve so that the population will include more hot stars to increase the ultraviolet flux density at earlier epochs. This is passive evolution in the sense that it is a simple ageing effect on a single population of stars. Secondly, even very small numbers of very young stars produced by star formation that is continuing at the epoch of observation can also have a very large impact on the ultraviolet flux density. This is active evolution because it is caused by the appearance of new stars in the population.

Figure 5.8 shows the data for the NLRG compared with three of Bruzual's (1981) models. These have been modified to account for the deficit of near ultraviolet light found in the original models when compared with nearby galaxies. Indeed the No-evolution (NE) model is actually based on the K-corrections of Schneider et al (1983a). The

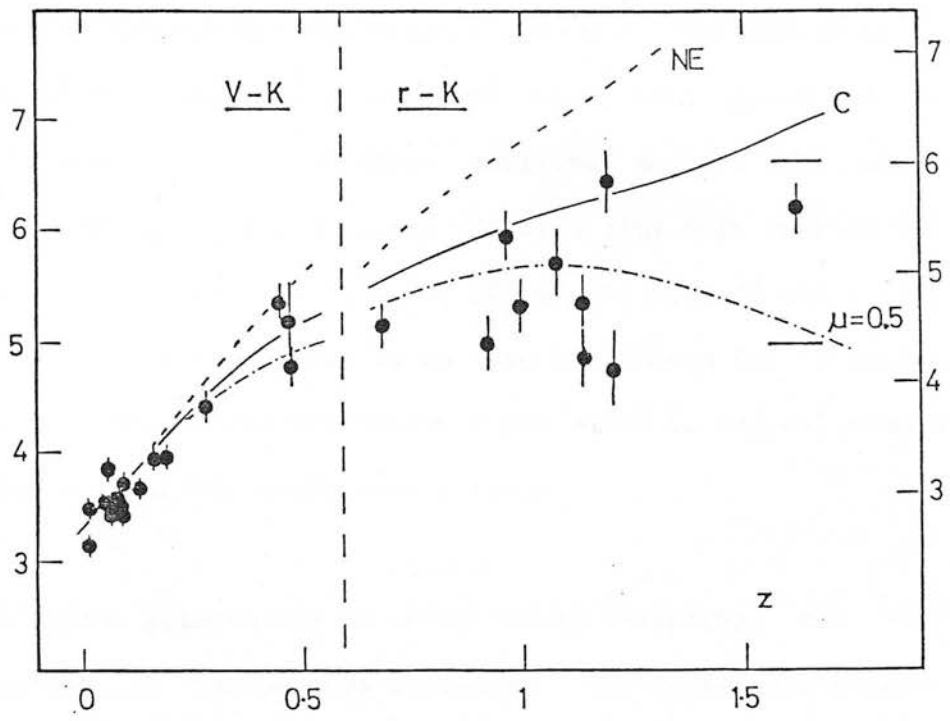


Figure 5.8: The optical-infrared colours of the NLRG. The solid line represents the passively evolving Bruzual model that has no star formation activity continuing at the epoch of observation. The $\mu$ = 0.5 line is an actively evolving model that has continuing star formation. Any burst of star formation will quickly move a previously passively evolving galaxy down from the C line to the region occupied by the high redshift data. When star formation ceases, the galaxy will quickly redden and return to it's original location.

C-model represents an old galaxy in which all the stars formed in a burst of duration 1 Gyr some 16 Gyr before the present epoch (b.p.). The relative differences between Bruzual's NE and other models (i.e. the differential evolutionary effects) have been preserved in producing the modified 'C', and other evolving models. The $\mu$=0.5 model has an exponentially decaying SFR with time such that at the end of the 1st Gyr, again 16 Gyr b.p., 50% of the mass of the galaxy was in the form of stars. There is no physical reason for favouring this particular form of the SFR history: the model is chosen simply to illustrate a plausible evolutionary track.

The difference between the NE and C models represents the Main Sequence ageing of the passive evolution. The difference between the C model and the $\mu$=0.5 model is largely due to the very youngest stars in the population, rather than those of 'intermediate' age. Consequently, similar effects to the colours can be produced by having a small burst of star formation immediately prior to the epoch of observation.

5.4.a The Basic Interpretation

A number of features of Figure 5.8 are noteworthy and contribute to the interpretation of the data. Many of these were mentioned in Chapter 3, but will be listed here prior to a description of the basic interpretation. Subsequently a few more detailed comments will be made and problems discussed.

Firstly, none of the high redshift galaxies lie anywhere near the NE curve. Secondly, none of the galaxies which have a secure

spectroscopically determined redshift, and which can hence be unambiguously placed on the diagram, are significantly redder than the passively evolving C model prediction. Thirdly, there is a significant range in the colours of the radio galaxies at redshifts greater than 0.9. It is not possible to draw a single colour-redshift relation through all the data. Finally, the position of 3C 241 only just below the C model line at a redshift of 1.62, shows that some galaxies can have very ordinary ultraviolet continua even at a redshift of 1.6. The r passband at such a redshift is at approximately 2500 A in the galaxy rest frame.

The favoured interpretation of these observational facts is that these galaxies are all old systems in which the vast majority of the stars were formed well before a redshift of 1.6. They are therefore basically passively evolving systems. Several of the galaxies, however, are also undergoing a burst of star formation, possibly involving much less than one percent of the total mass of the galaxy. Such a burst will rapidly move the colours of the galaxy on Figure 5.8 down from the C model to the areas occupied by the actively evolving $\mu$ models. The occurence of this burst might well be associated in some way, probably indirectly, with the production of the radio source in the galaxy. After the star formation ceases, the blue colour excess will rapidly fade away, and the colours of the galaxy will return to those of the original C model after a short period.

Another possible interpretation of the data is that there is a mix of morphological types amongst the high redshift radio galaxies, since the bluer galaxies have colours similar to those of spiral

galaxies of varying Hubble type. The rejection of this hypothesis is based primarily on the fact that the (K,z) relation shows virtually no change in the cosmic scatter with redshift. At low redshift, where morphological classification can be made, powerful double radio galaxies are without exception identified with elliptical types. If the high redshift population did exhibit a spread of morphological types then one might expect also to see a change in the (K,z) diagram. However, the distinction between a spiral galaxy and an elliptical undergoing a period of star formation may be difficult to define. It is simplest to think of the high redshift radio galaxies as elliptical systems with some continuing star formation.

The mass of young stars that are required to produce the colour changes in (r-K) depends on several unknown quantities, such as the slope and upper mass limit of the IMF, the metallicities of the stars, and the precise age distribution of the stars in the young population. Nevertheless, a number of order of magnitude estimates can be made. These range from the number of O stars required to match the observed ultraviolet flux density to the calculation of the instantaneous SFR in Bruzual's $\mu$=0.5 model to the realisation that these radio galaxies have colours which are broadly speaking similar to those of Sab and Sbc galaxies. These all suggest that star formation rates of the order of a few solar masses per year sustained over several million years will be sufficient. Such a burst need only contain a very small fraction (i.e. less than one percent) of the total galaxy mass.

How do the other relations with $\Delta$(r-K) found in Chapter 3 fit in

to this picture, and what relation, if any, is there between the star formation and the nuclear activity ? It will be recalled that a good correlation was found between the equivalent width of [O II] 3727 and (r-K), but not between the colour excess and either the core nuclear luminosity or the linear projected size of the radio source. The three diagrams are reproduced as Figures 5.9abc. The fact that there is no correlation between the colour and these radio parameters is interesting. The nuclear core luminosity is probably the best indicator of current nuclear activity, while the linear size may give some indication of the length of time that has elapsed since the onset of significant nuclear activity, although it should be recognised that any relation would be smeared out by the projection of random orientations onto the plane of the sky. The independence of the colour change, interpreted as measuring the integrated star formation rate over the last ten million years or so, and the radio parameters suggests that the young population of stars may not be closely related to the nuclear activity. For instance, it is possible to invisage a scenario in which the star formation seen in the radio galaxies represents the dying away of a massive burst associated with a phase in the life of the active nucleus in which its luminosity was much higher (e.g. when it was perhaps a quasar). Boroson and Oke (1982) have shown that 3C 48, a radio quasar, is surrounded by a young stellar population, and this effect could have been related to the present findings. However, such a relation does not recieve much support from the present investigation.

The relationship between the [O II] 3727 equivalent width and (r-K) is convincing. Apart from indicating that the variation in

Figure 5.9: The blueness parameter plotted against various other properties for the high redshfit 3C galaxies.

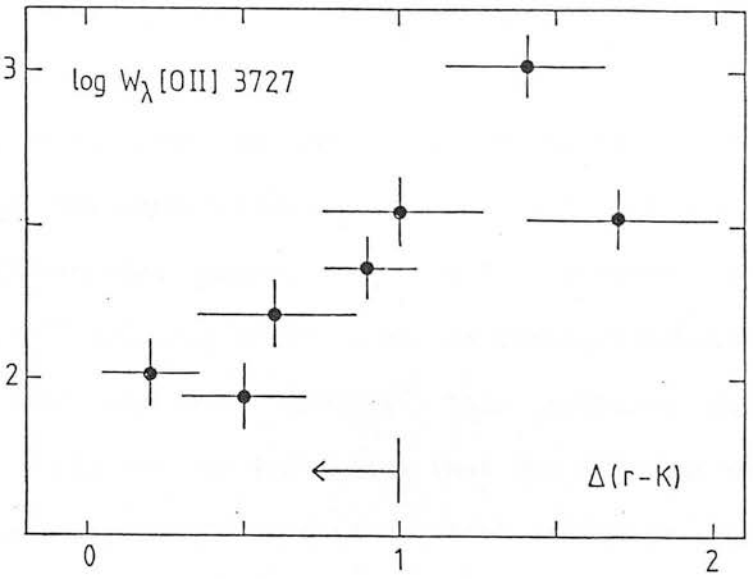


(a) The log of the rest-frame equivalent width of |O II| 3727.

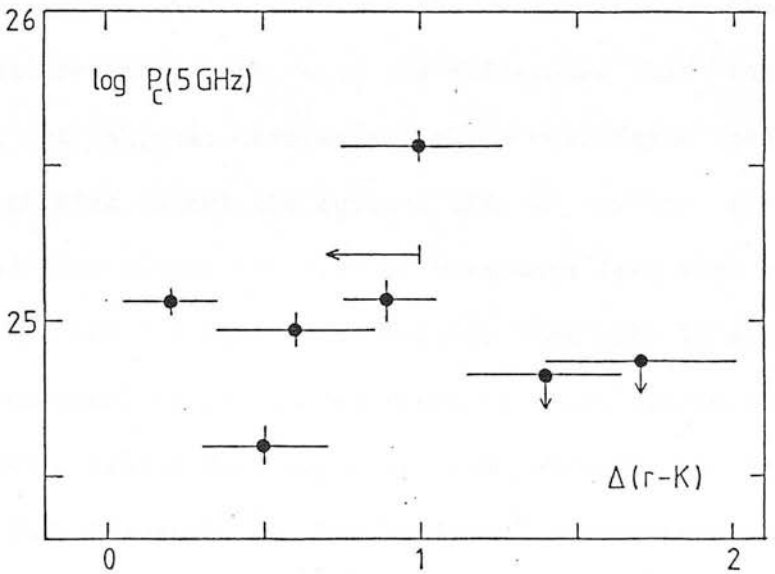


(b) The log of the radio luminosity at 5 GHz of the central core source.

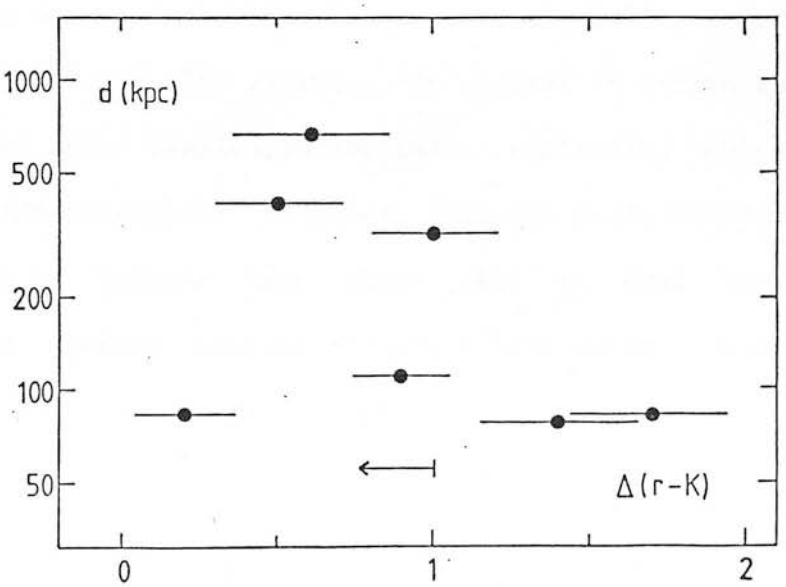


(c) The log of the linear projected size of the double radio source.

(r-K) must be real, since the spectroscopic measurement is completely independent, the correlation must contain information on the nature of the ultraviolet excess. A relation between the equivalent width of [O II] 3727 and (B-V) colour in ordinary spirals has been shown by Dressler and Gunn (1982). This relation was interpreted in these galaxies as indicating that the SFR must be constant with time, since the [O II] equivalent width indicates the current star formation rate given by the number of H II regions, while the (B-V) colour measures the mean SFR averaged over the previous Gyr or so. A similar explanation for the correlation in the radio galaxy data would be attractive, with the difference that the (r-K) colour, being at shorter wavelength in the rest frame than (B-V), measures to a greater extent the current SFR, or rather the average SFR integrated over a time interval of very much less than a Gyr. However, there are several reasons to believe that this is not the correct interpretation. In particular there is every reason to believe that the [O II] emission does not come from ordinary H II regions. Firstly, the strength of the emission is considerably stronger in the radio galaxies than in the spirals, even though the colours can be deduced to be comparable. The equivalent widths are an order of magnitude larger. Secondly, in the case of 3C 352, there was evidence that the [O III] 5007 emission was nuclear in origin in contrast to the excess short wavelength continuum radiation, which was clearly distributed throughout the galaxy (Section 4.3). Finally there is every reason to believe that there will be some hard ionizing non-stellar photons emitted by the active nucleus which could easily ionize any gas near the nucleus.

One interesting feature of the emission line spectra of many of

these high redshift 3CR galaxies is the low ionization state (Spinrad 1982). The ionization ratio [Ne V] 3426 / [O II] 3727, I, is in some cases less than 0.03, whereas in most active galaxies values of 0.2 to 0.3 are more typical. Spinrad has interpreted this as indicating that the lines are shock excited.

With only the very small number of galaxies for which complete data is presently available, it is difficult for a discussion to avoid being completely speculative. At present, it is believed that the observed correlation between the [O II] 3727 equivalent width and the colour excess may simply reflect the general gas content of the different radio galaxies. In galaxies with a high gas content, due perhaps to a recent merger with a nearby gas rich galaxy, one would expect to see more star formation, and there would also be a larger supply of gas to be ionized close to the nucleus.

Evidence for a higher gas content in radio galaxies at high redshift, whether from star formation or from emission lines, would be interesting as it would suggest an increased supply of gas to fuel the active nucleus. However, the details of any link have yet to be considered in any detail, but the simple observation that powerful radio sources are never found in (gas-rich) spiral galaxies at low redshift suggests that any link will not be straightforward.

5.4.b Problems

The principal problem with the scenario as described above arises directly from the evidence that has been used to argue in favour of a stellar origin for the change in colour. The young stars

must be distributed throughout the volume of the galaxy. Indeed, the crude values of the alpha parameter measured for these galaxies (Section 4.4) tentatively suggested that while the passively evolving systems (with low (r-K)) have alphas comparable with low redshift radio galaxies, the actively evolving galaxies have higher alpha than expected, which may indicate that the youngest stars in the population are in fact preferentially located away from the central regions of the galaxy.

Bailey and Macdonald (1981) and MacDonald and Bailey (1981) have investigated the evolution of supernova driven winds in elliptical galaxies, with a particular view to explaining the evolution of the radio source population. They showed that, while the winds could be total at the present epoch, because the evolution of the mass loss rate was faster than that of the rate of injection of energy from supernovae, they were unlkely to be total at earlier epochs. Gas would accumulate interior to the stagnation radius, and fuel the radio source, or , of course, form stars. However, the stagnation radius does not move more than a kpc or so from the nucleus in their models throughout their evolution, and the rest of the galaxy should still be swept clear of gas.

The gas could obviously have an external origin. Two sources that might be important are accreting gas from a cooling flow, and the merger of either a nearby gas rich galaxy or an intergalactic gas cloud. In the first case, accreting flows are known to occur in several nearby clusters that are strong X-ray emitters. Although star formation is a likely final outcome for this gas, a modified IMF has to be postulated in order that the number of massive stars

in the elliptical galaxies is not larger than observed at low redshift. It is conceivable that this modification of the IMF might not occur at earlier epochs, and that massive stars could be produced to change the (r-K) colour. However, in those galaxies that have been studied in detail, it is clear that the accreting gas falls to within 1-2 kpc of the nucleus, which is not where the young stars are seen in the high redshift ellipticals.

A merger does offer the possibility of young stars away from the nucleus. These could come either from the merged galaxy, if that had been forming stars as it was consumed, or from a disk of gas set up in the elliptical galaxy after the merger. Gunn (1980) has discussed the case of NGC 1052 which appears to have a disk of gas, of scale length 11 kpc, inclined to the axis of rotation of the stars. Star formation could be induced to occur in such a disk. The B image of 3C 352 (Figure 4.2 of the previous chapter) does give a hint of being a flattened structure, but the quality of the image is very poor indeed. High resolution data from the Space Telescope will greatly help in studying this problem.

## 5.5 : The Relationship of these Results to those of Other Investigators

One of the main attractions of the current work has been the extension of observations of galaxies with known redshift in to the relatively unexplored ranges of redshift beyond about 0.5. However, as well as the detailed comparisons with the data and conclusions of the other groups who have been working on the same sort of object (e.g. Lebofsky 1981, Puschell *et al* 1982), which have been made at

the appropriate point in Chapter 3, it is important to relate the conclusions that have been drawn from the 3CR radio galaxy observations to those drawn by other investigators.

Mention should first be made of the work carried out on the colours of galaxies identified with the faint radio sources in the Leiden-Berkeley Deep Survey (LBDS). These LBDS sources have flux densities at 1412 MHz of around 1 mJy, and are hence over three orders of magnitude fainter than the 3CR sources in the radio wavebands. They are correspondingly less luminous at a given redshift. Extensive optical photometry on the identifications has been carried out using deep 4 metre plates, and subsequently, infrared data has become available for most of these sources. The principal problem at the moment with this data is the lack of spectroscopically determined redshifts for the sources. Nevertheless, in the latest preprint describing this work, Thuan et al (1983) (but see also Windhorst et al 1983) reach the following conclusions.

The colours and magnitudes of two thirds of the sources are consistent with their being distant elliptical galaxies. About a half of these appear to have the colours of either non-evolving (NE) or passively evolving (C) model elliptical galaxies, while the remainder seem to require active star formation described by Bruzual $\mu$ models with $\mu>0.5$. The remaining third of the sample however are much bluer than the others at a given magnitude. They are probably either low luminosity spirals (or actively evolving ellipticals) at redshift less than 0.2. They could be higher redshift galaxies described by a very low $\mu$ model, but the presence of low redshift

Seyfert type spiral galaxies in the sample would not be unexpected in view of the very low radio flux density limit. These sources would be well below the break in the radio luminosity function. In contrast, all the 3CR galaxies studied in this Thesis are above this radio luminosity, and so the absence of this type of galaxy from the current investigation is not at all surprising. Indeed the LBDS sources only reach this break-point luminosity at redshifts of order unity.

As regards the results for the elliptical galaxies, the results are clearly rather similar, assuming that the redshift estimates are at least nearly correct. The range of behaviour indicated by the LBDS sources is quite consistent with that seen in the 3CR sample even though not all the 3CR galaxies can in fact be represented by models with $\mu>0.5$ (Figure 5.8). The lack of redshifts for the LBDS sample will tend to reduce the spread of models that are 'consistent' with the data, since all galaxies can be shifted in redshift by at least 30% (assuming a cosmic dispersion of 0.5 magnitudes in absolute magnitude) whilst still maintaining 'consistency'. In fact this effect can be seen in the present work by comparing Figures 5.8 and 6.7. The latter diagram is certainly 'consistent' with models with $\mu>0.5$, whereas the former is not. It appears quite likely that the LBDS radio galaxies at redshifts of order unity are showing the same range of behaviour as the 3CR galaxies despite having radio luminosities many orders of magnitude fainter. If this is confirmed by the measurement of spectroscopic redshifts for the LBDS sample, and by more comprehensive optical photometry for the 3CR galaxies, then this will be an important result. It will mean that the evolution seen in the 3CR colours is

not caused by the increase in radio luminosity but rather by the higher redshift, or equivalently earlier cosmological epoch.

Another important published work that is directly relevant to the present investigation is that of Ellis and Allen (1983) in to the range of optical to infrared colours (j-J) exhibited by a complete sample of optically selected faint galaxies. Although having the important feature of being an optically, as opposed to radio, selected sample, the interpretation of their data is made somewhat ambiguous by the complete lack of redshift information and the inevitable mix of morphological types in the sample. Despite this, Ellis and Allen were able to come to an important conclusion. Two features of their data were explained if early type galaxies at redshifts beyond 0.5 were about 1 magnitude bluer in (j-J). Such an increase in the short wavelength flux densities of these objects explains not only the large number of galaxies with red (J-K) colours (indicative of high redshift galaxies), but also the blue (j-J) colour distribution of those galaxies that have red (J-K) on their colour-colour plot. An examination of Bruzual's (1981) models suggests that passive evolution of about 0.6 magnitudes could be expected in (j-J) at a redshift of 0.8, so the Ellis and Allen result could imply that some active evolution is occurring too. However, the lack of redshift data makes all such comparisons slightly tentative. Perhaps the most important point is that the sort of evolution inferred in this optically selected sample, namely a change in colour of about 1 magnitude, is roughly the same as that seen in the radio galaxies at comparable redshift (i.e. between 0.5 and 1).

Gunn (1982) has shown a diagram of (g-r) colours for bright ellipticals with measured redshift, which extend to a redshift of 0.55. It is clear that the galaxies slowly diverge from the expected relation, and that by a redshift of 0.45 are about 0.3 magnitudes bluer than the unevolving prediction. This effect is probably accounted for by purely passive evolution, although the size is slightly larger than would be predicated by Bruzual's models. However, the highest redshifts covered by Gunn's work are still somewhat smaller than those at which strong active evolution is seen in the 3CR radio galaxies.

In summary of the above, there is certainly strong evidence for passive evolution of the stellar content of elliptical galaxies. It would have been rather surprising if this evolution had not been seen, if our ideas about cosmology, the present day stellar content of elliptical galaxies and stellar evolution were not to require drastic revision. Of course, the detailed models will still have to be refined to account for the precise effects observed. The unambiguous evidence for active evolution (i.e. star formation), in elliptical galaxies is less strong, and is based primarily on the observations of the radio selected objects described in the present work and, to a slightly lesser degree (because of their few known redshifts), by the LBDS investigation.

The situation regarding the number counts of faint galaxies is still rather confused. Shanks et al (1983) have at least claimed to have resolved several inconsistencies in previously published results to produce a generally acceptable form of the n(m) function for blue and red passbands. One problem with analyses of this kind

of data, even if the observational situation can be agreed upon, is the large number of input model parameters that must be specified before interpretation of the data in terms of the evolution of the galaxies can begin. Partly as a consequence of this the evolutionary models that are fitted to the data are usually rather crude, and sometimes take no account even of the variation of evolutionary history with morphological type. Aside from the obvious fact that evolution has been shown to take place in at least some galaxies, the most relevant aspect of the present work to the interpretation of the number counts is probably the demonstration that, even in what is believed to be a single morphological class selected according to well-defined criteria, there is a substantial variation in the observed colours at high redshift, even in fairly red passbands that are longward of 6000 A. This fact should be borne in mind when interpretations are made of number-magnitude n(m) or number-magnitude-colour n(C,m) data.

## 5.6 : Summary

The following conclusions have been drawn concerning the stellar populations of the 3C radio galaxies at redshifts of order unity.

(a) The form of the giant branch must be similar to that seen in nearby elliptical galaxies. This strongly suggests that the galaxies are old, but it is not possible to make a quantitative statement of this, on either theoretical or purely empirical grounds, because of the uncertainties that are presently associated with our understanding of the later stages of stellar evolution on the upper AGB. If the most reasonable assumptions

are made concerning the ages of the galaxies, then the data suggest that the number, or the total luminosity, of the AGB stars remains the same to within 10-20% out to a redshift of unity.

(b) The radio galaxies at high redshift contain a larger number of giant stars than those nearby. However, such a change is entirely expected in an ageing population, and the possibly surprising result is that if the effects of this change are corrected for as carefully as possible, then the corrected luminosity of the galaxies at high redshift is very similar to that of the nearby ones. In other words, the masses of the radio galaxies (or more strictly the total number of stars and stellar remnants) are the same at all the redshifts studied.

(c) All the galaxies show the effects of the evolution of the main sequence turnoff point due to the ageing of the population on the ultraviolet flux density.

(d) Many, but by no means all, of the high redshift galaxies contain a population of hot young stars in addition to the underlying old passively evolving population. This is apparently distributed throughout the galaxies, and is thought to be produced by a burst of star formation activity in an otherwise passively evolving galaxy. Little can be said at this stage about the properties of this star forming burst given the meagre data (i.e. the one optical-infrared colour), and the large number of input parameters required in any model (i.e. the

metallicity, IMF slope and cut-off mass, and the detailed SFR history). However, the total mass of stars formed need only be a very small fraction of the total mass of the galaxy. A galaxy that has undergone such activity will quickly revert to having the colours of a passively evolving system soon after the cessation of the star-forming activity.

# Chapter 6 : INFRARED OBSERVATIONS OF FAINTER RADIO SOURCES

## 6.1 : Introduction

There are several motivations for extending the programme of infrared observations of 3C radio galaxies, (which has been described in the preceding chapters), to the members of a somewhat deeper radio sample. Most of these stem from the fact that, in a radio flux density limited sample such as the 3CR, the radio luminosity of the sources is correlated with their redshifts since most of the sources will be close to the limit of the survey. The members of a radio sample selected at a fainter limiting radio flux density will, however, have, at a given redshift, a lower radio luminosity, or, for a given luminosity, will lie at a higher redshift. Observations of these sources, in combination with the 3CR observations, can differentiate between the effects of radio luminosity and of redshift. Also, a deeper sample would be expected to contain a larger fraction of sources at higher redshift.

In this Chapter, infrared observations of the members of a statistical sample of radio sources selected to have flux densities between 1 and 2 Jy at 408 MHz (Allington-Smith 1982) are presented. There were two theoretical and one practical attraction in choosing this particular sample for detailed study. Firstly, it is located at the range of radio flux density at which the radio source counts exceed by the greatest amount the predictions of uniform World Models. Therefore these radio sources may be thought of as being those that are directly responsible for the evolution of the radio

source population. Secondly the flux density difference between the two samples is ideal. It is sufficiently large that any difference in properties with radio luminosity should be apparent, and yet small enough that it is possible to be confident that the radio source identifications are basically the same sort of object (i.e. elliptical radio galaxies rather than Seyfert nuclei for example). Sources with the same radio luminosity as the well studied 3CR galaxies at redshifts of unity are found in the 1 Jansky sample at redshifts around two. Finally, the members of this sample have all been observed with the PFUEI CCD system at Palomar (Allington-Smith et al 1982), and hence a large and, as importantly, homogeneous set of optical photometry exists for these sources. In addition, relatively precise upper limits to the optical flux densities of those sources that were not identified may be derived.

The infrared observations of the identified sources were the same in all respects to those of the 3C galaxies described in Chapter 3. Some new considerations were relevant, however, when it came to attempting to detect the infrared emission of the objects associated with the radio sources for which no optical identification had been possible. These stem from both the uncertainty in the precise position of these associated objects relative to the radio source, and from their extreme faintness. These new aspects to the infrared observations will be discussed in the next sections after a brief introduction to the 1 Jansky sample.

6.1.a The '1 Jansky' Sample of Radio Sources

Allington-Smith (1982) defined the '1 Jansky' sample by selecting sources from the Bologna B2 catalogue of radio sources. The selection criteria were as follows: 1 Jy< $S_{408}$ <2 Jy, b>30°, 34°≤dec<40°, and RA<13$^{h}$02$^{m}$. Excluding one part of the giant 3C source, 3C 236, which appears in the sample, there are 59 individual sources that satisfy these criteria.

Radio maps were made by Allington-Smith (1982) for all these sources at 408 MHz, 1.4 GHz, and at least one of either 2.7 or 5 GHz. These radio data were used to derive the radio flux densities, and hence the spectral indices, and also the radio morphologies and angular sizes of the sources.

The sources in the sample have, in the main, steep radio spectra. To a certain degree this is a consequence of the relatively low selection frequency. Only 20-25% of the sources have $\alpha$ <0.5. The majority of sources have radio spectra that are either straight or which steepen at the higher frequencies. Morphologically, the sample is dominated by sources with extended radio emission. The morphology is ideally found from direct inspection of the higher frequency (and hence higher resolution) radio maps. For the sources with small or ambiguous morphological structure, however, the integrated spectral information can be used to indicate the likely structure. Synchrotron self-absorption in areas of high surface brightness causes the spectrum to flatten and turnover at low frequencies. Hence, those sources with flat spectra are likely to be small (less

than 10 pc) in extent, while those with steep spectra are likely to have large extended components of low surface brightness. In addition, the spectral curvature at high frequency can also provide clues to the nature of the source. Spectral steepening is likely to bd due to the synchrotron ageing process, while a flattening in the high frequency spectral index is probably the sign of the increasing effect of a flat spectrum compact central component, as the steep spectrum extended component decreases in intensity. Both these methods were used by Allington-Smith (1982) to classify the radio sources morphologically. 88% of the sample were adjudged to have extended structure. Indeed, over a half of the sample have clearly recognisable FR II classical double radio structure.

Allington-Smith et al (1982, APLGW) obtained CCD exposures of the fields of 47 of the 59 sources, with the aim of identifying the optical nbjects associated with the radio sources, using the accurate positions available from the high frequency radio maps. Including some earlier identifications, this work resulted in identifications for a total of 43 sources. APLGW showed from considerations of the background density of objects, that statistically almost all of these identificatinns were likely to be correct. Of the remaining 16 unidentified sources, 12 had very faint upper limits to the optical flux densities of the associated objects, while 4 had only somewhat brighter limits. In the cases of these latter sources, the CCD observation had either been obscured by a nearby bright star saturating the CCD chip, or had not been usable through a lack of secondary astrometric standards, or had not been taken at all. For the identified sources, a quantitative analysis was made by APLGW of the surface brightness profiles of the

images in an effort to distingtish between quasars (unresolved) and galaxies (extended). On the basis of this, 25% of the sample are probably quasars.

In all of these respects, the 1 Jansky sample has properties that are, broadly speaking, very similar to those of the slightly brighter 3C sample. Such differences as are evident, such as the lower identification rate, and smaller median radio source size, are consistent with the idea that the 1 Jansky sample contains essentially 3C-type sources at generally somewhat higher redshifts.

6.1.b The Methodology of the Identification of Radio Sources

Since Baade and Minkowski (1954) showed that the second brightest radio source in the northern sky (Cygnus A) was associated with a distant (z=0.06) galaxy, with the implication that radio sources observed at radio flux densities only a hundred times fainter, and hence still well within the 'bright source samples' such as the 3CR, would be at cosmologically significant distances, there has been a very large observational effort expended on identifying the optical objects that are associated with the sources of radio emmision.

During the 1960s increasing numbers of radio sources were identifified with extragalactic objects, including ,of course, the discovery in 1963 of the quasars (Schimdt 1963). However, it was only with the construction of large aperture synthesis radio telescopes in the early 1960s that major advances were possible in identifying the members of usefully large, statistically 'complete',

samples. These telescopes, and in particular the 5-km telescope at Cambridge, provided accurate positions and structural information from maps with a resolution of better than 2 arcsec (e.g. Longair 1975, Jenkins et al 1977 and references therein). Principally through the use of the 200 inch telescope at Palomar, the sources in the 3CR 'complete' sample (Jenkins et al 1977, JPR) were progressively identified with faint optical objects (Kristian et al 1974, 1978, Longair and Gunn 1975, Laing et al 1979, Riley et al 1980, Gunn et al 1981). Ultimately a prototype CCD camera was used on the 5 metre telescope at Palomar, and at the end of this programme, represented by the last paper in the above list, only three sources of the 177 sources in the JPR sample remained unidentified because of the faintness of the objects, although a further four were in obscured fields (e.g. very close to bright stars). Similar progress was made (Peacock et al 1981) on the high frequency, high flux density, equivalent of the 3CR, (Peacock and Wall 1981), but at lower radio flux densities, the fraction of sources that may be identified, even on CCD exposures, declines. As we have seen, the 1 Jansky sample is about 80% identified to a limit of about 23 in r, while the 5C6 and 5C7 samples (Perryman et al 1982) which are about 3 orders of magnitude fainter than the 3CR, have an identification rate to a similar optical depth of only 30-35%.

The 3CR sample is sufficiently completely identified, however, for a thorough analysis of the identifications to be made. This has been done by Laing et al (1983, LRL). They considered the possible biases that might exist in the 3CR sample and consequently adjusted the membership of the sample slightly. Subsequently, they derived

the definitive results of such classic cosmological tests as the V/Vmax test for various subsets of the revised sample. In the present context, however, the most important aspect of their analysis is their assessment of the reliability of the 3C identifications and in particular their investigation in to the quantitative distribution of the relative positions of the radio sources and associated optical objects.

The probability that an object seen at a given magnitude in a 'search area' around a radio source is not actually associated with the radio source may be estimated from the surface densities at that magnitude of the relevant types of object. Clearly, this chance is minimized by either having a smaller search area or by restricting the type of object so that the surface density of possible contaminants is lower. For instance the mean surface density of galaxies showing bright emission lines in their spectra is very much lower than that of ordinary ellipticals.

LRL found that for the compact sources, in which the optical and radio positions should agree to within the measurement uncertainties in both positions, there is a neglibible chance of confusion even at a V magnitude of 24. For extended objects, and in particular for the double sources, the situation is more complicated. LRL divided the FR II sources in to three categories. The first comprises those which also have weak central unresolved components. These sources are then effectively the same as the compact sources mentioned above, and the identification becomes completely unambiguous. The important consequence of this is that it is possible to plot confidently the position of the identification (or radio core)

relative to the two double components. Those double sources without cores were divided in to two groups depending on whether they are brighter or fainter than 19th magnitude. Those that are brighter have unambiguous identifications because their high optical brightness means that the 'background density' is low. Furthermore, spectroscopic data is available for all of them and many show strong emission lines too. The uncertainty of the correctness of the identifications for the remaining fainter objects is slightly higher, but in most cases is very small, especially for those with emission line spectra. The locations of the identifications with $\theta > 5$ arcsec, relative to the two hotspots in the outer radio lobes is shown in LRL's Figure 1. This is such an important diagram that it has been reproduced as Figure 6.1 in this Thesis. The important point to note is that for over 90% of the double sources for which there is no ambiguity in the identification (i.e. a and b), the identification lies within a circle of radius 0.2 $\theta$ centred on the midpoint of the line joining the two hotspots in the double lobes. It can be seen that the same is probably also true of the other sources (c), increasing numbers of which are also being found to have strong emission line spectra.

As well as indicating that virtually all of the 3CR identifications that have been observed in the preceding chapters are correct, the relevance of this analysis to the present work is that it demonstrates that nearly all the correct identifications will lie within this well-defined circle of radius 0.2 $\theta$ centred on the middle of the line joining the outer lobes.

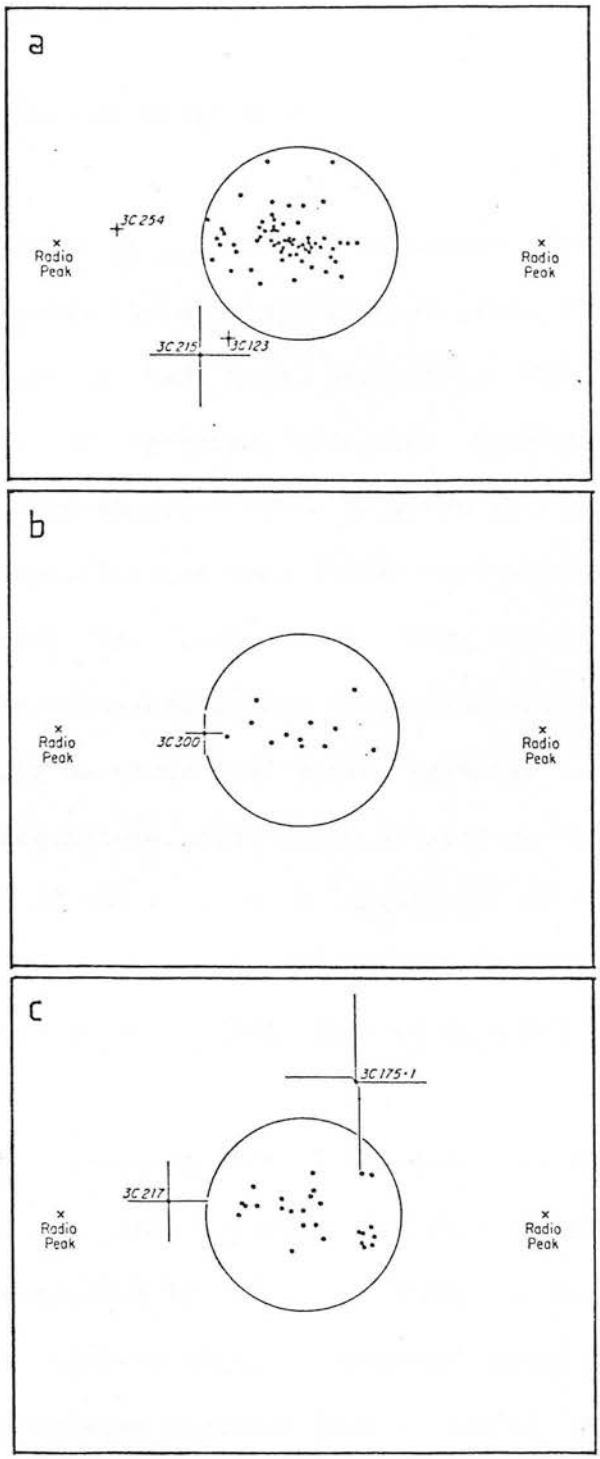


Figure 6.1: The positions of the identifications of double radio sources relative to the two outer lobes. In (a) and (b) the identifications are secure because of the presence of a nuclear core or because the identification is brighter than 19th magnitude. The identifications in (c) are less secure. Nearly all the objects lie well within a circle of radius 0.2 $\Theta$ centred on the midpoint of the line joining the lobes. (Taken from Laing et al 1983)

6.1.c Infrared Identifications of Radio Sources

Grasdalen (1980) and Riecke et al (1979) presented the first infrared detections of 'empty field' radio sources (i.e. those for which no optical identification had been proposed). These were single element detections of infrared radiation from the radio source position. Grasdalen had observed three 3C radio sources which at that time had no identification even though very deep optical plates of the of the fields had been taken. The sources were deliberately chosen to be classical double FR II sources, with the expectation that these would be elliptical radio galaxies at high redshift. After long integrations, convincing detections were made of two of these (3C 65 and 3C 427.1) at a K magnitude of between 16.5 and 17. Subsequently both these galaxies were in fact found on deeper optical exposures (Smith et al 1976, Gunn et al 1981).

Riecke et al (1979) investigated a larger number of flat-spectrum radio sources, and detected six that had not been visible on the Palomar Observatory Sky Survey (POSS) plates. The infrared detections were correspondingly somewhat brighter than Grasdalen's. This work did however indicate that a number of very red quasars exist, associated with such flat-spectrum radio sources, although Impey and Brand (1981) have subsequently shown that these do not constitute a distinct new class of QSO.

Subsequently, Lebofsky et al (1983) have extended this work to steep spectrum radio sources selected to have S(966)>2Jy. Such sources are thus comparable to the 3C sources which have

S(178)>10Jy. Again, their sample was selected to be unidentified below the POSS limit, and indeed several of these have published optical identifications (e.g. Gunn et al 1981). 11 out of 14 such objects were detected, which together with 4 other detections of 3CR galaxies by other observers (including the author) resulted in a very high identification rate for their sample, comparable to that for the 3CR. Three of these sources were thought to be 'red quasars' similar to the flat spectrum sources, but this classification does rely solely upon the redness of the (J-K) colour.

There are two main problems associated with extending this kind of work to the faintest possible limits. The major problem that must be addressed concerns the surface density of objects at progressively fainter infrared magnitudes. This is a problem because of the need to use a relatively large single aperture to be sure of covering the whole 0.2 θ circle, since there are at present no sensitive 2-dimensional detectors. The neccessity of chopping also introduces a further complicating factor which increases the chance of contamination. Secondly, the radio emission mechanism must produce, at some level, radiation in the infrared, and it is important to try to assess the level at which this may be significant.

6.1.c.(i) The Infrared Number-Magnitude Relation

There will be a certain background density of 'unrelated' objects at any given K magnitude limit. These contaminating objects can either occur in the 'object beam', mimicking the radio source identification, or in the reference beams, producing an

underestimate of the flux density of the radio source, or even producing a net negative signal. Because the two beams are of equal area, these two effects will statistically cancel out in a large enough sample of objects (i.e. the mean signal recieved from all the radio galaxies will be correct). The presence of these other objects will, however, introduce some confusion in to the detections, and it is important to attempt to estimate at what level this contamination is likely to be important. The probability that an aperture of radius r will contain one of the members of a population with mean background density $\rho$ is given by (provided $P \ll 1$)

$$P = \pi\, r^2\, \rho \qquad (6.1)$$

Unfortunately there is no observational data on the mean surface density of infrared objects due to the lack of a sensitive infrared array detector. Hence it is necessary to model the $\rho(K)$ function.

The calculation for the contribution from the population of external galaxies is familiar from the large amount of work done in interpreting the N(m) relations for optical passbands (see e.g. Ellis et al 1977) and proceeds as follows. In a cone of solid angle, $d\omega$ the incremental increase in comoving volume with redshift is given by:

$$\frac{dV}{dz} = \left(\frac{c}{H_0}\right)^3 \frac{(q_0 z + (q_0-1)\{(1+2q_0 z)^{\frac{1}{2}}-1\})^2}{(1+z)(1+2q_0 z)^{\frac{1}{2}}}\, d\omega \qquad (6.2)$$

At a redshift z, the density of objects, $\rho$ , at a given apparent magnitude can be computed from (a) a luminosity function for the different galaxy types, (b) the appropriate cosmological relations

between distance and redshift and (c) the K-corrections for each galaxy type. To a good approximation over the redshifts of interest, the 2.2 micron K-correction is not dependent on the morphological type of the galaxy, and the K-correction appropriate to a passively evolving elliptical galaxy (Bruzual 1981) has been used. In fact, the evolution of infrared luminosity is likely to be smaller for other morphological types because of the more steady rate of star-formation over cosmic time. The luminosity function has been taken from Felten (1977), with the assumption that B-K is constant, irrespective of galaxy luminosity or morphological classification. Integration over all the redshifts in the solid angle produces the total predicted number of galaxies brighter than a given K.

In the calculation, a $q_0$ of 0.5 was chosen, and the prediction was computed for a solid angle of 1 arcmin square.

This prediction is shown in Figure 6.2 as a function of limiting K magnitude. The number density at which there is a 10% chance that either the 12 arcsec object beam or one of the two 12 arcsec reference 'sky' beams will contain an object is shown on the vertical axis of the Figure. This model prediction, and the derived probabilities, may be uncertain by a factor of about 2. Furthermore, a number of additional considerations, such as the possibilty of cluster members near the radio identification enhancing the local background density, have been omitted.

However, an important aspect of the observational method has still to be included in the model. In most cases, some form of optical plate material is available, either at the very least the

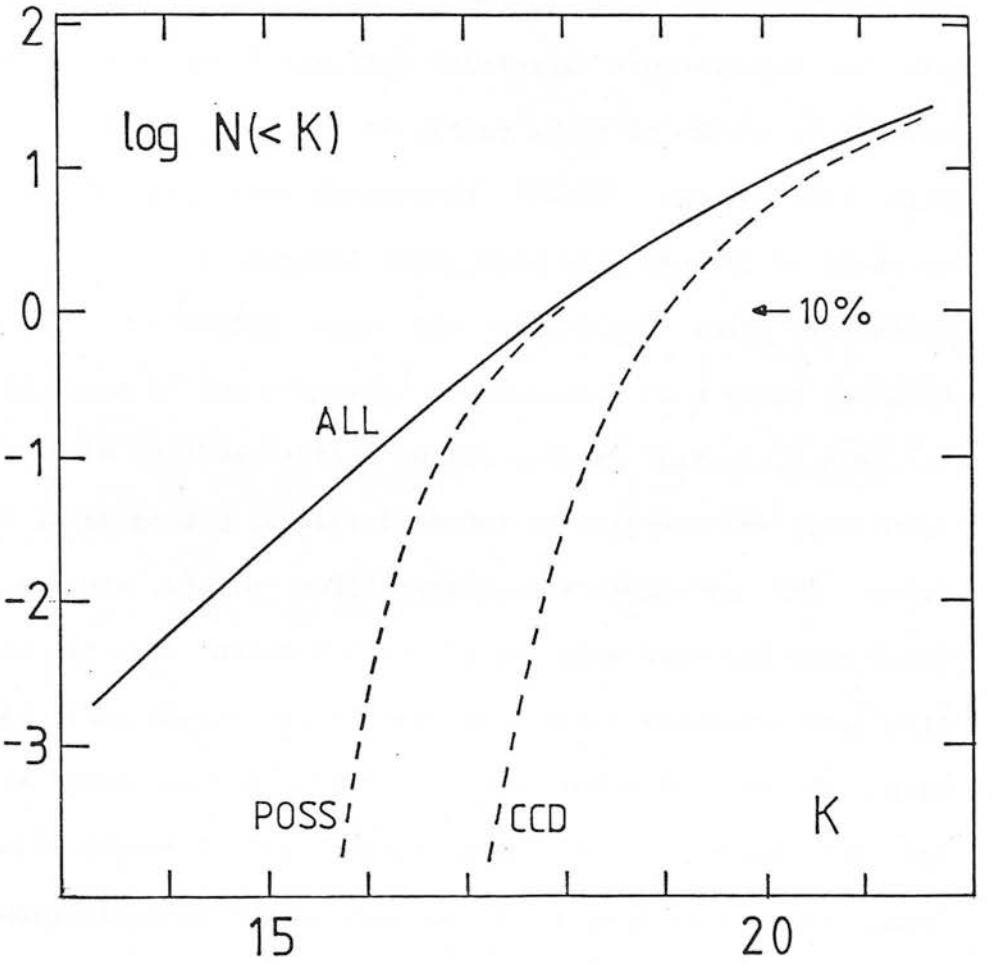


Figure 6.2: The predicated integral number-magnitude counts for galaxies in the K passband. The prediction is plotted as the number of galaxies per square arcmin that are brighter than a given K magnitude. The density at which there is a 10% chance that one of the 12 arcsec infrared beams will contain a contaminating galaxy is shown. The two dashed curves represent the N(K) relations for those galaxies that will not be visible on the POSS and on a 5 minute CCD exposure respectively.

POSS survey, or preferably, some rather deeper images. For instance in the case of the 1 Jansky sample, deep CCD exposures to a limiting magnitude of r=23.5 are available. Since most 'random' field galaxies at a given K will be at a somewhat lower redshift than the radio galaxies (because of the high intrinsic luminosities of the latter), they will tend to be rather bluer in colour at a given magnitude. Furthermore, the foreground 'field' sample will also contain a mix of morphological types that will tend to be bluer on average at a given redshift than the elliptical radio galaxies. Consequently, many of the potential contaminants at a given infrared magnitude will in fact be visible on the optical material even if the actual radio galaxy is not. In order to estimate the importance of this, a very simple modification was made to the model calculation. It was assumed that all galaxies have the same (r-K) colour, that of an elliptical galaxy, at a given redshift. This will be quite a good approximation at low redshift, but at higher redshifts will depend on the assumed evolutionary models for the different morphological types. However, it represents a 'worst case' since no galaxy is likely to be redder than the elliptical at each redshift. The colour was assumed to be equal to 3.0+2.5z. The number counts were then recomputed, omitting all those galaxies that would appear above a given optical plate limit in r. This was done for two different plate limits corresponding to the CCD limit of r=23.5, and the limit of POSS, assumed to be around r=20. The two resulting curves are also shown in Figure 6.2. If care is taken to avoid objects visible on the optical material when positioning the reference beams on the sky, then these are the curves that indicate the likely degree of contamination. When working in the important faint magnitude range of $17<K<18.5$, the value of having the deepest

possible optical material is clear from the large decrease in background density of potential contaminants when objects with $20<r<23.5$ are excluded. If CCD, or comparable material is available when choosing the chop direction and size, then there is only a 10% chance that there will be a galaxy brighter than a K magnitude of 19 in any of the three beams. This limit reduces to slightly brighter than 18 if only POSS is available.

On the basis of these curves it is apparent that confusion from galaxies is unlikely to be important at the K magnitudes of interest if deep material (r=23.5) is available.

That galactic stars will also be negligibly important as contaminents, particularly at high galactic latitude, may be seen from the fact that very few stars have an (R-K) colour that is redder than 2.5. Hence if deep plate material is available, no potential contaminent at 20 th magnitude in K will not be clearly seen on that material.

6.1.c.(ii) Infrared Radiation from the Radio Emitting Regions

The possibility that at a very faint level infrared radiation from the radio emitting regions may be confused with stellar or other radiation from the identification (radio galaxy or quasar) itself needs to be addressed. This infrared emission could have several causes (c.f. the discussion on optical emission by Miley 1979), the most plausible being that of synchrotron radiation from the same electron population that produces the radio emission. Theoretically, the spectrum of the radio emitting regions between

the radio and the optical wavebands is very uncertain, depending mainly on the spectrum of the electron energy distribution at high energies.

There have been several claims to have discovered optical emission at low light levels associated with the radio emitting lobes of 3CR double radio sources (e.g. Saslaw et al 1978, Simkin 1978). The number of radio sources, however, where convincing associations have been found is small, and there are several reasons why this form of contamination is not believed to be important, particularly for infrared measurements brighter than 19th magnitude at K, for the present work.

In order to make a significant contribution at K (e.g. at least 10 μJy in the present context) the mean spectral index between 408 MHz and 2.2 microns must be at least about 1.1. Such a slope, on its own is not implausible, since the extended components alone have spectral indices typically around 0.8, whereas the compact 'flat spectrum' component that is sometimes associated with the active nucleus itself, usually has a spectral index somewhat lower than this, being often about 0.2. However, the spectral indices between, say, r and K, that can be inferred from the lower limits to the (r-K) colour from an infrared, but not an optical, detection are considerably steeper than this value. The spectral index is given approximately by:

$$\alpha = -1.2 + 0.76\ (R-K) \qquad (6.3)$$

So, for an (R-K) colour of 5 or 6 , spectral indices steeper than 2.5 or 3.3 respectively are required. To maintain a mean slope of 1 between 408 Mhz and 2 microns, and to then steepen to these higher values between 2.2 and 0.7 microns would be an unlikely coincidence. Since, the optical fields of the unidentified 1 Jansky sources have been searched to a limit in r of 23.5, or roughly $R < 23$, it is unlikely that a infrared source brighter than around 18 to 18.5 could be seriously contaminated by this non-thermal radiation from the extended radio-emitting regions.

This argument may be extended further by the observation that optical radiation from radio emitting regions is not seen to a similar limit in r for the great majority of 3C sources, which are between 5 and 10 times brighter than the 1 Jansky sources in the radio. Hence, it may be argued that the effective limit to the optical radiation in the case of the 1 Jansky sources should be lowered by at least 1.5 magnitudes below the actual limit, with a corresponding decrease in the upper limit to the infrared contribution fron these regions, to around a K magnitude of 19.5 to 20.

## 6.2 : Observations and Data Reduction

Observations were made of 39 of the 1 Jansky radio sources during the period 11-18 March 1983, with the 3.8 m UKIRT teescope. The telescope was operated at f/35, and the observing procedures were identical to those used for the programme of infrared photometry of 3CR galaxies described in Chapter 3. All the 1 Jansky sources were observed at K (2.2 microns) only. The data reduction followed the procedures described in Chapter 3. The sole difference was that for the longest integrations on very faint sources, a statistical test was applied to the data to test for randomness in the noise.

### 6.2.a The Selection of Sources

The 1 Jansky sources may be conveniently grouped according to the existence or otherwise of an optical identification, and the appearance of the optical identification image, i.e. stellar (quasar) or extended (radio galaxy) (Allington-Smith et al 1982).

Every effort was made to ensure that the sample of optically unidentified sources that was observed was 'complete' in a statistical sense. 12 out of 16 unidentified soures were observed in the infrared. These 12 represent all the 'really empty' fields in the sample, i.e. those for which no object is seen to the limit (r 23.5) of a 'good' CCD image. These will be referred to as optically empty fields (OEF). The remaining four are 'empty' only to a somewhat brighter limiting magnitude, typically the limit of the

Palomar Observatory Sky Survey (POSS) plates. These will be referred to as optically obscured fields (OOF). The four OOFs were not observed because of the lack of deep CCD material. The principal effect of not having the CCD images is the difficulty encountered in selecting areas of sky uncontaminated by other objects for the refernce beam position. The EOF observations therefore form a well defined sample.

The completeness regarding the remaining, optically identified, sources is less satisfactory. The observing conditions prevalent during the run in March 1983, and particularly the strong winds that were encountered, severely constrained the areas of sky accessible to observation. The sample that was observed in the infrared is not therefore complete, particularly at the larger RA s. Unfortunately, this incompleteness is most severe in the important magnitude range just above the CCD optical plate limit, between $21 < r < 23$. In addition to this unavoidable bias, the identifications classified as galaxies were accorded a higher priority in the observing programme, and the observations of the quasar candidate identifications are correspondingly less complete. The magnitude distribution of the complete sample and of those members observed is shown in Figure 6.3 according to their classifications.

All 39 objects were measured at K (2.2 microns) only. Table 6.1 lists the fully reduced photometry and uncertainties for both the objects observed and those that were not. The uncertainties attributed to each measurement are, as in Chapter 3, derived from the statistics of each set of integrations. In the case of the 12 empty fields observed (indicated by an asterisk), the uncertainty is

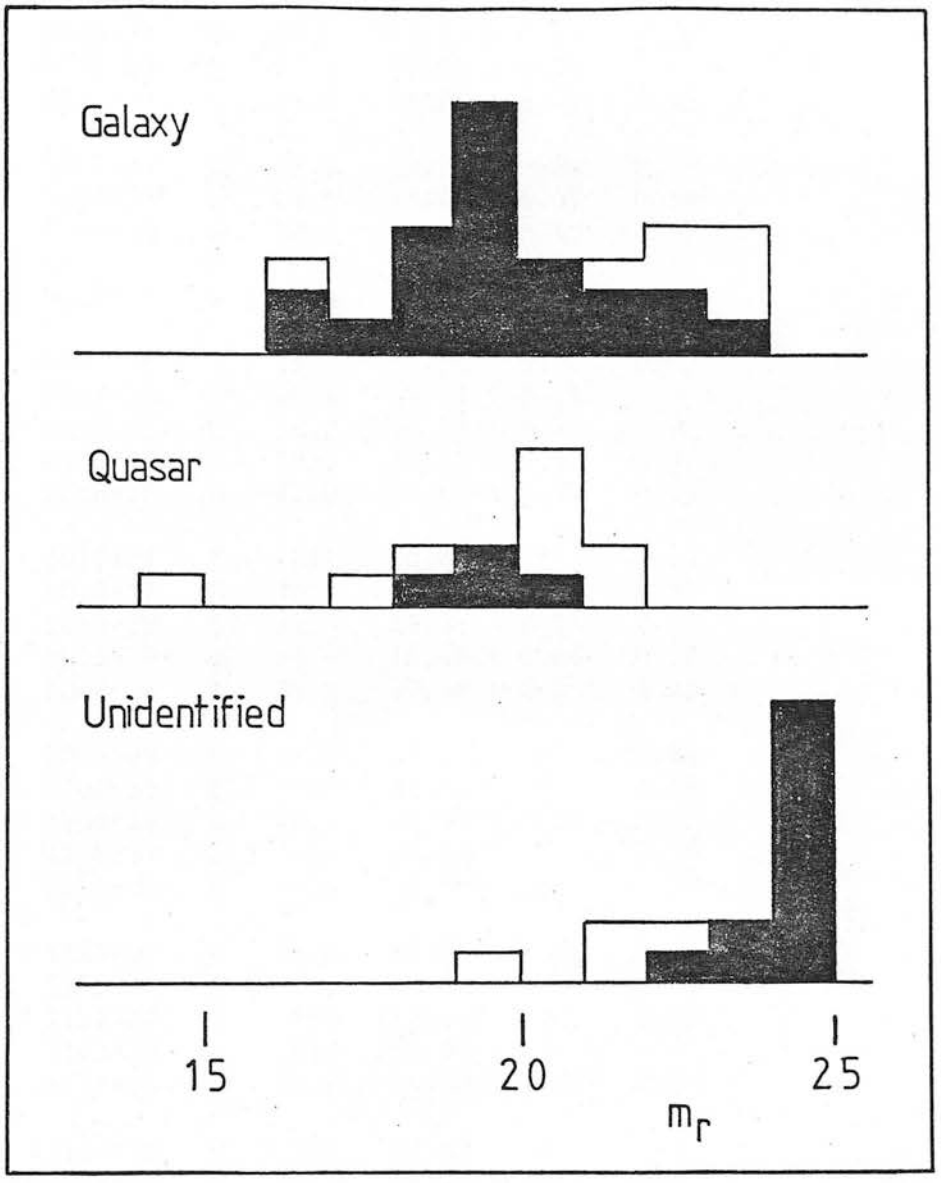


Figure 6.3: The distribution of apparent r magnitude of the sources in the '1 Jansky' sample. The classification of the identifications is on the basis of their morphology and the magnitudes of the unidentified sources are lower limits. Those sources that were observed in the infrared are shown shaded.

Table 6.1: Infrared Photometry of '1 Jansky' Radio Sources.

| | | r | K | z* |
|---|---|---|---|---|
| 0822+34 | G | 19.5 | 15.27 ± 0.06 | 0.42 |
| 0822+39 | U | >23 | 17.43 † * | 1.45 |
| 0823+37 | G | 17.8 | 13.75 ± 0.02 | 0.16 |
| 0824+35 | Q | 20.5 | 17.01 ± 0.24 | - |
| 0835+37 | G | 19.5 | 15.28 ± 0.06 | 0.42 |
| 0847+37 | G | 19.5 | 15.05 ± 0.03 | 0.37 |
| 0857+39 | G | 18.6 | 15.03 ± 0.07 | 0.36 |
| 0854+39 | G | 20.6 | 15.39 ± 0.10 | 0.45 |
| 0902+34 | U | >22 | 18.75 * | ? |
| 0908+37 | G | 16.1 | 12.70 ± 0.01 | 0.07 |
| 0922+36 | G | 16.3 | 12.60 ± 0.01 | 0.07 |
| 0927+35 | Q? | 19.6 | 14.77 ± 0.05 | - |
| 0952+35 | Q | 19.1 | 16.27 ± 0.14 | - |
| 0955+38 | G | 19.5 | 16.21 ± 0.11 | 0.74 |
| 1016+36 | G | 22.0 | 16.61 ± 0.11 | 0.93 |
| 1017+37 | U | >21 | 20.84 * | ? |
| 1018+37 | G | 20.2 | 16.49 ± 0.17 | 0.87 |
| 1019+39 | G? | 22.7 | 16.35 ± 0.14 | 0.80 |
| 1025+39 | G | 18.4 | 14.48 ± 0.05 | 0.26 |
| 1043+37 | ? | 21.2 | 17.38 ± 0.29 | 1.40 |
| 1056+39 | U | >23 | 17.91 * | 1.84 |
| 1100+35 | U | >22 | 17.11 * | 1.19 |
| 1104+36 | G | 18.0 | 14.87 ± 0.09 | 0.33 |
| 1106+37 | U | >23 | 17.68 † * | 1.59 |
| 1113+34 | U | >23 | 16.84 * | ? |
| 1129+37 | G | 23.0 | 16.94 ± 0.20 | 1.11 |
| 1130+34 | G | 19.9 | 15.76 ± 0.09 | 0.57 |
| 1132+37 | U | >23 | 17.36 * | 1.38 |
| 1143+37 | U | >23 | 19.20 * | ? |
| 1148+36 | G | 18.8 | 14.63 ± 0.08 | 0.28 |
| 1159+36 | U | >23 | 17.65 * | 1.57 |
| 1201+39 | G | 19.5 | 15.46 ± 0.15 | 0.46 |
| 1220+37 | Q | 18.6 | 15.30 ± 0.06 | - |
| 1245+34 | G | 19.5 | 15.11 ± 0.13 | 0.38 |
| 1256+36 | U | >23 | 17.58 * | 1.53 |
| 1257+34 | G | 20.9 | 16.65 ± 0.21 | 0.94 |
| 1301+38 | G | 19.8 | 14.98 ± 0.05 | 0.35 |
| 1301+35 | U | >23 | 18.97 * | ? |

Notes (for the last two columns):

* Observation of 'Empty Field' Source, See also Tables 6.2 and 6.3.

? Very faint source, see analysis of Fig. 6.11.

- No redshift estimate (QSO) candidate.

† 8 arcsec aperture used. All other measurements were taken with a 12 arcsec aperture.

not listed here as it is the subject of further analysis later.

6.2.b Observations of the Optical Empty Field Sources

In view of the obvious difficulties involved, particular care was taken in making and analysing these observations. The direction and size of chop was chosen, after close examination of high contrast prints of the CCD fields, to avoid all objects visible in the optical waveband. For all EOF sources with extended radio structure, and hence with corresponding uncertainty (0.2 θ)in the position of the associated object, and in fact for most of the remainder also, a 12 arcsec aperture was used. For three observations of compact sources with unresolved radio structure, a smaller aperture of 8 arcsec was used. This was to maximise the sensitivity of the photometer by reducing the sky background signal, since the position of the identication is unambiguous for such sources. A total of 14 observations were made of the 12 EOFs, including two repeat observations. Except for two of these 14 observations, each integration was continued until either 64 or 128 pairs of 30 seconds integration had been obtained. The decision to integrate for either 64 or 128 pairs was taken after about 15 minutes when the brightness of the object was beginning to be apparent. Of the two exceptions when these standard length observations were not used, one was terminated by a computer crash, fortunately after a good detection ($6\sigma$) had been made, while the other was terminated after only 50 integrations (reaching $4\sigma$) because a $2\sigma$ detection at H after 1 hour had already been obtained (by mistake). For the remainder it was possible to analyse the noise in the 128 or 64 individual pairs to test whether it was

random. This was done as follows:

In each observation, the data was progressively subdivided in to groupings of the pairs that make up the integration. For the observations with 128 pairs, two groups of 64 pairs, four of 32, eight of 16 and finally 16 groups of eight pairs were considered. For the observations with only 64 pairs the process was terminated at eight groups of eight pairs. At each level of subdivision, the mean and standard error of the pairs in each group was computed, and the consistency of the mean values of all the groups in that level with the mean value of the complete observation was evaluated using the $\chi^2$ statistic. Figure 6.4 illustrates the analysis for 1113+34, a typical member of the sample of EOFs, for which a 2 $\sigma$ detection was obtained after 128 pairs. The statistic was defined thus.

$$\chi^2 = \sum_i \frac{(\bar{m}_i - \bar{m})^2}{\sigma_i^2} \qquad (6.4)$$

In other words, this analysis tests for the existence of any non-random trends in the data that are present on timescales of longer than about eight pairs, or four minutes. This timescale is much less than the total length of integration which was either 32 or 64 minutes. The results of this analysis are shown in Table 6.2, which lists the observations and the values of $\chi^2$ derived from the analysis of the subgroups containing the number of pairs listed at the head of each column. For reference, Table 6.2 lists the values of $\chi^2$ which will only be exceeded with given probability, for the analyses with the appropriate degrees of freedom. Of course, the $\chi^2$ statistic can indicate that the mean value of the data is too

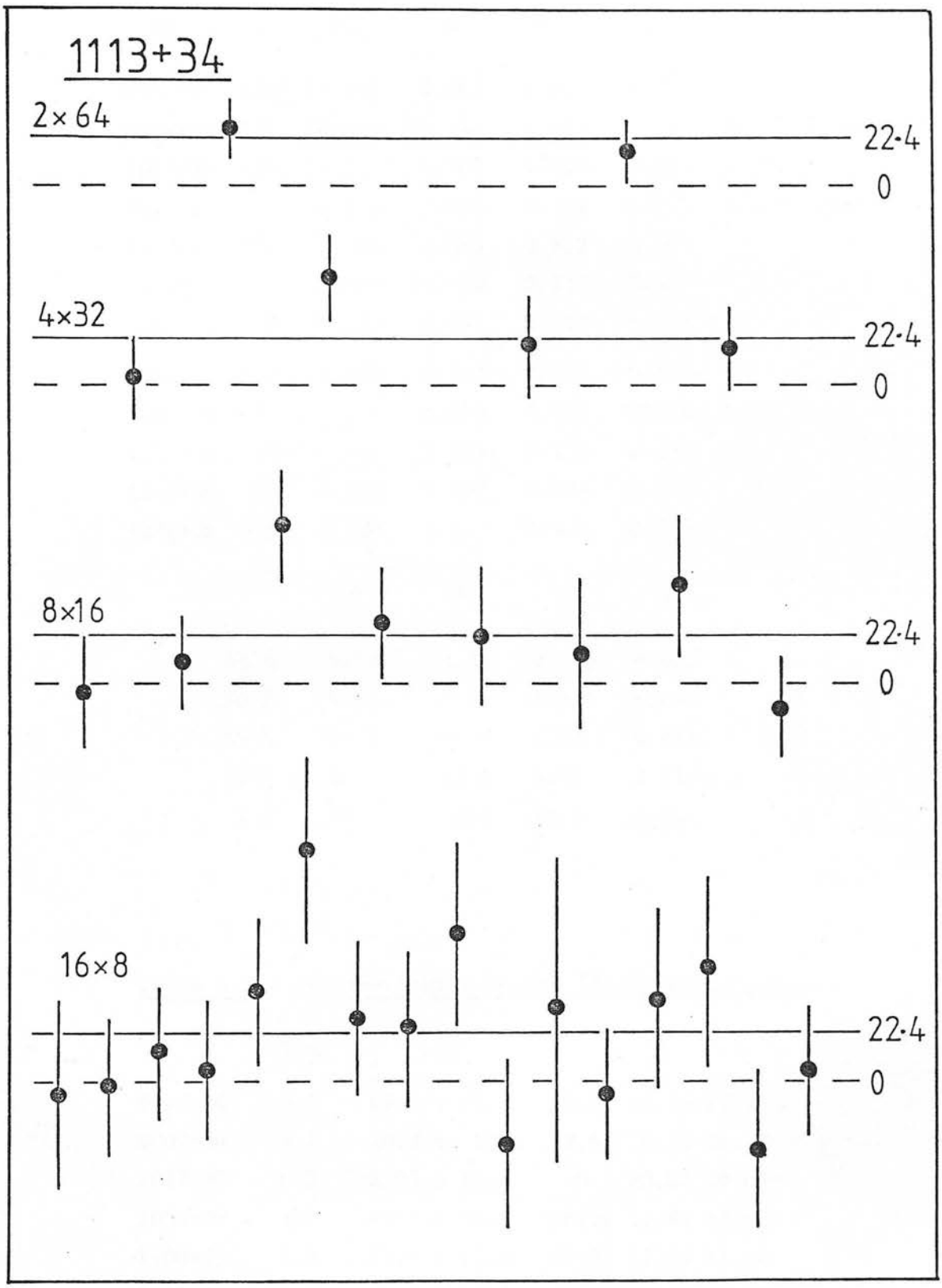


Figure 6.4: A diagram illustrating the statistical analysis that was performed on each of the long integrations. The set of 128 (or 64) pairs was progressively subdivided and at each stage a $\chi^2$ analysis was carried out to ensure that each group was consistent with the mean, which was 22.4 μJy in the case of 1113+34.

Table 6.2: Statistical Analysis of the 'Empty Field' Observations.

| ID | N | 16 | 8 | 4 | 2 | % | |
|---|---|---|---|---|---|---|---|
| 0902+34 | 128 | 11.738 | 4.383 | 1.557 | 0.270 | - | |
| 0902+34 | 128 | 38.040 | 25.347 | 19.210 | 0.159 | 0.5 | Reject |
| 1017+37 | 128 | 13.252 | 3.399 | 1.807 | 0.000 | 17 | |
| 1017+37 | 128 | 28.310 | 9.658 | 2.426 | 0.504 | 1.5 | Reject |
| 1113+34 | 128 | 12.460 | 7.885 | 3.812 | 0.260 | - | |
| 1143+37 | 128 | 21.045 | 10.710 | 0.133 | 0.008 | 17 | |
| 1301+35 | 128 | 10.129 | 5.741 | 2.781 | 1.675 | 20 | |
| 1056+39 | 128 | 16.320 | 4.317 | 1.577 | 0.194 | - | |
| 1100+35 | 64 | - | 5.843 | 4.717 | 0.352 | 17 | |
| 1132+37 | 64 | - | 2.206 | 1.136 | 0.028 | - | |
| 1159+36 | 128 | 15.006 | 5.096 | 1.904 | 0.041 | - | |
| 1256+36 | 128 | 6.338 | 1.853 | 1.466 | 0.712 | - | |

| | 15 | 7 | 3 | 1 |
|---|---|---|---|---|
| 99 % | 5.23 | 1.24 | 0.115 | 0.000 |
| 90 % | 8.55 | 2.83 | 0.584 | 0.016 |
| 50 % | 14.3 | 6.35 | 2.37 | 0.455 |
| 10 % | 22.3 | 12.0 | 6.25 | 2.71 |
| 1 % | 30.6 | 18.5 | 11.3 | 6.63 |

Table 6.3: Precise Limits to the 'Empty Field' Data.

| | S/N | μJy | K | | |
|---|---|---|---|---|---|
| 0822+39 | 5.8 | 68.3 ± 11.7 | 17.63 | 17.43 | 17.26 |
| 0902+34 | 2.1 | 20.2 ± 9.6 | 19.45 | 18.75 | 18.33 |
| 1017+37 | 0.2 | 2.95 ± 11.8 | ∞ | 20.84 | 19.09 |
| 1056+39 | 4.0 | 43.9 ± 10.9 | 18.22 | 17.91 | 17.66 |
| 1100+35 | 5.9 | 91.6 ± 15.5 | 17.31 | 17.11 | 16.94 |
| 1106+37 | 3.8 | 54.2 ± 14.4 | 18.02 | 17.68 | 17.42 |
| 1113+34 | 2.2 | 22.4 ± 8.6 | 19.16 | 18.64 | 18.28 |
| 1132+37 | 5.9 | 72.8 ± 12.3 | 17.56 | 17.36 | 17.19 |
| 1143+37 | 1.4 | 13.5 ± 9.5 | 20.51 | 19.19 | 18.61 |
| 1159+36 | 5.4 | 55.7 ± 10.3 | 17.87 | 17.65 | 17.47 |
| 1256+36 | 5.7 | 59.5 ± 10.4 | 17.79 | 17.58 | 17.40 |
| 1301+35 | 1.9 | 16.5 ± 8.5 | 19.76 | 18.97 | 18.52 |

constant, given the noise in each pair. This situation is indicated by a value of $\chi^2$ that is improbably small. It is noticeable in Table 6.2 that this occurs only in the analyses involving a small number of groups, whereas those which have $\chi^2$ too large occur in those with a larger number of groups. Although slightly puzzling, the occurence of 'spuriously good' data is not a problem. The penultimate column of Table 6.2 lists the lowest probability associated with the four values of $\chi^2$ in the Table, but only if this worst case is smaller than 25%. Those values of $\chi^2$ associated with low probabilities (i.e. less than 5%) are indicated by underlining.

Only two of the observations have sequences of pairs that could only have arisen by chance less than 15 times out of a hundred. The probabilities that these two did in fact occur by chance are small (less than 2% in both cases). The degree of independence represented by the four individual analyses of each object is difficult to assess. Nevertheless, the number of independent trials represented in Table 6.2 must be much less than 46, and so these two worst observations should be rejected. It is important to note that the whole observation is rejected rather than just those parts which contribute to the high $\chi^2$. By good fortune, the two observations which had to be rejected both had repeat observations, which passed the test. This was a coincidence. In one case the first observation was rejected and in the other it was the second which failed.

It is important to note that this analysis examines the noise on the mean signal, and should be independent of the actual level of the mean signal with respect to zero.

Having rejected the two observations whose probabilities were only of the order of 1%, the remaining observations are listed in Table 6.3. For each of the twelve objects, the S/N ratio of the detection, the mean flux density and (linear) standard error in this, and the mean magnitude and upper and lower limits to the magnitude are listed.

The astronomical discussion of the observations of the OEFs will be presented later. One important fact, however, is readily apparent from Table 6.3. A net positive signal had been recorded at the end of all the integrations. Indeed, in only one case, 1017+37, was the net signal not more than one standard error removed from zero. This fact alone confirms the theoretical expectation (Section 6.1c(i)) that confusion from objects not visible on the CCD images is not the dominant soure of noise.

## 6.3 : Analysis and Results

### 6.3.a The Absolute Magnitudes of Galaxies with Known Redshifts

Five galaxies and four quasars in the complete sample have measured redshifts. All of the galaxies have redshifts smaller than 0.15. Four of these galaxies have infrared measurements, and may therefore be directly compared with the 3CR galaxies. The other has an r magnitude, and an estimated K magnitude has been derived for this galaxy, by comparing this r measurement with the r magnitudes of the other 4 galaxies, for which K magnitudes are available.

These five galaxies are plotted on the 3CR K(z) relation in

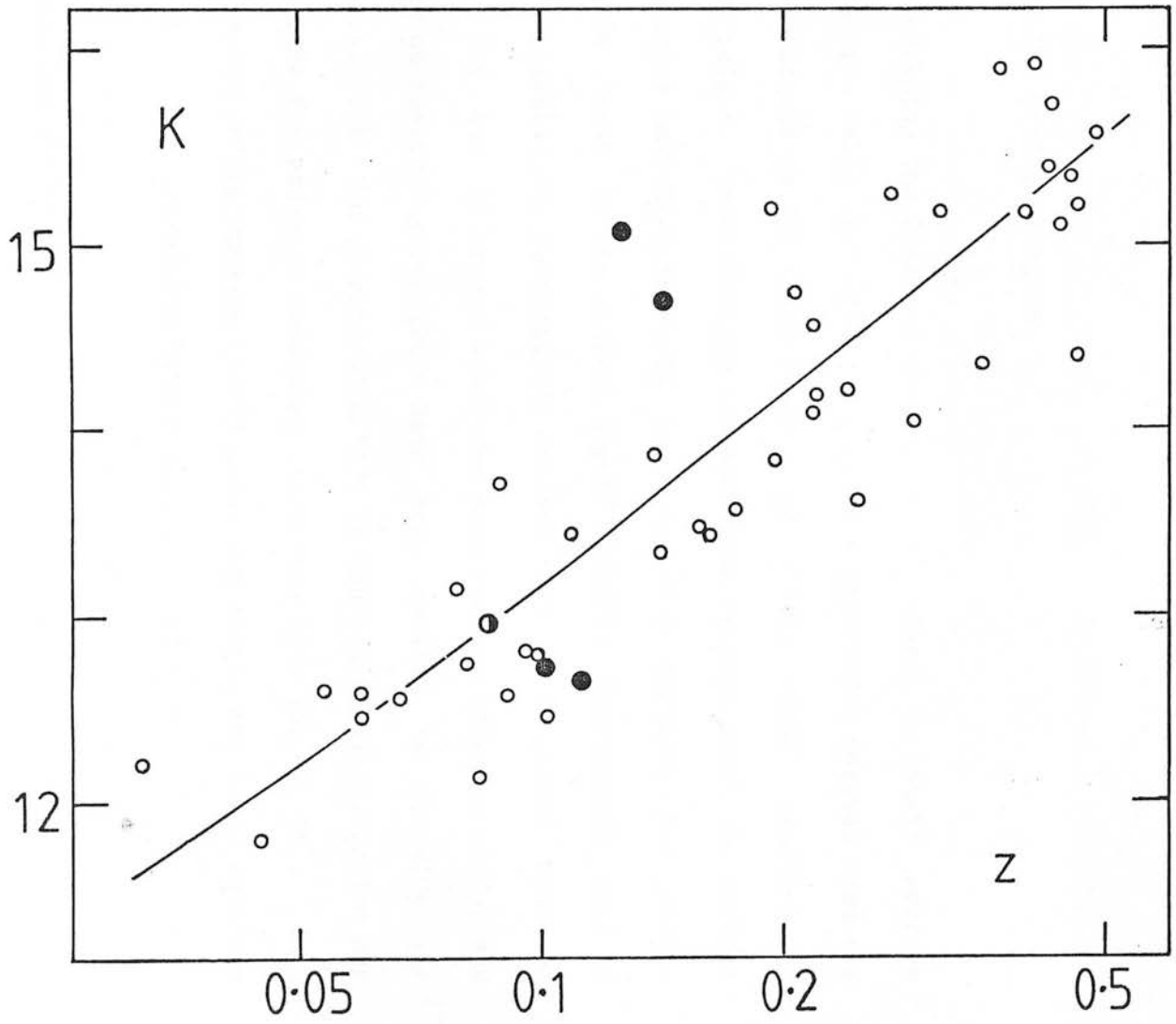


Figure 6.5: The K(z) relation for 1 Jansky radio galaxies with known redshift (solid circles). The half-filled circle represents the galaxy whose K magnitude is derived from its r magnitude. The open circles are the data for the 3C sample, and the line is a modelled best-fit to that data.

Figure 6.5. The agreement is not as good as might have been expected. In particular 1301+38 (at z = 0.126) is rather fainter (by about 1.3 magnitudes) than the mean 3CR galaxy at that redshift. The dispersion in absolute magnitudes of the five galaxies is about 1 magnitude, while the mean absolute magnitude is over 0.3 magnitudes fainter than that of the 3C galaxies. However, given the small number of objects involved this deviation is not formally significant. More redshifts will have to be obtained before a definitive answer to the question of whether the mean absolute magnitudes of the 1 Jansky and 3CR galaxies are the same can be provided.

6.3.b The (r-K),K diagram

Combining the infrared photometry of these 1 Jansky sources given in Table 6.1 with the optical r magnitudes derived from the CCD exposures by Allington-Smith et al (1982, APLGW) produces an (r-K) colour. Unfortunately the apertures through which the optical magnitudes have been measured are not well defined, but should include "most of the optical light" (APLGW). Fortunately, most of these galaxies are sufficiently distant that this should also be true for the 12 arcsec apertures used for the infrared study, and hence no aperture corrections have been applied in deriving the colours. For the objects with RA < 10 hours a small correction has been made for galactic reddening since they have $|b| < 50^{\circ}$. This was based on the Sandage (1973) polar cap model, and in no case was this reddening correction larger than 0.07 magnitudes. The (r-K) colours, and in the case of the "empty fields", lower limits to that colour, for the galaxies that have been observed in the infrared are

listed in Table 6.1. These lower limits for the colours of the empty field sources are based on the optical limit of $r > 23$ given by APLGW (but see Section 6.3.d), and the K magnitude derived from the mean infrared flux density, rather than the lower limit to this infrared brightness. They should be regarded as indicative only.

These data are plotted on Figure 6.6. The lower limits to the colours of the empty fields are plotted as horizontal bars whose length corresponds to the limits to the K magnitudes given in Table 6.3. Distinction has also been made in plotting the data for sources that have optical identifications. This has been done in accordance with the appearance of the optical morphology of the identification as classified by APLGW. Those with stellar profiles and classified as quasars (Q) by them are represented by open circles, while those with resolved appearances, classified as galaxies (G), are plotted as solid circles. Two objects whose classification is somewhat less certain are indicated by question marks while one whose nature is completely open is represented by a semi-solid circle. Typical error bars on these points are indicated near the bottom of the diagram.

Under the assumption that the 1 Jansky galaxies do in fact follow the empirical (K,z) relation defined by the 3CR galaxies (but see the discussion in the previous section) it is possible to plot on the (r-K),K diagram the equivalent curves to those used on the (r-K),z diagram for 3C galaxies (Figure 5.8). This has been done on Figure 6.6. The curves have been terminated on this diagram at a redshift of two. The mean redshift as a function of K magnitude used for this is shown along the top of the Figure. The (K,z) relation

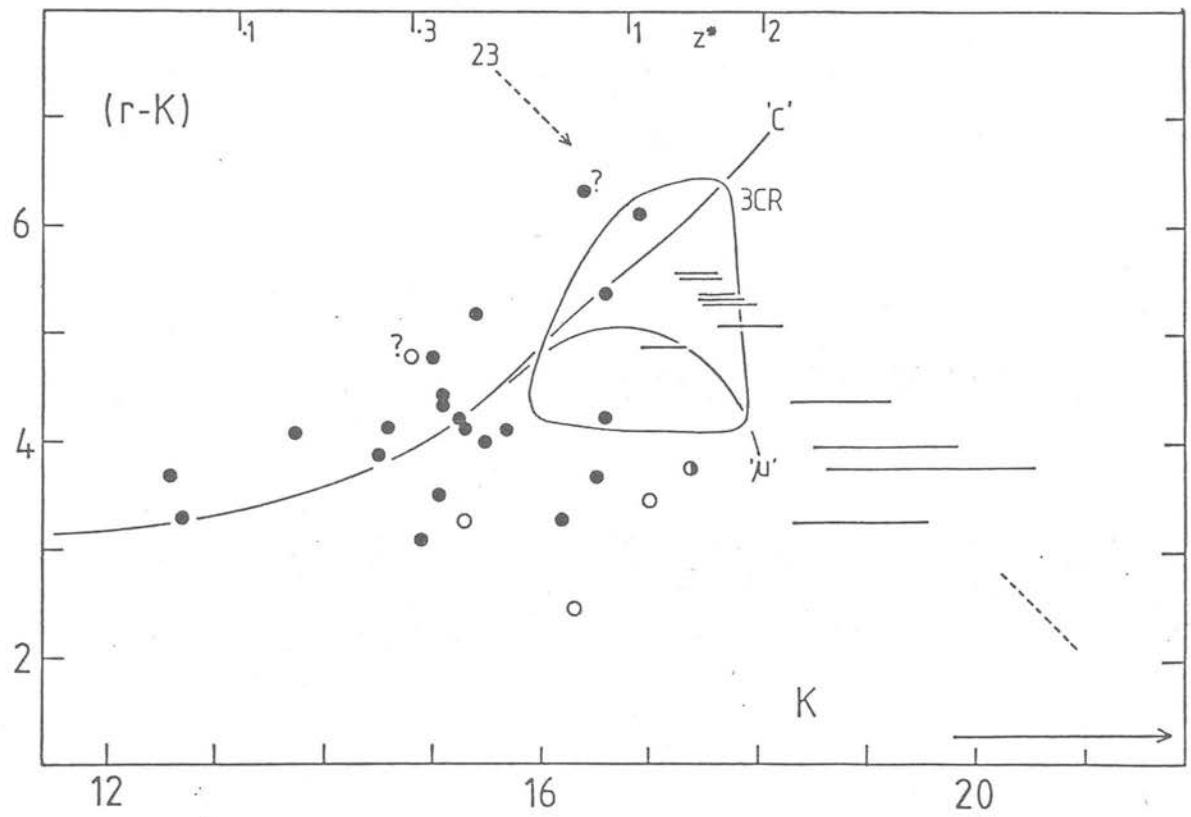


Figure 6.6: The (r-K),K diagram for 1 Jansky radio sources. The data are plotted for galaxies (solid circles), quasars (open circles) and the optical empty fields (horizontal bars). Question marks indicate a less certain classification, and the half-filled circle is an object whose nature is completely uncertain. The two solid curves represent a passively and an actively evolving Bruzual model respectively. They are plotted using the 3C K(z) relation shown on the top of the diagram. The area occupied by the 3C galaxies is shown, as is the limiting r magnitude of 23.

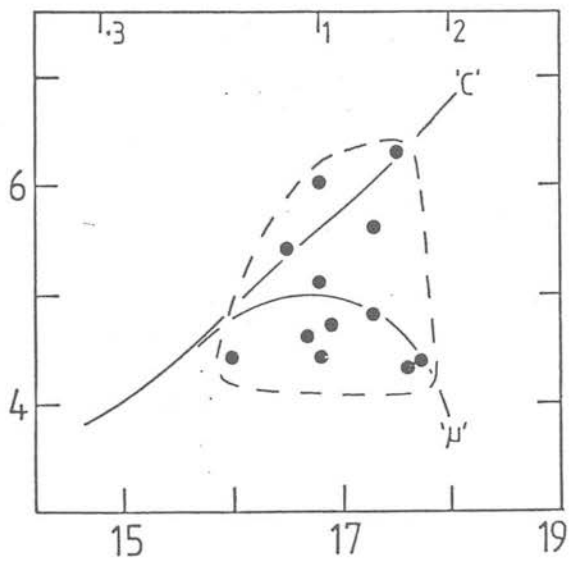


Figure 6.7: The (r-K),K diagram for the 12 3C galaxies at high redshift that were discussed in the previous Chapters.

for redshifts greater than 1.5 has been assumed to follow the modelled extrapolations of the curves that are satisfactory fits to the 3CR data.

The area on the (r-K),K diagram occupied by the 12 3CR galaxies with good (r-K) colours (see Chapter 3 and 5) is shown. Indeed, the positions of the 3CR galaxies on such a diagram is shown in Figure 6.7. Comparison of Figure 6.7 with Figure 5.8 shows that, while there is an obvious degradation in the information due to the neglect in Figure 6.7 of the redshift data for the 3C galaxies, the basic trends in the colours are still evident. In particular the absence of objects significantly redder than, and the scatter below, the C model prediction is clear.

Several important results are evident in Figure 6.6. Before discussing these, however, it is necessary to note the effect of the incompleteness of the subsample for which infrared data is available. For the galaxies, which are the sources most of interest, the sample is essentially complete for $r < 22$ and for the EOFs with $r > 23.5$. However, less than half the galaxies in the important range of apparent optical magnitude $22 < r < 23.5$ have been observed in the infrared. Correspondingly, there is a dearth of measurements in the strip of width about 1.5 magnitudes parallel to the r=23 limit marked. Unfortunately, this strip runs through the important area of the diagram that is occupied by both the passively and the actively evolving 3CR galaxies. It is therefore difficult to assess at this stage whether the 1 Jansky galaxies exhibit the same range of behaviour as seen in the 3CR sample.

However, it is clear from Figure 6.6 that the filled circles, representing the resolved 'galactic' identifications broadly follow the predicted behaviour of a gradual reddening in (r-K) colour with increasing faintness in K. It should be remembered that there is expected to be a scatter in absolute magnitude at a given redshift of about 0.5 magnitudes, and that this will be reflected as a spread in apparent magnitude at a given colour. The two rather blue galaxies are not anomalous in the radio, both being classical double sources. They may be similar to 3C 265 (see Section 3.4.d.(iii)), but a redshift determination is required before their nature can be confirmed.

One question that can easily be addressed, however, is whether the position of an object on the (r-K),K diagram can yield information on its nature. It is clear from Figure 6.6 that the three objects (open circles) with unambiguously stellar profiles (i.e those which were found to be optically unresolved by APLGW and hence classified by them as quasars [Q]) have amongst the bluest (r-K) colours found in the whole sample. The object which they were unable to classify morphologically (the half filled circle) also has a rather ambiguous colour. From its location on the diagram, it could be a nuclear dominated quasar, or a highly actively evolving galaxy similar to those found in the 3CR sample. The two objects whose nature was uncertain (i.e. either G? or Q? in APLGW's scheme) are most likely to both be galaxies. Their colours and magnitudes are quite consistent with those of a passively evolving gE galaxy, and, in the case of the colours, somewhat redder than the other quasars. The very red colour of the Q? source may possibly reflect the trend in Figure 4.4.c, in which there was some evidence that the

reddest objects were the most compact in r.

The observations of the 'empty field' sources illustrate an important point which will be explored further in Section 6.3.d. Assuming for the moment that they are 'ordinary' elliptical radio galaxies similar to those sources just above the optical plate limit (their nature will be discussed in more detail in the next section), then their location on the diagram, redder than the actively evolving $\mu$=0.5 model, indicates that there must be many radio galaxies at large redshift which are comparatively 'inactive', in the sense of having little star-forming, or other, activity to enhance the ultraviolet flux density. As the redshift increases, the r passband will penetrate further into the ultraviolet, reaching 2000 A at a redshift of about 2.2. This lack of activity was also demonstrated by 3C 241, at a redshift of 1.62, on the (r-K),z diagram (Figure 3.9). In other words, the apparent onset of activity in the 3CR radio galaxy sample as the redshift approaches unity, is not the herald of very widespread activity in all radio galaxies at $z > 1.5$.

### 6.3.c Analysis of the Empty Field Detections

Of the 12 optically empty fields (EOF) with nominal r > 23 (APLGW) that were observed on UKIRT, unambiguous detections were made for over half. Five sources were detected at more than 5 times the level of statistical fluctuations (5$\sigma$), and a further two at over 3$\sigma$. Of the remainder, 3 were about 2$\sigma$ detections, while the others were not very significant at 1.4$\sigma$ and 0.2$\sigma$ respectively.

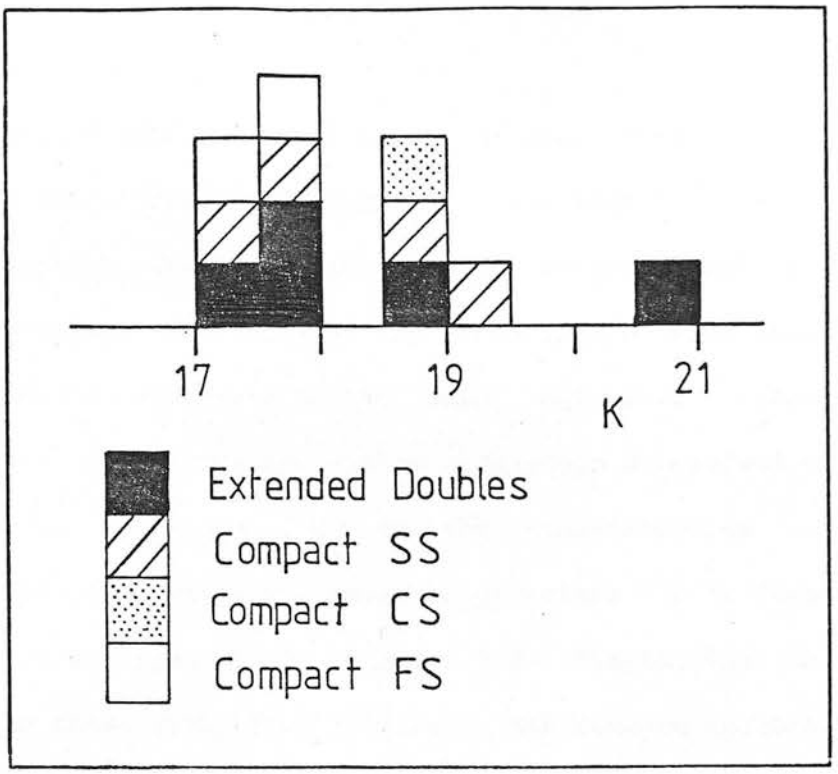


Figure 6.8: The distribution of K magnitudes that were measured for the 12 optical empty fields in the 1 Jansky sample. The morphological classification is based on radio maps and on whether the spectrum is steep, concave, or flat.

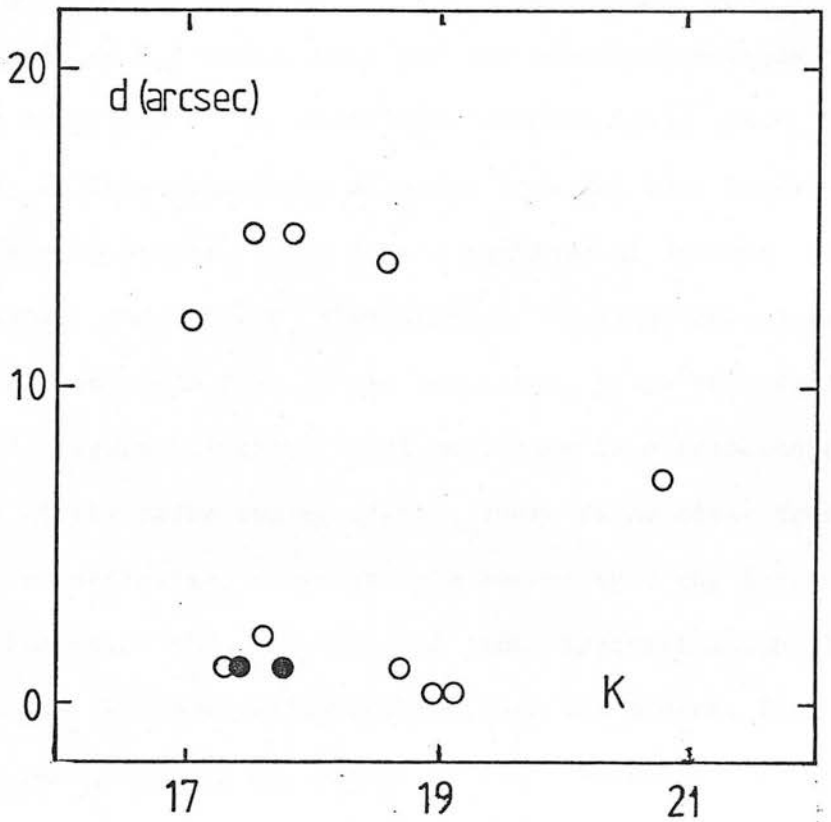


Figure 6.9: The K magnitudes of the empty fields plotted against the angular size of the radio source which determines how well the position of the identification is known.

Figures 6.8 and 6.9 show the K magnitudes of these detections as functions of the radio properties of the sources. Figure 6.8 shows the distribution of K magnitude with radio morphological and spectral classification. Distinction has been made between those with recognisable double structure on the maps, all with 'steep' radio spectra, and those that are either completely unresolved by the Cambridge 5 km telescope ('U' in the classification of Allington-Smith 1982) or have no recognisable structure ('E'). These are both referred to as 'compact' in Figure 6.8. Distinction has been made between those with 'flat', 'steep', and concave spectra. The flat spectrum sources are probably genuinely compact. The steep spectrum sources are probably small extended doubles, while the concave sources are probably composite sources, with extended emission dominating at low frequencies, but compact flat spectrum emission emerging at higher frequencies. The K magnitudes have been binned in intervals of 0.5 magnitudes, and the precise positions of the faintest are obviously rather uncertain. Nevertheless, there is no obvious trend in this histogram. Although both the flat spectrum sources are relatively bright, their actual rankings of 3rd and 6th brightest indicates that their distribution of magnitude is not significantly different from that of the remainder, given the small samples involved. Figure 6.9 shows the K magnitude as a function of the angular size of the radio source. Again, there is no clear trend in the data. In particular, there is no evidence that the largest double sources, for which the location of the identification is least certain, are systematically fainter than the others. Such a trend would have been worrying for either of two reasons. Firstly, it could have indicated that some light from the double source identifications, with their more uncertain positions, was being

missed because it lay outside the aperture. Secondly, it could have suggested that some infrared radiation was being detected from the radio-emitting regions.

The $2\sigma$ level of detection after an integration of about an hour corresponds to a K magnitude of slightly brighter than 19 magnitude. Since it would be expected that a giant elliptical at a redshift of around 3 would have this infrared brightness, it is of interest to analyse the more marginal infrared detections both to determine the overall detection rate, and to try to set plausible constraints on the redshift distribution of the objects, within the limitations imposed by the data and by the uncertainties in the predicted behaviour with redshift.

One analysis has been carried out as follows. For any given 2.2 micron flux density, it is possible to determine, for each source, a probability that that object has, in reality, a K flux density that is brighter than the flux density limit being considered. This probability may be derived from the statistics of the integration pairs. For instance the probability that a source with observed flux density $f_i \pm \sigma_i$ (in the 3rd column of Table 6.3) has a real K flux density brighter than f′ is given by:

$$P_i(f') = (2\pi)^{-\frac{1}{2}} \exp\left(-\frac{(f_i - f')^2}{2\sigma_i^2}\right) \qquad (6.5)$$

Hence it is possible to calculate the probability that, say, N of the 12 sources are, in reality, brighter than the given limiting flux density f′:

$$P(f',N) = \sum \prod_i \left[ \frac{P_i(f')}{(1-P_i(f'))} \right] \qquad (6.6)$$

In this expression, the summation is carried over all the possible combinations that yield a total of N galaxies brighter than f′.

This analysis is clearly related to the binomial probability distribution. However, the important difference is that for a given f′, the probability of 'success' or 'failure', (i.e. that the galaxy really is brighter or fainter than f′) is different for each galaxy.

The results of this analysis are shown in Table 6.4. A range of flux density limits f′ have been considered, including negative values. For each of these the probability that N galaxies were brighter has been calculated for different N, and tabulated. These results are also represented graphically in Figure 6.10, in which the 5% probability contour has been shown. Note that the sum of the 13 probabilities for each f′ limit must equal unity.

This analysis is essentially a method for combining the 5 or so statistically less significant detections. In particular, it is interesting to see the number of sources that must have a flux density greater than zero in Table 6.4 and Figure 6.10, since this is effectively the number of sources that have been positively detected. One can say from the results in Table 6.4 that at the 95% level of confidence (i.e. one would be wrong only one time in twenty) at least 10 of the 12 sources have infrared flux densities that are greater than zero. There is only a 0.2% chance that only 9 objects have non-zero K flux densities.

Table 6.4: The Number of sources detected as a function of limiting flux density.

| Flux | N | | | | | | | | | | | | |
|---|---|---|---|---|---|---|---|---|---|---|---|---|---|
| μJy | 0 | 1 | 2 | 3 | 4 | 5 | 6 | 7 | 8 | 9 | 10 | 11 | 12 |
| 100 | 0.691 | 0.304 | 0.005 | 0.000 | 0.000 | 0.000 | 0.000 | 0.000 | 0.000 | 0.000 | 0.000 | 0.000 | 0.000 |
| 80 | 0.129 | 0.519 | 0.298 | 0.052 | 0.003 | 0.000 | 0.000 | 0.000 | 0.000 | 0.000 | 0.000 | 0.000 | 0.000 |
| 60 | 0.000 | 0.009 | 0.086 | 0.282 | 0.366 | 0.207 | 0.047 | 0.003 | 0.000 | 0.000 | 0.000 | 0.000 | 0.000 |
| 50 | 0.000 | 0.000 | 0.002 | 0.026 | 0.152 | 0.370 | 0.356 | 0.094 | 0.000 | 0.000 | 0.000 | 0.000 | 0.000 |
| 40 | 0.000 | 0.000 | 0.000 | 0.000 | 0.007 | 0.091 | 0.403 | 0.477 | 0.022 | 0.000 | 0.000 | 0.000 | 0.000 |
| 30 | 0.000 | 0.000 | 0.000 | 0.000 | 0.000 | 0.004 | 0.092 | 0.567 | 0.284 | 0.050 | 0.003 | 0.000 | 0.000 |
| 20 | 0.000 | 0.000 | 0.000 | 0.000 | 0.000 | 0.000 | 0.002 | 0.094 | 0.312 | 0.370 | 0.184 | 0.036 | 0.002 |
| 10 | 0.000 | 0.000 | 0.000 | 0.000 | 0.000 | 0.000 | 0.000 | 0.001 | 0.015 | 0.115 | 0.354 | 0.406 | 0.109 |
| 0 | 0.000 | 0.000 | 0.000 | 0.000 | 0.000 | 0.000 | 0.000 | 0.000 | 0.000 | 0.002 | 0.050 | 0.424 | 0.524 |
| -10 | 0.000 | 0.000 | 0.000 | 0.000 | 0.000 | 0.000 | 0.000 | 0.000 | 0.000 | 0.000 | 0.001 | 0.143 | 0.856 |
| -20 | 0.000 | 0.000 | 0.000 | 0.000 | 0.000 | 0.000 | 0.000 | 0.000 | 0.000 | 0.000 | 0.000 | 0.027 | 0.973 |

Note: This Table lists the probabilities that N, and only N, sources have true flux densities that are brighter than the various limits listed on the left.

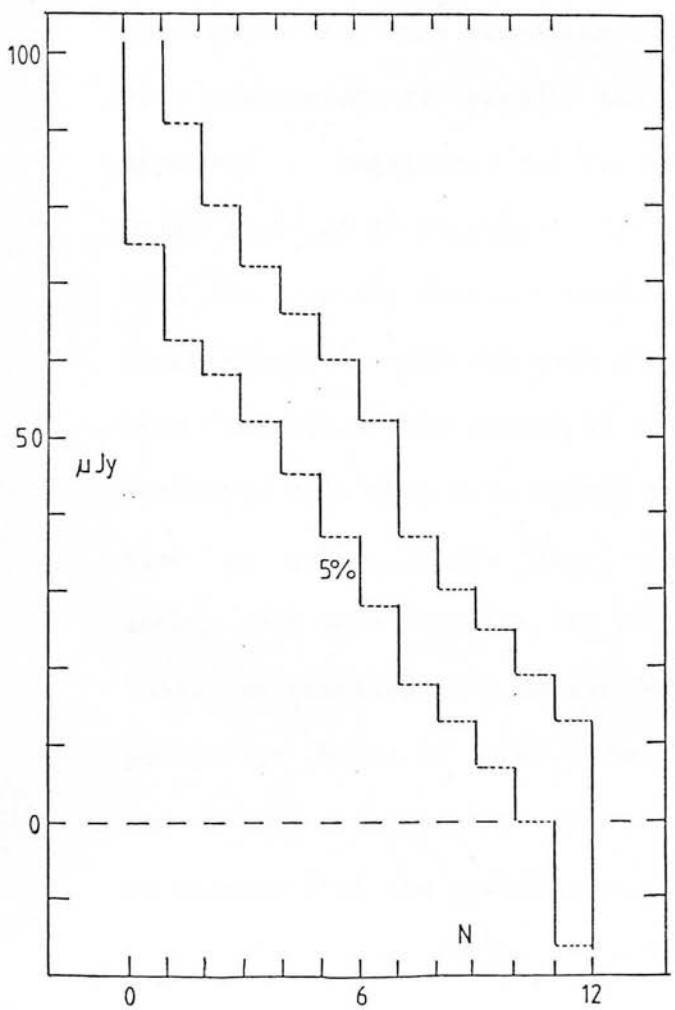


Figure 6.10: A graphical representation of Table 6.4. This shows the number of sources N which are likely to be brighter than a given flux density limit. The two lines represent the 5% levels of confidence. i.e. one can say with 95% confidence that between 5 and 7 sources are really brighter than 40 μJy, and that at least 10 are brighter than zero flux density, and have hence been detected.

A similar analysis may be carried out in terms of redshift, rather than flux density. In other words, for each source, it is possible to calculate the probability that the source really lies at a redshift that is smaller than the one being considered. Since, however, this is considerably further removed from the basic data than a simple flux density limit, a number of assumptions must be made. Firstly, it must be assumed that the 1 Jansky empty field sources are all indeed radio galaxies (rather than quasars or other objects), and hence follow a well-defined (K,z) relation. For the empty fields with relatively high infrared brightnesses, and hence rather red lower limits to their (r-K) colours, this is probably justified. For the remainder, however, the main justification for this assumption is simply the peaking of the distribution of apparent r magnitudes for the Q identifications well above the CCD plate limit of 23 (Figure 6.3). Furthermore, it must also be assumed that the 1 Jansky galaxies follow the same (K,z) relation as the 3CR radio galaxies, with the same degree of cosmic scatter about the mean relation. This empirical 3C (K,z) relation is well-defined for redshifts less than 1.5. Beyond this redshift, however, the relation must be extrapolated. This has been done, using a range of the models that were found to fit the 3CR data with $z < 1.5$ (Section 5.3). In practice, the extrapolations are rather insensitive to the particular choice of model, provided that the model is a good fit to the lower redshift data. Nevertheless, there is no a priori reason to believe that the combination of evolution, cosmology, and any biases introduced by the selection methods, that is appropriate for redshifts out to 1.5 will still be so at a redshift of 3. The actual formal uncertainty in these model extrapolations to a redshift of 3

is only around 0.2 magnitudes. Despite the restrictiveness of these assumptions, the analysis is nevertheless sufficiently of interest in possibly indicating any large trends exhibited in the data on these optically empty fields as to be worthwhile.

The analysis is further complicated, however, by the existence of the scatter in the (K,z) relation of at least 0.5 magnitudes. This, of course, effectively increases the range of acceptable redshifts for each galaxy beyond that indicated by the simple observational uncertainties. Furthermore, it is neccessary to carry out the analysis in terms of magnitudes rather than flux density. The drawback of this is that the observational uncertainties are not symmetrical in magnitude space. In other words, a low significance detection has a smaller magnitude error bar in the brighter direction than in the fainter. Given the uncertainty in the whole analysis, the effect of this was was reduced by simplying having two values for $\sigma_i$ for each measurement. These two values were derived from the differences between the upper and lower limits and the mean K magnitude given in Table 6.3. Depending on whether the sampling magnitude was brighter or fainter than the mean magnitude of the object, one or other of these two were used. The lower $\sigma$ for the source detected at less than 1 $\sigma$ was set to infinity. To produce the $\sigma_i$ required in Equation 6.5, the appropriate observational uncertainy was added in quadrature to the cosmic dispersion of 0.5 magnitudes.

The results of this analysis are shown graphically in Figure 6.11. It should be remembered that these results apply only to the optically empty fields and that, particularly at $z < 2$, there will

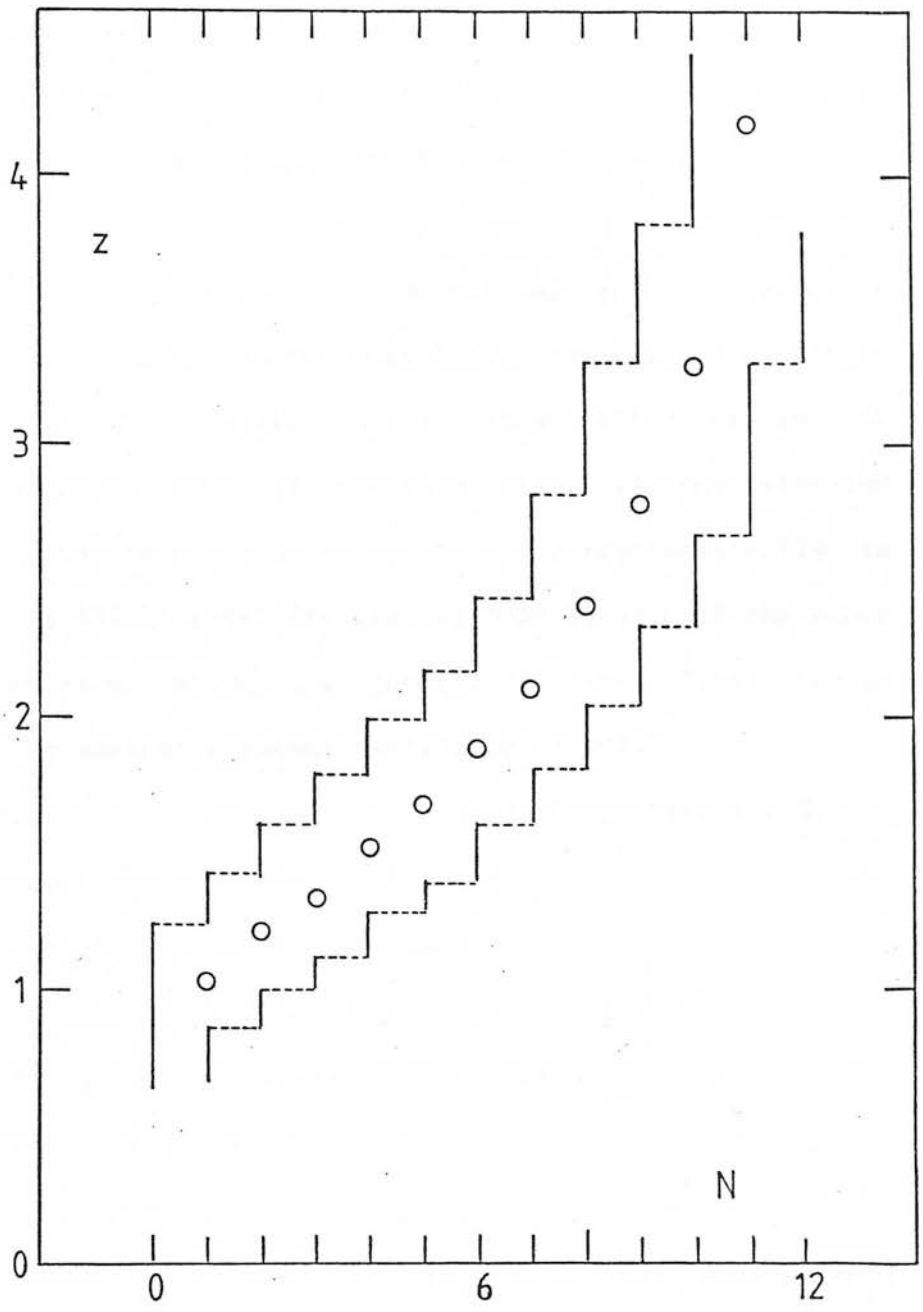


Figure 6.11: The equivalent diagram to Figure 6.10 showing the most likely numbers of galaxies that are nearer than a given redshift z. The two lines represent 5% confidence levels, and the open circles represent the most probable $z_N$ such that N galaxies are closer than $z_N$.

be a substantial number of galaxies that will have been identified on the CCD. One consequence of this is that there will an inverse Scott effect. The bright end of the sample may be biased towards the inclusion of intrinsically faint galaxies. The redshifts of these galaxies will therefore be systematically overestimated.

On the basis of Figure 6.11 a number of quite interesting statements may be made. At the very least, however, it should be remembered that the uncertainties in the extrapolation of the 3C (K,z) relation alone make it possible that all the estimated redshifts quoted in the next few sentences may be systematically in error by at least 15% at redshifts greater than 2, even if the other assumptions described above are justified. The first three statements may be made at a formal confidence of 90%.

(i) Between 4 and 7 of the empty field sources have $z > 2$.

(ii) Between 1 and 4 of them have $z > 3$.

(iii) Not more than 2 sources can have $z > 4$.

(iv) All objects could (10% confidence) have $z < 3.5$.

(v) It is quite plausible (25% confidence) that all the sources have $z < 4$.

The ridge line in Figure 6.11 represents the most likely distribution of redshifts in the sample of empty field sources, if the many assumptions made above are valid. For the remainder of this section, a brief analysis of this distribution is carried out to investigate whether this redshift distribution is broadly as expected, or whether the data shows gross discrepancies from these expectations. In order to do this, a comparison is made with the redshift distribution found in the 3CR sample.

Because it has been assumed that all of the 1 Jansky empty field sources are radio galaxies, as opposed to quasars, it is neccessary to make this comparison with the 3C radio galaxies only, and exclude the quasars completely from this analysis. Fortunately, recent progress (e.g. Spinrad 1982 and private communications, Chapter 2 of this thesis) in determining redshifts for faint 3CR identifications has resulted in redshifts being available for a large fraction (more than 85%) of the statistical sample (Laing et al 1983, LRL). For the few remaining sources infrared magnitudes were used wherever possible to estimate the redshifts, since these are less susceptible to evolutionary effects

Figure 6.12 shows the (P,z) plane. The axes are linear in log P(408) and log (1+z). Assuming a $q_0 = \frac{1}{2}$ geometry, and a mean spectral index of 0.7, the limiting flux densities of S(178)=10 Jy for the 3CR and 1Jy<S(408)<2Jy for the 1 Jansky sample have been plotted on this diagram. Since the sample of empty fields is almost certainly not representative of the total radio galaxy population at $z < 2$, (since many of the galaxies at $z < 2$ will have been identified and, unfortunately, not observed as yet in the infrared), the region of the (P,z) plane that is most of interest for the 1 Jansky sample is at $z > 2$. This has been divided in to 4 sections. The corresponding sections of the 3CR sample are clear, and have been shown in Figure 6.12. The numbers of radio galaxies in each 3C section is indicated.

Taking in to account the different solid angles of sky covered by the two surveys and the different comoving volume elements, the number of 1 Jansky radio galaxies that would be expected in each 1

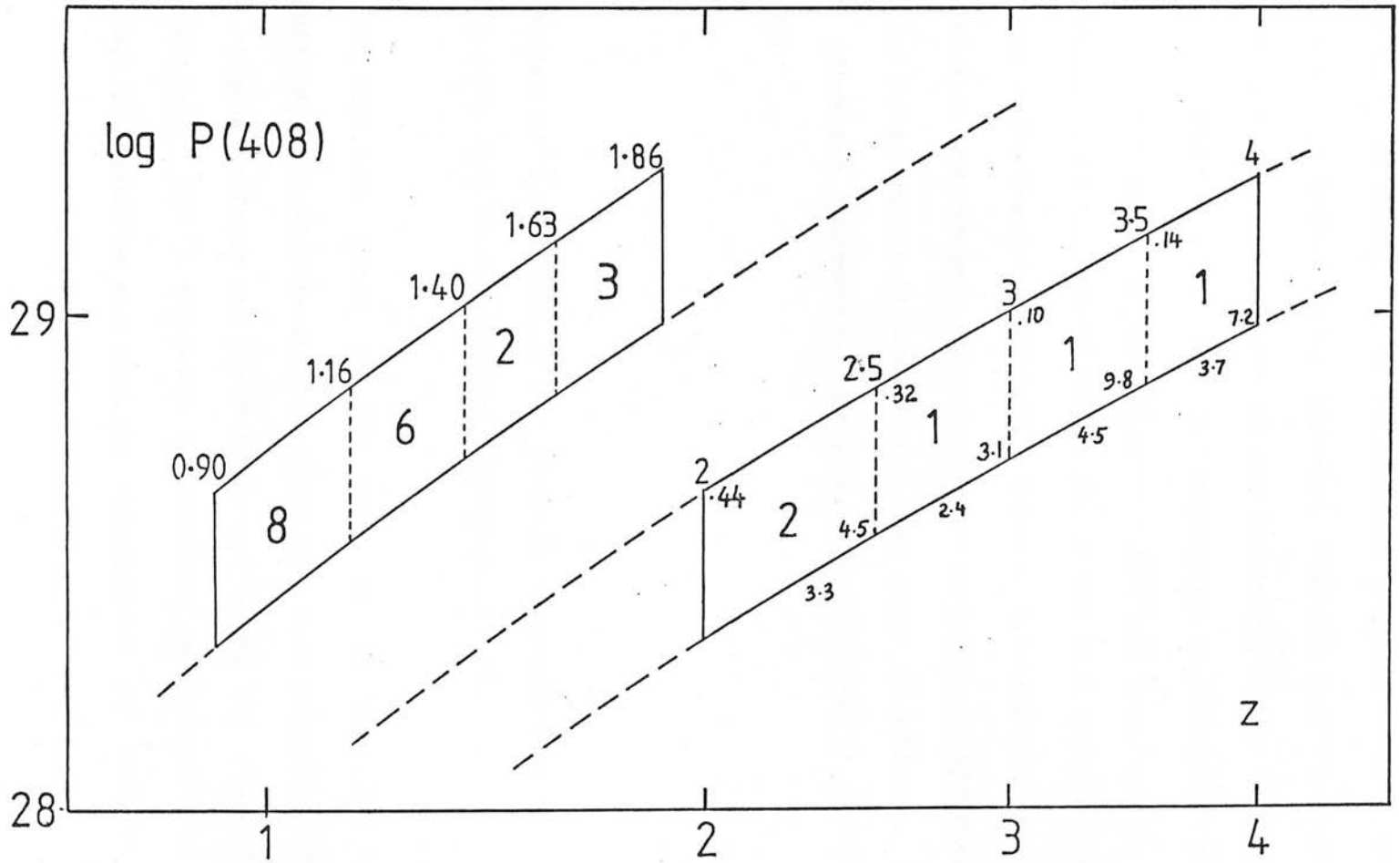


Figure 6.12: The (P,z) plane showing the locations of the 1 Jansky sample (right) and the 3CR sample (left). The numbers of radio galaxies in each 3C bin is shown. Based on these the predicted number of 1 Jansky sources is shown in the upper left of each 1 Jansky box. The observed number is the large central figure, and the enhancement factor is in the lower right. These have been converted to an approximate $\beta$ and these values are the small numbers outside each box.

Jansky section is shown as the small number in the upper left of each 1 Jansky box. This number has been computed assuming a constant co-moving space density of objects. The actual number observed, on the basis of the best-guess redshift distribution, derived from Figure 6.11, is shown. It is immediately apparent that there are many more 1 Jansky radio galaxies than are predicted under the assumption of a constant comoving space density. This, of course, is merely a demonstration of the well-known evolution of the radio source population. It is nevertheless a striking illustration of the enhancements, by factors of about 5-10, of the comoving space density of these radio sources between redshifts of approximately 1 and 2. The actual enhancement factors, highly uncertain in all cases, are also indicated on the Figure in the lower right of each box. To show that these are reasonable, they have been converted to an effective $\beta$ where:

$$\rho \propto (1+z)^{\beta} \tag{6.7}$$

The values of $\beta$ thus derived are shown by each box, and as far as can be said with so few sources, are quite normal.

The important point in this analysis is that the infered redshift distribution is much as would have been predicted. The data show no gross effects and there is no evidence, of even marginal significance, for a turn-over in co-moving space density at $z > 3$, although it should be stressed that the numbers of objects is so small as to make even the formal uncertainties very large.

6.3.d Possible constraints on the Epoch of Last Star Formation

The observations of those empty field sources for which good detections (i.e. better than $4\sigma$) were obtained can set fairly precise limits on the colours of the associated objects. Indeed, because of the long standard integrations used for these observations, the infrared measurements for many of the 1 Jansky empty field sources are better than those of some of the faint 3C galaxies described in Chapter 3. Assuming that the associated objects are indeed elliptical radio galaxies like the 3CR identifications in at least most, if not all cases, these colour limits have the potential to impose constraints on possible scenarios for the formation and evolution of the radio galaxies, and in particular on the time that has elapsed since the epoch of last major star-formation in these particular galaxies. An investigation in to this has been carried out as follows.

The five OEF observations of radio sources with steep 'radio' spectra for which detections were made at the $4\sigma$ level or greater were selected for more detailed study. The CCD images of the fields of these five sources published by Allington-Smith et al (1982), and rereduced by the author as described in Section 3.4.d , were examined to produce more precise upper limits to the optical flux density. One source was dropped from the analysis at this stage because it had a small pixel defect at the position of the radio source leading to a less severe constraint of $r > 22$ (Allington-Smith et al 1982). For the remaining four fields, however, the rms fluctuations in the background around the radio

source position were measured through an aperture whose size was matched to the seeing disk. An upper limit of three times this rms value was chosen as a reasonable upper limit to the optical flux densities of the infrared identifications. The very faintest objects that could be seen on the CCD were at about this level. These upper limits are listed for the 4 sources in Table 6.5. Of these 4 sources, two had 15 arcsec double structure (1056+39 and 1256+36) while the other two had marginally resolved structure of indeterminate form (Allington-Smith 1982).

From these optical upper limits, more precise lower limits to the (r-K) colour may be set. These lower limits are also listed in Table 6.5, and have been calculated in each case from the most likely K value and the $3\sigma$ r lower limit. The range of likely redshifts has been deduced for each identification. This is derived from the K magnitude of each identification and the 3C (K,z) relation, incorporating both observational uncertainties and an assumed cosmic dispersion of 0.6 magnitudes. Although the range of redshifts for each object is high (spanning a factor of about two in z) the mean redshift of about 1.6 is quite close to the range in which the 3C (K,z) relation is well defined, and the principle concern is the assumption that these infrared identifications are basically 3C-type radio galaxies, rather than the actual extrapolation of the relation. The possible biases in the redshift distribution discussed in the previous section may be present here, but they will only tend to push the correct redshift to one or other end of the uncertainty range, and should not extend that range in either direction. In practice these redshifts are not central to what follows, although the assumption that these are basically

Table 6.5: Upper Limits to Optical Flux Densities.

| | $r_{min}$ | K | $(r-K)_{min}$ | z* |
|---|---|---|---|---|
| 1132+37 | 23.8 | 17.9 | 5.9 | 1.2 - 2.4 |
| 1132+37 | 24.4 | 17.4 | 7.0 | 1.0 - 1.9 |
| 1159+36 | 24.2 | 17.6 | 6.6 | 1.1 - 2.2 |
| 1256+36 | 23.6 | 17.6 | 6.0 | 1.1 - 2.1 |

Note: $r_{min}$ is the r magnitude of the flux density that is three standard deviations above the sky.

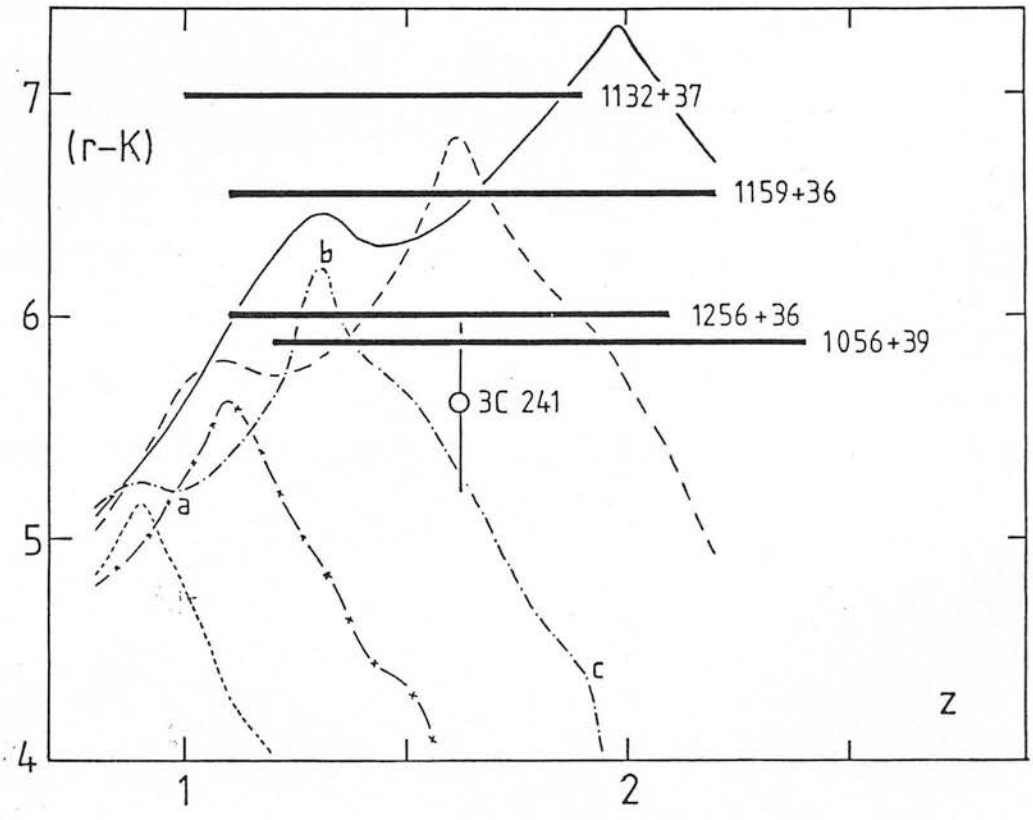


Figure 6.13: The (r-K),z diagram for the four brightest optical empty fields and 3C 241. The 1 Jansky sources have estimated redshi-ts only. The 5 curves represent passively evolving 'C' models of Bruzual which have different ages at a redshift of two. The solid line is a model in which the PLMSF ceased 2 Gyr prior to the epoch corresponding to z=2, and the others are progressively 1 Gyr younger. The curve of the galaxy which has the PLMSF ending at z=2, is labelled at epochs a) 4 Gyr after PLMSF, b) 2 Gyr after and c) at PLMSF.

stellar systems is. These colour limits are plotted as a function of redshift in Figure 6.13.

The curves on Figure 6.13 represent four passively evolving stellar populations. They differ only in their ages, and have kindly been computed for the author by Dr. Bruzual. These models are all 'C' models (Bruzual 1981) in which a uniform burst of star-formation occurs for 1 Gyr, after which there is no subsequent star-forming activity. The models, which are appropriate for an $H_0=50$ $q_0=0$ cosmology have different zero-redshift (i.e. present epoch) ages. These are respectively 16, 15, 14 and 13 Gyrs. For the present purposes, these translate to ages, at a redshift of two, of 3, 2, 1, and 0 Gyrs respectively (since in such a cosmological model, the age of the universe at a redshift of two is 6.7 Gyr, and at a redshift of zero is 20 Gyr). The curves represent, effectively independent of the precise cosmology that was adopted in computing the models, the appearance of a coeval population at any given high redshift, at various ages after its birth. The (r-K) colour has been computed from the data provided by Dr. Bruzual using the relation between (r-K), (V-R) and (V-K)

$$(r-K) = (V-K) - 0.77\ (V-R) + 0.34 \qquad (6.8)$$

No attempt was made to modify the model relations in the way described in Section 5.4 since the aim of the present investigation is to relate the observations to the ageing of a simple coeval stellar population, rather than to study the differential effects with redshift which was the motive for the earlier adjustment. It can be seen in Figure 6.13 that, as the epoch of last major

star-formation is approached the colour redshift relations become more complex as short lived populations become evident. The essential features of the evolution are recognisable in all the curves however.

As one looks back in time, towards the youth of the stellar populations, the curves for the different populations are virtually the same (to within 10% or so) until the epoch about 4 Gyrs after the period of last major star formation (PLMSF) is reached. At this point, as one continues to look back, the model galaxy becomes intrinsically bluer than the other models representing galaxies which are still older at that redshift. Nevertheless, except for a brief period, the observed (r-K) colour of the galaxy continues to redden with redshift and runs parallel on the diagram to the older populations. However, when one approaches to within about 2 Gyrs of the end of the PLMSF, the galaxy colour that is observed becomes progressively and steadily bluer with redshift. Continuing to look back in time, the (r-K) colour will be between 4 and 5 at the epoch corresponding to just after the end of the PLMSF. Finally as the PLMSF is actually observed, the colour sharply declines a further two magnitudes or so. Parenthetically, it is of course this last sharp decline that makes the (r-K) colour so sensitive to even very small amounts of continuing star formation in otherwise passively evolving galaxies (c.f. Section 5.1.a).

A consequence of this behaviour is that there is a maximum (r-K) colour that is attained by a model galaxy. This maximum colour varies as a function of the epoch, or redshift, of the PLMSF. In view of the position of the two identifications with the reddest

lower limits in (r-K), it is unlikely that they are being observed at epochs less than 2 Gyrs before the PLMSF. In other words, it is likely that the PLMSF for these galaxies was at least 1 Gyr before the epoch corresponding to a redshift of two. Reference to Figure 6.14 shows that in terms of the formation redshift this limit is not dramatic, requiring only that the PLMSF occured sometime before a redshift of about 2.6 to 3 (depending on whether $q_0$ is closer to 0.0 or 0.5).

It should be stressed that, although the extrapolation of the 3C K(z) relation has been used to place the 'empty field' sources on the (r-K)-redshift diagram (Figure 6.13), this does not enter into the argument concerning the minimum redshift of the PLMSF. This limit is based purely on the models of the stellar populations (used in the regime of quite modest turnoff masses, e.g. less than 2 solar masses), and an assumption that the colours of the galaxies have not been reddened by any dust at moderately high redshifts. There is no evidence from quasar spectra that reddening at a redshift of two is significant. The result is therefore reasonably secure.

## 6.4 : Summary

The main conclusions that have been drawn from the infrared observations of 39 radio sources selected from the '1 Jansky' sample are concerned with the properties of the 'empty field' sources that have not been seen in optical passbands to a limiting r magnitude of 23.5. Other important results will be obtained when redshifts are measured for these sources, and when the programme of infrared photometry is completed. Nevertheless, two interesting results have

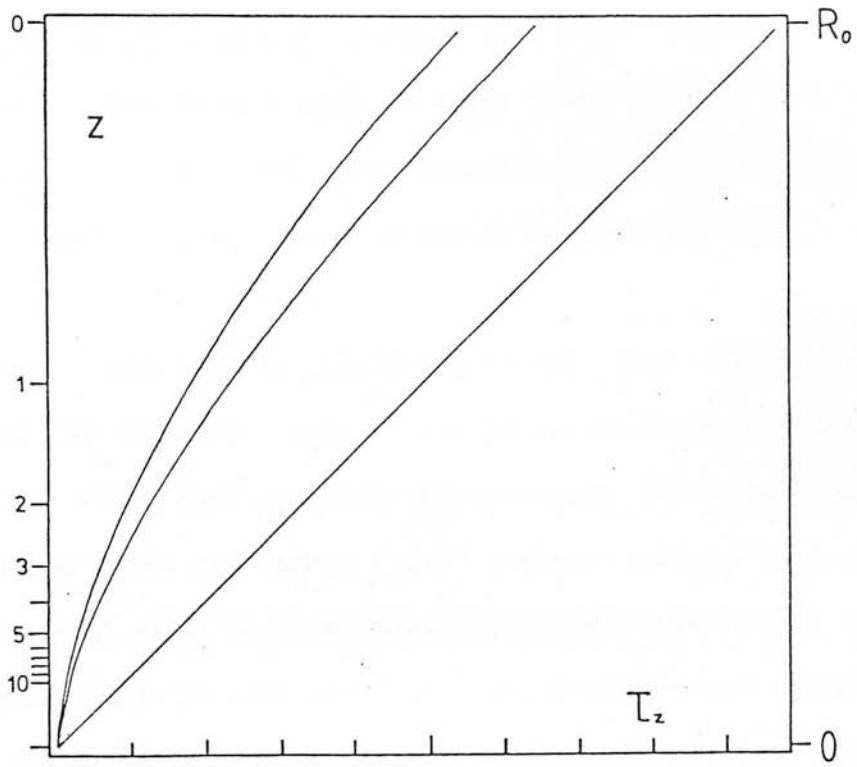


Figure 6.14: The change in cosmic time after the Big Bang with redshift for three different cosmological models. These all have $H_0$= 50 $kms^{-1}Mpc^{-1}$, and have $q_o$ = 0 (diagonal line), 0.5 and 1 respectively. The vertical scale is linear in the scale factor R.

been derived.

(a) The 'empty field' sources that were brightest in the infrared have colours and magnitudes that are consistent with those that are expected of passively evolving elliptical galaxies at high redshifts. The lower limits to their (r-K) colours suggest that the period of last major star formation must have occurred in these galaxies prior to a redshift of between 2.6 and 3.

(b) Based on a modelled extrapolation of the K(z) Hubble relation defined by the 3C radio galaxies in the redshift range from 0.05 to 1.5, the redshift distribution of the galaxies associated with the 'empty field' sources that were faintest in the infrared shows no gross discrepancy with that which may be predicted from the redshift distribution of 3C radio galaxies at lower redshift using conventional models for the evolution of the comoving space density of radio sources.

# Chapter 7 : SURFACE PHOTOMETRY OF TEN 3CR RADIO GALAXIES

## 7.1 : Introduction

Ostriker and Tremaine (1975) first suggested that the merging of cluster galaxies with the central giant galaxy could be a large evolutionary effect in shaping the appearances of 1st ranked cluster galaxies, and since then much work has been done to investigate this effect. Much of the motivation for this has come from the realisation that this process must be understood if 1st ranked cluster galaxies are ever to be used as standard candle cosmological probes. As regards radio galaxies, the idea of merging galaxies had been at one time very popular following the identification of 3C 405 (Cygnus A) by Baade and Minkowski (1954) with, as they then thought, two colliding galaxies. This was the first identification of an extragalactic radio source. However, this idea became less tenable later as numerous giant elliptical galaxies with more normal morphology were identified with radio sources (e.g. Matthews et al 1964), and as the morphology of Cygnus A was interpreted in terms of a superposed dust lane, rather than as two separate galaxies. However, galaxy mergers have long been regarded as a convenient source of fuel for the radio sources associated with nuclear activity, and the original idea has been revived recently in a different form by the observation of Hutchings et al (1982) that many low redshift quasars appear to have interacting companions (see also Stockton and McKenty 1983).

Mergers between satellite galaxies and the central giant are

caused by the loss of orbital energy of the former through the action of dynamical friction forces. Theoretical work (e.g. Gunn and Tinsley 1976 and Hausman and Ostriker 1978) has indicated that, under the assumption of homology during the merging process, these mergers should result in relations being found between various photometric parameters of the remnants. These arise because the merger remnant must have the same total mass and binding energy as the initial two galaxies, assuming that mass loss is negligible.

Hoessel (1980) has presented a large body of data on 104 Abell cluster 1st ranked cluster galaxies, and interpreted his data in terms of the models of merging in these clusters. This work has recently been extended by Schneider et al (1983b). In addition, Thuan and Romanishin (1981) have also published data on nine 1st ranked cluster galaxies selected from poorer systems than the Abell clusters. They also interpreted their data in terms of these models.

7.1.a The Alpha Structure Parameter

Much of the theoretical and observational work on the effects of galaxy mergers has used the dimensionless structural parameter $\alpha$ introduced by Gunn and Oke (1975). This parameter was used by them to describe the logarithmic slope of the growth curve of enclosed galactic flux density at a given metric sampling radius, $\gamma$. It therefore entered in to the aperture correction that they used to convert their metric magnitudes appropriate for one cosmological geometry in to those appropriate for another. Hence $\alpha$ also appears in the equation giving the effective sensitivity of the Hubble diagram to the cosmological geometry. If L(r) is the luminosity

enclosed within a radius r, then:

$$\alpha_{\gamma} = \left. \frac{\delta \log L(r)}{\delta \log r} \right|_{\gamma} \qquad (7.1)$$

The sampling radius $\gamma$ is usually chosen, for historical reasons, to be 19.2 $h^{-1}$kpc, where $H_0 = 50h$ kms$^{-1}$Mpc$^{-1}$ (Gunn and Oke 1975). It should be noted that this parameter therefore measures the properties of the main body of the galaxy, and to a large degree excludes the outer envelope that is the defining characteristic of cD galaxies (Matthews et al. 1964). Henceforth in this Chapter, the sampling radius will be assumed to be as above, and the subscript $\gamma$ will be dropped from $\alpha$ and the metric absolute magnitude (measured through an aperture of metric size $\gamma$), $M_V$.

Algebraically, it is trivial to show that $\alpha$ is equivalent to twice the ratio of the mean surface brightness at $\gamma$ to the mean surface brightness interior to $\gamma$:

$$\alpha = \frac{\text{Mean Surface Brightness at } \gamma}{\text{Mean Surface Brightness within } \gamma} \times 2 \qquad (7.2)$$

Alpha is clearly related to the characteristic scale length of the galaxy, and may be computed as a function of this length for any of the well-known surface brightness distribution laws. In Figure 7.1, $\alpha$ as a function of the de Vaucouleurs effective radius $r_e$ is shown, together with the magnitude difference between the 'total' absolute magnitude and the metric magnitude $M_V$. It is clear from Figure 7.1 that for $\alpha$ less than 0.25, $\alpha$ varies at least approximately linearly with log $r_e$.

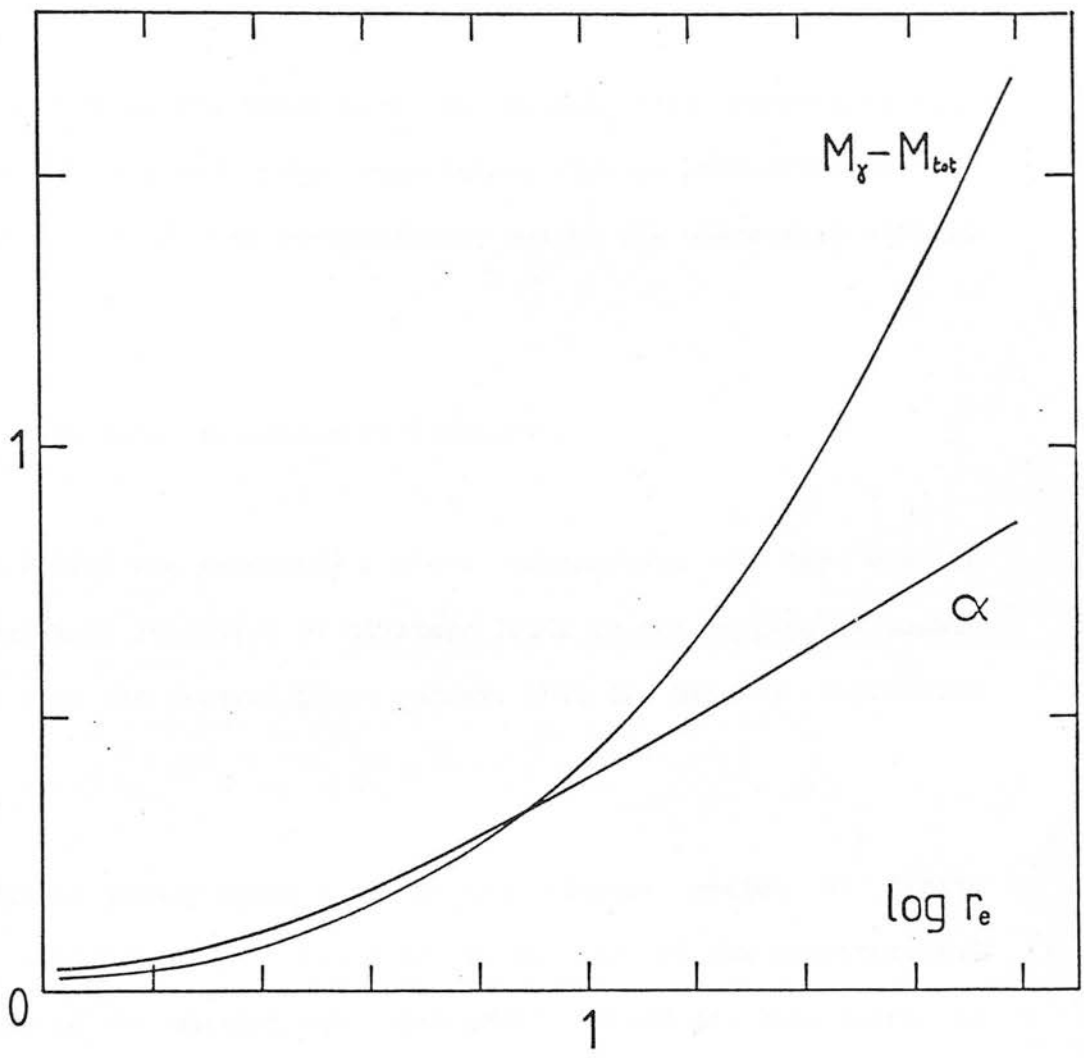


Figure 7.1: The variation of $\alpha_\gamma$ and $M_\gamma - M_{tot}$ as a function of the de Vaucouleurs effective radius $r_e$.

7.1.b Theoretical Models

Due in part to its importance in cosmological investigations, there has been considerable theoretical work on predictions of the merger rate in different environments, and of the observable effects of each merger.

7.1.b'The Dynamical Evolution of Clusters

Gunn (1978) has presented a clear explanation of the way in which dynamical evolution of clusters leads to the merging of member galaxies with the central giant galaxy. This is briefly reproduced here.

A cluster galaxy moving through the cluster medium of finite density experiences a retarding force due to the gravitational attraction of the massive wake that trails behind it. This force is known as dynamical friction, and the deceleration suffered by a galaxy of mass m, moving with speed v through a medium of density $\rho$ is given (Gunn 1978) by (within approximate numerical factors):

$$\frac{dv}{dt} = \frac{8\pi\ G^2\ m\ \rho}{v^2} \qquad (7.3)$$

Depending on the precise assumptions that are made about the distribution of mass in the cluster, the circular velocity v may be found. In the particular case of a galaxy moving outside of the core of an isothermal cluster, the density will be given by:

$$\rho = \rho_0 r^{-2} \tag{7.4}$$

In this case the enclosd mass will be proportional to the radius and hence the circular velocity will be constant. The loss of energy, given by vdvdt, will appear as a loss of potential energy as the galaxy spirals in to the centre of the cluster.

$$v \frac{dv}{dt} = \frac{8\pi G^2 m \rho}{v} = \frac{dr}{dt} \cdot \frac{v^2}{r} \tag{7.5}$$

But since $8\pi G\rho r^2 = v^2$, it follows that

$$r \frac{dr}{dt} = \frac{G m}{v} \tag{7.6}$$

Hence, after a time t, all galaxies of mass m that were initially within a critical radius $r_c(m,t)$, will have reached the centre of the cluster, where $r_c$ is given by:

$$r_c = \left[\frac{2Gm}{v}\right]^{\frac{1}{2}} \cdot t^{\frac{1}{2}} \tag{7.7}$$

Note that the more massive satellite galaxies are preferentially moved to the centre of the cluster. This is because they experience more dynamical drag. The total mass consumed is proportional to the critical radius for this particular density distribution, and so the mass of the giant will grow as $t^{\frac{1}{2}}$ .

For the density distribution that is appropriate to the central regions of a cluster (and hence to the early evolution) the dependence of the total mass of the cannibal on t actually increases

to the first power (Hausman and Ostriker 1978), and more massive galaxies are also more preferentially consumed, the dependence again increasing to the first power.

### 7.1.b Individual Mergers of Galaxies

When the cluster galaxy eventually spirals into the centre of the cluster, it will merge with the galaxy that is already located there. The form of the remnant that remains after these two have merged together is difficult to predict. If, however, it is assumed that the merger is homologous, i.e. that the form of the remnant is the same as that of the two constituent galaxies, then very simple relations will hold between the properties of the galaxies. This assumption of homology can be criticised on several grounds (see e.g. White 1978). On the other hand, the fact that the surface brightness profiles of elliptical galaxies which span a wide range of luminosity can all be fitted by simple two-component models (e.g. the Hubble or de Vaucouleurs profiles) lends support to this assumption of homology, if some of them are indeed formed from mergers of other galaxies.

For galaxies having surface brightness distributions that are fitted by two-parameter models that may be described by a total luminosity (or mass, m) and a characteristic radius, r, the binding energies of the systems will be proportional to $m^2 r^{-1}$. Similarly the specific binding energies will be proportional to $m\, r^{-1}$. Since low mass galaxies are very weakly bound, it follows that in a merger between two galaxies of very unequal mass, the total binding energy of the remnant will be equal to that of the more massive progenitor.

In contrast, if both galaxies are of similar mass, then it is the specific binding energy which will be the same after the merger.

Hence, if the mass and characteristic radius of the galaxies are related as $r \propto m^k$, then an unequal merger will result in k=2, while a merger between galaxies of comparable mass will yield k=1. For a given increase in the total mass (or luminosity), the characteristic size will increase more in the k=2 case, as the remnant expands to accomodate the extra mass without increasing its total binding energy. These two different scenarios, involving mergers between galaxies of similar and dissimilar masses, will therefore lead to different predicted evolutionary tracks on any diagram that relates the two photometric parametres of luminosity and size (Gunn & Tinsley 1976).

7.1.c Previous Observational Work

Hoessel (1980) presented surface photometry of a large sample of 104 Abell cluster 1st ranked galaxies. Hoessel parameterized the observed surface brightness distributions of these galaxies by fitting a modified Hubble profile. From the parameters of this fit $\alpha$ and $M_v$ were deduced. From an analysis of these two quantities for the galaxies in his sample Hoessel found a number of relations which provide support for the hypothesis that the merging process caused by dynamical friction strongly affects the structure and luminosity of the 1st ranked Abell cluster galaxies.

Before describing these, however, it is important to note that the best and most direct evidence in favour of the merging hypothesis comes from his observation that 28% of the galaxies have

multiple nuclei (see also Schneider et al 1982). It is difficult to envisage mechanisms for creating these except through their being the surviving dense cores of merged galaxies.

The first result that Hoessel found was that the diagram of $(M,\alpha)$ (Hoessel's Figure 8, and reproduced here as part of Figure 7.5) shows a clear relationship between $M_v$ and $\alpha$ in the sense that the galaxies with higher $\alpha$ generally have higher metric luminosities. If total luminosities were considered, the effect would be even stronger since the galaxies with high $\alpha$ will have large differences between total and metric magnitudes. The application of an $\alpha$-correction, based on the mean relation, reduces the cosmic scatter in the absolute magnitudes of these galaxies from 0.4 to about 0.25 magnitudes. When the data is binned in $\alpha$, the mean absolute magnitude as a function of $\alpha$ follows well the relation that is predicted for the k=1 case homologous mergers. Recall that this is the case appropriate to the merging of galaxies of comparable mass. Note, however, that the 'best fit' in Hoessel's Figure 9 would in fact have k rather larger than unity, although still smaller than two. This may be important for the following reason: Figure 17 of Hoessel (1980) shows that the Abell galaxies follow the Kormendy (1977) relation between core radius and central surface brightness found in elliptical galaxies in the Virgo cluster. Since all these galaxies are assumed to be representable by Hubble profiles the galaxies in Hoessel's Figures 8 and 9 must also follow the equivalent relation between $M_v$ and $\alpha$ derivable from the Kormendy relation between $B_e$ and $r_e$. Indeed, the Kormendy relation is equivalent to the case k=1.45, and it is clear from his Figure 9 that such a value of k would be an acceptable fit to the data. The

relation between $M_V$ and $\alpha$ appropriate to the Kormendy relation has been derived and is plotted on Figure 7.5. Hoessel's interpretation of his Figure 17 was that it possibly indicated that all ellipticals might be formed from mergers of smaller units. However, there are reasons (Kormendy 1982) for believing that not all ellipticals do form by mergers, and the continuation of structural properties between 'normal' ellipticals and the 1st ranked cluster galaxies could be caused by the, as yet unknown, process that causes low luminosity ellipticals to have k=1.45.

Secondly, Hoessel demonstrates relations between o and the Bautz-Morgan (Bautz and Morgan 1970) Classes and Richness Classes of the clusters that are in the sense predicted by the theoretical models described above, since the merging rate will be higher in richer, denser systems.

Finally, Hoessel deduced, from comparisons of the mean $\alpha$ and $M_V$ of those galaxies with, and without, multiple nuclei, that the typical change in $M_V$ and $\alpha$ caused by the accretion of a single galaxy was approximately 0.12 magnitudes and 0.05 respectively. He therefore deduced that about four mergers had occurred in a typical member of the sample, since $M_V$ and $\alpha$ had evidently increased by about 0.5 magnitudes and 0.2 respectively from the 'primordial' galaxies that had $\alpha$ around 0.3. He pointed out that this number of mergers is consistent with the, admittedly rather uncertain, theoretically predicted merging rate of $10^{-9}$ $yr^{-1}$ and the time interval of around $5.10^9$ yr since cluster collapse. He also noted that the fraction of galaxies displaying multiple nuclei was consistent with this merging rate and the expected duration of each

merging event of approximately 2.5 $10^8$ yr.

In view of these facts, it appears that $\alpha$ probably does measure in some statistical way, at least in these galaxies, the number of mergers that have taken place. However, particularly in view of the doubts about the applicability of the assumption of homology during the merging process, this interpretation should still be treated with some caution.

Schneider et al (1983b) have extended this work to include a further 84 Abell clusters. The new sample extended to redshifts of 0.3, and included several systems that are much richer than those which are found in the Hoessel (1980) sample. Although there are some detailed differences in the conclusions as a consequence of the different samples and slightly different methods of analysis employed, the conclusions of Schneider et al (1983b) were essentially similar to those of Hoessel (1980).

Thuan and Romanishin (1981, TR) presented photographic surface photometry for nine cD 1st ranked cluster galaxies in the poor clusters of Morgan et al (1975,MKW) and Albert et al (1977, AMW). TR presented three basic results. These were firstly that these galaxies had large de Vaucouleurs effective radii. They must therefore from Figure 7.1, have large values of $\alpha$. Secondly, they showed that these galaxies did not have extended envelopes, the occurence of which they showed to be related to the total luminosity of the cluster. Hence these galaxies were not, after all, genuine cD galaxies. Finally they showed that the poor cluster galaxies had luminosities that were considerably higher than would be predicted

from fitting a Schecter (1976) luminosity function to the distribution of the luminosities of the other cluster members. This effect was larger than the similar one found in Abell clusters. These results were all interpreted as indicating that the central galaxies in these poor clusters had actually consumed rather more of their neighbours than those in the richer, Abell, systems. A higher merging rate in these systems is indeed predicted by equation 7.7, because these poor clusters have a lower velocity dispersion (and hence circular velocity). The low velocity dispersion results in a high central density of galaxies, even if the total number of galaxies in the cluster is smaller than in the Abell clusters.

One criticism should be made of this work however, and although it does not alter their basic conclusions, it does illustrate an important point. It is correctly claimed by TR that these galaxies may be represented by a de Vaucouleurs surface brighness distribution. Hence only two independent photometric parameters may be found for the profile of each galaxy. Any others must be a combination of these two. Hence TR's Figures 10 and 12 must convey the same astronomical information. The fact that the cluster galaxies appear to lie on the relation labelled 'ellipticals' in Figure 10 but lie well away from the 'ellipticals' relation in Figure 12 (they are displaced by about 1.5 magnitudes) must indicate that the two 'ellipticals' relations, the one from Kormendy (1977) and the other derived from the work of Strom and Strom (1978), must be inconsistent. It is easy to show that they are, and the apparent difference between Figures 10 and 12 cannot be, as TR claimed, significant.

7.1.d Motivation for the Investigation of $\alpha$ for 3C Radio galaxies

In this chapter, the initial results of a project to measure the $\alpha$ parameter for a sample of giant ellipticals associated with 3CR radio sources at moderate redshift (less than 0.3) are presented. There are several motivations for such a study.

Firstly, it is of interest to examine the relationship between the structures of the powerful radio galaxies and of other giant elliptical galaxies, and in particular with those found at the centres of rich Abell-type clusters and the poorer clusters found by AMW and MKW. This is important not only because of the light it may shed on the general active galaxy phenomenon, but also because several recent studies in to the evolution of galaxies and cosmology generally, have used samples of galaxies composed of Abell cluster galaxies at low redshift and 3CR galaxies at high redshift (where they are the only galaxies known). This has been done on the assumption that they are essentially the same type of galaxy with similar evolutionary histories. Earlier qualitative studies on the nature of 3CR radio galaxies, (e.g. Matthews et al (1964) concentrated on those with redshifts generally less than 0.1. These are somewhat less luminous in the radio wavebands than those studied at high redshift.

Secondly, if $\alpha$ can be taken as a crude indicator of the degree of dynamical evolution that has taken place, then it is of interest to assess the importance of this evolutionary process for two reasons. The first is that this information may suggest whether it

is likely that the radio source is indeed fuelled from the debris of merging galaxies, and it may thus provide clues as to the nature of the link between the cosmological evolution of the radio source population and the evolution of the host galaxy. The second is that this information is required in order to interpret the (K,z) infrared Hubble relation presented in Chapter 3 in terms of the combination of both various evolutionary effects and the cosmological geometry.

Thirdly, a study of the range of growth curves exhibited by these radio galaxies is required to produce the corrections that must be applied to aperture photometry (see Chapter 3) both to derive the optical to infrared colours such as (V-K) and to produce metric magnitudes required in the analysis of the Hubble diagram.

Finally, when this investigation is extended to a larger sample of radio galaxies in the southern hemisphere, where quantitative information is available on the cluster environments of the radio galaxies, it will be of interset to examine the (M,$\alpha$) relation in a sample of giant elliptical galaxies that have been selected without direct regard to their cluster environment. This will be in contrast to the investigations in to the 1st ranked cluster galaxies in Abell and poor MKW and AMW clusters described above.

### 7.1.e A sample of ten 3CR Radio Galaxies

Ten 3CR radio galaxies have been observed with the aim of measuring $\alpha$. These were selected from the complete sample of 3CR radio galaxies described in Chapter 3. All the galaxies have

redshifts less than 0.3, and were chosen to have Fanaroff-Riley class II structure (Fanaroff and Riley 1974), i.e. to be classical double radio sources. No Broad Line Radio Galaxies (BLRG) were observed since these have prominent optical nuclei, being generally associated with N-type morphology.

Althogh not a complete sample in a statistical sense, the sample was nevertheless randomly selected within the constraints described above, and should be representative of the population.

The ten radio galaxies are listed in Table 7.1 (p. 301 ). Their radio structures have a range of physical size from $48\bar{h}^{1}$kpc (3C 277.3) to $5.7\bar{h}^{1}$ Mpc (the giant source 3C 236), but they are typically a few hundred kpc in extent. They are evenly distributed in the 'quality of double', defined by Longair and Riley (1979), having approximately equal numbers of 'good', 'doubtful', and 'one-sided hotspot' sources.

## 7.2 : Data Acquisition, Reduction and Analysis

### 7.2.a Observations

Surface photometry for all these radio galaxies was obtained using the Royal Observatory Edinburgh Imaging Spectropolarimeter (ISP) system (McLean et al.1981). Except for 3C 33, which was observed by Dr. McLean with the University of Arizona 1.54 metre telescope in November 1981, the data for the galaxies was obtained with the instrument mounted on the 3.8 metre United Kingdom Infrared Telescope (UKIRT) on Mauna Kea during April 1982. These latter

observations were made in conditions of reasonably good seeing, but of generally poor and varying atmospheric transparency.

The ISP camera is a versatile instrument that may be used in a variety of modes. The CCD detector used was a thinned backside illuminated RCA device with 30 micron square pixels in a 512 by 320 array format. Readout noise was approximately 70 electrons rms per pixel. In the direct imaging mode, only the central 256 by 256 area of the chip is read out, and in fact within this area only that region within a circular aperture of diameter approximately 180 pixels is illuminated. This limitation is due to the fact that the camera optics are designed around some components associated with the polarimetric and spectrographic modes which are of neccessity rather small. The UAO 1.54 metre and UKIRT gave plate scales of 0.75 and 0.49 arcsec per pixel respectively. Hence the UKIRT data had a circular field of view of only about 90 arcsec. The chief drawback of this when doing surface photometry of galaxies is the relatively small area available to determine the sky background around the nearest galaxies.

Most of the exposures were taken through a red interference filter with half peak transmission at 7200 and 7980 A. The seeing, defined as the FWHM of a gaussian fitted to the stellar profiles, varied slightly between exposures, but was less than 1.5 arcsec for all the exposures except that for 3C 219, for which it was 1.7 arcsec. The exposure times varied between 5 minutes and 15 minutes depending on the apparent magnitude of the galaxies and the atmospheric conditions that were prevalent at the time of observation.

7.2.b Reduction of the CCD data

The raw CCD exposures were reduced in the following way. First, the effect of the electronic bias offset was removed. The value of this offset was determined by finding the median pixel value in numerous zero exposure readout frames obtained regularly throughout the observing period. The median was chosen to avoid the degradation of the signal to noise ratio in the astronomical image that would have occurred had the whole bias frame been subtracted, pixel by pixel, and to avoid the effects of two defects in the system. Firstly, every 16 rows, or 4096 pixels, there was an interruption in the readout process while the data was written to disk, after which the application of the (negative) bias was intermittent for a few hundred pixels. Secondly, the analogue to digital converter did not function correctly close to zero and in fact set all pixel values between -3 and +3 to zero. The first problem was also present, of course, in the astronomical exposures, but the second was not, because the exposed sky level was in all cases considerably greater than zero. In addition to this bias offset level, a dark current signal appropriate to the length of integration was also subtracted. This was not large and was derived from long integrations at the start of each night's work with the camera shutter closed. The resulting image was divided by a normalised flat-field exposure (similarly bias subtracted). This was obtained from observations of the twilight sky. Finally the exposure was normalised to a standard exposure time of one minute.

Figure 7.2 shows the CCD image of 3C 223, a typical galaxy in

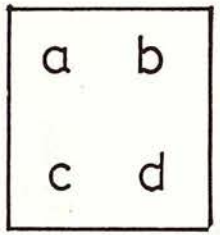


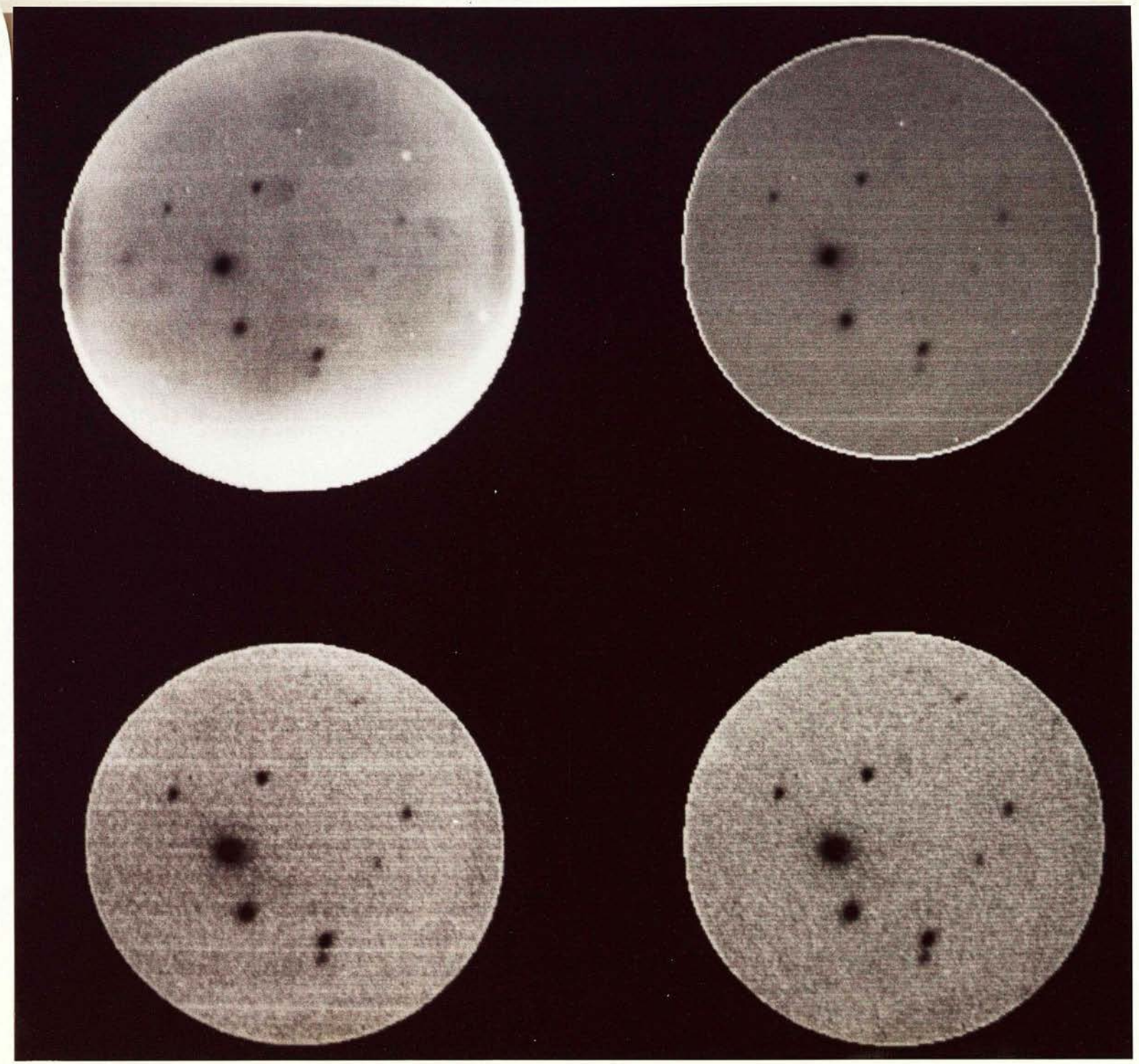

Figure 7.2: Stages in the reduction of the CCD images for 3C 223 (z = 0.137): (a) The raw exposure; (b) After flat-fielding; (c) As (b) but with increased contrast; (d) After the removal of columnar sensitivity variations. (a) and (b), and (c) and (d) are set at the same greyscale. All the images have been rotated to have North at the top.

the sample at a redshift of 0.137, at various stages in the reduction process. The upper left image shows the raw data, and the upper right image shows the effect of applying the flat field correction.

After these standard operations had been carried out two further cosmetic defects were removed as follows. The first was a form of non-linearity in the response of the RCA CCD chip which resulted in certain columns of the device being systematically less sensitive as a function of exposure. These were not completely removed by the flat-fielding process because the flat-field exposures were generally of a higher background level in order to maximise the signal to noise ratio of the flat field correction. In Figure 7.2, this effect can be seen as horizontal streaks (the images have been rotated so that north is at the top) on the top right image, and the one in the bottom left, which is the same image with an expanded grey scale. Even the worst columns, clearly visible in the images, were affected at only the 1-2% level, although virtually every column was affected to a certain degree. It was found that a single multiplicative correction applied to all the pixels of each affected column was sufficient to remove this defect, and an iterative algorithm was developed to find and apply this correction. By traversing the CCD image in a direction parallel to the defects, the background sky level was determined by iteratively rejecting both astronomical images and other defects such as cosmic ray events, whose pixel values lay more than 2 standard deviations from the mean. This process was continued until on average only one pixel per column had been rejected on each pass. The mean value of the remaining pixels in each column was calculated, and a correction

applied to each column so that the means became constant across the image. While all such image processing must be regarded as undesirable, the degradation in information is formally small since only one correction is applied to all the pixels in each column. The effectiveness of this procedure, however, can be judged by comparing the two lower images in Figure 7.2.

When this correction had been applied, a further defect was apparent on those images with short exposure times or dark sky backgrounds. This was caused by the intermittent application of the bias offset described above. This was at a very low level because the bias level was so much smaller than the sky background in most images, and the effect of it was removed by the reapplication of the algorithm described above, with the difference that the correction applied was additive rather than multiplicative. The application of these processes resulted in extremely clean images.

### 7.2.c Derivation of the Alpha Parameter

The derivation of the alpha parameter itself was carried out in the following way. The center of the galactic image was found by fitting a gaussian profile to the central regions of the galaxy. Stars, other fainter galaxies and the effects of cosmic ray events were then removed from around the image of the radio galaxy. These were identified interactively. If the object lay more than $2\gamma$ from the centre of the radio galaxy, the pixel values were replaced by a sky value (produced from the defect removal routines described above) with the addition of a gaussian noise component of appropriate amplitude. If the object to be removed lay closer than

this limit, the pixel values were replaced by those found by a 180° rotation about the centre of the radio galaxy, interpolating where neccessary. An improved value of the mean sky background was found by constructing the histogram of pixel values in the anulus of inner and outer radii $2\gamma$ and $4\gamma$ centred on the nucleus of the radio galaxy. A gaussian curve was fitted to the top of the histogram to determine the best sky value. This is shown in the case of 3C 223 in Figure 7.3a. This procedure was adopted in order to apply the same method to all galaxies, irrespective of their redshift, and hence of their apparent size and brightness on the sky. Any contamination in this sky value from the outer regions of the galaxy itself should be the same for any given galaxy profile irrespective of distance. The sky at such large radii (about 60 $h^{-1}$ kpc at the galaxy) may still be slightly contaminated by the outermost parts of the galaxy, but the size of the effect on $\alpha$ should be small. A de Vaucouleurs $r^{\frac{1}{4}}$ surface brightness distribution has a surface brightness at $3\gamma$ that is a factor of 20 down on that at $\gamma$, while 60 kpc is in any case close to the cutoff radius. A contamination in the sky level equivalent to 5% of the galactic surface density at $\gamma$ leads to a 5% (i.e. only about 0.02) error in $\alpha$, in the sense that the measured value is too low. It was decided not to attempt to correct for any error introduced in this way. This 'accurate' sky level was subtracted from every pixel in the image.

An empirical growth curve of integrated enclosed luminosity as a function of radius was constructed by plotting the cumulative flux density progressing outwards from the centre. The effects of digitization are obviously important in the first few pixels, but are negligible at $\gamma$, which was typically at about 10 pixels radius.

This empirical curve was extended to $2\gamma$, and a sixth order polynmomial was fitted to the curve for radii smaller than $1.5\ \gamma$. This fitting was done to smooth out small variations in the growth curve due to noise in each individual pixel, and to parameterize the empirical growth curve to aid in the analytical calculation of alpha and of the upper and lower bounds to alpha that are introduced by uncertainty in the sky background level.

This growth curve is shown for 3C 223 in Figure 7.3b. The solid line represents the polynomial fit to the growth curve, while the dashed lines show the effects of the uncertainty in the sky value. This approach is slightly different from that taken by Hoessel (1980) who derived $\alpha$ from the parameters of a fitted Hubble surface brightness law. The 6th order polynomial is essentially a free form fit.

As a check on this growth curve, the three polymonials were plotted in the form of a surface brightness in magnitudes against the radius to the one quarter power. A de Vaucouleurs $r^{\frac{1}{4}}$ distribution would be a straight line on such a plot, although the radius used here is a circular radius and not an effective radius (defined as the geometric mean of the semi-major and semi-minor axes at a given isophote). Figure 7.3.c shows this diagram for 3C 223. The galaxy is clearly well represented by the de Vaucouleurs distribution, and there is no evidence of an error in the sky background level that would be made apparent by a sudden steepening or lessening of the slope at large radii.

Finally, the observed value of $\alpha$ was determined from the

Figure 7.3a-d:
Stages in deriving $\alpha$ for 3C 223 (z=0.14).

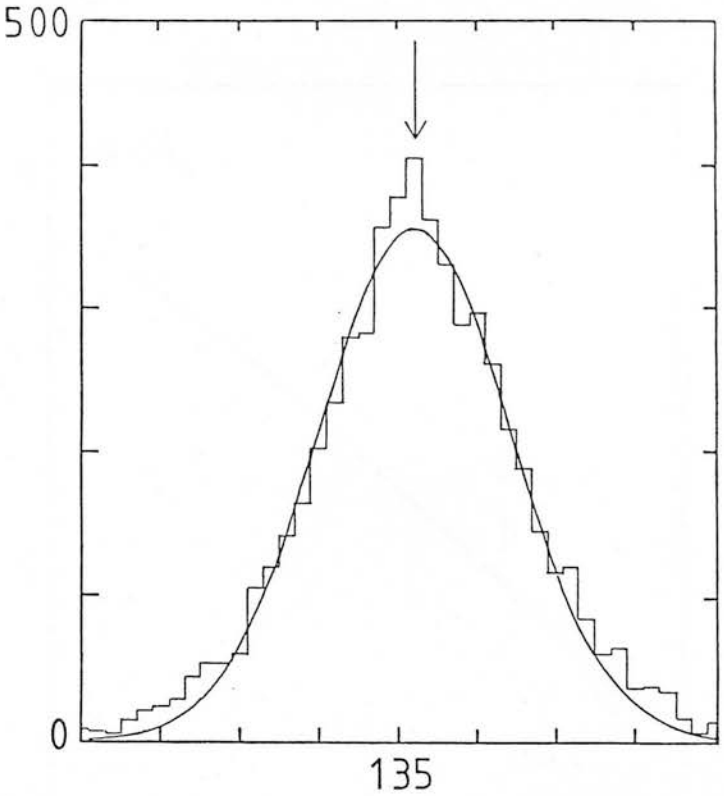


(a) The histogram of pixel values found in an anulus of inner and outer radii $2\gamma$ and $4\gamma$ is fitted by a gaussian curve, and an accurate sky value is found (arrow).

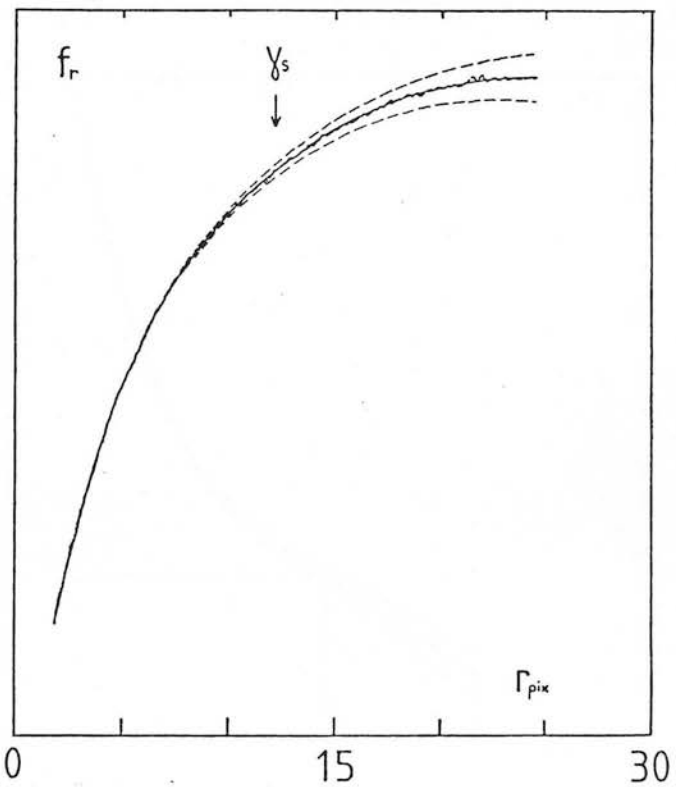


(b) The cumulative growth curve of enclosed luminosity is plotted and then fitted by a sixth order polynomial in r (solid line). The two dashed curves are derived by taking extreme values for the sky background.

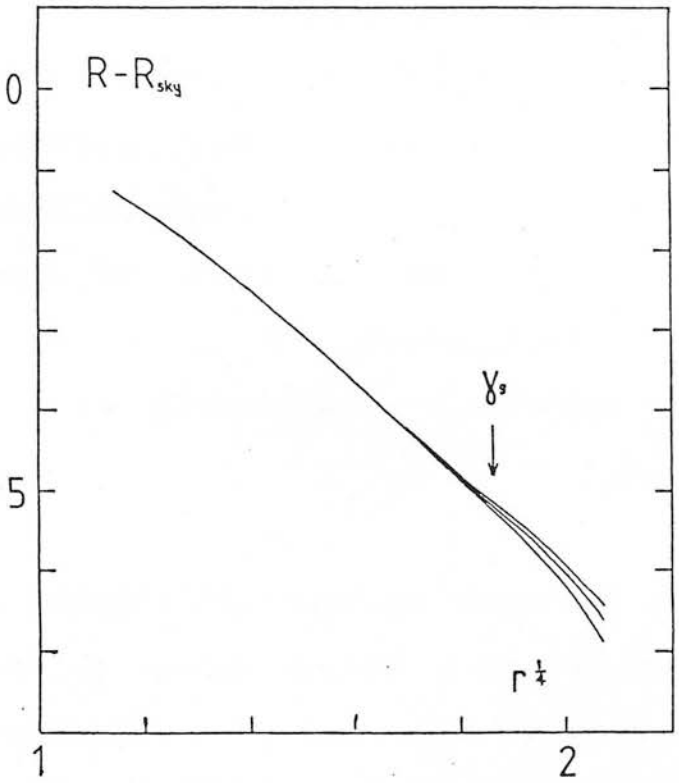


(c) The surface brightness profiles that are derived from the three polynomials are plotted in the form of magnitudes against the $r^{\frac{1}{4}}$. The de Vauscouleurs profile is a straight line on such a diagram.

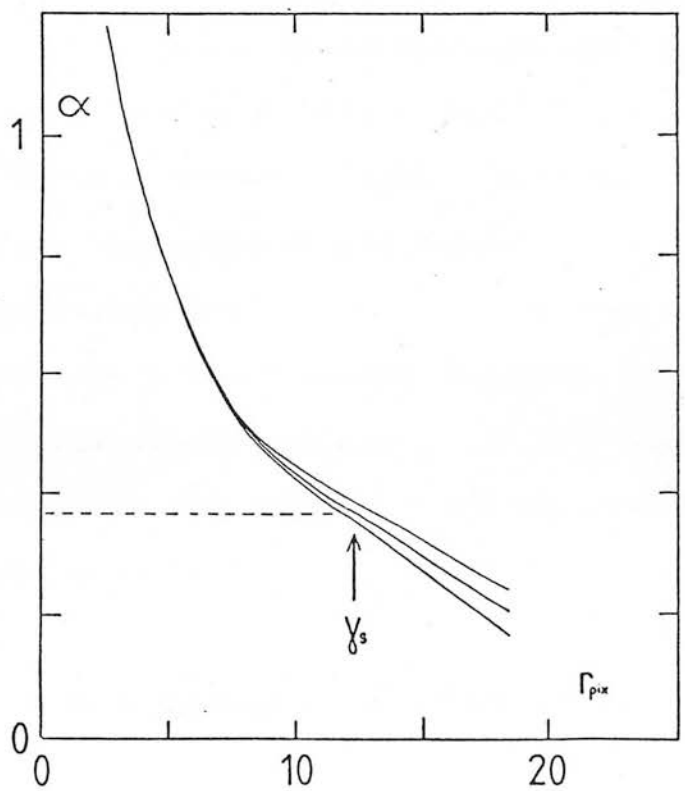


(d) $\alpha(r)$ and hence $\alpha_\gamma$ are computed for each of the three polynomials.

polynomial using the definition together with upper and lower bounds corresponding to the appropriate limits to the sky background. While the value of $\alpha$ at the sampling radius $\gamma$ is of most interest, $\alpha$ may be calculated at all radii. The variation of $\alpha$ with sampling radius for 3C 223 is shown in Figure 7.3.d. The observed limits on $\alpha$, determined at $\gamma$ are listed for all the galaxies in the third column of Table 7.1.

A correction must be applied to the observed values of $\alpha$ to account for the effects of seeing. Because $\alpha$ is essentially a measure of the surface brightness at a relatively large radius, typically around five arcsec, the effect of seeing is not as critical as when one is attempting to measure nuclear parameters such as the core radius. In order to assess the effects of seeing a number of simulations were carried out. These involved constructing model galaxies with different de Vaucouleurs characteristic radii (and hence different intrinsic values of $\alpha$) and degrading them with gaussian seeing profiles of different widths relative to the characteristic radii of the model galaxies. Figure 7.4 shows the results of these simulations. It is evident that provided the seeing standard deviation is smaller than about 0.2 $\gamma$ , the corrections to $\alpha$ are small and can therefore be safely applied. The ratio $\sigma/\gamma$ was less than 0.2 for even the most distant galaxies, and the seeing correction was in all cases less than 0.025. $\sigma/\gamma$ and the corrected ranges for alpha are listed in Table 7.1.

Absolute magnitudes in the V passband are available for the six nearest radio galaxies and were derived from the fully corrected V photometric data of Sandage (1972) since the present CCD data for

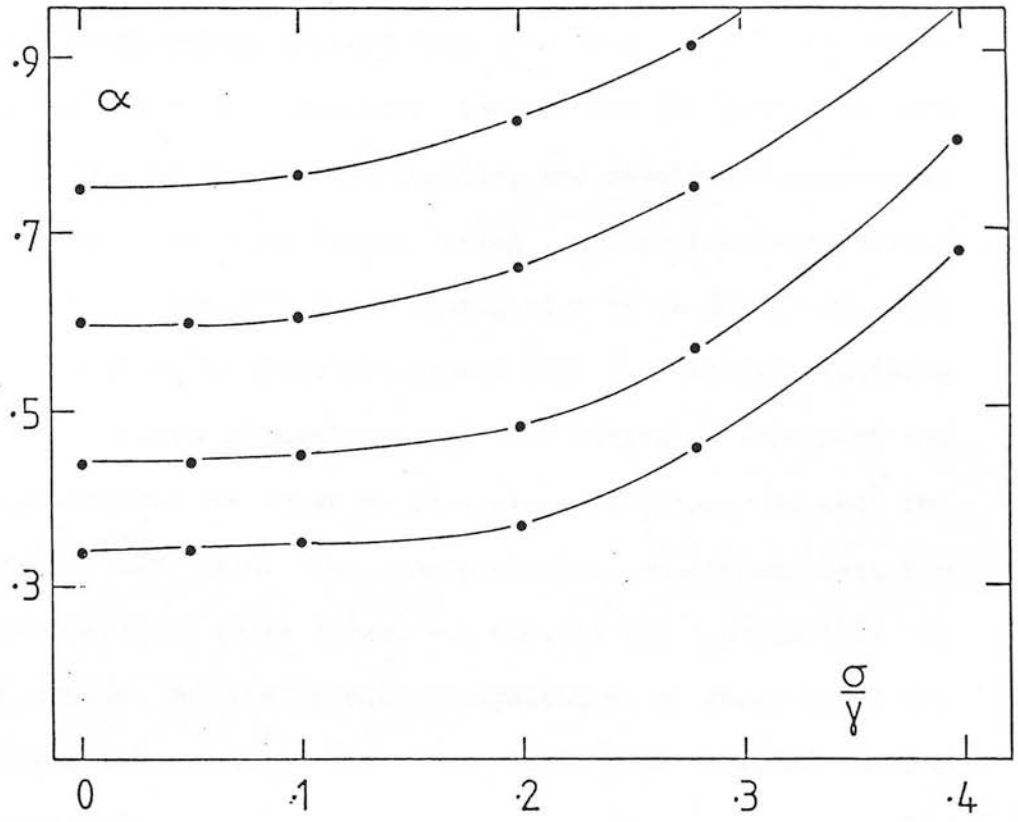


Figure 7.4: The effect of atmospheric seeing on the observed value of $\alpha$. The four curves represent model galaxies with different effective radii $r_e$ and hence different intrinsic $\alpha$ (given by the intersection on the left hand axis). The values of $\alpha$ that would be observed in conditions of seeing $\sigma$ have been computed for several ratios of the seeing width to the sampling radius $\gamma$. $\sigma/\gamma$ was less than 0.2 for the images of all the radio galaxies discussed in this Chapter.

these objects were not obtained in photometric conditions. A small correction was applied to these magnitudes so that they were appropriate to a $q_0 = 0.5$ cosmology, and an aperture correction, based on the growth curves derived from the CCD data, was applied to produce $M_V$. For two of the remainder, (3C 284 and 3C 349) the CCD data were in fact of photometric quality, and absolute V magnitudes have been derived from these images using the photometric system described in connection with the investigation in to 3C 352 (Chapter 4). The uncertainties in these are around 15%. For the two remaining galaxies, an absolute V magnitude has been estimated from both the 2.2 micron photometry for these objects given in Chapter 3, and the 'unphotometric' CCD data. The uncertainties in these last two galaxies are therefore quite large, but none of the conclusions of this work depend on the precise magnitudes of these final two galaxies. The final column in Table 7.1 lists the adopted metric absolute magnitudes.

In order to ensure consistency with the large data set of Hoessel (1980) an exposure of the central cD in Abell 104 was taken with the UAO 1.54 metre telescope in November 1981. This exposure was reduced in an identical manner to those of the radio galaxies. The corrected value of $\alpha$ was $0.71 \pm 0.01$, in good agreement with Hoessel's $0.70 \pm 0.03$.

Table 7.1: The $\alpha$ parameter for 10 3C Radio Galaxies.

| 3CR | z | $\alpha_{obs}$ | $\sigma/\gamma$ | $\alpha_o$ | $M_{v\gamma}$ |
|---|---|---|---|---|---|
| 33 | 0.060 | 0.32 ± 0.02 | 0.07 | 0.31 ± 0.02 | -22.58 |
| 285 | 0.079 | 0.34 ± 0.02 | 0.07 | 0.33 ± 0.02 | -22.45 |
| 277.3 | 0.086 | 0.39 ± 0.01 | 0.08 | 0.38 ± 0.01 | -22.63 |
| 236 | 0.099 | 0.49 ± 0.02 | 0.09 | 0.48 ± 0.02 | -22.88 |
| 223 | 0.137 | 0.37 ± 0.02 | 0.11 | 0.36 ± 0.02 | -22.65 |
| 219 | 0.174 | 0.43 ± 0.02 | 0.16 | 0.41 ± 0.02 | -23.05 |
| 319 | 0.192 | 0.19 ± 0.08 | 0.13 | 0.18 ± 0.08 | -22.15 |
| 349 | 0.205 | 0.37 ± 0.05 | 0.17 | 0.35 ± 0.05 | -22.05 |
| 284 | 0.239 | 0.48 ± 0.03 | 0.15 | 0.46 ± 0.03 | -22.95 |
| 300 | 0.270 | 0.24 ± 0.07 | 0.17 | 0.22 ± 0.07 | -22.07 |

## 7.3 : Results and Discussion

Figure 7.5 shows the location of the ten 3C radio galaxies on the $(M,\alpha)$ diagram. Also shown are the 108 Abell cluster 1st ranked galaxies from Hoessel (1980), plotted as open circles, the 84 Abell 1st ranked cluster galaxies from the richer cluster sample of Schneider *et al* (1983b), plotted as open squares, and the nine 1st ranked galaxies from the poor clusters of Morgan *et al* (1975, MKW) and Albert *et al* (1977, AMW) studied by Thuan and Romanishin (1981). The parameters for the Schneider *et al* galaxies have been derived from the values of the Reduced Absolute Magnitude (RAM) and log $r_e$ given by them, while those for the poor MKW and AMW clusters were derived from the total absolute magnitudes and r given by Thuan and Romanishin (1981). The solid line (shown as K77) represents the relation between M and $\alpha$ produced by the relation between $B_e$ and $r_e$ found by Kormendy (1977). His data scattered about 0.6 magnitudes above and below this line. The dashed line (labelled k=1) indicates the predicted evolutionary track for homologous mergers between galaxies of comparable mass.

Two things are evident from Figure 7.5. Firstly, all of the radio galaxies lie within the range of $(M,\alpha)$ combinations occupied by the normal elliptical galaxies observed by Kormendy (1977). Certainly in the seven brighter examples, the radio galaxies have values of M and $\alpha$ similar to those found in some Abell cluster galaxies. This implies that the radio galaxies do not have unusual surface brightness distributions. Since the colours of these NLRGs are also not anomalous in most cases (see the discussion in Chapter

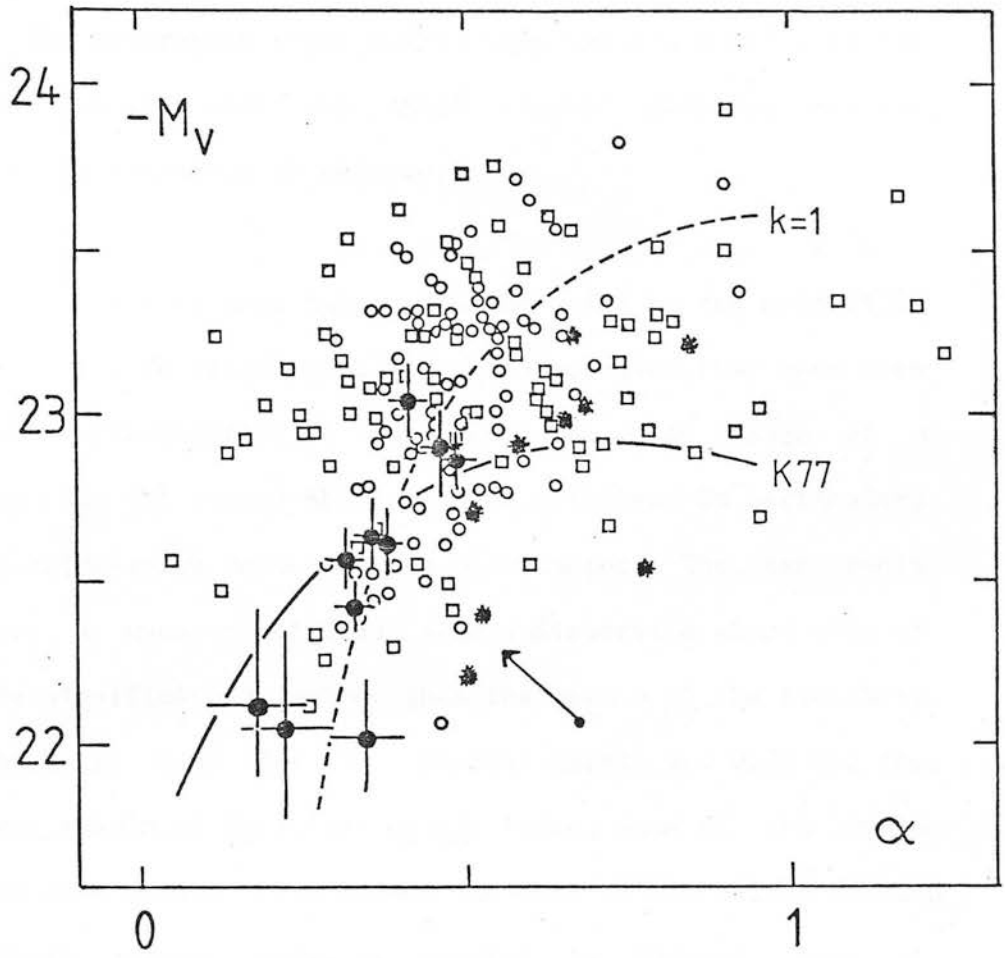


Figure 7.5: The ($M_V$,α) diagram. Data plotted are as follows: 1st ranked Abell cluster galaxies from Hoessel (open circles); (b) 1st ranked Abell cluster galaxies from Schneider et al (1983b) (open squares); cD galaxies from poor AMW and MKW clusters from Thuan and Romanishin (stars); Ten 3C radio galaxies (this study) (solid circles with error bars). The curve labelled k=1 represents the predicted evolutionary track for homologous mergers of galaxies of comparable mass, normalised as in Hoessel (1980). The curve labelled K77 is the relation between $M_V$ and α that is derived from the relation between $B_e$ and $r_e$ given by Kormendy (1977). The arrow shows the effect of adding an unresolved nuclear flux component that contributes 20% of the total light within γ to an otherwise normal galaxy.

3) it can be said that in the majority of cases one cannot distinguish photometrically at this level between giant ellipticals that do and do not have powerful double radio sources associated with them. The apparently tight correlation between M and $\alpha$ in the radio galaxies compared with the Abell cluster galaxies may be caused by the small numbers of objects.

The second result is more interesting and will be the subject of the remainder of this discussion. The radio galaxies that have been studied in this investigation do not span the wide range of $\alpha$ exhibited by the 1st ranked Abell cluster galaxies. In particular, they have relatively low values of the $\alpha$ parameter. The ten radio galaxies have a mean $\alpha$ of 0.35, with a dispersion about this of 0.08. This is significantly smaller than the mean $\alpha$ of the two Abell samples, which is 0.49 for the Hoessel sample and 0.70 for the richer cluster sample of Schneider et al. Indeed none of the radio galaxies has an $\alpha$ greater than either the mean or the median (0.48) of the 104 Abell cluster galaxies studied by Hoessel. Even if attention is restricted to those in the Hoessel sample with Richness class 0 or Bautz-Morgan Class III, the mean $\alpha$ are still significantly larger (0.41 and 0.47 respectively) than those of the radio galaxies.

Furthermore, the radio galaxies lie in a completely different part of the diagram to the 'poor' clusters of Thuan and Romanishin (1981).

These 3CR radio galaxies are clearly host to an active nucleus of some sort, and in this context it is important to note the effect

of the addition of an unresolved nuclear component onto an otherwise normal galaxy. In view of the definition of $\alpha$ in terms of the ratio of surface brightnesses, it is clear that the addition of, say, a 20% nuclear component in the R waveband, will decrease $\alpha$ by about 20% (around 0.08) while increasing the absolute magnitude in the V passband by about 0.2 magnitudes, depending on the precise relative spectral indices of the nuclear and galactic components. This vector is shown in Figure 7.5. It is clear from this that the addition of such a component cannot be the cause of the difference between the Abell cluster galaxies and the 3C radio galaxies. Furthermore, if the host galaxies are extracted from the same elliptical galaxy population as studied by Kormendy (1977), then it seems unlikely that the radio galaxies have substantial unresolved nuclear components. Crude estimates of the values of the alpha parameter for broad line radio galaxies may be made using the multiaperture optical photometry of several such galaxies presented by Sandage (1972b). These galaxies, which clearly have substantial nuclear components do indeed lie above and to the left of the ten 3C galaxies if they are plotted on Figure 7.5.

Possible relations between $\alpha$ and various radio parameters such as linear size, luminosity, spectral index, were searched for. None were found, however, although the sample is of course small.

Before discussing some of the implications of this difference between Abell cluster galaxies and the 3C radio galaxies, it is worth comparing the radio galaxy growth curve with that of Sandage (1972a) which, it will be recalled, was used in the construction of the optical-infrared colours of Chapter 3. The value of the alpha

parameter that is derived from Sandage's growth curve for 1st ranked cluster galaxies, is 0.44. This is similar to the mean $\alpha$ of the Hoessel sample (see above) of Abell cluster galaxies. The radio galaxies are significantly more compact with their mean $\alpha$ of 0.35. However, the error that will be introduced in to the optical-infrared colours is very small because the optical and infrared measurements were always made through apertures of similar size. In contrast, the analysis of the Hubble diagram does require as accurate a growth curve as possible, since the curve is used over a wide range of metric sizes because of the fixed measuring aperture. The mean value of $\alpha$ for the radio galaxies that has been found here was therefore used to construct the growth curve that was employed in Section 4.4.e.

### 7.3.a The Difference between 3CR Radio Galaxies and Abell cluster Galaxies

The major question that arises is why does the powerful radio activity associated with the classical double sources avoid the galaxies in the upper right quadrant of Figure 7.5. It is well known that radio activity generally occurs in more massive systems, yet these most powerful radio sources are not in the most massive (or strictly speaking, the most luminous) galaxies found in the universe. While it has been known for some time (Sandage 1972b, Yee and Oke 1978) that low redshift 3CR radio galaxies have a slightly lower mean absolute magnitude than the 1st ranked cluster galaxies, this has generally been thought to be due to the existence of a tail to the optical luminosity function extending to lower luminosities (Sandage 1972b). The explanation for this avoidance of the most

massive galaxies may lie either in some intrinsic property of the galaxy related to its mass, or in some property of the local environment. A different environment will certainly affect the radio power and morphology, and may also affect the mass and optical structure of the giant elliptical, particularly if the merging hypothesis is correct.

In this context, it is of interest to note the possible difference between the results of this work, and the qualitative investigation of Matthews et al (1964, MMS). The cD-type of optical galaxy morphology was originally introduced by MMS in order to describe the appearance of 3CR radio galaxies, and was subsequently found to be applicable to the first ranked cluster ellipticals in Abell clusters and also to the first ranked galaxies in the poorer AMW and MKW clusters. These latter certainly have high values of $\alpha$ even though they do not have the extended envelopes that are the defining feature of cD galaxies (Thuan and Romanishin 1981). Hence, it seems quite likely that the radio galaxies classified as cD galaxies by MMS have a higher $\alpha$ than those studied here. Such a difference, if confirmed in quantitative investigations, would be very interesting, since there is an important difference in the sample observed by MMS and that observed in the current investigation. The samples observed here is at generally higher redshift. This is important because the difference in redshift between the two samples results in a difference of radio morphology as well as a difference in radio luminosities, since morphology and luminosity are known to be related (Fanaroff and Riley 1974, FR). 70% of the radio galaxies classifies as cD's by MMS have FR I structure (i.e. are relaxed doubles or are extended in an

ill-defined way) whereas all of the sample investigated here have FR II morphology (i.e. are classical doubles with prominent hotspots in the radio lobes).

In connexion with this, the results of Longair and Seldner (1979) are relevant to this discussion. They investigated the amplitudes of the spatial cross-correlation function of galaxies around radio galaxies compared with that around randomly selected galaxies. Their quantitative statistic Bgg*/Bgg is the ratio of these amplitudes, appropriately corrected for the effects of the different redshifts on the projection of galaxies and clusters onto the sky. The method can, of course be applied to any particular galaxies of interest, and for Abell cluster galaxies Bgg*/Bgg ranges from about 13 for Richness Class 2 clusters to about 4.5 for Richness Class 0 clusters. Galaxies chosen at randon have, by definition, a mean Bgg*/Bgg of unity. Longair and Seldner's results were as follows. For the weakest radio sources, with P(178) only 10 to 1000 times larger than that of our own Galaxy, and in which the radio emission is from 'conventional' sources such as supernova remnants, they found $\langle Bgg^*/Bgg \rangle$ to be essentially unity. This implies that these galaxies are effectively random members of the galaxy population, which is not at all surprising. On the other hand, the more powerful radio sources, classified as 'radio galaxies' proper and associated with 'non-thermal' activity in the nuclei of the host galaxies, had a $\langle Bgg^*/Bgg \rangle$ of about 5. This indicates that they tend to be found in clusters and groups of galaxies that are comparable to the poorer Abell clusters. Longair and Seldner's surprising result, however, was that their eight most powerful 'good classical double' FR Class II sources had a value of

<Bgg*/Bgg> close to unity. They must therefore be in environments in which there is a considerably lower galactic density than is found around the less powerful, FR I, sources. This result is certainly consistent with the possible result described above concerning a difference in optical morphology of the radio galaxies associated with FR I and FR II sources, since ot would indicate that they occupy generally different cluster environments. There is a correlation between $\alpha$ and cluster richness in the sample of Hoessel (1980), although it should be remembered that the poor clusters of AMW and MKW have high $\alpha$. In terms of the merging hypothesis, the AMW and MKW galaxies are thought to have a higher merging rate due to the lower velocity dispersion of the cluster members. It would be interesting to obtain velocity dispersions for the, presumably poor, clusters surrounding the radio galaxies, which have been shown to have lower values of the $\alpha$ parameter, in order to compare them with the poor AMW and MKW clusters.

The location of these ten powerful 3CR radio galaxies at moderate redshift on the $(M,\alpha)$ diagram, and the results of Longair and Seldner (1979) indicates that the radio galaxies studied here and in the other parts of this Thesis, are not precisely the same sort of galaxy as typical Abell cluster cD galaxies. This strongly suggests that studies of the evolution of massive elliptical galaxies that use samples of galaxies that are a mixture of Abell cluster 1st ranked galaxies at low redshift, and 3CR radio galaxies at high redshifts, (i.e. greater than about 0.4 at which point the cluster samples peter out), may be difficult to interpret if this apparent difference between Abell cluster galaxies is maintained out to redshifts of order unity. In particular the infrared (K,z) Hubble

diagram of Lebofsky (1981) was constructed using predominantly Abell cluster galaxies for $0.05<z<0.50$, and predominantly 3CR radio galaxies at higher redshifts. The results will clearly be distorted if there is a difference in the mean intrinsic absolute magnitudes of the two types of galaxy. Similarly, the investigation in to the $(\theta,z)$ relation, and the evolution of alpha with cosmic epoch undertaken by Djorgovski and Spinrad (1981) used a sample of 25 galaxies in the redshift range from zero to 1.2. Again, most of the galaxies at redshifts less than 0.4 were 1st ranked cluster galaxies, many in Abell clusters, while two thirds of the high redshift sample were 3CR or PKS radio sources. Hence it is quite conceivable that the apparent decrease in $\alpha$ with redshift noted by Djorgovski and Spinrad could represent only the change in emphasis in the sample from 1st ranked cluster galaxy to radio galaxy as the redshift increases.

The sample examined in this investigation is very small however, consisting of only ten objects. It should nevertheless be representative of the population, although it is possible to find counter-examples to the trends that have been established in the ten galaxies studied here. For instance, Spinrad and Stauffer (1982) have presented photographic surface photometry of 3C 405 (Cygnus A), that indicates that this galaxy has both a high value for the alpha parameter and a high luminosity despite being the definitive classical double FR II radio source. 3C 405 lies in the upper right quadrant of Figure 7.5. There has also been speculation for some years that the environments of quasars may change with the redshift (e.g. Stocke and Perrenod 1981) and there are at least two 3CR radio galaxies with redshifts around 0.5 that have high alphas greater

than 0.7. These are 3C 295 (z=0.46) and 3C 34 (z=0.69).

If the small values of $\alpha$ found in the radio galaxies can be taken as indicating that the merging of cluster galaxies with the giant elliptical radio galaxies has been relatively unimportant compared to the situation in Abell cluster galaxies and the poorer AMW and MKW cluster galaxies then a number of interesting things may be said.

Firstly, this would suggest that the effect of dynamical evolution, in the sense of increasing the luminosities with cosmic time, is unlikely to be important in the (K,z) Hubble diagram for 3C radio galaxies, since the nearest galaxies, and hence presumably the oldest, are in a relatively unevolved state. Although bringing the determination of $q_0$ no nearer, since the other evolutionary terms, and selection effects, are still extremely uncertain, this does nevertheless simplify the discussion presented in Chapter 5.

Secondly the result would hint that mergers have not been important in fuelling these radio sources. However, the statement on the lack of dynamical evolution derived from the low values of the $\alpha$ parameter, refers only to evolution over cosmological timescales, and it is not possible on the basis of $\alpha$ to rule out that a single merger occurred around $10^7$ to $10^8$ years ago to trigger the radio activity. On the other hand there is no evidence on the CCD images, such as multiple nuclei, that such an event took place.

# Chapter 8 : CONCLUSIONS AND AN INDICATION OF FUTURE WORK

## 8.1 : Summary of the Results of the Investigation

The project described in this Thesis has demonstrated the feasibility of studying very distant galaxies using modern instruments on large 4 metre class telescopes. The redshift range of the galaxies studied certainly extends to 1.6, and several of the faintest galaxies studied probably lie at redshifts considerably larger than 2.0.

In addition to the seven new redshifts for faint 3CR source identifications presented at the begining of the Thesis, the main results of this work may be summarized as follows:

(a) A large programme of infrared photometry of 81 members of a well defined sample of 90 3C radio galaxies has enabled comparisons to be made of the optical and infrared colours and magnitudes of such galaxies over a large range of redshift $0.03 < z < 1.6+$. These comparisons have produced the following results:

(i) The infrared colours longward of 7000 A in the rest frame do not change out to a redshift of at least unity. This effectively means that the integrated colours of the giant branch population cannot have changed over the last 10 Gyr, and this indicates that the form of this population and the relative contributions of the stars on different parts of the giant branch must have remained much the same over this

period. This suggests that the bulk of the stellar population in these galaxies is relatively old, even at a redshift of unity.

(ii) The optical to infrared colours, effectively measuring the ratio of ultraviolet to red/infrared light, however show significant changes at high redshift. Attention was concentrated on the small but representative sample for which both infrared and optical CCD imaging r photometry was available. On the basis of evidence presented that demonstrated that these changes were due to changes in the stellar populations of the galaxies, it was deduced that all the galaxies at high redshift exhibited the colour changes caused by the ageing of the main sequence turnoff point in a passively evolving old stellar population. In addition, however, many of the galaxies had ultraviolet flux densites that were further enhanced. This effect was interpreted as being caused by a minority young population produced by a burst of star formation involving a very small fraction of the total galaxy mass. The strength of this second effect is correlated with the strength of the [O II] 3727 line in the spectra of the galaxies, but not with the radio properties. The precise cause of the correlation is not known, but it probably reflects the overall gas content of the galaxy. However, an important observation is that 3C 241 at a redshift of 1.62 has a ultraviolet flux density only slightly enhanced over that expected for an inactive, passively evolving old elliptical galaxy. At all redshifts greater than about 0.8, there appears to be a range of star

formation activity found in the radio galaxies.

(iii) The infrared (K,z) relation for the 3C radio galaxies is well defined at all redshifts up to about 1.4, and has a cosmic scatter of approximately 0.5 magnitudes. The apparent value of $q_0$ that is indicated by the diagram is substantially greater than unity, with values between 3 and 4 being found. There is no reason to believe, though, that this should be any where near the true value. The most important result is that if the effects of the evolution of the stellar population on the infrared luminosity are corrected for, as carefully as possible, then the corrected value of $q_0$ lies in the range $0 < q_0 < 0.6$. Since this is the range in which other experiments suggest the true vlue should lie, this indicates that the net effect of any other evolutionary effects, and of any biases introduced by the sample selection criteria, is probably less than 0.3 magnitudes, which is much smaller than the 'stellar' evolutionary effect (which is about one magnitude in size). In other words, under an evolutionary change caused simply by the changing number of red giant stars in the galaxy, and which would be expected to occur in all galaxies regardless of their radio activity, the 3CR radio galaxies are apparently rather good 'standard candles'.

(b) Infrared observations of 39 other radio sources, selected to be about six times fainter in the radio than the 3CR sources, were also made. The most interesting aspect of this work was the clear detection at 2.2 microns of eight out of twelve of the

sources that had remained unidentified to the faint limiting red optical magnitude of 23.5. The brightest examples of these infrared identifications are probably passively evolving elliptical galaxies at a redshift of about 2. They must have rather red (r-K) colours, and the lower limits to these colours suggest that the epoch of last major star formation in these galaxies occured prior to a redshift of about 2.6 to 3. The best estimate that can be made of the redshift distribution of the faintest radio galaxies, which are likely to have redshifts greater than 2, shows no gross discrepancy from that which is predicted, on the basis of existing models for the evolution of the radio source population, from the redshift distribution of the 3CR galaxies.

(c) An analysis of the optical surface brightness distributions of ten 3CR galaxies at low redshift ($z < 0.3$), and a comparison of these profiles with those of other giant ellipticals found in rich (Abell) and poor (AMW and MKW) clusters, suggests that the radio galaxies have undergone relatively few mergers with other galaxies. This result is consistent with previous quantitative estimates of the cluster environments of these galaxies. The optical morphology and radio structure may be related through the different effects of the local cluster environment. The apparent statistical difference between the radio galaxies and 1st ranked Abell cluster galaxies at low redshift strongly argues that the two should not be mixed in samples of giant elliptical galaxies that are used to study galactic evolution or in other investigations of a cosmological nature. The lack of evidence for dyamical evolution in the lowest redshift (and

hence the oldest) radio galaxies suggests that this evolutionary process may not be important in biasing the Hubble diagram for these objects, and may explain why the 'stellar' term appears to be the dominant evolutionary effect (see (iii) of (b) above).

The picture that emerges of radio galaxies at high redshift is therefore really rather conventional. A self-consistent scenario is envisaged in which the radio galaxies form at redshifts of 3 or greater. By a redshift of unity, they are already several Gyrs old and, although bursts of star formation are still occuring in some of the galaxies possibly related to either the nuclear activity or to a merging event, the vast bulk of the stellar population is already formed and is passively evolving towards the populations that we see today around us.

Although this picture will surprise few contemporary cosmologists, the importance of establishing it on the basis of direct observation rather than speculation is clear.

## 8.2 : Future Work

### 8.2.a Immediate Prospects

Observations of respectably sized samples of faint objects, such as those undetaken in the investigations described in this Thesis, are time consuming, even on the largest telescopes. Hence, there are always many programmes that would directly and substantially advance current work that could be undertaken immediately with presently

available equipment, if sufficient time could be made available.

For instance, some of the most interesting results presented in this Thesis have concerned the changes observed in the optical to infrared colour (r-K). Nevertheless, nearly all these results have been based on observations of this single colour in just the twelve galaxies for which both good optical and good infrared data are available. However, even south of +55° declination (which is neccessary for UKIRT observations), there are over 40 3CR galaxies at redshifts that are almost certainly greater than 0.4. Most of these have spectroscopically confirmed redshifts. A programme to obtain high quality photometric CCD images in four colours (e.g. griz) for all these high redshift galaxies would substantially improve the amount of observational data available. As well as simply increasing the sample size, with all the advantages of clarifying some of the correlations indicated by the original small sample, such data would also allow a more thorough investigation in to the nature of the ultraviolet excess. In particular, with multi-colour optical photometry, the two different effects of the redshift, namely the changing rest-frame wavelength and the changing cosmological epoch, may be distinguished, and the epoch at which the evolutionary effects first become apparent could be found. If taken in good seeing, these data would also allow an extension of the investigation in to the alpha parameter (Chapter 7) to higher redshifts. Again, the multi-colour approach has the advantage of enabling that particular investigation to be carried out at a fixed rest wavelength. Related to this, such data would allow the investigation described (Chapter 4) in to 3C 352 to be carried out on a much bigger sample, most of the members of which would not be

next to a 17th magnitude star

As regards the '1 Jansky' sample (Chapter 6), much work remains to be done. It will have been clear to the reader that the available information on a galaxy increases dramatically when a redshift is determined. This is because it is then possible to relate the observable measurements to the intrinsic properties of the galaxy unambiguously. Most of the galaxies in the 1 Jansky sample, and some of the quasars even, do not have redshift information at present. A much more detailed interpretation of the existing photometry would be possible if redshifts could be measured for all the 1 Jansky sources with $r < 22.5$. A proper comparison with the 3CR galaxies at higher radio luminosities could be undertaken, and this sample, with its existing complete r data and nearly complete K data, would be ideal for investigating the relationship between colour and emission line properties if homogeneous spectroscopic data could also be obtained. Another high priority is the very deep imaging of the optically empty fields in which significant infrared detections were made. The existing CCD exposures were relatively short (5 minutes) and there seems no reason why much longer exposures, perhaps of two hours or so, could not lower the limiting magnitude by a very significant amount. The already rather red lower limits to the (r-K) colours in the context of the models for elliptical galaxies suggests that these galaxies will not be far below the existing plate limit. They are almost certainly passively evolving galaxies and, presumably, clusters of some sort, at redshifts near to two. Deep exposures of the remaining empty fields should also be taken, but for these the prospects for detection are not so hopeful.

Finally, the alpha parameter investigation should be extended by firstly increasing the size of the sample, and secondly having more detailed information available on the cluster environments of the individual sources. Fortunately, an investigation in to the clusters surrounding many southern radio galaxies has begun in Edinburgh using the deep UKST plates which are available for the southern hemisphere. It will be relatively easy to obtain good CCD images of these galaxies. Such data will allow the measurement of the alpha parameter, the accurate calibration of the UKST plates, the searching for very faint nearby companions to the radio galaxy that may have been missed by the UKST plates, as well as providing a more systematic set of low redshift colour data in UBVR for comparison with the optical and infrared data on high redshift galaxies. It is envisaged that after an initial analysis of the relationship between alpha, the radio source structure and the cluster environment, further data should be obtained on such cluster parameters as the velocity dispersion, in order to investigate the general merging hypothesis in more detail. An important aspect to this investigation is the selection of a sample of giant ellipticals (i.e. the radio galaxies) by a means that is not directly related to the form of the cluster. Previous investigations have had to use gE galaxies selected because of their membership of either rich Abell clusters or poor, but centrally dense (to provide sufficient contrast to the background), clusters which may not be representative of poor groups in general.

8.2.b New Technologies

In addition to the specific examples of projects which could be undertaken at the present time using existing facilities which were described in the previous section, the introduction in the next few years of two particular instruments will make feasible many new projects and make existing investigations so much easier that it will be well worth repeating them. In order of their likely appearance, these two instruments are the multi-element 1-dimensional, and later 2-dimensional, array detectors for the near infrared 1-5 micron waveband, and the Space Telescope (ST). 1-dimensional 32 element array detectors are will be tested on UKIRT in early 1984, and the larger 2-dimensional format devices should become available about a year later. The Space Telescope is presently scheduled for launch in 1986.

Infrared arrays will be very important in both spectroscopy and direct imaging. For instance, the arrays will have sufficient detector elements for it to be possible to undertake medium resolution spectroscopy right through any one of the atmospheric windows corresponding to the J, H and K passbands, in a single integration. This will make it feasible to attempt to determine redshifts for faint galaxies in the infrared. At present, say with the seven-element CGS II instrument on UKIRT, a minimum of about 8 integrations must be made to cover a single window. This requires a prohibitive expenditure of telescope time. It is clear that many of these radio galaxies have very strong emission lines, particularly in [O II] 3727 and [O III] 5007. These are however redshifted out of

the optical passbands for $z > 1.5$, but from this redshift on, will move through the near infrared. The equivalent widths that can be reasonably expected in these galaxies (several hundred A in the restframe, multiplied by (1+z) in the observed frame) are sufficiently large, and the lines sufficiently narrow, that a significant detection of the continuum is not required. Particularly in view of the reduction in noise that will be associated with the spectrograph in those passbands that are at present dominated by the photon statistics of the sky background, it will be worth taking the spectra of all the faint radio galaxies for which decent broad-band detections have been made, including those in the 1 Jansky sample which have not been detected optically.

In the direct imaging mode, aside from the obvious advantages of having an array detector in terms of the amount of sky that can be mapped in a given time, a two-dimensional array also offers the possibility of large increases in effective sensitivity in those passbands that are are presenty sky noise limited. Principally because of the uncertainties in the precision of the relative positions of the offset guide star and of the faint galaxies, large apertures have been used in the present work. This is pariculary true in the case of the 'empty field' sources, for some of which the position of the radio galaxy is formally uncertain (on account of the extended radio structure) to 3 arcsec. In the present investigation on UKIRT a 12 arcsec aperture was used as standard. Other investigators have used smaller apertures (e.g. 7-8 arcsec), although it is believed that in some cases at least, their 'anomalous' results are probably due to this difference in technique. These apertures are, of course, substantially larger than

the area that contains most of the light on, for instance, the CCD images of the most distant radio galaxies. Consequently, unneccessary noise is introduced into the measurement by the surrounding sky. With an array detector, the precise positioning of the array is not important, particularly if the image can be analysed astrometrically later, and hence much smaller pixels can be used. If the pixel size can be reduced by a factor n, then in principle, the limiting flux density of the detector will be reduced to fainter light levels by a similar factor, depending on such considerations as the precise degree by which the background noise dominates, and the actual size of the galaxy images. Hence, an improvement in sensitivity of well over a magnitude appears to be quite feasible. It is clear from Chapter 6 that this improvement is just that which is required to enable giant elliptical galaxies at a redshift of around 3, i.e. those with a K of around 19, to be studied effectively.

The instruments, capabilities and scientific opportunities offered by the Space Telescope have been described many times in various publications (see e.g. Longair and Warner 1979). ST has esentially two unique capabilities. These are high resolution imaging (0.1 arcsec resolution) in the optical shortward of 1 micron, and an imaging capability in the ultraviolet shortward of the terrestrial atmospheric cutoff at 3000 A. Although ST has a relatively small mirror, at 2.5 metres in diameter it has only a quarter of the collecting power of the Palomar 5 metre, some of the work described in this Thesis has demonstrated how important spatial information on the distribution of light at different wavelengths is. In particular, the investigation in to the appearance of the

single galaxy 3C 352 (Chapter 4) through BVRI filters was crucial in establishing the stellar nature of the colour changes observed in the larger sample of galaxies which had little imaging information. One of the most interesting features of the present investigation has been the inferred location of the star forming regions in the elliptical galaxies. The contrast between the young and old populations in these galaxies is greatest at short wavelength and much could be learnt from a sequence of high resolution multicolour images of a large sample of these high redshift galaxies. Many of the ST filters are sufficiently narrow that in many cases it would be possible to map in detail the distribution of the sources of the strong emission lines. This would prove invaluable in understanding the nature of the correlation between the ultraviolet flux density enhancement and the [O II] line strength.

Ten years ago, galaxies at a redshift of 0.2 were at the limits of the observable universe and were at the forefront of observational cosmology, although one (predictably a radio galaxy) was known at a redshift of 0.46. Today galaxies at redshifts of unity are being studied in some detail, and some are known at redshifts of as high as 1.6. The changes in the colours and magnitudes caused by an evolution of the stellar populations of elliptical galaxies, which have long been expected have now been convincingly shown to be found at these high redshifts. It is very likely that the starlight of stellar populations at a redshift of three has already been detected on UKIRT, and even if detailed study of these systems is not yet feasible, the prospect of substantial

further advances in our ideas on the evolution of galaxies over the whole history of the universe in the near future is very real.

Non-Bibliographic Abreviations.

AGB Assymptotic Giant Branch.
AGN Active Galactic Nuclei.
BLRG Broad Line Radio Galaxy.
BLQ Broad Line Quasar.
CCD Charge Coupled Device.

CMB Cosmic Microwave Background.
CRS Compact Radio Source.
CTIO Cerro Tellolo Interamerican Observatory.
EOF Empty Optical Field.
EOR Extended Operating Region.

FWHM Full Width at Half Maximum.
FR Fanaroff-Riley (1974) Class.
GUT Grand Unified Theory.
HB Horizontal Branch.
IMF Initial Mass Function.

ISP Imaging Spectropolarimeter.
KPNO Kitt Peak National Observatory.
LBDS Leiden Berkeley Deep Survey.
MS Main Sequence.
NLRG Narrow Line Radio Galaxy.

ODG Old Disk Giant.
OEF Optically Empty Field.
OOF Optically Obscured Field.
OVV Optically Violently Variable.
PFUEI Prime Focus Universal Extragalactic Instrument.

PLMSF Period of Last Major Star Formation.
PMS Post Main Sequence.
POSS Palomar Observatory Sky Survey.
QSO Quasi-Stellar Object (Quasar)
RAM Reduced Absolute Magnitude.

RGB Red Giant Branch.
RLF Radio Luminosity Function.
RMS Root Mean Square.
SED Spectral Energy Distribution.
SFR Star Formation Rate.

SSP Simple Stellar Population.
ST Space Telescope.
UAO University of Arizona Observatory.
UKIRT United Kingdom Infrared Telescope.
3C Third Cambridge Radio Catalogue.

3CR Revised Third Cambridge Radio Catalogue.
4C,4CT Fourth Cambridge Catalogue.

## REFERENCES


Aaronson, M., Frogel, J.A., & Persson, S.E.; 1978a, Ap.J., 220, 442.

Aaronson, M., Cohen, J.G., Mould, J.R., & Malkan, M.; 1978b, Ap.J., 223, 824.

Aaronson, M., & Mould, J.R.; 1982, Ap.J.Suppl, 48, 161.

Albert, C.E., White, R.A., & Morgan, W.W.; 1977, Ap.J., 211, 309. (AMW)

Allington-Smith, J.R.; 1982, Mon.Not.Roy.astr.Soc., 199, 611.

Allington-Smith, J.R., Perryman, M.A.C., Longair, M.S., Gunn, J.E., & Westphal, J.A.; 1982, 201, 331. (APLGW)

Audouze, J.; 1982, In "Proc. Study Week on Cosmology and Fund. Phys." Pont.Acad.Sci.; (eds. Bruck, H.A., Coyne, G.V., & Longair, M.S.,) p.395.

Baade, W., & Minkowski, R.; 1954, Ap.J., 119, 206.

Bailey, M.E., & Macdonald, J.; 1981, Nature, 289, 659

Baldwin, J.R., Frogel, J.A., & Persson, S.E.; 1973, Ap.J., 184, 427.

Bautz, L.P., & Morgan, W.W.; 1970, Ap.J., 162, L149. (BM)

Becklin, E.E., Matthews, K., Neugebauer, G., & Wynn-Williams, C.G.; 1973, Ap.J., 186, L69.

Bennet, A.S.; 1962, Mem.Roy.astr.Soc., 68, 163.

Blanco, V.M., McCarthy, M.F., & Blanco, B.M.; 1980, ApJ, 242, 938.

Boroson, T.A., & Oke, J.B.; 1982, Nature, 296, 397.

Bruzual, G.; 1981, PhD Dissertation, Univ. California, Berkeley.

Bruzual, G.; 1983, Ap.J., 273, 105.

Burstein, D., & Heiles, C.; 1982, A.J., 87, 1165.

Cohen, J.G., Frogel, J.A., Persson, S.E., & Elias, J.H.; 1981, Ap.J., 249, 481.

Coleman, G.D., Wu, C.C., & Weedman, D.W.; 1980, Ap.J.Suppl, 43, 393.

Corwin, H.G., & Emerson, D.; 1982, Mon.Not.Roy.astr.Soc., 200, 621.

Costero, R., & Osterbrock, D.E.; 1977, Ap.J., 211, 675.

Davis, M.; 1980, In "Objects at High Redshift" IAU Symp. 92, (eds. Abell, G.O., & Peebles, P.J.E.) Reidel, Dordrecht, p.57.

Davis, M.; 1982, In "Proc. Study Week on Cosmology and Fund. Phys." Pont.Acad.Sxi,. (eds. Bruck, H.A., Coyne, G.V., & longair, M.S.) p.113.

De Veny, J.; 1982, "An Observer's Manual for the Cryogenic Camera", Kitt Peak National Observatory.

Djorgovski, S., & Spinrad, H.; 1981, Ap.J., 251, 417.

Dressler, A., & Gunn, J.E.; 1982, Ap.J., 263, 533.

Edge, D.O., Shakeshaft, J.R., McAdam, W.B., Baldwin, J.E., & Archer, S.; 1959, Mem.Roy.astr.Soc., 68, 37.

Elias, J.H., Frogel, J.A., Matthews, K., Neugebauer, G.; 1982, A.J., 87, 1029.

Ellis, R.S., Fong, R., Phillips, S.; 1977, Mon.Not.Roy.astr.Soc., 181, 163.

Ellis, R.S.; 1983, In "The Origin and Evolution of Galaxies" (eds. Jones, B.J.T., & Jones, J.E.) Reidel, Dordrecht, p.255.

Ellis, R.S., & Allen, D.A.; 1983, Mon.Not.Roy.astr.Soc., 203,685.

Fabbiano, G., Miller, L., Trinchieri,G., Longair, M.S., & Elvis, M.; 1983, ApJ, in press.

Faber, S.M.; 1972, Astr.Ap., 20, 361.

Faber, S.M.; 1977, In "The Evolution of Galaxies and Stellar Populations" (eds. Tinsley, B.M., & Larson, R.B.) New Haven, Yale University Obs., p.199.

Fabian, A.C., Ku, W.H.M., Malin, D.F., Mushotzky, R.F., Nulsen, P.E.J., & Stewart, G.C.; 1981, Mon.Not.Roy.astr.Soc., 196, 35P.

Fanaroff, B.L., & Riley, J.M.; 1974, Mon.Not.Roy.astr.Soc., 167, 31P. (FR)

Felten, J.E.; 1977, A.J., 82, 861.

Frogel, J.A., Persson, S.E., Aaronson, M. & Matthews, K.; 1978, Ap.J., 220, 75. (FPAM)

Frogel, J.A., Persson, S.E., & Cohen, J.G.; 1980, Ap.J., 240, 785. (FPC)

Glass, I.S.; 1976, Mon.Not.Roy.astr.Soc., 175, 191.

Goad, J.; 1982, "A Partial Guide to the IPPS RV Menu", Kitt Peak Nat. Obs.

Grandi, S.A., & Osterbrock, D.E.; 1978, Ap.J., 220, 783.

Grasdalen, G.L.; 1980, In "Objects at High Redshift", IAU Symp. 92, (eds. Abell, G. & Peebles, J.), Reidel, Dordrecht, p.269.

Gunn, J.E., & Oke, J.B.; 1975, Ap.J., 195, 255. (GO)

Gunn, J.E., & Tinsley, B.M.; 1976, Ap.J., 210, 1

Gunn, J.E.; 1978, In "Observational Cosmology" 8th Adv. Course SAAS-FEE, (eds. Maeder, A., Martinet, L., & Tammann, G.) Geneva Obs. p.1.

Gunn, J.E.; 1980, In "Active galactic Nuclei", Cambridge Univ. Press, eds. Hazard, C., Mitton, S., p.213.

Gunn, J.E., Hoessel, J.G., Westphal, J.A., Perryman, M.A.C., & Longair, M.S.; 1981, Mon.Not.Roy.astr.Soc., 194, 111. (GHWPL)

Gunn, J.E., Stryker, L.L., & Tinsley, B.M.; 1981, Ap.J., 249, 48.

Gunn, J.E.; 1982, In "Proc. Study Week on Cosmology and Fund. Phys.", Pont.Acad.Sci., (eds. Bruck, H.A., Coyne, G.V., & Longair, M.S.) p.233.

Hausman, M.A., & Ostriker, J.P.; 1978, Ap.J., 224, 320.

Hewitt, A., & Burbidge, G.R.; 1980, Ap.J.Suppl., 43, 57.

Hine, G., & Longair, M.S.; 1979, Mon.Not.Roy.astr.Soc., 188, 111.

Hoessel, J.G.; 1980, Ap.J., 241, 493.

Hutchings, J.B., Campbell, B., & Crampton, D.; 1982, Ap.J., 261, L23.

Hyland, A.R., & Allen, D.A.; 1982, Mon.Not.Roy.astr.Soc., 199, 943.

Impey, C.D., & Brand, P.W.J.L.; 1981, Nature, 292, 814.

Jenkins, C.R., Pooley, G.G., & Riley, J.M.; 1977, Mem.Roy.astr.Soc, 84, 61. (JPR)

Johnson, H.L.; 1966a, Ap.J., 143, 187.

Johnson, H.L.; 1966b, Ann.Rev.astr.astrophys., 4, 193.

Kellerman, K.I., Pauliny-Toth, I.I.K., & Williams, P.J.S.; 1969, Ap.J., 157, 1.

Kormendy, J.; 1977, Ap.J., 218, 333.

Kormendy, J.; 1982, In "Morphology and Dynamics of Galaxies" 12th Adv. Course SAAS-FEE (eds. Martinet, L., & Mayor,

M.) Geneva Obs. p.177.

Kristian, J., Sandage, A., & Katem, B.; 1974, Ap.J., 191, 43.

Kristian, J., Sandage, A., & Katem, B.; 1978a, Ap.J., 219, 803.

Kristian, J., Sandage, A., & Westphal, J.A.; 1978b, Ap.J., 221, 383.

Kurucz, R.L.; 1979, Ap.J.Suppl., 40, 1.

Laing, R.A., Longair, M.S., Riley, J.M., Kibblewhite, E.J., & Gunn, J.E.; 1978, Mon.Not.Roy.astr.Soc., 184, 149.

Laing, R.A., Riley, J.M., & Longair, M.S.; 1983, Mon.Not.Roy.astr.Soc., 204, 151. (LRL)

Lebofsky, M.J.; 1980, In "Objects at High Redshift", IAU Symp. 92, (eds. Abell, G.O, & Peebles, P.J.E.), Reidel, Dordrecht, p.257.

Lebofsky, M.J.; 1981, Ap.J., 245, L59.

Lebofsky, M.J., Riecke, G.H., & Walsh, D.; 1983, Mon.Not.Roy.astr.Soc., 203, 727.

Lee, T.J., Beattie, D.H., Brand, P.W.J.L., Jones, T., & Hyland, A.R.; 1982, Nature, 295, 214.

Lilly, S.J., & Longair, M.S.; 1982a, Mon.Not.Roy.astr.Soc., 199, 1053.

Lilly, S.J., & Longair, M.S.; 1982b, In "Extragalactic Radio Astronomy" IAU Symp. 97, (eds. Heeschen, D.S., & Wade, C.M.)Reidel, Dordrecht, p.413,

Lilly, S.J., & Longair, M.S.; 1982c, In "Proc. Study Week on Cosmology and Fund. Phys." Pont.Acad.Sci., (eds. Bruck, H.A., Coyne, G.V., & Longair, M.S.) p.269.

Lilly, S.J., Longair, M.S., & McLean, I.S.; 1983, Nature, 301, 488.

Lilly, S.J.; 1983, In "Proc. RAL Workshop on the Spectral Evolution of Galaxies", Rutherford Laboratory, in press.

Lilly, S.J., McLean, I.S., & Longair, M.S.; 1983, Mon.Not.Roy.astr.Soc., in press.

Longair, M.S.; 1966, Mon.Not.Roy.astr.Soc., 133, 421.

Longair, M.S.; & Gunn, J.E.; 1975, Mon.Not.Roy.astr.Soc., 170, 121.

Longair, M.S.; 1975, Mon.Not.Roy.astr.Soc., 173, 309.

Longair, M.S.; 1978, In "Observational Cosmology" 8th Adv. Course SAAS-FEE (eds. Maeder, A., Martinet, L., & Tammann, G.) Geneva Obs., p.125.

Longair, M.S., & Riley, J.M.; 1979, Mon.Not.Roy.astr.Soc., 188, 625.

Longair, M.S., & Seldner, M.; 1979, Mon.Not.Roy.astr.Soc., 189, 433.

Longair, M.S., & Warner, J.W.; 1979, "Scientific Research with the Space Telescope", IAU Coll. 54, NASA CP-2111.

McAlary, C.W., McLaren, R.A., & Crabtree, D.R.; 1979, ApJ, 234, 471.

McLean, I.S., Cormack, W.A., Herd, J.T., & Aspin, C.A.; 1981, Proc. Soc. photo-opt. Engng, 290, 155.

Macdonald, J., & Bailey, M.E.; 1981, Mon.Not.Roy.astr.Soc., 197, 995.

Matthews, T.A., Morgan, W.W., & Schmidt, M.; 1964, Ap.J., 140, 35.

Morgan, W.W., Kayser, S., & White, R.A.; 1975, Ap.J., 199. 545. (MKW)

O'Connell, R.W.; 1976, Ap.J., 206, 370.

Mrley. G, 1980; Am Rev astr. Astr., 18, 165.

O'Connell, R.W.; 1980, Ap.J., 236, 430.

O'Dell, S.L., Puschell, J.E., Stein, W.A., Warner, J.W., & Ulrich, M.H.; 1978, Ap.J., 219, 818.

Osmer, P.S.; 1982, Ap.J., 253, 28.

Ostriker, J.P., & Tremaine, S.D.; 1975, Ap.J., 202, L133.

Peacock, J.A., & Gull, S.F.; 1981, Mon.Not.Roy.astr.Soc., 196, 611.

Peacock, J.A., & Wall, J.V.; 1981, Mon.Not.Roy.astr.Soc., 194, 331.

Peacock, J.A,, Perryman, M.A.C., Longair, M.S., Gunn, J.E., & Westphal, J.A.; 1981, Mon.Not.Roy.astr.Soc., 194, 601.

Peacock, J.A.; 1983, In "The Early Evolution of the Universe and Its Present Structure" IAU Symp. 104, (eds. Abell, G.O., & Chincarini, G.) Reidel, Dordrecht, p.43.

Pence, N.; 1976, Ap.J., 203, 39.

Penston, M.V.; 1973, Mon.Not.Roy.astr.Soc., 162, 359.

Persson, S.E., Frogel, J.A., & Aaronson, M.; 1979, Ap.J.Suppl., 39, 61.

Persson, S.E., Aaronson, M., Cohen, J.G., Frogel, J.A., & Matthews, K.; 1983, Ap.J., 266, 105.

Perryman, M.A.C., Longair, M.S., Allington-Smith, J.R., & Fielden, J.; 1982, Mon.Not.Roy.astr.Soc., 201, 957.

Puschell, J.J., Owen, F.N., & laing, R.A.; 1982, Ap.J., 257, L57. (POL)

Rees, M.J.; 1978, In "Observational Cosmology" 8th Adv. Course SAAS-FEE (eds. Maeder, A., Martinet, L., & Tammann, G.) Geneva Obs. p.259.

Renzini, A.; 1981, Ann.Phys.Fr., 6, 87.

Riecke, G.H., Lebofsky, M.J., & Kinman, T.D.; 1979, Ap.J., 232, L151.

Riecke, G.H., & Lebofsky, M.J.; 1979, Ann.Rev.astr. astrophys., 17, 477.

Riley, J.M., Longair, M.S., & Gunn, J.E.; 1980, Mon.Not.Roy.astr.Soc., 192, 233.

Ryle, M., & Clarke, R.W.; 1961, Mon.Not.Roy.astr.Soc., 122, 349.

Salpeter, E.E.; 1955, Ap.J., 121, 161.

Sandage, A.; 1972a, Ap.J., 173, 485.

Sandage, A.; 1972b, Ap.J., 178, 25.

Sandage, A.; 1973, Ap.J., 183, 711.

Saslaw, W.C., Tyson, J., & Crane, P., 1978, Ap.J., 222, 435.

Schecter, P.; 1976, Ap.J., 203, 297.

Scheuer, P.A.G.; 1974, Mon.Not.Roy.astr.Soc., 166, 513.

Schmidt, M.; 1963, Nature, 197, 1040.

Schmidt, M.; 1965, ApJ, 141, 1.

Schneider, D.P., Gunn, J.E., & Hoessel, J.G.; 1983a, Ap.J., 264, 337.

Schneider, D.P., Gunn, J.E., & Hoessel, J.G.; 1983b, Ap.J., 268, 476.

Scott, P., Hammond, S., & Goad, J.; 1982, "Long slit Batch Reduction Manual", Kitt Peak Nat. Obs.

Searle, L., Wilkinson, A., & Bagnuolo, W.G.; 1980, Ap.J., 239, 803. (SWB)

Shanks, T., Stevenson, P.R.F., Fong, R., & MacGillivray, H.T.; 1983, preprint, submitted to Mon.Not.Roy.astr.Soc..

Simkin, S.M.; 1978, Ap.J., 222, L55.

Smith, H.E., Burbidge, E.M., & Spinrad, H.; 1976, Ap.J., 210, 627.

Smith, H.E.; 1977, In "Radio Astronomy and Cosmology" IAU Symp. 74, (ed. Jauncey, J.L.), Reidel, Dordrecht, p.279.

Smith, H.E., Junkkarinen, V., Spinrad, H., Grueff, G., & Vigotti, M.; 1979, Ap.J., 231, 307.

Smith, H.E., & Spinrad, H.; 1980a, Pub.astr.Soc.Pac., 92, 553.

Smith, H.E., & Spinrad, H.; 1980b, Ap.J., 236, 419.

Smith, M.G.; In "Galactic and Extragalactic Infrared Spectroscopy" XVIth ESLAB Symp. (ed. Scoville, N.Z.), Toledo. 1983

Soifer, B.T., & Neugebauer, G.; 1981, In "Infrared Astronomy" IAU Symp. 96, (eds. Wynn-Williams, C.G. & Cruikshank, D.P.), Reidel, Dordrecht, p.329.

Spinrad, H., & Smith, H.E.; 1976, Ap.J., 206, 355.

Spinrad, H., Stauffer, J., & Butcher, H.; 1981, Ap.J., 244, 382.

Spinrad, H.; 1982, Pub.astr.Soc.Pac., 94, 397.

Spinrad, H., & Stauffer, J.R.; 1982, Mon.Not.Roy.astr.Soc., 200, 153.

Stocke, J.T., & Perrenod, S.C.; 1981, Ap.J., 245, 375.

Stockton, A., & McKenty, J.W.; 1983, Nature, 305, 678.

Stone, R.P.S.; 1977, Ap.J., 218, 767.

Strom, S.E., Strom, K.M., Goad, J.W., Vrba, F.J., & Rice, W.; 1976, Ap.J., 204, 684

Strom, K.M., Strom, S.E., Wells, D.C., & Romanishin, W.; 1978, Ap.J., 220, 62.

Strom, K.M., Strom, S.E.; 1978, A.J., 83, 73.

Sweigart, A.V., & Gross, P.G.; 1978, Ap.J.Suppl., 36, 405.

Telesco, C.M., Becklin, E.E., Wynn-Williams, C.G.; 1980, Ap.J., 222, 14.

Thuan, T.X., & Gunn, J.E.; 1976, Pub.astr.Soc.Pac., 88, 543.

Thuan, T.X., & Romanishin, W.; 1981, Ap.J., 248, 439. (TR)

Thuan, T.X., Windhorst, R.A., Puschell, J.J., Isaacman, R.B., & Owen, F.N.; 1983, preprint, submitted to Ap.J..

Tinsley, B.M.; 1972, Ap.J., 178, 319.

Tinsley, B.M., & Gunn, J.E.; 1976, Ap.J., 203, 52.

Tinsley, B.M.; 1978, Ap.J., 222, 14.

Wall, J.V., Pearson, T.J., & Longair, M.S.; 1980, Mon.Not.Roy.astr.Soc., 193, 683.

Wall, J.V., Pearson, T.J., & Longair, M.S.; 1981, Mon.Not.Roy.astr.Soc., 196, 597.

White, S.D.M.; 1978, Mon.Not.Roy.astr.Soc., 184, 185.

Whitford, A.E.; 1975, In "Stars and Stellar Systems" Vol IX, (eds. Sandage, A., & Kristian, J.), Chicago, p.159.

Whitford, A.E.; 1977, Ap.J., 211, 527.

Windhorst, R.A., Puschell, J.J., & Thuan, T.X.; 1983, In "The Early Evolution of the Universe and its Present Structure" IAU Symp. 104, (eds. Abell, G.O., & Chincarini, G.) Reidel, Dordrecht, p.83.

Yee, H.K.C., & Oke, J.B.; 1978, Ap.J., 226, 753.

Yee, H.K.C.; 1980, Ap.J., 241, 894.

ACKNOWLEDGEMENTS

I should particularly like to thank Professor Malcolm Longair, Astronomer Royal for Scotland, who was my supervisor, for his enthusiastic support of this project, and for the many interesting ideas that he suggested.

In addition to him, I have actively collaborated with several astronomers on the different investigations described in this work. Dr. Ian McLean (ROE) built the versatile CCD camera which was used in the work described in Chapters 4 and 7, and helped in obtaining and reducing that data. Drs Mike Perryman (ESTEC) and Ann Downes (Cambridge) collaborated in obtaining and partly reducing the spectroscopic investigation described in Chapter 2. Dr. Jeremy Allington-Smith (MSSL) contributed to the work described in Chapter 6. I thank all of them for their friendly collaboration.

Most of the observations described in this Thesis were made on the UKIRT telescope on Mauna Kea. The efforts of all the Staff Astronomers in Hawaii, which led to a steady improvement in the telescope during the past three years, are greatly appreciated. I am particularly grateful to those who actually assisted with taking these observations, during the many observing runs. Above all, I thank Dr. Terry Lee, but also Drs. Peredur Williams and Rich Isaacman, Dolores Walther and Alan Pickup. David Beattie and the various day-crews were also always at hand with their excellent support. I had many useful conversations in Hilo with Drs. Andy Longmore and Peredur Williams.

In Edinburgh, I have had very interesting discussions with too many colleagues to name them all individually. However, Drs. Russell Cannon, Malcolm Smith, Peter Brand and, in particular, Mike Hawkins and John Peacock, have helped develope my ideas on this and other subjects. I owe a great deal to the last two named. Drs. Peter Brand and David Emerson have both taught me a great deal during my three years at the Department of Astronomy. I thank them both.

I learnt much from all of my fellow Research Students, but particularly would like to thank Chris Impey, Paul Hewett, Neil Reid and Richard Prestage.

I am appreciative of the excellent computing, library and photographic facilities at the Royal Observatory, and would like to thank Bernie McNally and Ann Fraser especially for their help. Photolabs produced the two photographic prints in this Thesis. I have also made extensive use of the UKSTU plate library at the Observatory, and I am grateful to Sue Tritton for her assistance.

I attended several conferences during the course of this research. Two however were particularly valuable, that at Herstmonceux in January 1983, and that at Abingdon in June 1983. They were both very stimulating, and I should like to thank the organisers and all the participants of these, but especially Drs. Hy Spinrad, Richard Ellis, Gustavo Bruzual, Alvio Renzini and Richard Kron.

I am very grateful to Dr. Hy Spinrad for the prompt communication of his new redshift measurements as they have been obtained. Many of the interesting results of this investigation would have been impossible without the redshifts of the very faint 3C galaxies that he has measured. I have also had a continuous and fruitful dialogue with Dr. Richard Ellis during the course of this project.

I am grateful for the observing time on UKIRT that has been awarded to this programme, and I also thank the Kitt Peak National Observatory in Arizona for observing priveleges on the Mayall 4-metre telescope.

I acknowledge financial support from the UK SERC in the form of a Research Studentship and other grants.